WETTABILITY ALTERATION IN ROCK RESERVOIRS AND ITS EFFECT IN PETROLEUM RECOVERY

by

Talal Jamal Mubarik Al-Aulaqi

Submitted in accordance with the requirements for the degree of

Doctor of Philosophy

The University of Leeds

School of Earth and Environment

October 2012

The candidate confirms that the work submitted is his/her own, except where work which has formed part of jointly-authored publications has been included. The contribution of the candidate and the other authors to this work has been explicitly indicated below. The candidate confirms that appropriate credit has been given within the thesis where reference has been made to the work of others.

2012 "The University of Leeds and Talal Al-Aulaqi"

Some of the work contained in this thesis is also contained in the following posters and papers:

1. Al-Aulaqi, T., Grattoni, C., Fisher, Q., 2010, Effect of temperature in crude oil/brine/rock interaction in silicate surface. Poster present in 10th international wettability symposium, University of Calgary, Canada.
2. Al-Aulaqi, T., Grattoni, C., Fisher, Q., Musina, Z. and Al-Hinai, S., 2011, Effect of Temperature, Oil Asphaltene Content, and Water Salinity on Wettability Alteration. SPE 149071/DGS Saudi Arabia Section Technical Symposium and Exhibition, Society of Petroleum Engineers, Al-Khobar, Saudi Arabia.
3. Al-Aulaqi, T., Fisher, Q.,2012, Crude Oil, Brine Salinity and Sandstone Interaction - Nanoscale Resolution. SPE 155658 SPE EOR Conference at Oil and Gas West Asia, Muscat, Oman.

Abstract

Reservoir wettability is controlled by crude oil/rock/brine interactions. Wettability plays an important role in oil recovery because of its effect on fluid location, flow behaviour and residual oil distribution. In mature oil fields, a development programme is initiated to maintain oil production in economic size. Understanding reservoir wettability is a central issue in such field development plans which can be optimised to boost oil production rate. However, there is a considerable uncertainty in understanding the reservoir wettability especially in terms of effect of brine composition and temperature. This thesis serves to minimise such uncertainty.

In the present work, several experimental techniques are employed to investigate crude oil/brine/rock interaction in mineral surface. A protocol of contact angle measurements is developed to mimic the drainage of oil through receding contact angle and imbibition of water through advancing contact angle. Experiments are designed carefully to investigate the role of water film, brine composition, asphaltene content, crude oil solvency and temperature in wettability of mineral surface. The consequence of wettability alteration is studied in how fluid behaviour is developed and affects the trapping fluids. A two dimensional glass micromodel gives new visual insights into the type of flow behaviour as a function of brine salinity and temperatures. Furthermore, the role of capillary number is investigated in three distinctive wettability scenarios that exist in oil fields. Real rock surfaces, which are extracted from underground reservoirs in Oman, are studied extensively to understand the role of mineralogy in rock surface. A novel experimental combination between Nuclear Magnetic Resonance (NMR) and capillary imbibition test are utilised to track the wettability alteration in core samples as brine salinity and temperature manipulated. For the first time, the introduction of optical interferometry to petroleum recovery literature is achieved successfully by using vertical scanning interferometry. A detailed investigation of surface profile of crude oil adsorption gives new information on nanoscale wettability.

Application of the above-mentioned techniques to different crude oils on different reservoir conditions allows the establishment of fundamental wettability understanding to current enhance oil recovery techniques such as smart water flooding and steam injection. To our best knowledge, some of these finding are reported for the first time.

Acknowledgment

I would like to express my sincere gratitude to my supervisor Prof. Quentin Fisher who has always been a source of inspiration for me. I consider myself privileged to be one of his research students. His continuous encouragement during this journey has a great positive impact on me. The entrepreneurship skills that Quentin implants in his students surely will shape their future career in oil industry.

I would also like to thank my second supervisor Dr.Carlos Grattoni for his supervision with experimental set-up and his suggestion with safety issues during experimental progress in Chapter 6. Furthermore, the useful references in understanding the flow behaviour gives me more in depth understanding in discussing Chapter 5. Also, sincere thanks go to Mr. Phil Guise for monitroing safety issues and health hazardous during my experiments.

I would like also to thank Prof. Yulong Ding from Institute of Particle Science for his kind permission to use his laboratory during Chapter 4 for contact angle and interfacial tension measurements. I would like also to thank Dr. Nik Kapur , Mr. Ron Cellier and Mr. B. Leach from Institute of Engineering Thermofluids, Surfaces and Interfaces for their generous support to use the high resolution camera and syringe pumps during Chapter 5.

I would also like to thank Dr. Louise Jennings from Leeds Musculoskeletal Biomedical Research Unit to allow using their medical lab. Without the generous support from Dr. Louise Jennings, it will not be possible for a student who carries crude oil samples to get access to ultra clean medical lab. Also, I would like to thank Mr. Adrian Eagles for his very useful discussions in meteorology and surface profile. His encouragements and exciting discussion in optimising the fringes of vertical scanning interferometry help me in create Chapter 7.

My sincere thanks go to my external examiner Prof. Andrew Aplin from University of Newcastle for his fruitful discussion during the viva examination. I found there are many research future frontlines should be tackled in wettability especially from geochemistry point of view. Also, my sincere thanks go to my internal examiner Dr. James Lawrence for his interesting discussion in wettability alteration especially how chalk can be approached in wettability studies.

I would like also to thank Petroleum Development Oman (PDO) for financial support during my PhD. The continuous support of Mr. Hamed Al-Hadhrami (HLD), Suad Al-Battashi and Asad Al-Maherzi is much appreciated. Also, I thank Dr. Suleiman Al-Hinia from EOR study centre for supplying the crude oil and reservoir core samples which help me in creating Chapter 6.

I was very fortunate to have nice friends during my staying at Leeds University. Sanjeeva Witharana,Ruquia Al-Zadjali,Farah Al-Zadjali, Mohamed Al-Rajhi, Mahmood Al-Harrasi and Mohamed Mahroos. Their kind friendship was another source of knowledge.

I thank my parents Jamal Mubarik Al-Aulaqi and Zaida Awadh Al-Aulaqi for their continuous prayers and supports during my PhD. Their influence in my life will last forever. My brothers Moutaz and Muatasam for their continuous support. Also, thanks to my younger sisters Sarah and Fatimah for their love and support.

Table of Contents

Table of Figures:

Chapter 1
Introduction

In the opening years of the twenty-first century, peak oil production has been one of the dominant issues in the headlines. Forecast of the imminent depletion of oil have forced energy companies to extract more oil from underground reservoirs in efficient manner. Several major oil producing countries have hit peak oil production and are currently in declining production mode. To maintain sustainable growth, industries start looking to secure the vast amount of oil that is trapped in the reservoir. By supporting scientists in research laboratories, novel method of extracting oil have been designed and tailored to specific fields; these methods can often be classified as enhanced oil recovery (EOR). Investing in EOR research activity was very rewarding in different countries. For example, in the United States, EOR may provide more than 137 billion barrels of additional technically recoverable domestic oil (Kovscek et al., 2006).

EOR requires a rigorous understanding of how oil interacts with other components present within petroleum reserovirs. In particular, reservoirs contain a mixture of fluids with various minerals that compromise a geological system formed millions of years ago. These fluids include formation brine and crude oil, which interact with rock surfaces. Crude oil/brine/rock (COBR) interacts in a complex manner that affects the outcomes of EOR. Many aspects of COBR interactions need to be investigated to assure the successful implementation of EOR strategies. It is the basic aim of the following thesis to improve understanding of COBR interactions with particular emphasis on the feasibility of enhancing oil recovery by increasing the reservoir temperature or diluting brine composition.

Steam injection is potentially the most important EOR application in the oil industry (Al-Mjeni et al., 2011). It used widely to decrease oil viscosity and increase the volumetric sweep efficiency. Enormous pilot field applications appeared in the late 1990s, some which succeeded while others failed (Babadagli et al., 2009). In this thesis, the role that temperature has on the way in which oil

resides on mineral surfaces (often referred to as wettability) has been investigated. Furthermore, brine composition is a variable that can be altered during water flooding as part of an EOR scheme. The development of research on effect of brine composition during EOR was boosted throughout 2000s, which create an urgent necessity of a fundamental understanding. **Figure 1.1** shows that publications on brine composition and oil recovery increased 30 fold in very short period. Different field trails have been initiated to investigate the feasibility of brine EOR at various geographic locations. However, the absence of a general fundamental understanding of the controls of brine composition of oil recovery means that it is difficult to extrapolate results from one field pilot to a field with different reservoir conditions. Therefore, this thesis builds a systemic investigation to understand COBR interaction as brine composition changed.

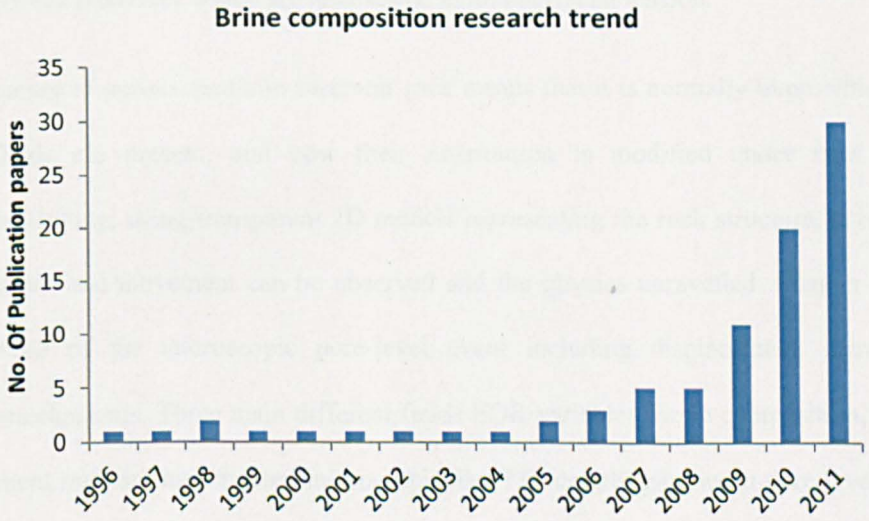

Figure 1.1 *Trend in brine composition EOR research.*

The thesis is divided into seven futher chapters. Chapter 2 provides an extensive literature review to the impact of wettability on oil production. Furthermore a detailed discussion is presented of methods that are currently used to measure wettability. The new frontier of physics that emerge by EOR is discussed in terms of capillarity phenomena, which govern the microscopic displacement efficiency in porous media. The chapter also provides field examples whereby wettability plays a critical role in field development plans.

Chapter 3 provide an overview of techniques used during this research to investigate wettability at the core scale and mineral scale. The physical principles behind each tool is explained and contrasted with others.

Using crude oil as a wettability agent modifier is a necessary condition to reproduce reservoir wettability. However, the complex chemical nature of crude oil makes it difficult to identify the causes of wettability alteration. Chapter 4 will offer details investigation to the role of three main components of crude oil (alkane components, asphaltene macromolecules and water soluble components) that might govern the wettability alterations. Details of wettability alteration are assessed through measurement of advancing, receding and static contact angles between brine and oil on a silicate surface. The interfacial activity between oil and brine interface are studied in detail through the energy between interfaces which are manifested as an interfacial tension.

The opaque nature of porous media in reservoir rock means that it is normally impossible to observe where the fluids are present, and how their distribution is modified under flow conditions. Microvisual modelling, using transparent 2D models representing the rock structure, is one way that fluid distributions and movement can be observed and the physics unravelled. Chapter 5 will offer detailed analysis of the microscopic pore-level event including displacement, entrapment and mobilisation mechanisms. Three main different fields EOR variables, brine composition, temperature and displacement rate, are investigated microscopically. The coupling between pore level events and numerating relative permeability gives a new insight into understanding of interaction between wettability and COBR.

The porous media in the petroleum reservoir involve many factors including the bulk physical properties of the fluid (e.g. viscosity, interfacial tension and density), as well as those of the rock framework and clay infillings (such as wettability and pore morphology). Nevertheless before further design of the various methods of EOR can be made, investigations are needed to describe the flow of water and oil in core plugs that are extracted from reservoir. Chapter 6 report details study in core plugs extracted from reservoirs with different rock surface characteristic. Spontaneous imbibition

plays an important role in oil recovery from fractured reservoirs, for which mass transfer between the rock matrix and the fractures determines the rate of oil production. Oil recovery by water imbibition was first recognized as a mechanism in the early 1950's after the discovery of the highly fractured Sparaberry field in West Texas (Brownscombe and Dyes, 1952). Production from the North Sea chalk reservoir further confirmed the importance of imbibition to oil recovery (Tohmas et al., 1987). Since then, there has been rapid growth in the technical literature on oil recovery by spontaneous imbibition from fractured reservoirs (Morrow and Mason 2001). The combination between spontaneous imbibition tests and the non destructive Nuclear Magnetic Resonance (NMR) techniques provide a powerful tool to probe the effect of wettability in petroleum recovery. The effect of brine salinity and temperatures are key issues addressed in Chapter 6.

Generally the studies of intermolecular interaction between crude oil and rock surface were hampered by the ability of observing the movement of oil-brine menisci and subsequent adsorption into rock surface. Chapter 7 offers new insights into the nanoscale adsorption of oil into rock surfaces. Vertical scanning interferometry was utilised to provide details topography of oil adsorption morphology into rock surface. The role of asphaltene in wettability alteration development was investigated to the scale that never reached before this study. Furthermore, the effect of brine composition and temperature was determined through direct visualisation of the thickness adsorption.

The mechanistic understanding of the interactions that can occur between crude oils, brine and rock surface that has emerged from this study will pave the road to more accurate implementation of EOR projects. Fundamental knowledge of reservoir wettability will impact various petroleum application that range from estimation of oil reserve to production technology issues.

Conclusions and recommendations for future work are presented in Chapter 8 and the references used in the thesis are presented in Chapter 9.

Chapter 2
Fundamentals of Wettability in Petroleum Recovery

The understanding of oil field wettability has developed significantly in the past 50 years. The critical understanding to such complex parameter impacts many field development plans to extract more oil. In this chapter, an extensive literature review is provided on oil field wettability and how it impacts oil production. The science behind enhanced oil recovery is outlined and discussed. One of the ongoing challenges in petroleum engineering is the accurate determination of wettability. Thus, the methods of wettability measurements are described and different standard methods compared. The feasibility of wettability adjustment to enhance oil recovery by altering temperature and brine salinity is reviewed.

2.1 General overview of petroleum recovery

Oil is generated by the thermal maturation of organic matter within a source rock, such as shale, as it is buried. Once expelled from the source rock, a process known as primary migration, oil migrates as a result of buoyancy forces through pore space or fractures in the subsurface (Morrow, 1991). If migration is prevented by the presence of impermeable strata, known as a trap, it forms an oil reservoir. The oil will be situated within pore space or fractures along with water, which was not expelled from the reservoir during oil migration; this water is often referred to as connate or irreducible water. Rocks that form source rocks, reservoirs and traps vary widely both in terms of lithology and age (Krauskopf and Bird, 1993). Although in general, most rocks that source, trap or act as reservoirs to petroleum are Cambrian (~500 Ma) to Neogene (>2 Ma) in age. Sandstone and limestone are the most common reservoir rocks; shales and evaporites the most common seals and shales are the most common source rocks.

Oil is found in porous rock starta, usually referred to as reservoir rocks, at depths down to 10 km, at temperature up to 300 °C and pressure > 1000 bar (Dawe, 1991); although it is possible that petroleum will be found in more harsh environments in years to come.

Oil contains a range of hydrocarbons from lighter (e.g. methane, ethane etc.) to heavy (asphaltenes, wax, sulphur compounds) fractions. Oil also varies in nature from very viscous, with a viscosity in the range 100-100000 cp to extremely light, with a viscosity < 0.5 cp. Oil is produced by drilling a well (borehole) through the impervious cap rock formation into the reservoir. The oil is usually at a pressure near or above the hydrostatic head of connate water at the reservoir depth but below the lithostatic pressure (i.e. pressure created by the weight of the overburden). Oil production initially occurs because it has a higher pressure than the connate water present in the reservoir. The rate at which the oil moves towards the well depends on the pressure differential between the wellbore and the reservoir as well as the permeability of the rock to oil. For oil to move through the reservoir rock to the well, the pressure under which the oil exists in the reservoir must be greater than at the wellbore. Eventually, oil production causes the reservoir pressure to decline and the rate of oil production to fall to a point below which the field is uneconomic to produce by natural pressure drive; this marks the end of the "primary recovery". Energy must then be supplied to the reservoir if more oil is to recovered. Waterflooding is a very common technique that maintains the reservoir pressure at allowing further recovery. For example, the majority of the North Sea oil fields have facilities on their platforms to optimise water injection, and around 50% of the current U.S. annual production is by waterflooding. Over time, the amount of oil produced declines during a water flooding operation and the amount of water increases eventually reaching a level where secondary recovery is also no longer economically viable. In some reservoirs a large proportion (> 75%) of the stock tank oil originally in place (STOIIP) may remain unproduced and trapped within the reservoir. This is the target of oil recovery by special methods known as tertiary or enhanced oil recovery (EOR).

2.1.1 Enhanced oil recovery

The main aim of tertiary stage of production is to recover more oil from an exhausted reservoir. In the end of secondary recovery, oil is trapped as a residual oil by physical force known as "capillary

forces". Capillary forces are controlled by the interfacial tension and/or wettability of the crude oil, brine, rock (COBR) system; a key strategy for EOR is to manipulate the injection fluids to minimize the interfacial tension between fluids or change the rock wettability. Moving the residual oil requires an amount of energy expressed in terms of a viscous force initiated by difference of pressure between reservoir and wellbore. This viscous force is affected by a range of physical phenomena such as capillary pressure, contact angle, interfacial tension and capillary number. In the following section, a review is presented of the physical definition of major phenomena occurred during EOR process.

2.1.1.1 *EOR physics*

Capillary pressure

Capillary pressure, P_c, is defined as the pressure difference that exists between the two immiscible fluids in contact with each other in a porous media; capillary pressure controls the curvature of the interface separating the two fluids. This difference in pressure, P_c, is given by:

$$P_c = P_{nw} - P_w$$

where P_{nw} is the pressure in the non-wetting phase and P_w is the pressure in the wetting phase. If the two immiscible fluids are oil and water then

$$P_c = P_o - P_w$$

The general expression for calculating P_c at any point on a curved interface between oil and water is given by the Laplace equation

$$P_c = P_o - P_w = \sigma(\frac{1}{r_1} + \frac{1}{r_2})$$

where:

σ = the interfacial tension between the two fluids;

r_1, r_2 = the principle radii of curvature of the local interface within a pore measured perpendicular to each other.

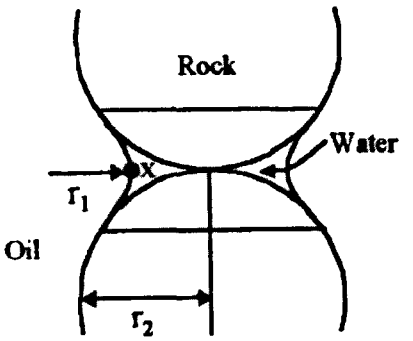

Figure 2.1 ***Water trapped between two spherical sand grains in a water-wet reservoir.***

For an immiscible fluid pair confined in a circular cross-section pore (**Figure 2.1**) of radius, r, and making the assumption that $r_1 = r_2$, we can write (Morrow, 1990):

$$P_c = \frac{2\sigma cos\theta}{r}$$

where θ is the angle measured through the wetting phase (water) fluid. The capillary pressure is thus a measure of the tendency of a porous medium to suck in the wetting fluid phase or to repel the non-wetting phase.

Phase saturation is the amount of fluid that filled the pore volumes inside the rock. The combination of capillary pressure and phase saturation give a valuable information known as the capillary pressure curve and is measured routinely in the laboratory. **Figure 2.2** shows an example of drainage and imbibition capillary pressure functions measured in a water-wet core plug. Starting at point A, with core sample 100% saturated with wetting fluid (e.g. water), the wetting fluid is displaced by the non-wetting (e.g. oil), which is a drainage process. At point B, the irreducible saturation of the wetting fluid (or connate water saturation), the wetting saturation cannot be reduced further irrespective of the imposed difference in phase pressure. If the experiment is reversed, by displacing the non-wetting fluid (e.g. oil) with wetting fluid (e.g. water), the result would be the imbibition curve (**Figure 2.2**). When the wetting fluid saturation has risen to its maximum value, $S_w=1-S_{nwo}$, the capillary pressure is

zero (point C). At this point the residual saturation of the non-wetting fluid, S_{nwo}, cannot be reduced if fluids of oil and water move under free buoyancy forces (Tiab and Donaldson, 2011).

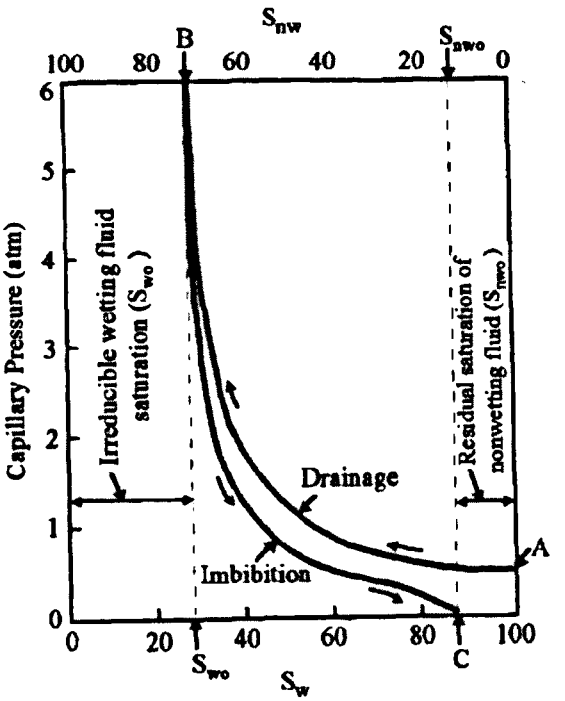

Figure 2.2 *Drainage and imbibition capillary pressure functions (Tiab and Donaldson,2011)*

Wettability and contact angle

Wettability can be defined as the tendency of one fluid to spread on or adhere to a solid surface in the presence of other immiscible fluids. **Figure 2.3** shows two immiscible fluids, A and B, in contact with a solid surface, *S*. The angle, θ, is called the contact angle and exists as a result of the mechanical equilibrium of a drop resting on a plane solid surface under the action of three specific interface free energies: σ_{SA}, σ_{SB}, σ_{AB} at the interface of the solid and fluids A and B (Morrow,1991). Hence at equilibrium,

$$\sigma_{AB} \cos\theta = \sigma_{SA} - \sigma_{SB}$$

This is known as Young's equation. Wettability is therefore characterised by a contact angle. By convention, the contact angle θ is measured through the denser liquid phase and ranges from 0 to

180°. Water is always present in oil reservoirs and the minerals present range from oil-wet through neutral to being water-wet (Hirasaki and Zhang, 2004). Oil-wet means that oil preferentially adheres to the rock surface. The two dynamic situations of two phases, shown in **Figure 2.4**, are described as (a) imbibition; in which the wetting phase saturation is increasing and (b) drainage in which the wetting phase saturation is decreasing. In imbibition displacement, the advancing contact angle defines the wettability. In drainage displacement, the receding contact angle defines the wettability (Morrow, 1990). The difference between advancing and receding contact angle are defined as the hysteresis.

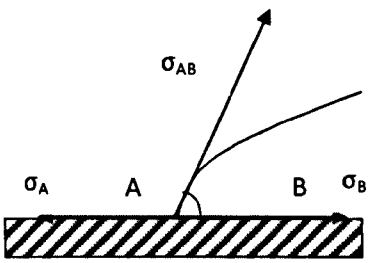

Wettability and contact angle.

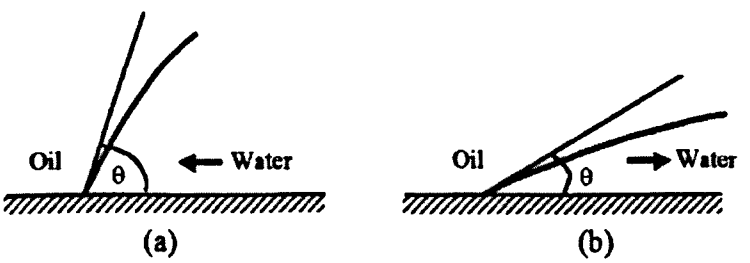

Figure 2.3 *Hysteresis in contact angle in a water-wet reservoir (a) wetting phase increasing (imbibition); (b) wetting phase decreasing (drainage) (Morrow,1991)*

Surface and Interfacial tension

Surface and interfacial tension of fluids result from molecular properties being different at the surface or interface between two immiscible liquids and a gas and a liquid. The interfacial energy arises from the difference between the inward attraction of the molecules in the interior of each phase and those at the interface. The free interfacial energy manifests itself as interfacial tension. The interfacial tension, $\sigma_{AB,}$ is defined as the amount of work that must be performed to separate a unit area of substance A

from substance B. The interfacial tension between a substance A and its own vapour is called the surface tension. The interfacial tension between substances A and B, and the corresponding surface tensions, is related to each other by Dupre's formula

$$W_{AB=}\sigma_A + \sigma_B - \sigma_{AB}$$

where W_{AB} is the amount of work required to separate a unit area of an interface between substances A and B into two interfaces. Surface and interfacial tension can be measured in the laboratory using the pendent drop technique.

Capillary number

Capillary forces and the network nature of pore space cavities are responsible for the entrapment of oil by water during waterflooding. Previous work of Chatiz and Morrow (1984) concluded that residual oil can be recovered if the displacing phase causes viscous forces to exceed a critical capillary retention forces. The magnitude of the capillary forces is set by oil/water interfacial tension, wettability conditions, and the pore geometry in which the trapped oil located. A dimensionless group known as the capillary number, N_{ca}, which is the ratio of viscous to capillary forces, has been used in the literature to demonstrate the relative importance of viscous and capillary forces on the mobilisation of residual oil. Capillary number in this thesis will be defined using the formulation of Lenormand and Zarcone (1984):

$$N_{ca} = \frac{q\mu}{A\sigma}$$

where,

q = the injection rate (ml/s).

μ = the displacing fluid viscosity (Poise).

A= cross-sectional area of the porous media (m^2).

σ = the interfacial tension between the fluids (mN/m).

2.1.1.2 *EOR implementation*

In the opening years of the twenty-first century, EOR has been one of the emerging technologies that will change the future of the oil industry. In 2006, it is attributed to the production of roughly 240 million barrels in the U.S. or about 12% of U.S. production alone (Kovscek, 2006). Enhanced production in Canada accounted for more than 94 million barrels. China, Venezuela, Mexico, and Norway also have significant fractions of their oil production originating from EOR (Kovscek, 2006). In this section, EOR methods are summarised in terms of definition and implementation.

Thermal processes

Thermal processes supply heat energy to the reservoir, which reduce the oil viscosity, thereby increasing its mobility so that it can be effectively swept to the producing wells. The oil viscosity can be reduced by several orders of magnitude in heavy oil reservoirs (Thum et al., 2010). Beside reduction in viscosity, the ability of oil to adhere to mineral surfaces can be changed by increasing temperature (i.e. increase in temperature results in wettability alteration). Adjustment of wettability of reservoir rock is widely investigated to obtain maximum oil recovery as will be discussed later (**Section 2.5**). A variety of thermal techniques is applied to different reservoirs which include steam injection and in situ of combustion.

Steam injection

Steam is injected into an oil reservoir where it condenses, giving up its latent heat to the reservoir rocks and fluids (Dawe, 1991). Most steam floods are based on very close well spacing, high rock porosity, shallow wells. There are two main restrictions in steam flooding are depth and reservoir thickness (Al-Bahlani and Babadagli, 2010). Recent development in horizontal well drilling opens the door for new techniques of steam injection. Steam assisted gravity drainage (SAGD) is used as horizontal wells to introduce steam into reservoir. Butler (1991) described the technique as steam is injected; steam chamber is formed above the injector well **Figure 2.4**.

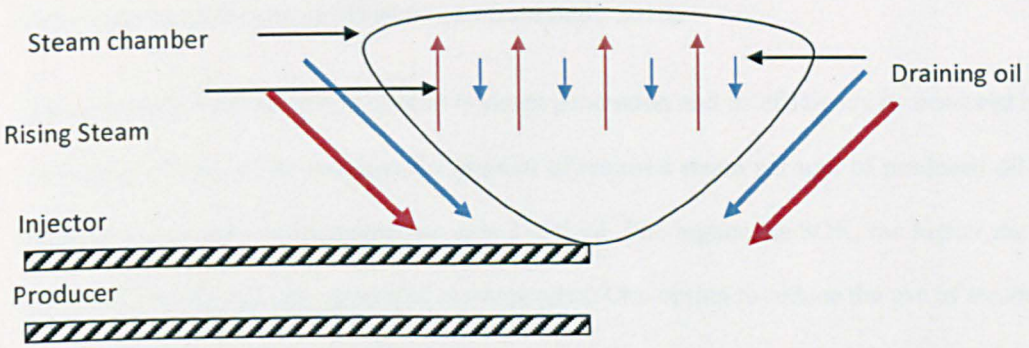

Figure 2.4 *SAGD mechanism which shows movement of steam and sweeping of oil.*

The heat from the steam is transferred by thermal conduction into the surrounding reservoir (**Figure 2.4**). As the oil viscosity is reduced, it starts to drain by gravity to the production well. The key to achieving high production by using SAGD is to maintain the region between two wells at high temperature during the operation. Typically the injector is placed approximately 5 m above the producer. This close spacing results in high oil production rates especially in early production phase. However, the main disadvantage with the SAGD technique is "short circuiting" between the injector and producer. Short circuiting is defined as when steam flows in channels and bypasses the residual oil as a result of reservoir heterogeneity (high permeability streaks) or high pressure differences between the injector and producer. The consequence of short circuiting is the high steam to oil ratio during the production to an extent that makes the SAGD uneconomic option. Stalder (2007) suggested a new technique, cross-SAGD (XSAGD), to mitigate short circuiting. The main features of this configuration are to create injector wells perpendicular to producing wells. Portions of the wells near the crossing points are plugged after a period of steam injection. The restriction to flow induced by plugging some parts of the injector and producing wells provides a control of short circuiting effect. This allows rates to be increased while avoiding live steam production. However, the disadvantage in using XSAGD is that only points near where the wells cross are effective in establishing the initial steam chamber whereas in SAGD the steam chamber is established in the entire length of the wells . As a result, the initial production in XSAGD is lower than SAGD. Also, from a production

technology point of view, plugging operation during steam injection poses serious challenge to apply under high temperatures (Al-Bahlani and Babadagli, 2010).

The most expensive activity in SAGD is steam generation and its efficiency is measured by the steam-to-oil ratio (SOR). SOR measures the amount of required steam per unit of produced oil. In the field, the SOR is typically in the range between 2 and 10. The higher the SOR, the higher the steam usage and consequently, the less economic is the process. One option to reduce the use of steam is to replace it or some fraction of steam with solvents. A novel approach is combined steam and solvent during injection process known as Expanding Solvent Steam-Assisted Gravity Drainage (ES-SAGD) (Nasr, 2003). The solvent is selected in such way that it would evaporate and condense at the same condition as the water phase. Solvent phase would condense, with condensed steam, at the boundary of the steam chamber. During the condensation of solvent, dilution starts between the solvent and the oil around their interface. In conjunction with steam, dilution will enhance reducing the viscosity of the oil increasing sweep efficiency.

In general, the application of steam in oil fields is either for steam flooding or cyclic injection. Steam flooding is established by direct continuous injection of steam from one well which sweep oil to production well. Cyclic steam injection is known as "cyclic-huff and puff" (**Figure 2.5.**) A slug of steam is injected into the reservoir. The reservoir is then shut-in for a few weeks to soak, and the steam condenses and heats the reservoir, then the well put back into production until the rate of oil flow drops. Another slug of steam is then injected and the process repeated several cycles.

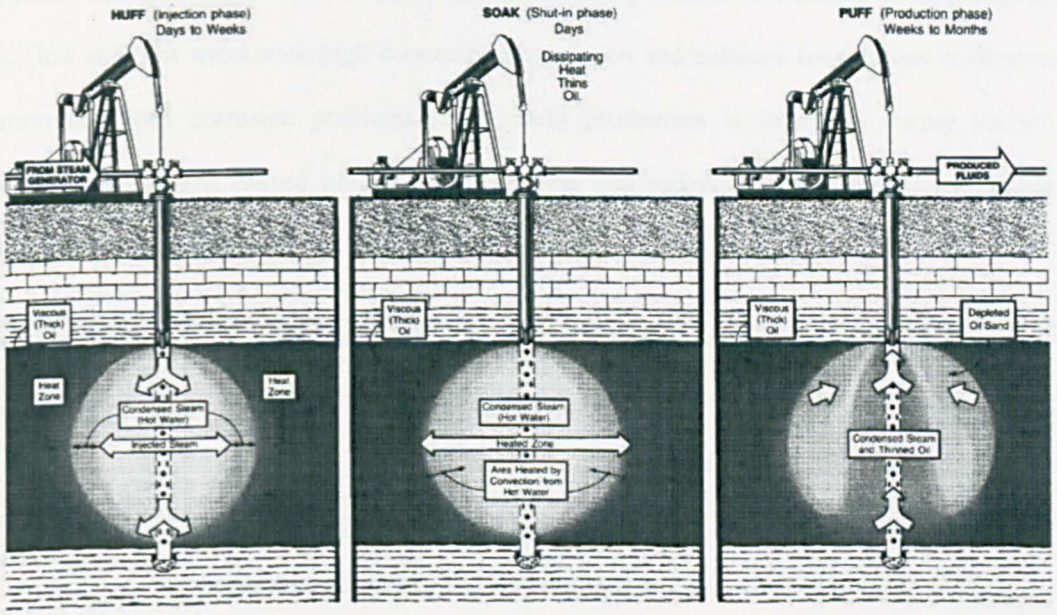

Figure 2.5 *Cyclic steam injection concept, vertical sections view (Kovscek, 2006).*

In situ combustion

Steam flooding is only suitable for shallow reservoirs. In deep reservoirs, due to high pressure, steam cannot work effectively. Moreover, the distance between the heat source and the reservoir can reach up to 7 km, which results in greater heat loss in comparison to short wells used in shallow reservoirs. *In situ* combustion is an alternative option for steam injection to enhance oil recovery. Air is injected into the deep reservoir using compressors. The hydrocarbon in the reservoir is prepared for combustion by a process known as ignition, which can occur spontaneously or using downhole tools. If the reservoir temperature is very high or sufficient heat is released by the oxidation of oil, spontaneous ignition will occur a few days after air injection is started. Typical temperature for spontaneous ignition is above 140°F. If spontaneous ignition does not occur, ignition can be achieved by artificial means such as a special downhole ignition equipment. Three main methods used for ignition are electrical heaters, natural gas burners and exothermic chemical reactions. The average oil recovery by employing *in situ* combustion is nearly 50% according to (Donaldson et al., 1985). The major amount of oil is recovered before breakthrough of the combustion zone. The breakthrough of combustion zone can be recognized by an increase in gas production and its oxygen content. The

main pitfall in *in situ* combustion is the serious operational problems. For example, the production of acidic (low pH) hot water with high concentrations of iron and sulphate ions causes environmental pollution and well corrosion problems. Also, sand production is increased during the *in situ* combustion which can caused plugging of well line and reducing well productivity. **Table 2.1** summarises previous thermal EOR methods with advantages and disadvantages.

Thermal EOR	Advantages	Disadvantages	Reference
Steamflood	Early oil production	Not effective in deep reservoir	Al-Bahlani and Babadagli (2009)
XSAGD	Early oil production with lower water content	Limitation in establishing steam chamber	Stalder (2007)
ES-SAGD	Less cost of steam input	Serious environmental impact due toxic solvent	Nasr (2003)
In situ combustion	Effective in deep reservoir	Formation damage and sand production	Donaldson et al.(1985)

Table 2.1 *Comparison between thermal enhanced oil recovery techniques.*

Miscible flooding

The principle of miscible displacement is to eliminate interfacial tension between the displacing and displaced fluids so that residual oil saturation in the swept zone may be reduced to near zero. Miscibility occurs if two substances are mixed and form a single homogenous phase. Carbon dioxide is the most popular choice of a miscible injection gas due to its availability and favourable miscibility at moderate pressure and temperature. The injected fluid contacts the reservoir fluids but it does not become miscible of the first contact. The carbon dioxide takes time until it develops a dilution process and then becomes completely miscible. During the design of EOR miscible process, the pressure of the injected fluid is important parameters in determining the miscibility with crude oil. For a given reservoir temperature, the minimum pressure at which the injected fluid is either first contact or

multiple contact miscible in the crude oil is referred to as the minimum miscibility pressure (MMP). If the MMP is too great, the possibility of applying miscible EOR would be very low due to difficulty of bring up the reservoir pressure to high level without formation damage problem.

Chemical processes

Chemicals are introduced to the displacing water, which changes its physico-chemical properties to make the displacement process more effective. Two main examples for chemical process are reviewed:

Surfactant flooding

Surfactant flooding aims at recovering the residual oil in the swept areas by reducing the oil-water interfacial tension. Different types of surfactant widely used including anionic petroleum sulphonates and alkyl phendpropoxysulphates. Anionic surfactants are usually preformed because they are relatively stable and can be made relatively cheaply from available feedstocks (Standnes and Austad, 2003).

Polymer flooding

Reservoir heterogeneity is considered one of the major uncertainties in field development plans. During water injection, flow can go through high permeable area and bypassing the oil trap in lower permeable layers resulting in early breakthrough. One way to reduce bypassing is to block the zone or lower its permeability by forming gells by crosslinking polymers. A monomer solution with crosslinking agent is injected into the reservoir and naturally moves into the high permeability area. Crosslinking agent reaction forms, in principle, a gelled (non-moving) polymer *in situ* in the high permeability area. In practice the whole high permeability area has to be blocked to prevent water injection passing through. Also, polymer is used where the oil being displaced in a waterflood is more viscous than the water, and the displacement process is less efficient than when viscosities are equal. Viscosifying the water that is injected by adding a polymer can lead to better sweep efficiencies. Polymers such as polyacrylamides are added to the injection of water to increase its viscosity typically to between 10 and 40 cp (water is 0.5 cp in the reservoir).

Chemical processes have significant technical advantages because a process can be designed to have high displacement efficiency. However, chemical processes can be expensive to implement. Expense is derived mainly from the purchase of chemical and the fact that significant injection of chemical solutions is usually needed before any incremental oil production occurs. Moreover, the toxic nature of some chemical materials makes the application dangerous to environment.

2.2 Fundamentals of wettability in petroleum recovery

Rocks often contain many types of mineral so the surfaces in contact with oil and water are chemically heterogeneous. For uniform systems, the wettability can range from the strongly water-wet to strongly oil-wet depending on the interactions between solid surface, oil and water. In the early years of reservoir engineering, it was generally believed that all reservoirs were uniformly water wet. This understanding was postulated by the geological assumption that during or soon after deposition pores were originally filled by water (Morrow, 1990) and that oil migrating into the rock simply displaced water in the larger pore spaces; it was argued that water was retained by capillary forces in the finer pore spaces and films on pore surface overlain by oil. However, this simple view of oil field wettability is no longer generally accepted. Salathiel (1973) postulated a mixed wettability condition observed in East Texas field based on results from laboratory experiments. In particular, following standard protocol, cores were fired at 400°C to remove major clays and then filled with brine. An oil flood was then initiated until no water was produced. The water saturation following the oil flooding is referred to as irreducible water saturation. The core was then flooded with water until no oil was produced, which is known as the residual oil saturation. The main result from Salathiel work is that using crude oil as the non-wetting phase results in less than 10% residual oil saturation. This amount is dramatically different when using refined oil which can reach up to 40%. The main conclusion is less oil is trapped when crude oil is used. This conclusion resulted in the mixed wettability concept, which Salathiel used to explain his observations for the core flooding experiment. It was argued that a crude oil film remained on the surfaces of large grains, which provided a continuous oil path from pore to pore reducing oil trapping. Furthermore, Salathiel's experimental work in core flooding enhances the assumptions of heterogeneous wetting condition in previous work (Holbrook, 1958).

Development work was undertaken in mixed-wettability systems to address the important issues of wettability and wettability alteration at the pore scale. This approach was explained by the physical relation between the stability of film and disjoining pressure, which has been ignored in previous pore models in porous media, which exhibit mixed-wettability condition (Heiba, 1983; Mohanty, 1983). Kovscek et al. (1993) established a model to include the effect of pore shape and thin film forces in determining the thickness of wetting film through the cycle of primary drainage, spontaneous imbibition, forced imbibition and secondary drainage. The new feature of the Kovscek model is the type of pore shape, which is totally different from cylinder pores used in previous work (Mohanty, 1983). More importantly, Kovscek developed a pore-level picture of how mixed wettability might form and evolve in a reservoir initially filled with brine. The main theoretical result was that the presence of asphaltene in the oil phase is indispensable for the generation of mixed wettability than the underlying mineralogy of the rock. In a distribution of star-shaped pores, the largest pores are prevented from becoming oil wet due to thick water films, which makes the critical capillary pressure too high to be exceeded by oil; hence, they remain water wet. In pore of intermediate size in star shape model, the water film thins more, which allows the asphaltene to be adsorbed on the pore wall to render it oil wet. The smallest pores, which are never entered by oil remained water wet. Skauge (2004) studied the effect of pore geometry in mixed wetting (MW) state and identified two subcategories: mixed wetting large (MWL) and mixed wetting small (MWS). Fogden (2009) confirmed experimentally that oil can even invade the small micropores during primary drainage and render them oil-wet state especially in pores with high convex curvature. This result developed the mix wettability understanding to further direction, which shows clearly how pore geometry can affect the stability of the water thin film and the consequence of mixed wettability states.

2.3 Wettability evaluation

The complexity of wettability induced by COBR interaction makes wettability evaluation methods varied and different. Many approaches have been presented in the literature such as contact angle (Treiber, 1972), Amott method (Amott, 1959), USBM method (Donaldson et.al, 1969), spontaneous imbibition method (Shouxiang et al., 1999), relative permeability method (Raza et al., 1968) and

nuclear magnetic resonance method (Brown and Fatt 1956). In this section, a detailed review of advantages and disadvantages of wettability measurements are presented.

2.3.1 Contact angle method

On a flat surface the wettability is defined by contact angle measurement, which is a result of the force balance between two fluids, at the contact line between the two fluids, and the solid surface (Buckley, 2001). The main advantage of the contact angle test is the quantitative feature, which enables to compare different wetting surface by each other. However, smooth mineral surface can exclude many features that involve with real rocks such roughness, pore geometry and mineral heterogonous.

For the contact angle method, a drop of reservoir fluid is placed on a pure mineral surface that is representative of the mineralogy of the reservoir rock (i.e. quartz, mica and glass). The contact angle is measured as static, advancing or receding angle in ambient or reservoir conditions. Several modes can be utilised to measure contact angle. These are including tilting plate method, sessile drop method, captive bubble method and Wilhelmy plate method. The tilting plate method captures the contact angles measurements on both the left and right sides of a drop while the solid surface is being inclined typically from 0° to 90° (**Figure 2.6**). As the surface is inclined, gravity causes the contact angle on the downhill side to increase while the contact angle on the uphill side decreases. Respectively, these contact angles are referred to advancing and receding angles. The graphic below shows a contact angle measurement by tilting method.

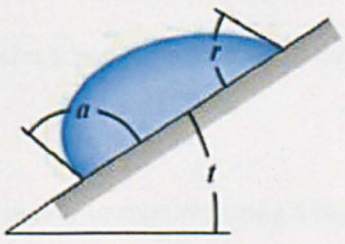

Figure 2.6 *Advancing and receding contact angles captured by tilting base method (Adamson,2007).*

The sessile drop method involves placing a liquid drop on a solid and viewing it through a microscope fitted with a goniometer scale so that the contact angle can be measured directly. During the captive bubble method the drop is enlarged or shrunk through a syringe in constant rate. As the drop is released, the advancing angle is formed whereas as drop retracts, receding angle is formed. The Whilemy plate provides a direct method of measuring adhesion tension, ε (the product of interfacial tension, σ, and contact angle, θ, acting along the perimeter of the plate

$$\varepsilon = \sigma \cos \theta$$

when the plate, of width, w, and thickness, t, contacts the interface, the change in force, F, acting on the plate due to adhesion tension along the perimeter of the plate, p, where $p = 2(w+t)$, is

$$F = \sigma p \cos \theta$$

If the interfacial tension is known, the contact angle is given by

$$\theta = arc \cos \theta \frac{F}{p} \sigma$$

The contact angles for a system differed according to the way of fluids advance or recede in the solid surface. The contact angle at the surface newly exposed to water is known as water advancing angle, (θ_a), while the reverse is water receding contact angle, (θ_r). The difference, (θ_a - θ_r) is known as contact angle hysteresis. Water advancing contact angles are reported as defining wettability because these are considered relevant to waterflooding (Morrow, 1990). Contact angle hysteresis can arise from surface roughness, heterogeneous distribution of adsorbed impurities on the solid surface or the mechanism by which liquid molecules adsorb or desorb when fluid interface is advance or recede (Xie et al., 2002).

Although the reservoir wettability is easy to captured using direct visualisation of contact angle, there is no way to measure the contact angle within a porous medium. There are therefore major limitations to the use of this method for characterising reservoir wettability. Another problem is in deciding the range of contact angle for a particular type of wettability. Various ranges of contact angles have been

suggested in the classification of wettability, but no single value has been accepted as the standard cut-off for wettability classification. Morrow (1976) suggested water advancing contact angles in the range 0° to 62°, 62° to 133° and 133° to 180° to classify as water-wet, intermediate-wet and oil-wet. All the previous factors limit the method of contact angle measurement in determine the reservoir wettability. Nevertheless it can give some indication of tracking the wettability alteration if external conditions are varied (Sharma and Wunderlich, 1999).

2.3.2 Amott test method

The Amott method (Amott, 1959) assesses wettability based on the ratio of the change in water saturation for spontaneous imbibition (S_{ws}) to the combination of water saturation change of spontaneous imbibition and waterflooding (S_{wf}). The Amott procedure is based on displacing water by oil to reach irreducible water saturation, S_{wi}. The next step is to immerse the sample in water and measure the oil recovered by spontaneous imbibition. The sample is then subjected to what is known as forced displacement either by centrifuging or by waterflooding. If the increase in water saturation by forced displacement is ΔS_{wf}, the Amott wettability index to water, I_w, is then defined as

$$Iw = \frac{\Delta S_{ws}}{\Delta S_{ws} + \Delta S_{wf}}$$

Similarly, the Amott wettability index to oil, I_o, is obtained by measuring the spontaneous imbibition of oil, followed by forced displacement by oil. A continuous wettability scale from -1 to 1, known as the Amott-Harvey wettability index, I_{AH}, is given by the difference between I_w and I_o. A positive unity of the Amott-Harvey wettability index indicates more water-wet state whereas a negative value of the Amott-Harvey wettability index indicates more oil-wet state. Cuiec (1991) provide a specific range for wettability degree as following: from -1 to -0.3 is oil wet, from -0.3 to -0.1 is slightly oil wet, from -0.1 to +0.1 is neutral wet, from +0.1 to +0.3 is slightly water wet and from +0.3 to +1 is water wet (**Table 2.2**).

The main drawbacks of using the Amott test is practically the imbibition of oil or water does not reach distinct equilibrium saturation which makes cessation time of oil or water uncertain (Morrow and

Mason, 2001). Also, the Amott index is insensitive near neutral wettability which make using Amott test alone for wettability evaluation in mixed-wet cores very difficult to discriminate between wetting states that located in neutral area (Anderson, 1986c).

-1	-0.3	-0.1	+0.1	+0.3	+1
	Slightly oil wet	Neutral	Slightly water wet		
Oil wet	Intermediate			Water wet	

Table 2.2 *Scale of wettability categories using Amott wettability and USBM (Cuiec, 1991)*

2.3.3 USBM test

The USBM method by (Donaldosn et al., 1969) compares the work needed to displace the other fluid in a rock. This is achieved by comparing the area under oil-displacing drainage capillary curve to the area under brine-displacing-oil imbibition capillary curve. If the logarithmic ratio (*N)* of the area under drainage capillary curve to the area under imbibition capillary curve is greater than zero, the core is water-wet. If N is less than zero, the core is oil-wet. If N is zero means the core is neutrally wet.

$$N = \log\left(\frac{A1}{A2}\right)$$

where: $A1$ = area under the oil-brine-displacing drainage curve and $A2$ = area under brine-oil-displacing imbibition curve (**Figure 2.7**).

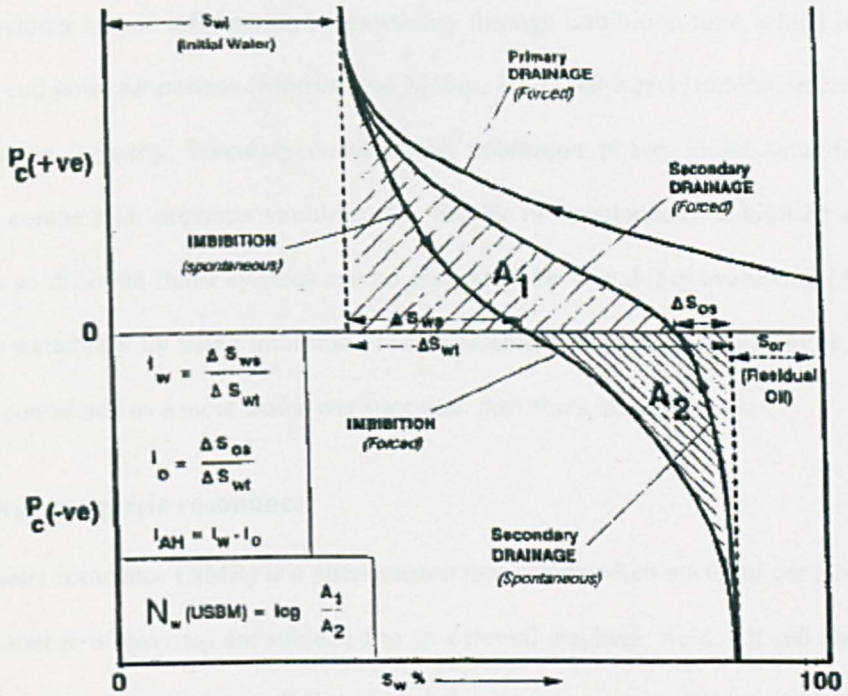

Figure 2.7 *Amott index and USBM number (Morrow, 1990).*

The main advantage of using USBM is that it is a fast quantitative technique compared to Amott-Harvey wettability index. However, USBM during drainage does not provide a good quantitative measure of the wetting variation close to water-wet (Shouxiang et al., 1999).

2.3.4 Spontaneous imbibition

Spontaneous imbibition is driven by surface energy dominated capillary forces which are strongly wettability dependent (Morrow and Mason, 2001). The spontaneous imbibition test involves placing a saturated rock samples in a denser fluid to allow the imbibition to take place. The volume of fluid produced from rock samples is monitored through the imbibition time. Two quantitative parameters can be gained from spontaneous imbibition technique: rate of imbibition and extent of imbibition. The former is an indication of wettability and the latter is an indication of microscopic displacement efficiency (Tang et al., 2005). Bobek et al. (1958) and Denekas et al. (1959) did both oil and water imbibition tests. They plotted imbibition fluid volume against time and used the strongly water-wet case as reference to evaluate the wettability. The main advantage of using spontaneous imbibition

method is providing kinetic information of wettability through imbibition time, which is excluded in Amott test by end point saturations (Morrow and Mason, 2001). However, imbibition rate depends on interfacial tension, porosity, boundary condition of imbibition phase, initial saturation and pore structure. To compensate previous variables, the results of spontaneous imbibition can be made dimensionless so different fluids systems can be compared for wettability evaluation (Zhang, 1996). To assess the wettability by using imbibition rate, a reference wetting state should be attained first which can be considered as a more water-wet state than the others imbibition tests.

2.3.5 Nuclear magnetic resonance

Nuclear magnetic resonance (NMR) is a phenomenon that occurs when nuclei of certain atoms (those with an odd number of protons) are subjected to an external magnetic field. All sub atomic particles (electron, protons) have a property called spin. As an external magnetic field is applied to a sample, the spin of atoms responds in a similar manner to a small bar magnet (**Figure 2.8**). The spinning charges start to align themselves according to the magnetic field (low energy state) or against the field (high energy state). Net magnetisation is developed as groups of atoms align with the external magnetic field. Experimentally, net magnetisation can be expressed in two measured parameters. The first parameter is described as longitudinal relaxation and is characterised by time constant (T_1). Longitudinal relaxation is the return of the magnetisation to its equilibrium state along the external magnetic field, B_o, after they are perturbed from their equilibrium state by a ratio frequency (RF) pulse and can be expressed by as

$$M_z(t) = Mo(1 - e^{-\frac{t}{T_1}})$$

where $M_z(t)$ is the magnetisation at time, t, and M_0 is the equilibrium magnetisation.

The second parameter of expressing net magnetization is described as spin-spin relaxation or transverse relaxation and is characterised by a time constant (T_2). It involves the decay to zero of the magnetisation perpendicular to the external magnetic field and can be expressed by:

$$M_{x,y}(t) = Mo(e^{-\frac{t}{T_2}})$$

where $M_{x,y}(t)$ is the signal intensity at time, t, and M_o is the signal intensity at time 0.

NMR is sensitive to wettability because of the strong effect that the solid surface has on promoting magnetic decay (relaxation) of contacting fluid. Two main mechanisms are involved in the relaxation: Bulk relaxation and surface relaxation (Kleinberg and Vinegar, 1996). Bulk relaxation is caused primarily by the nature of the spin-spin interaction between neighbouring protons. Surface relaxation is caused by multiple interactions between the molecules of the fluid and a solid surface. The molecules in the fluid make many random movements across the pores. By colliding with the grain surface the protons lose energy and return to equilibrium. In small pores, the probability for the protons to collide with a grain surface is high, therefore the relaxation is rapid. In large pores, the opposite occurs as protons have more space to move, therefore these collisions are less frequent and there is a slower relaxation. Another factor contribute to surface relaxation is the surface relaxivity, which is the ability of the surface to cause relaxation of proton magnetisation. If the total relaxation is only governed by surface relaxation, the relaxation rate of the fluids is directly proportional to surface to volume ratio of the pores

$$\frac{1}{T_{1,2}} = \rho_{1,2}\,\frac{S}{V}$$

where $T_{1,2}$ represent the T_1 and T_2 relaxation times, $\rho_{1,2}$ is the corresponding pore surface relaxivity, and $\frac{S}{V}$ is the pore surface-to-volume ratio. The above equation shows that the surface relaxation depends upon $\frac{S}{V}$, which is essentially a description of the pore size characteristics and the strength of the interaction between fluid and rock. For example, in a water-wet rock the water spread in pore wall, which will prevent any interaction between oil phases and the pore wall. The relaxation decay of hydrocarbon phase here is equal to bulk hydrocarbon relaxation decay because there is no interaction between oil and the pore wall. On this basis, NMR has been used as a quantitative interpretation of wettability by measuring the fluid response to NMR (Fleury and Deflandre, 2003). The response of

fluid is characterised by measuring T_1 or T_2 relaxation distribution at different rock saturation of oil and water.

Wettability determined from NMR measurements has been successfully compared with other laboratory wettability indices such as Amott-Harvey wettability index. Hsu et al. (1992) used NMR relaxation methods to characterize the wettability of water-wet and oil-wet carbonate cores. They observed that water-wet cores gave shorter relaxation rates than oil-wet cores. This is a result of the dominant surface relaxation of the water phase since water is in contact with most of the grain surfaces. Their experimental measurements also showed that relaxation rates in oil-wet cores were longer than water-wet cores because the water phase decays at its low bulk relaxation rate, since water is no longer in contact with the grain surface. Also, Freedman et al. (2003) used NMR relaxation methods to determine wettability, saturation and oil viscosity in rocks partially saturated with oil and brine. In mixed-wet samples they observed a shortening in the relaxation times of the oil distribution compared to the oil bulk distribution which provides a clear evidence of surface relaxation of the oil. In oil-wet samples, the brine molecules do not contact the pore surfaces and therefore experience reduced relaxation. As a result, the brine T_2 values were shifted towards higher values approaching bulk value.

The main advantage of using NMR is the short time required to obtain the measurement compared to Amott and USBM tests. However, NMR relaxation time is sensitive to the pore structure, which can means that the wettability evaluation from relaxation time data is not a straightforward process.

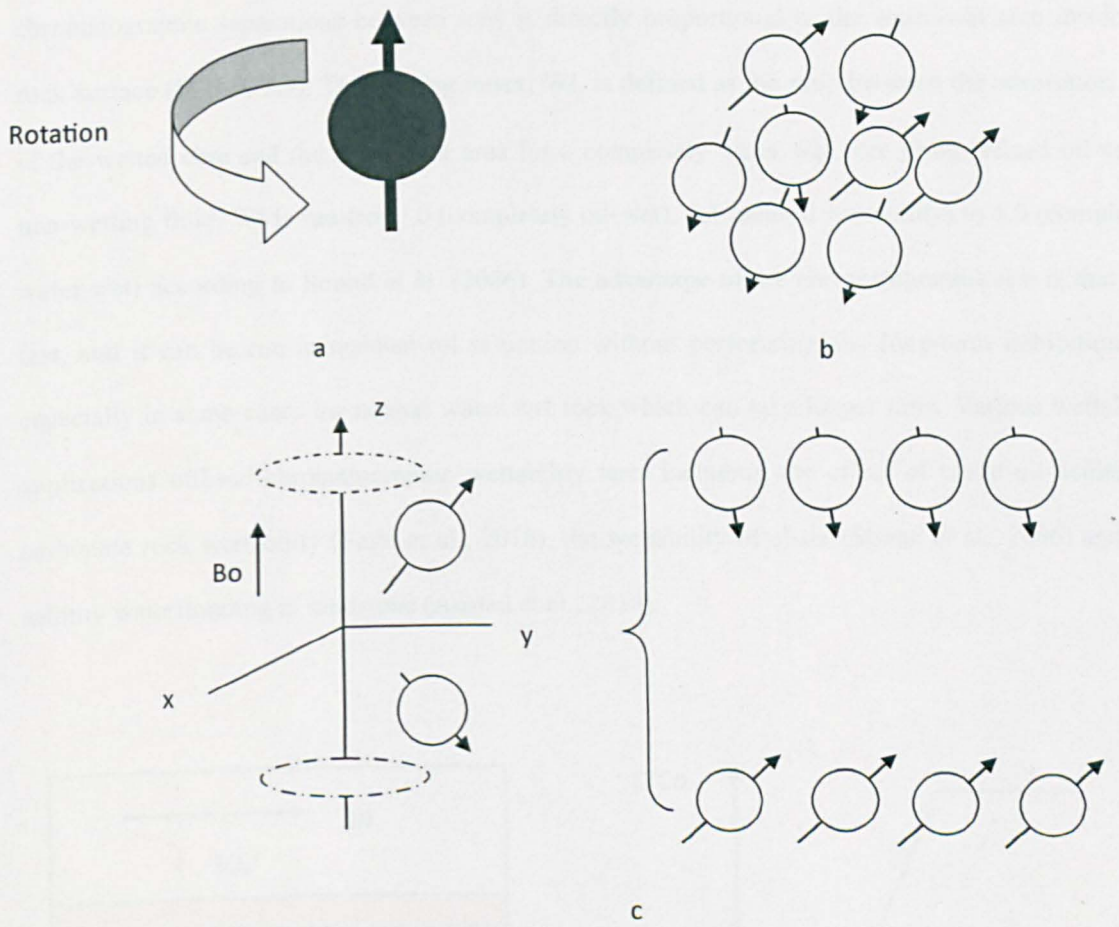

Figure 2.8 *a) Hydrogen nuclei (proton or spin) behave like small bar magnets. b) Protons randomly orientated in free space in the absence of an external magnetic field. c) Nucleus arranges around a magnetic field.(Coates et al.,1999)*

2.3.6 Chromatographic wettability test

One of the major drawbacks in Amott test is the insensitivity tracking of natural wetting states of some rocks such as carbonate. The chromatographic wettability test can serve as a quantitative and qualitative interpretation to such cases where neutral wettability is expected (Strand et al., 2006). The test is based on dynamic adsorption of specific ions onto a surface. It is achieved on a chromatographic separation of the water-soluble tracer thicyanate, *SCN*, and the potential determining ion sulphate, SO_4^{2-}. Thicyanate, which is a non-potential determining ion towards the rock surface, is used as the non-adsorbing water tracer. The test is conducted on a core sample that

has reached residual oil saturation, and the chromatographic separation of the two components of sulphate and thicyanate only takes place at the water-wet areas. The difference between the chromatographic separations between ions is directly proportional to the water-wet area inside the rock surface (**Figure 2.9**). The wetting index, WI, is defined as the ratio between the adsorption area of the wetted core and the adsorption area for a completely water wet core using refined oil as the non-wetting fluid. WI is run from: 0 (completely oil-wet), 0.5 (neutral wettability) to 1.0 (completely water-wet) according to Strand et al. (2006). The advantage of the chromatographic test is that it is fast, and it can be run at residual oil saturation without performing any long-term imbibition test especially in some cases for neutral water wet rock which can take longer time. Various wettability applications utilised chromatographic wettability tests including the effect of crude oil acidity on carbonate rock wettability (Fathi et al., 2010), the wettability of chalk (Strand et al., 2006) and low salinity waterflooding in sandstone (Austad et al., 2010).

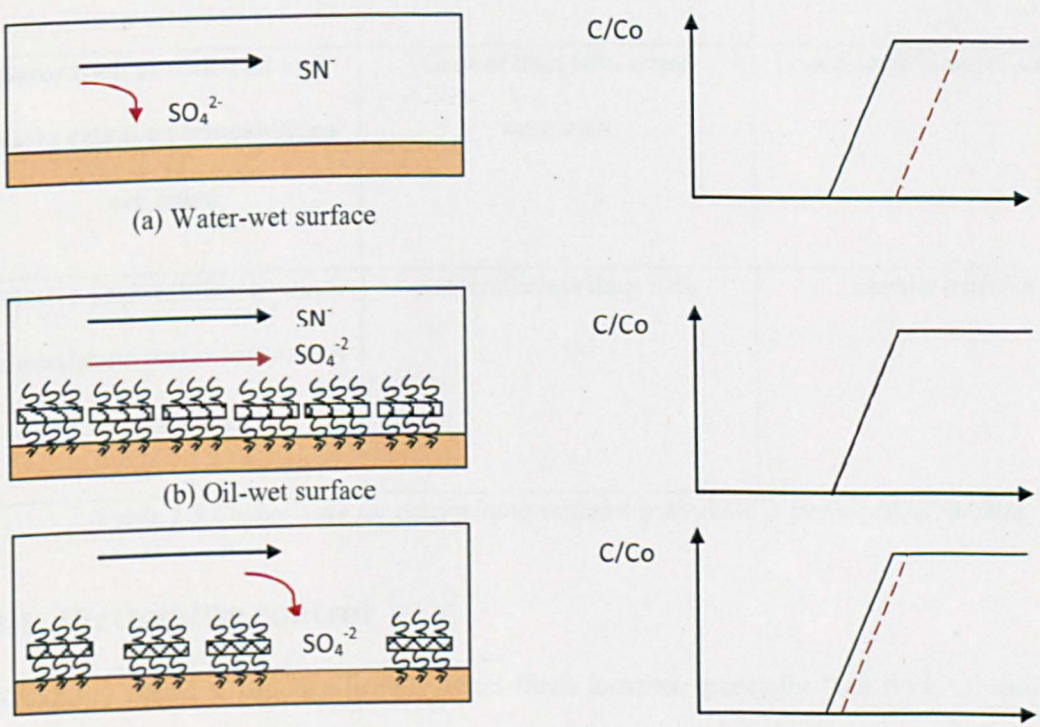

Figure 2.9 *Area between SCN⁻ and SO_4^{2-} curves is proportional to sulphate adsorption by comparing between injection concentration (C_o) and effluent concentration (C).*

2.3.7 Relative permeability

The relative permeability characteristics are a direct measure of the ability of the porous system to conduct one fluid when one or more fluids are present. This method is based on the fact that wettability has a major effect on the shape of the two phase relative permeability curves. Craig (1971) introduced a rule-of-thumb to differentiate between strongly water-wet and strongly oil-wet core. In general, for water-wet cores the crossover point in relative permeability occurs at high water phase saturation. Crossover at about equal wetting and non-wetting phase saturation indicates neutral wettability. A second indicator is the water relative permeability value at the oil residual saturation in which the higher water permeability is the more oil-wet. A third indicator is the connate water saturation in which usually greater than 20% for water-wet whereas in oil-wet is generally less than 15%. The details of previous indicators in which Craigs' rule is listed in the (**Table 2.3**).

	WATER-WET	**OIL-WET**
Connate water saturation	Usually Greater than 20%	Generally less than 15%
Saturation at which oil and water relative permeabilities are equal	Greater than 50% water saturation	Less than 50% water saturation
Relative permeability to water at maximum water saturation i.e. floodout.	Generally less than 30%	Greater than 50%

Table 2.3 *Craigs' rule for determining wettability by relative permeability method.*

2.4 Wettability control

Wettability alteration can significantly affect fluids location, especially fluid flow, oil recovery and residual oil distribution in porous media (Anderson, 1987a) through affecting relative permeability (Owens and Archie, 1971) and capillary pressure (Morrow, 1976). Furthermore, wettability can influence well logging results which are critical to evaluation of reservoir reserves and field

development plans (Anderson, 1986c). Reservoir wettability alteration occurred after crude oil migrated into a reservoir trap where it displaced the water content down to the reservoir connate water saturations. The alteration is mainly caused by adsorption of polar components from crude oil (Denekas et al., 1959; Buckley, 1996).

Typical practise is assumed by reservoir engineers that wettability to be strongly water-wet in oil reservoir (Anderson, 1986a). Moreover, the interpretation of non-water-wetness observed in oil field was frequently attributed to the artifacts of core recovery and the cleaning process. The possible diversity of reservoir wettability conditions was first indicated by (Treiber et al., 1972). They reported wettability evaluation results on 55 reservoir rocks through contact angle measurement on representative mineral surfaces (quartz for sandstones and calcites for carbonates). Later on, Chilingar and Yen (1983) and Cuiec (1984; 1990) confirmed the conclusions reached by (Treiber et al.,1972). Since then, more and more attention has been given to a form of wettability described by (Salathiel, 1973) as mixed wettability. The main result from Salathiel (1973) core waterflooding is that using crude oil as non wetting phase makes less than 10% residual oil saturation. Similar experimental observation is obtained by (Morrow et al.,1986) when the interaction of crude oil/rock/brine was investigated. According to (Morrow et al., 1986), a form of mixed wettability described by as speckled mixed wettability whereby water imbibes strongly but there is no spontaneous imbibition of oil. Consequence of wettability in oil recovery has changed over time. Early investigations suggest water-wet state is the optimal condition for oil recovery in which oil that not adhered to surface is totally produced when it displaced by the wetting phase (Donaldson and Thomas, 1971). Later, the view that mixed wettability gives the maximum oil recovery became accepted and supported by most laboratory investigations (Salathiel, 1973; Rathmell et al., 1973; Jadhunadan and Morrow, 1995). However, the mechanism by which wettability determines oil recovery is still somewhat unclear. Much remains to be learned about crude oil/brine/rock interactions and wetting properties in order to establish a satisfactory working knowledge of reservoir wetting behaviour.

In studying wettability at the laboratory scale, it is important to attain a reproducible wetting state to obtain accurate results. There are two main methods to control wettability: chemical treatment and

crude oil treatment. First, coating of a clean core by chemical treatment, generally organochlorosilanes for sandstone cores and naphthenic acids for carbonate cores. **Figure 2.11** shows an organochlorosilanes compound forming covalent bonds with a silicon dioxide surface and changing it from water-wet to oil-wet. The advantage of this method is obtaining uniform wetting state. However, the chemical coating may not be stable due to hydrolysis and desorption of silanes (Wei et al., 1993). The second approach is to use crude oil to control the wettability in rocks, which provide the opportunity to capture the essential features of petroleum reservoir wettability. This is achieved by immersion rocks in crude oil in the presence of brine. The advantage of using crude oil to control wettability is that it is a representative for secondary migration of oil to reservoir rocks. However, using crude oil to control the wettability does not provide a universal wettability state due to different composition of the individual crude oils.

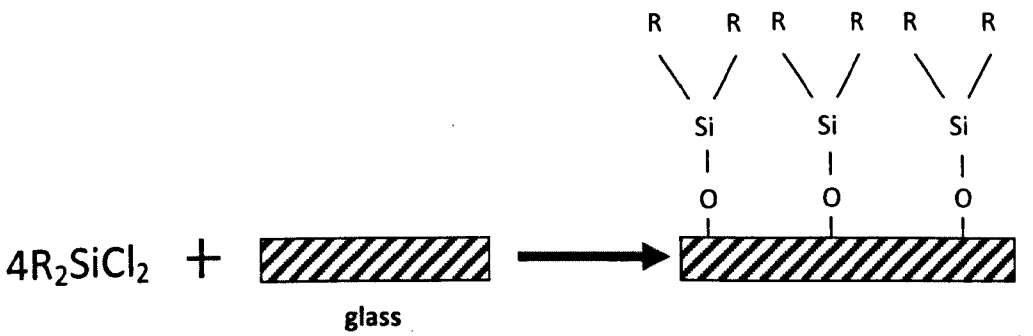

Figure 2.10 Deposition of silane (dimethyldichlorosilane) on a glass surface.Chemical treatment used widely to change the wettability of silicate surface from water-wet to oil-wet.

2.5 Application of wettability adjustment in oil recovery

In the past decade, progress has been made in understanding the role of wettability modification in oil reservoir management. This can start from understanding the *in situ* condition of wettability in the reservoir and extend to the use of wettability modification as an option for EOR. The wettability of rock surface is reported to be sensitive to factors such as temperature and brine salinity. Here previous

works are reviewed, which investigate how temperature and brine salinity affect wettability of the rock/oil/brine system.

2.5.1 Effect of Temperature

In the reservoir management, rock/oil/brine interaction in deep reservoirs might have different wetting characteristic than rock/oil/brine interaction at shallower zone due to different effect of reservoir temperature. This implies the accurate estimation of oil column will be directly affected if wettability is a function of temperature. During the reservoir production, temperature is also considered as a critical parameter to enhance oil recovery in light, medium and heavy oil reservoir.

In heavy oil reservoir, temperature is mainly used to reduce the oil viscosity sharply from 100000 cp to 100 cp, which increases sweep efficiency. Various temperature techniques are emerged targeting better oil sweeping efficiency were discussed extensively in **Section 2.1.1.2**. In medium and light oil reservoirs, the viscosity is low so the contribution to oil recovery from viscosity reduction cannot be considered attractive. The goal from using temperature in medium and light oil reservoir is to modify the wettability of reservoir matrix so increasing the capillary forces to allow the imbibition of hot water or steam to displace the oil trapped (Al-Hadhrami and Blunt, 2001).

In the following section, a review of previous work in studying the effect of temperature in the wettability of rock surface. The review is classified based on the experimental approaches from small scale of mineral surfaces to larger core scale of reservoir rocks.

2.5.1.1 *Smooth mineral surfaces*

The contact angle at which two fluid phases meet a smooth solid surface is the macroscopic indication of wetting preference that depends upon solid/fluid and fluid/fluid interfacial energies. It is the boundary condition for interfaces between those two fluids in a porous medium composed of that solid. Wetting thus controls fluid distribution and the capillary pressure between immiscible phases in a porous medium. Contact angle measurements on reservoir crude-oil/brine system provide an initial step to characterise reservoir wettability under control experimental variables. Initial work (Treiber, 1972) used advancing and receding water contact angle as an indication of wettability in different

reservoirs during the waterflooding. Afterwards, the use of contact angle measurement as a universal measure of wettability expands more to study the effect of many other reservoir variables such as temperature, which is the focus of this review.

Hjelmeland and Larrondo (1984) studied the effect of temperature on contact angles with calcite surfaces. The experimental approach used is known as the "single-crystal technique", which enlarges and reduces the drop of oil to simulate water advancing and receding angle during drainage and imbibition in porous media. Their main finding is that calcite surface tends to become less oil-wet as temperature increase up to 60°C. Sharma (1984) used glass slides that were initially immersed in the crude oil and aged at 65°C for a week prior to measuring the contact angle by a probe fluid. Their main result was that a shift in a contact angle from 73° at 25°C to 115° at 65°C, which is less water-wet. Sayyouh et al. (1991) used actual surface of core samples to represent the solid surface in contact-angle measurements. Their procedure is involved contacting oil droplet with downward surface of a core sample and then immersed the system in the aqueous solution in a glass container. The main result was that surface become more oil-wet as temperature increased up to 50°C. Wang and Gupta (1995) found different responses of contact angles on quartz and calcite to temperature change. For quartz system, the surface is more water-wet (θ=22°) at room condition, but the contact angle increased to 34° as the temperature increased. However, calcite surfaces were found to be weakly water-wet with a contact angle of about 60° and became progressively more water-wet as the temperature increased to 70°C. Improvement of the contact angle technique was achieved by Rao (1999) using a technique known as the Dual-Drop-Dual Crystal (DDDC). The DDDC method is describing in the following: i) placing the two separate crude oil drops on two similar solid surfaces previously immersed and equilibrate in brine, (ii) allowing the system to age for 1 to 7 days to attain equilibrium of the rock-fluids interactions, (iii) turning the lower crystal upside down to mingle the two oil drops, and (iv) shifting the lower crystal position laterally to create advancing and receding angle Figure 2.11. The main result is that a quartz surface tends to become more oil-wet whereas a calcite surface becomes water-wet as the temperature of oil/brine/solid increased. However, one of the

main drawbacks with this technique is the pinning between the three phase lines due to forming of rigid film at high temperature, which in some case prevent the advancing water angle to be formed.

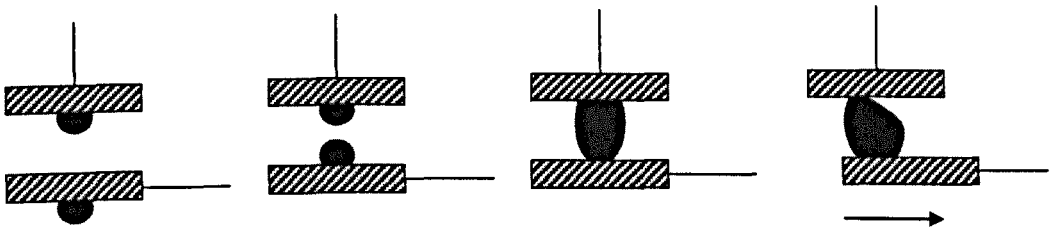

Figure 2.11 ***Dual-Drop-Dual Crystal (DDDC) technique used to measure dynamic oil angle during fluid imbibition and drainage.***

Hamouda (2008) studied the effect of temperature on the wettability of calcite. Instead of using a crude oil as a wettability control, 0.005 M steric acid dissolved in decane was utilized to mimic the role of crude oil. The advantage of using steric acid is to have a defined fluid system whereas the crude oil considered as a heterogeneous fluid system including different composition of functional groups. The main results that contact angle decrease with temperature, which indicates the surface is becoming more water-wet as a function of temperature. Roosta (2009) used glass slides, smooth calcite, mica and quartz surface as solid surface to investigate the effect of temperature in wettability established by aging the surfaces in crude oil only. After a period of aging time, the mineral surface was exposed to steam at high temperature (120°C). Then the contact angle of probe fluid (water/kerosene) is measured at the four different surfaces. The main finding was that a consistent shift of wettability to water-wet after exposure the glass, calcite, mica and quartz to steam.

2.5.1.2 *In core-scale experiment*

Studying the effect of wettability in surface plate minerals provide a better, wider control over the experimental parameters such as temperature of the system. However, the limitation of pore structure on simple mineral surfaces necessitates applying more experiments in porous media that more similar to reservoir rock structure. Thus core-scale experiments are used in literature to translate the major effect in wetting condition of surface substrate to porous media. In Buckley et al. (1998), oil recovery

characteristics were studied by spontaneous imbibition experiments in porous media while increasing the complexity from synthetic core (Aeroliths) to outcrop sandstone (Berea). The main objective of their work was the comparison between wettability of the COBR system in different porous media with that of mineral surfaces. The result shows a good agreement between interaction with the mineral surface and the core scale.

The impact of temperature on the wettability of core scale depends on how wettability is evaluated. As mention in the section of measurement of wettability, spontaneous imbibition, Amott-Harvey index, USBM index and relative permeability measurements are used widely in tracking the wettability change during the temperature; below the effect of temperature on wettability through observed using these four measurement methods is reviewed

Spontaneous imbibition measurement:

Jadhunandan and Morrow (1995) studied the effect of aging temperature on the wettability of sandstone core and oil recovery factor. The main result is that as aging temperature increased, there was a continuous decrease in water-wetness in which Amott-Harvey index for a Moutray crude oil aged at 26°C, 50°C and 80°C yield an Amott index (I_{w-o}) of 0.89, 0.73 and 0.33 respectively. Also, they concluded for COBR systems, oil recovery by waterflooding increased as wettability changed from strongly water-wet to a maximum at close-to-neutral wettability. Their conclusion also agrees with Zhou et al., (1995) when the effect of aging temperature is studied on the imbibition rate of water for short time period. Cuiec (1995) investigated the response of Amott test to thermodynamic effects in sandstone and carbonate cores. Novel apparatus, made of Hastelloy, was used for the first time up to 120°C during the four stages of the Amott test. The main results demonstrate that an increase in temperature changed sandstones affinity towards water whereas carbonate reservoir cores did not show any sensitivity to the temperature. Tang and Morrow (1997) extend the previous work to investigate the effect of displacement temperature on wettability and the recovery of crude oil by spontaneous imbibition in sandstone with three different crude oil compositions. The main result was the transition toward water wetness when the temperature is raised during the course of displacement to 75°C. Tang and Kovscek (2002) investigate the effect of temperature by a series of spontaneous

imbibition of water in outcrop diatomite cores at temperatures up to 240°C and pressures up to 600 psi. Their study showed that temperature has a positive impact in oil recovery by spontaneous water imbibition in which imbibition rate and oil recovery increase with temperature systematically.

The studies discussed above are essentially mixed wettability imbibition studies in which mixed wettability states (MXW) were induced by adsorption from crude oil onto rock surface in the presence of low initial water saturation. Tong et al. (2005) developed an experimental approach known as mixed-wet film (MXW-F) that provides a reproducible wettability state. According to Tong et al. (2005), MXW-F wetting states is defined by displacement of the crude oil with decalin, which was in turn displaced by mineral oil to leave a film of adsorbed organic polar components at the rock surfaces. Use of the MXW-F wetting control method is particularly suited to the study of the wetting properties and stability of adsorbed organic films without the complication of further adsorption from the bulk oil phase. The main results in Tong et al. (2005) is that imbibition behaviour indicates the wettability of MXW-F tends to change towards water wetness during the course of spontaneous imbibition at elevated temperature.

Computed Tomography (CT) is used initially in characterising the general physical properties such as pore geometry in rock cores. In imbibition experiments, a CT scanner was used, originally by Akin et al. (2000), to provide a visual mean of water frontal advance inside the core samples filled with oil. Recently, Schembre et al. (2006) utilised the CT imbibition cell technique for measuring water imbibition. Oil displacement test were conducted with diatomaceous reservoir cores between temperatures of 45°C and 230°C. Three main results emerge from their experimental work. First, there was a substantial increase in imbibition rate and extent of oil recovery. Second, there was a slight reduction in residual oil saturation. Third, a significant shift in the Amott wettability index is observed from intermediate and weakly water-wet to strongly water-wet. From the previous three results, a transition of wettability towards more water-wet state as temperature increased for diatomaceous reservoir cores.

Zhang and Austad (2005) studied the effect of aging temperature in chalk samples based on Amott water index, I_w, with three aging temperatures are varied 40°C, 80°C and 120°C. Their main results indicate there is a minor shift towards more water-wet state as the temperature increased in chalk cores. Strand et al. (2008) studied the effect of different displacement temperature at recovering light oil from chalk formation. Their experimental approach was using seawater coupling with three high temperatures (90°C, 110°C and 120°C). Their main finding that the high incremental recovery is observed only at temperatures above 90°C during spontaneous imbibition of seawater. Their conclusion that enhanced oil recovery from chalk by wettability modification using seawater is very restricted to the temperature.

Relative permeability

Wettability has a major effect on the relative permeabilities. Early work by Fatt and Kikoff (1959) used a mixture of sand, which was fractionally treated by organosilane vapors to produce a fractional wettability state. They found that the relative permeability characteristics of a sandpack alter continuously as the fractional oil wettability is changed. Donaldson and Thomas (1971) extend the previous work by using a crude oil and Cottage Grove sandstone cores 25 cm long and 4 cm in diameter. Wettability of the sandstone is controlled by Dri-Film at 0, 0.02, 0.2, 2 and 10.0 % in toluene. The wettability of the cores is determined by centrifugal method (USBM) to yield 0.649, 0.176, -0.222, -1.250 and -1.33 respectively. It was found that at any given water saturation greater than the initial water saturation, the relative permeability to water at the oil-wet system is much greater than the relative permeability to water at the water-wet system. Donaldson and Thomas (1971) attribute this change in relative permeability characteristic to change in wettability of the cores. Owens and Aarcher (1971) studied the effect of wettability in steady-state relative permeability. Torpedo outcrop sandstone is used as a porous media with refined oil and NaCl brine. The wettability control is established by adding barium dinoyl naphthalene sulfonate (BNDS) to the refined oil. By changing the concentration of BNDS in the oil phase, two extreme wetting states are established. Contact angle test on a flat quartz surface were used to develop a calibration between the degrees of wetting, as indicated by BDNS concentration in the oil phase. Two results emerge from their study:

first, that rock wetting preference has a significant and qualitatively predictable effect on oil-water relative permeability measurement. In particular, at a given saturation, as the water wetness decreases, the relative permeability to oil decrease and the relative permeability to water increases. Second, there was no consistent trend in the change in magnitude of residual oil saturation as the wettability was altered.

McCaffery and Bennion (1974) investigated the effect of wettability in steady-state relative permeability tests but with different approach from previous works. The wettability control is achieved by using consolidated porous media composed of polytetrafluoroethylene (PTFE) and various pure fluid pairs with nitrogen, which displayed constant and uniform wetting properties with solid surface. No measurable difference in relative permeability-saturation properties was found for systems with contact angle of 20°, 42° and 49°. As the contact angle was increased to higher values, the relative permeability of liquid is higher when it was the displacing phase.

Morrow et al. (1973) investigates the effect of wettability in a dolomite pack. Wettability controlled by dissolving octanic acid in refined oil to produce three different wetting state which are water-wet, intermediate wet and oil-wet to give advancing water/oil contact angle of 15°, 100° and 155° respectively. Four main results emerge from their studies: First, for the oil-wet case, oil relative permeability at initial water saturation was 20% less than that observed for water-wet condition. Second, for intermediate wet system, oil relative permeability at initial water saturation was reduced by only 6%. Third, the corresponding oil and water relative permeability curves cross over at lower water saturations as advancing water contact angle is increased. Four, the relative permeability to water at a given water saturation is 0.3 for the water-wet condition and 0.8 for the oil-wet system. Hence, water relative permeability at residual oil saturation is the least for water-wet and the most for the oil-wet.

All the previous work devoted to wettability that established by chemical treatment which can be classified as uniform wettability as discussed extensively in **Section 2.4**. Wang (1988) pushed the literature further to investigate another type of wettability, which is induced by contacting a crude oil

with porous surface. Steady-state relative permeability is investigated in natural Berea sandstone; crude oil aged Berea sandstone and preserved reservoir sandstone. Natural Berea sandstone without crude oil aging shows high residual oil saturation (47%) with low relative permeability to water (3.4%). For aged Berea sandstone, the water relative permeability was 35%, which is higher than natural Berea sandstone. Also, residual oil saturation is only 17%, which is lower than natural Berea sandstone (47%). For preserved reservoir sandstone, 20% is observed for water relative permeability with 19% residual oil saturation. The large difference between natural and aged Berea sandstone is attributed to a Salathiel-type mixed wettability that established by crude oil contact of surface for aged and reservoir samples whereas the natural Berea sandstone is still water-wet state. Similar work by Chang (1997) used crude oil to alter the wettability of clean composite core. The comparing between the cleaned cores and aged cores were assessed by measuring the steady-state relative permeability. The study showed an increasing in the water relative permeability and decreasing in oil relative permeability for the cores that aged in crude oil.

Effect of temperature on relative permeability

Test environment is generally acknowledged to have a significant effect on measurement of relative permeability. Therefore, accounting for how temperature affects relative permeability is an essential requirement to modeling thermal recovery processes. In this section, previous works that studied the effect of temperature on relative permeability are reviewed.

Edmondson (1965) studied the effect of different temperatures range between 75°F-500°F using Berea sandstones. Refined oil and crude oil were used to render different wetting state for the sandstone. Three main results were recorded. First, the residual oil saturation decrease with increasing temperatures. Second, relative permeability ratio is different for different temperatures. Third, the crude oil shows distinctly different relative permeability behaviour than refined oil floods.

Weinbrandt (1972) used sandstone to investigate the effect of two temperatures (80°F and 175°F) on relative permeability. Refined oil was used only as a displaced phase by brine. Three main results were obtained. First, the individual relative permeability to oil increased for all water saturations.

Second, the individual relative permeability to water exhibit two different behaviours. At intermediate water saturation, the water relative permeability is decreased slightly by 3% as temperature increased. However, at flooded out, the water relative permeability is increased by 5%. Third, for all water saturations, the ratio of relative permeability (k_w/k_o) decreased when the temperature was raised.

Lo and Mungan (1973) used a new approach to study the effect of temperature in relative permeability by isolating the effect of temperature in wettability and observing the consequence of other factors in the relative permeability. Dependence of wettability on temperature was isolated by using refined oil in two porous media: Berea sandstone and consolidated porous Teflon. Berea sandstone is water-wet whereas Teflon is oil-wet when using water/refined oil as fluid system. The independence of wettability on temperature is validated by measuring the contact angle of refined oil/brine on flat quartz and Teflon, which only changes in the range of 10°. Three types of refined oil were used, each with different viscosities: Kaydol (130 cp), Protol (68 cp) and tetradecane (2 cp). Relative permeability was measured by the steady-state method in isothermal conditions at room temperature and 200°F for the teflon and 300°F for the sandstone cores. Two main results were reported in their paper. First, no dependence of relative permeability is observed for a system that used a low viscosity refined oil tetradecane. Second, for a system that used other higher viscosity refined oil, a change in relative permeability is observed for both water-wet system and oil-wet system at two different temperatures. At higher temperature, relative permeability to oil was found to be higher, residual oil saturation was lower and the rate of increased water relative permeability with increasing water saturation is higher. They attribute this change in relative permeability to change in the viscosity ratio with temperature.

Maini and Batycky (1985) used a preserved sandstone core and heavy crude oil with viscosity 16400 cp to investigate the effect of temperature in the relative permeability. By using unsteady state method, four main results were obtained. First, the initial water saturation is increasing noticeably with temperature whereas residual oil saturation appeared to be minimized at temperatures between 60°C and 160°C. Second, effective permeability to oil at irreducible water saturation declined with increasing temperature. Third, effective permeability to water at S_{or} was not a strong function of

temperature. With using the heavy crude oil, increasing of initial water saturation with temperature was suggested the main driving force for decreasing the oil relative permeability.

Schembre et al. (2005) used a tight reservoir diatomite core with heavy crude oil (640 cp) at temperatures of 120°C and 180°C. A novel method applied to estimate relative permeability and capillary pressure from *in situ* saturation profile obtained from CT scanning during imbibition experiment. The main result that the remaining oil saturation, S_{or}, and the water relative permeability end point decreased as the temperature increased. These results confirm that temperature increased the water wettability of diatomite core after applying elevated temperatures 120°C and 180°C.

Hamouda et al. (2008) investigate the effect of temperature on outcrop chalk treated by model oil. Three model oils were used in the relative permeability experiment: decane, decane with 0.005 M steric acid, decane with 0.005 M 18-phenyloctadecanoic acid. Relative permeability was estimated from the monitored differential pressure data and produced fluids at temperatures 23°C, 50°C, 80°C and 130°C. The main result was a large shift of cross over saturation in the relative permeability toward the higher water saturation. Also a decrease in residual oil saturation is observed as the temperature increased from room temperature to 50°C and 80°C indicating an increase of the water-wetness. However, at 130°C, an increase of about 45% of residual oil saturation is detected. According to their paper, they attribute that based on oil trapping caused by fine detachment and migration at temperatures above 80°C creating dead ends and forming localised high residual oil saturation areas in the porous medium that falsely indicate more oil-wet.

2.5.1.3 *Field application*

Thermal EOR is one of the examples of how understanding the effect of temperature in oil fields can lead to increases in production. Thermal EOR has been applied in various reservoir type including sandstone and carbonate reservoirs with different type of crude oils ranging from heavy to light crude oil. **Table 2.4** illustrates the main fields with different EOR status. In the following sections, the main results from recent field applications are described

Country	Field	EOR status	Rock type	Permeability (md)	Porosity (Φ)	Reference
Oman	Amal	Full field scale	Sandstone	19	25	Thum et al. (2010)
Oman	Qarn Alam	Pilot test	Carbonate	5-14	29	Macaulay et al. (1995)
Oman	Fahud	Pilot test	Carbonate	4-10	23	Shahin et al. (2006)
Kuwait	Ratqa-Lower Fars	Pilot test	Sandstone	3	33	Sanyal. (2009)
Saudi Arabia	Wafra	Pilot test	Carbonate	250	37	Barge et al. (2009)
Turkey	Bati	Pilot test	Carbonate	10-100	14-20	Babadagli et al. (2008)
United States	Yates	Full field scale	Dolomite	137	21	Snell et al. (1999)

Table 2.4 *Thermal EOR projects in different reservoir type worldwide.*

(i) Yates field

The Yates Oil Field is a giant oil field in the Permian Basin of west Texas, which was discovered in 1962. The Yates San Andres reservoir is a naturally fractured dolomite formation. Several improved oil recovery methods have been evaluated in this prolific field with cumulative production greater than 1.3 billion bbl of a 30° API crude oil. A steam pilot was initiated in December 1998 to assess the economic viability of improving the vertical gravity drainage process. Usually, steam is injected into a fracture to displace the oil from the matrix. However, in Yates field, steam is injected to heat the oil in the matrix and improving gravity drainage from dolomite matrix toward highly conductive fractures. Oil mobilized due to heat drains vertically to the oil column, then laterally via fractures to offset producers

Figure 2.12. The main result from applying thermal EOR in Yates field was a noticeable increase in oil production rate since steam injection began in December 1998 (Snell et al, 1999).

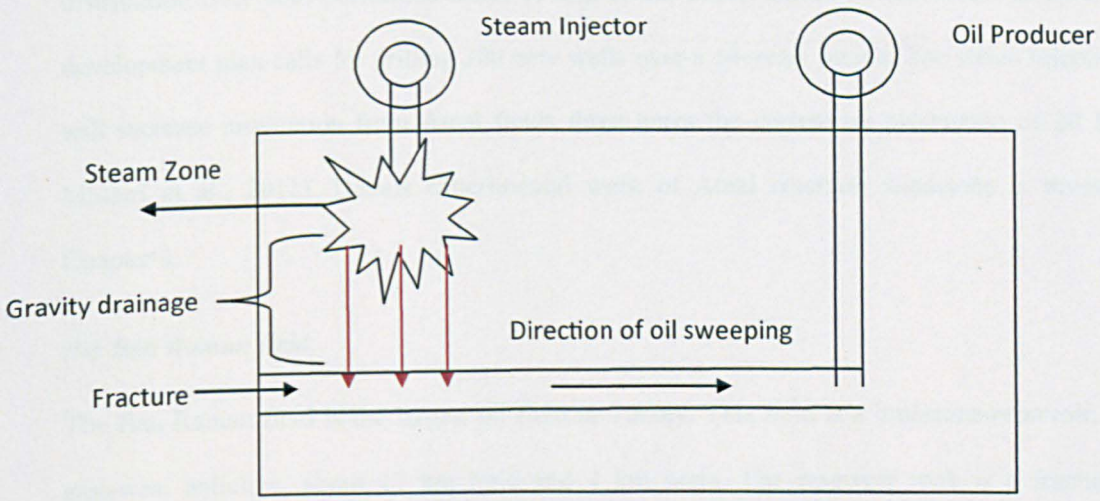

Figure 2.12 *Schematic of steam injection into Yates field.*

(ii)- Qarn Alam field

Qarn Alam is a densely-fractured chalky limestone containing 213 million m^3 of heavy viscous (220 cp) crude oil. The structure is approximately 3 km x 6 km in size, gently dipping with a maximum oil column of 165 m. The chalky reservoir has an average porosity of 30%. The field come on production in 1975 at a rate of 6000 m^3/d from six gas lifted vertical wells. After two years, the water-cut climbed to 95% making the primary recovery of the Qarn Alam field about 2% of STOIIP, which makes the Qarn Alam field economically unviable. To mitigate the field failure, steam injection was considered as an EOR option. Initial studies indicate that heating the oil from 50˚C to 250˚C reduces the viscosity in the reservoir from 240 cp to about 2 cp, which will greatly increase the recovery factor. A pilot test indicated a shift in initial oil saturations from 95% to below 50%, which indicates that significant drainage had occurred (Penney et al., 2007).

(iii) Amal field

The Amal field is located on the eastern flank of the south Oman salt basin and contain a 200 m thick column of heavy oil sandstone reservoir. It has been in production for over 25 years and is currently in decline. A thermal EOR project was started in 2007 on continuous steam injection mode in Amal

West and cyclic steam injection mode in Amal East. The field trails conclude with two main results. First, 400 tonnes per day of steam injectivity was achieved, which meet the required injectivity for thermal EOR. Second, temperature logs during steam injection indicated a uniform vertical steam distribution over both perforated zones (Thum et al., 2010). Based on successful of field trails, the development plan calls for drilling 300 new wells over a 14-years period. The steam injection project will increase production from Amal fields three times the current oil production of 20 MBD (Al-Mutairi et al., 2011). Details experimental work of Amal reservoir sandstone is investigated in Chapter 6.

(iv) Bati Raman field

The Bati Raman field is the largest oil field in Turkey. This field is a limestone reservoir, elongated east-west anticline, about 17 km long and 4 km wide. The reservoir rock is a fractured vuggy limestone in the western and central part of the field, but is chalky and tighter to the east. Porosity and permeability values are 14-20% and 10-100 md respectively. The reservoir contains heavy oil with an API gravity of 6.5-13.5 at an average depth of 4300 ft. The reservoir temperature is 150°F and the original reservoir pressure was 1800 psi. Due to the fact that the recovery factor by primary recovery was limited to only 2% of nearly 1.8 billion bbl oil in-place, thermal EOR techniques had been proposed to develop the field production.

A five-spot steam injection pilot was performed by injecting steam at well and producing from different wells during 172 days. The main result from the pilot was that water breakthrough was observed after 114 days. Oil production at the breakthrough was 30,738 bbl. Overall recovery efficiency at breakthrough was low (1.16%). According to Babadagli et al. (2008), the very low recovery factor could be attributed to the more fractured-heterogeneous character of the reservoir.

2.5.2 Effect of brine salinity

As the oil production starts from new oil fields, reservoir pressure starts to decline, which affects the oil production rate. To maintain the reservoir pressure after primary depletion, water is injected to the reservoir, a process which known as "waterflooding", which is one of the techniques widely adopted

in improved oil recovery (IOR). The reservoir connate water composition usually differs significantly from the composition of water available for injection. One of the early works by Martin (1959) used fresh water to displace a core saturated with reservoir brine and heavy crude oil. The main observation was improved heavy oil recovery by injection of fresh water. He ascribed clay swelling and emulsions as the possible mechanisms for improvement of oil recovery by fresh water in the high permeable zone. Bernard (1967) verified previous work of Martin (1959) by using fresh water to displace a sandstone core saturated with reservoir brine and mineral oil. Improved oil recovery by injection of fresh water is observed as a result of clay swelling and/or dispersion along with an increase in pressure drop.

Since previous studies only explore the effect of fresh water, change in invading brine composition and its effect in oil recovery was studied later by Jadhunandan and Morrow (1995). By using a Berea sandstone and Moutray crude oil, the Amott-Harvey index was observed to decrease when the calcium ion content increased in the invading brine. Yildiz and Morrow (1996) extended the study later by extensive waterflooding using two different brine compositions: brine 4% NaCl + 0.5% $CaCl_2$ and brine 2%$CaCl_2$ known as brine 1 and brine 2 respectively. They found that waterflood recoveries were improved significantly if the core was initially equilibrated with brine 2 and subsequently flooded first with brine 1 and then with brine 2.

Tang and Morrow (1997) reported an increase in oil recovery by using low salinity for spontaneous imbibitions for outcrop sandstone when the connate and imbibed water were low salinity. All previous core flooding experiments were conducted at reduced condition until Webb (2005) conducting the first investigation of effect of low salinity brine at real reservoir condition (live crude oil, high confining pressure and reservoir temperature). Their results indicate that low salinity waterflood confirm the core floods experiments seen previously in experiment with incremental benefits in oil recovery range from 5% to 40%. Based on previous encouraging results, Webb (2004) conducted the first field test using log-inject-long at producing well. The results were support the previous laboratory test from other fields, and showed 25-50% reduction in residual oil saturation when

waterflooding with low salinity brine. In the following section, we are reviewing in details the effect of brine salinity in core scale experiments and field test applications.

2.5.2.1 *Core scale experiment*

Jadhunandan and Morrow (1995) was first who investigate the effect of brine salinity in oil recovery. Two brines were used formulated as 4% NaCl + 1% $CaCl_2$ and 4% NaCl + 0.5% $CaCl_2$. Three main results obtained from their work. First, Amott-Harvey index, I_{w-o}, for Moutray crude oil tends to decrease as Ca^{2+} content increases. Second, displacement of Moutray crude oil after aging at room temperatures showed the greatest sensitivity of I_{w-o} and imbibition rate behaviour to brine composition. Third, for system aged with Moutray crude oil at higher temperatures, the sensitivity to brine composition decreased significantly.

Tang and Morrow (1997) used diluted reservoir brine (RB) from Dagang field to investigate the response in oil recovery. Two main experimental methods were used to characterise the effect of brine salinity: spontaneous imbibition and waterflooding tests. The salinity of the brine was adjusted in three systematic manners. First, adjusting the brine salinity while making the invading brine salinity equal to connate brine salinity. Second, adjusting the invading brine salinity only while the connate brine salinity is kept constant. Third, adjusting the connate brine salinity while the invading brine salinity is kept constant.

Sharma and Filoco (2000) used a high speed ultracentrifuge to investigate the effect of brine salinity in sandstone outcrops during drainage and imbibition displacement mode. Three different crude oils were used: Shell A-20, Prudhoe Bay and Mars A-1. In the capillary de-saturation curves of primary drainage, changing the composition of the brine in the core from 3% to 20% NaCl does not have a significant impact on the residual brine saturations. During imbibition displacement mode, three different results were noticed. First, when brine salinity invading is equal to brine salinity connate, oil recovery is reach to 70% with 0.3% NaCl brine, 61% with 3% NaCl brine and 57% with 20% NaCl brine. In other words, a dramatic increase in oil recovery results from the use of lower brine salinity. Second, when brine salinity connate is varied only, oil recovery is reached to 70% with 0.3% NaCl brine, 61% with 3% NaCl brine and 58% with 20% NaCl brine. Third, when the waterflooding brine

salinity is changed only, the oil recovery does not change when brine salinity is varied from 0.3% to 20% for a fixed connate water salinity of 3%.

Webb (2005) extend the previous investigation in low salinity core flooding by using core flood facilities operated up to temperature of 150°C and pressure of 10000 psi. *In situ* saturation monitoring by gamma ray was used to validate the average saturation across the core and minimized the uncertainty of determine the saturation volumetrically. The main experiment is operated by unsteady state waterflood with live crude oil and three different concentrations of formation brine 1400 ppm, 5600 ppm and 28000 ppm. Two scenarios of running waterflooding experiment were used: secondary waterflood and tertiary waterflood. The secondary waterflood is defined by running waterflooding at core that still in irreducible water saturation, comparison between high salinity brine and low salinity brine gives the incremental benefits of using low salinity in secondary mode. The tertiary waterflood is defined by injecting low salinity brine at remaining oil saturation point (ROS), which has previously been achieved through high salinity brine injection. Three main results obtained from outlined in Webb (2005). First, in secondary waterflooding reservoir condition, the oil recovery at breakthrough was 0.62 pore volumes (PV) for 1400 ppm, 0.5 PV for 5600 ppm and 0.45 PV for 28000 ppm. Also, remaining oil saturation after 11 pore volumes injection was 0.65 PV for 1400 ppm, 0.55 PV for 5600 ppm and 0.52 PV for 28000 ppm. Second, in tertiary waterflooding reservoir condition, after injection of 20 PV of simulated formation brine with salinity of 15,000 ppm, a 5 to 10 PV of low salinity brine of 1500 ppm is injected. As a result, the oil recovery increased from 63% to 71%. Both secondary and tertiary mode shows an increasing in the dry oil production and final oil production after low salinity brine injection.

Loahardjo et al. (2007) present a laboratory investigation and analysis for recovery from four cores taken from a sandstone reservoir that contained chert, lithic fragments and kaolinite. Cores were flooded with low salinity brine either in secondary or tertiary mode. Injection rate ranged from 0.2 to 0.25 ml/min. The volume of oil production and the pressure change along with effluent brine pH were recorded. The four main results in their work show that low salinity flooding of reservoir sandstone cores gave large increase in oil recovery in both secondary and tertiary modes. First, As injected

seawater, the final oil recovery was 50.9%. Recovery after injection of 0.1 seawater was 66.7% which is an increase of 16% over that given by seawater. The recovery after injection of 0.01 seawater was 80%, an increase of nearly 30% over that given by seawater. Second, the pressure response shows a systemic increase as the brine salinity decreased. Around 3 psi is obtained with seawater brine salinity, 4.5 psi is obtained with 0.1 seawater brine and 5 psi is obtained with 0.01 seawater. Third, the effluent brine pH for all three tests was close to neutral. Fourth, no clay particles were observed in brine effluent or at oil/brine interface.

Berg et al. (2009) used an open flow model geometry that allows a direct observation of single oil droplets. The novel approach represents the situation inside a pore in the rock where some of the residual oil is bound to clay particles that are attached to rock grains. The clay surface is fabricated from a standard microscope glass slide where clay particles were glued. Oil droplets were attached in the surface by releasing from a syringe. The experiment start with passing high salinity brine with TDS=25.95 (g/l) and switch to low salinity brine with TDS=2 (g/l). The main results was that a release of more than 80% of crude oil is observed when brine salinity is switch to TDS=2 (g/l) whereas no releasing of oil is observed when high salinity brine is applied. Moreover, the releasing of oil was accompanied with expansion of clay layer thickness without de-flocculation or fine migration when high salinity brine is diluted to half. Breg et al. (2009) ascribes the extra releasing of oil by low salinity brine to weaking of adhesion force between oil and rock grains.

Cissokho et al. (2009) investigated the role of clay type by using an outcrop sample that contains 9.2% clay without kaolinite. Oil production, pressure response and pH variation were monitored throughout the experiment. A 11% increase in tertiary mode oil recovery was gained when diluted NaCl brine (1 g/L) was injected after mixture of $CaCl_2$ and NaCl brine (50g/L). As the lower salinity brine is invading the core, the pH was increased from 7.0 to 9.5 and the pressure response increase from 120 psi to 205 psi. The author ascribes the incremental increase in recovery factor due to two reasons. First, the ionic exchange between rock surface and invading low salinity brine which is observed in increasing of pH from 7.0 to 9.5. Second, the expansion of clay layer when electrical

forces are modified by dilute brine injection which causes the differential pressure to increase resulting in higher incremental oil recovery.

Wickramathilaka et al. (2011) extended the previous investigation in reservoir sandstone by using a conductivity measurement. Two main sets of displacement were conducted: spontaneous imbibition and waterflooding. The main results was when the seawater brine invading switch to $1/15^{th}$ dilute seawater brine, the imbibition rate increased significantly and incremental oil recovery jump from 22% to 55%. Second, the pressure response across the core is doubled when the brine invading is switched from high salinity to low salinity. Third, the conductivity shows a spike before it is stabilised when brine is switched to low salinity brine. However, the spike in conductivity has not observed when brine is switched from low salinity to seawater. According to Wickramathilaka et al. (2011), the core samples which did not show a bump in conductivity for low salinity waterflood is indicating that the rock did not react with invading brine.

2.5.2.2 *Field applications*

Endicott field:

Endicott is a mature offshore oil field located on the North Slope of Alaska. Endicott was brought on line in 1987. Current production is 11 Mbpd of oil and 1 Mbpod of LNG. Average water cut is 94%. To date, 129 wells, including 27 side tracks have been drilled. Currently 82 producers and 25 injectors are active. The Endicott formation is sandstone, which is fairly continuous across the field and contains discontinuous shales. Due to high water-cut, low salinity brine was selected as a field development option. The pilot was conducted with permeability of 100 md and average porosity of 20%. In December 2007, produced formation water was re-injected to the reservoir; water-cut of 95% was observed. Reduced-salinity water injection commenced June 2008, an increase in oil rate and a reduction in water-cut were observed. The average oil residual after secondary high salinity waterflood is 41%, the residual oil saturation after tertiary reduced-salinity EOR waterflooding is 27%. Low salinity EOR waterflooding increase displacement efficiency by 26% relative to conventional waterflooding (Seccombe et al., 2010; Lager et al., 2011).

Middle East giant clastic reservoir:

Webb et al. (2004) investigate the response of a giant clastic reservoir to low salinity brine injection. A major producing interval were selected to run a "log inject log" to determine the incremental reduction in residual oil saturation during low brine salinity injection. The log inject log technique is based on running multiple passes of pulsed neutron capture (PNC) logs after injection of two or more different brines which is required to calculate the residual oil saturation. By injecting three different brines, it is possible to determine the residual oil saturation after normal waterflooding and after injection of low salinity water. Three types of NaCl brine was used 220,000 ppm, 170,000 ppm and 3000 ppm which represent high salinity, intermediate salinity and low salinity brines. When high salinity brine commenced, logging passes were performed every hour. Around 700 bbls of high salinity brine is injected representing 10-15 pore volumes of throughput required to displace the oil away from the wellbore. In intermediate and low salinity brine, around 300 bbls were required to attain equilibrium. The main result after low salinity brine injection was a decrease in remaining oil of around 50% around wellbore. Based on encouraging result from their filed test, several possible applications for injection low salinity brine is proposed. There are including low salinity alternating gas, low salinity alternation regular salinity, low salinity slug, low salinity with surfactant, low salinity with microbes, hot low salinity water and low salinity polymer.

Prudhoe Bay Field:

Prudhoe Bay oil field is a large oil field on Alaska's North Slope. It is the largest oil field in both the United States and in North America, covering 213,543 acres (86,418 ha) and originally containing approximately 25 billion barrels (4.0×10^9 m^3) of oil. It is giant reservoir sandstone which started production in 1971.

McGuire et.al. (2005) used single well chemical tracer tests (SWCTT) to evaluate the efficiency of low salinity brine in Prudhoe Bay field. The field trail is carried out by injecting, and then producing back through the same well, a volume of the injected brine labelled with appropriate chemical tracers. The method of SWCTT can be described in four main steps. First, a volume of test reservoir water containing about 1% primary tracer, which is typically ester, is injected into the target zone. Second,

injection of reservoir water without ester to push the water injected in the first step further into the reservoir, typically 10-15 ft around wellbore. Third, the well is shut in for ten days to allow a sufficient time for ethyl alcohol to be formed in situ as a result of reaction between ester and reservoir water. Ehyl alcohol is considered the secondary tracer which is soluble only in water. Fourth, the well is produced back and fluids are periodically sampled and analysed for unreacted ester, ethanol and propanol content by gas chromatography. The separation between these two tracers, primary and secondary tracer, is used to calculate the residual oil saturation. Two SWCTT were conducted in Prudhoe Bay field in 2003. The purpose of these tests was to measure the residual oil saturation before and after low salinity water injection. In the first SWCTT, the residual oil saturation was 0.21. After injecting 3000 ppm of lower salinity brine, the second SWCTT is started. The in situ residual oil saturation dropped to 0.13. The test shows an improvement of 18% in oil recovery compared to high salinity waterflooding.

Omar Field:

With an approximate STOIIP of 750 MMbbl, the Omar field is the largest field in Syria. Omar field is a sandstone reservoir with uniform high permeability leading to a good lateral connectivity between wells. The field was discovered in 1987 and production started 1989. After an initial production of 80 k barrel/day, production starts to decline to only 25 k barrel/day. To recover the oil production, 500 mg/L low salinity brine is injected to the reservoir. During the injection of low salinity brine, clear oil bank signals have been observed. Open hole logging indicates an average oil saturation of 85%, before the lower salinity brine is commenced. After lower brine salinity started, an average of oil saturation of 50% is recorded. The oil recovery factor has an incremental increase around 10-15% after lower brine salinity injection (Vledder et al. 2010).

From previous works, there is an agreement of wettability alteration as function of brine salinity and temperature. Despite the change of brine salinity or temperature, there is a knowledge gap between the characterising of wettability of the mineral surface and field scale. None of previous works carried a consistent investigation at different scales using same COBR system. How residual oil saturation is trapped inside the complex porous media and whether distinctive flow behaviour is exists during both

different brine salinity and temperature variations are still unknown. Moreover, all of special core analysis programmes focus on using single wettability test as an indicator for reservior wettability. This can be a huge uncertainty of trusting single wettability measurement method such as Amott-Harvey index which required a detail independent experimental investigation of wettability. A Non-destrictuve NMR wettability measurement shows to be a promising indicator for wettability alteration. However, non of previous works utlise NMR to challange the wettability alteration as function of brine salinity and temperature in sandstone and carbonate reservoir. More fundamentally, the pattern of wettability evolution during primary migration of oil from source rock to reservior trap needs to be probe at more nanoscale resolution in terms of thickness of adaorption layer , surface roughness and the oil aggreagation volume. All the previous work focus on using surface analyatical techniques such atomic force microscopy (AFM) which has a major risk of removing the soft deposited crude oil by contacting. Looking of a method that characterise the surface profile without contact method will increase the confidence on understading the wettability at nanoscale resolution.

Chapter 3
Experimental Procedures

Throughout this thesis, various techniques have been used to investigate the effect of wettability in petroleum recovery. This chapter describes the experimental tools used and reviews the basic theory behind them. It is not intended to describe the theoretical fundamentals and development history of each technique. Nevertheless, the applications between various techniques are compared to emphasise their differences.

3.1 Effective wettability of mineral surfaces

3.1.1 Contact angle measurement

The sessile drop method method is used to measure contact angle; advancing and receding contact angles are measured through the brine phase **Figure 3.1**. The apparatus is mounted on a pressurized vibration isolation table, and the video system includes a Plunix video camera, a Cole-Parmer fiber-optic light source, and two polarisers. The positions of the camera, sample holder, and drop dispenser (Gilmont micro syringe stainless steel needle of 0.5 mm in diameter) are adjustable in vertical direction. The position of the 50-mL optical glass cell, filled with aqueous phase, is also adjustable by movement of a support plate attached to optical support column. Drop images are captured by KRUSS frame grabber and interpreted by Drop Shape Analysis (DSA) software. The DSA determines drop edge coordinates, drop height, diameter of drop-liquid contact, and left, right, and average contact angles with a maximum speed of 30 measurements per minute. The profile of the drop is extracted using Drop shape analysis (DSA) software. Young Laplace equation fitting is applied to determine the contact angle. To check for consistency, an open source software provided by ImageJ is also used for contact angle determination. Agreement between the two angle determinations is always within ± 5°. All contact angles in this work are measured through the water phase.

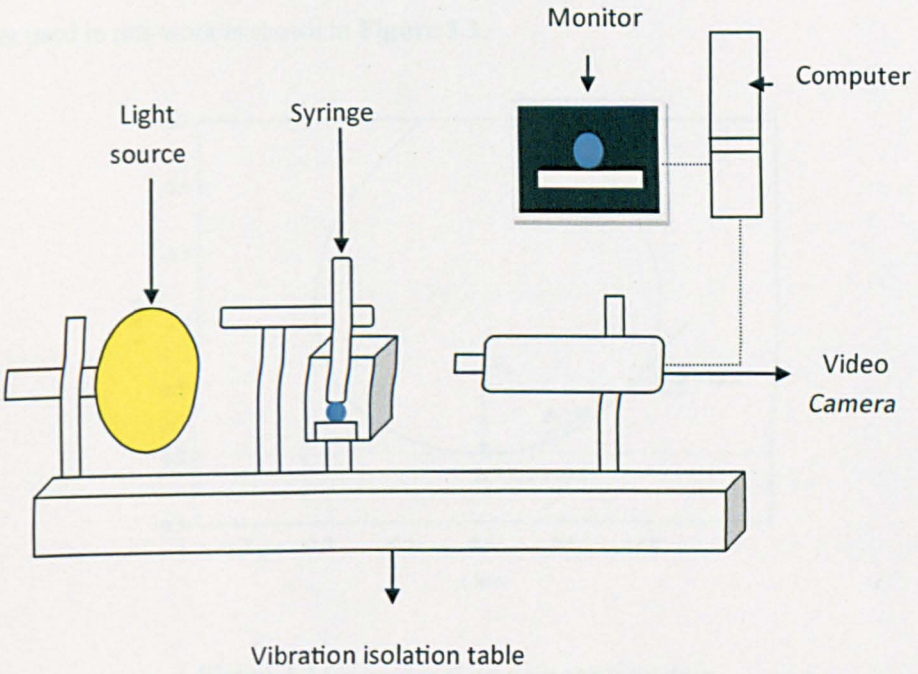

Figure 3.1 *Contact angle measurement apparatus to measure static and dynamic contact angle of water surrounding by oil in silicate surface.*

3.1.2 Interfacial tension

Although many techniques to measure interfacial tension have been developed, axisymmetric drop shape analysis (ADSA) has proven the most accurate. In ADSA, the interfacial tension is determined from the profile of a static pendent drop using Young-Laplace equation. A typical shape of an axisymmetric pendent drop is shown in **Figure 3.2** as a function of the r and z coordinates. The Young-Laplace equation can be written for the axisymmetric drop as follows:

$$\frac{\partial \emptyset}{\partial s} = 2 + \frac{\Delta \rho g {R_o}^2}{\gamma} z - \frac{\sin \emptyset}{R}$$

where ∂S is the differential arc length (cm), $\emptyset$ is the tangent angle to the surface (degree), $\Delta\rho$ the difference in density between oil and brine (g/cc), R_o radius of the drop (cm) and γ is the interfacial tension (mN/m).

Interfacial tension is determined by fitting the above equation into the extracting drop profile. Drop shape analysis software (DSA) from KRUSS Company is used for profile fitting. The interfacial tensiometer used in this work is shown in **Figure 3.3**.

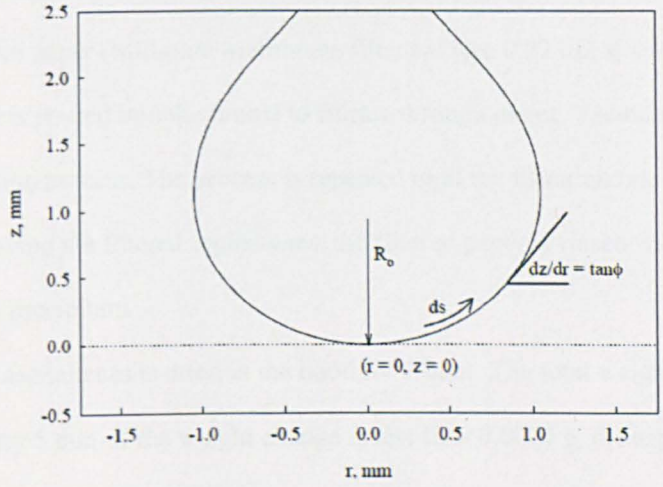

Figure 3.2 *Geometry of an axisymmetric drop.*

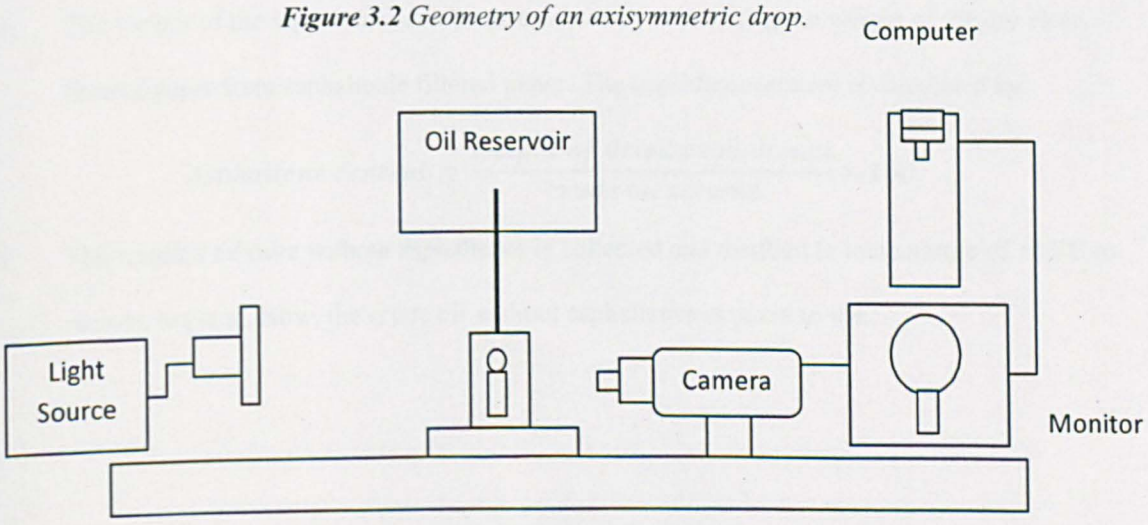

Figure 3.3 *Interfacial tension tensiometer to measure oil/brine interfacial tension.*

3.1.3 Fluid properties

The crude oils used in this thesis were separated to isolate the effect of asphaltene. The procedure of separating asphaltenes is based on American Society for Testing and Materials (ASTM D2007-80) with some modification. The method for asphaltene separation is provided as follows:

i. 20 ml of crude oil is taken out of centrifuged **Figure 3.4** crude oil and added to 800 ml of heptane to be mixed. The flask is sealed and left in equilibrates for two days at ambient conditions.

ii. A funnel filter glass used to separate the precipitated asphaltenes from the oil/heptane mixture. Filter paper (Millipore Membrane filter) of size 0.22 μm is used.

iii. The mixture is poured into the funnel to filtrate through paper. Vacuum pump is used to speed up the filtration process. The process is repeated until the filtration rate becomes very slow.

iv. Before removing the filtered asphaltenes, the filtered paper is rinsed with several aliquots of the n-alkane precipitant.

v. The filtered asphaltenes is dried in the hood for 1 hour. The total weight of filtered paper is checked every 5 min. If the weight change is less than 0.0001 g, the asphaltenes are dry **Figure 3.5**.

vi. The weight of the asphaltenes can be determined by subtracting the weight of the dry clean filtered paper from asphaltenic filtered paper. The asphaltene content is calculated by:

$$Asphaltene\ content = \frac{weight\ of\ dried\ asphaltenes}{crude\ oil\ volume} \times 100$$

vii. The residual mixture without asphaltenes is collected and distilled to temperature of 105°C to remove heptane. Now, the crude oil without asphaltenes is ready to use.

Figure 3.4 Centrifuge to remove the water and sand from crude oil.

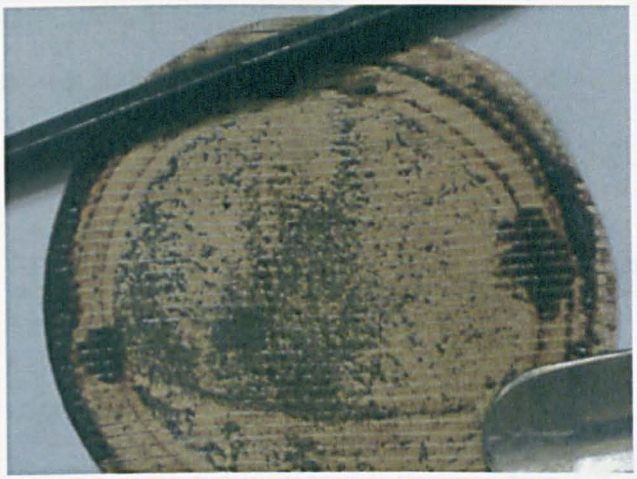

Figure 3.5 Asphaltene aggregation in the filtered paper.

3.2 Micromodel construction

Micromodels are two-dimensional (2-D) flow cells which have a network pattern of flow channels which represent idealized porous media. The models are constructed from transparent material such as glass which allows the pore scale phenomena to be observed and recorded. The author of this thesis used the micromodel without doing the construction. Nevertheless, it is worth mentioning the step by step procedure used to construct the micromodel which is as follows **Figure 3.6**:

i. A piece of 4 mm thick mirror glass was cut to the required size. The surface is coated with a thin layer of photo resist and kept for 20 min at oven under temperature of 100°C.

ii. A photomask, which is a piece of lithographic negative film with the pore network, is placed on the photoresist covered surface and sandwiched between glass plates. The photoresist was then exposed to ultra-violet light for approximately 1 hour. The image was then developed in the photoresist.

iii. The glass was then dipped in a 5.6 M nitric acid solution to remove the copper and silver layers where the photoresist had removed.

iv. The glass is coated with paraffin wax, except the area with pore network, to protect it from the hydrofluoric acid (HF) used for etching. The glass was then etched by immersing it in a 5-

% w/w HF solution for 20 minutes. Inlet and outlet channels were then drilled into the glass surface using a diamond cutting wheel.

v. The micromodel was sealed by heating to 720°C for 20 minutes in a furnace. **Figure 3.6** shows the complete stages of producing glass micromodels.

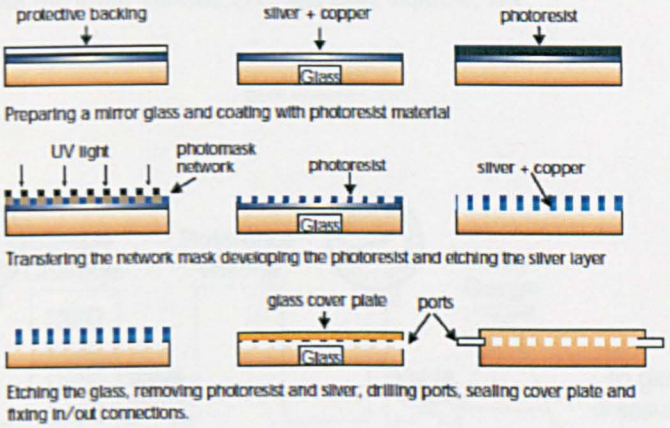

Figure 3.6 *Micromodel construction steps. After Dawe and Grattoni (1998).*

3.3 Core scale experiments

3.3.1 Routine core analysis

Routine core analysis is defined as the set of measurements normally carried out on core plugs which include the porosity and permeability of core plugs.

3.3.1.1 *Porosity*

Two main techniques used to measure the porosity of the rock in this thesis: Helium porosimetry and weights difference techniques.

Helium poroesimetry:

A helium gas expansion porosimeter is used to determine the grain volume of the dry samples. **Figure 3.7** shows the experimental set up. The porosimeter is first calibrated yielding the reference chamber volume, V_r, and the sample chamber volume, V_c. A dry core plug is then placed in the sample chamber. Helium gas is admitted into the reference chamber at a predetermined pressure, typically 100 to 200 psig. About 30 seconds should be allowed for pressure equilibrium and then P_1 (pressure

indicated by the transducer digital readout) should be recorded. The gas is then allowed to expand into the sample chamber. The resulting lower pressure, P_2 should be measured after the system has reached equilibrium. The grain volume of the sample is calculated using the gas law equation. The bulk volume is determined by measuring the sample diameter and length with a calliper. The porosity, ϕ, is then determined from the grain volume,GV, and bulk volume, BV,

$$\Phi = \frac{BV - GV}{BV}$$

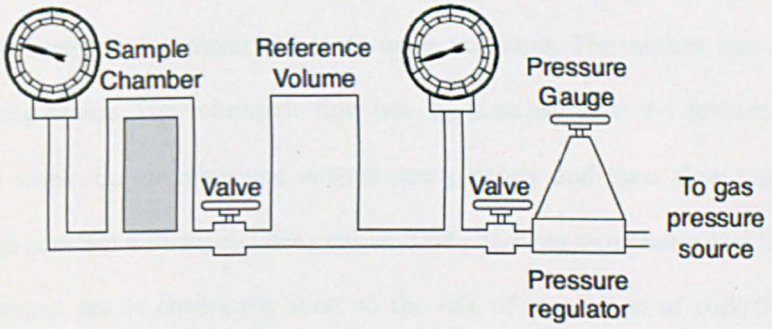

Figure 3.7 *Porosity measurement by Helium*

The advantages of using Helium gas are due to the following properties:

- Very small size of helium molecules makes the gas rapidly penetrate even into small pores,
- Helium is an inert gas and will not be absorbed on the rock surfaces which would otherwise cause erroneous results.

Dry and wet weight:

Other techniques have been used to verify the measurements of pore volumes. Using Archimedes' principle of mass displacement, the sample is first measured dry. Then the sample saturated with brine and its weight is measured. By knowing the dry weight of the samples and the weight of the samples after saturating with brine, the pore volumes of the sample are calculated as follow:

$$PV = \frac{mass\ (Sw = 100\%) - mass\ dry}{Density\ brine}$$

3.3.1.2 *Permeability*

Figure 3.8 shows a steady state experimental setup for flow of gas or liquid phase. In case of permeability measurement by gas, a dry core plug is installed in the core holder. In case of brine permeability, a fully saturated core plug is installed in the core holder. The saturation of core should achieved by high pressure to assure the tight pores are covered by brine. The core holder contains a flexible sleeve to isolate the seal between core plugs and core holder by compressing the radial confing stress. Axial stress can be transmitted to the sample by applying force to one or both end plugs. The end plugs have an axial port for transporting fluid to and from the sample. Each end plug contains a port for measuring upstream and downstream pressures. The outflow line is connected to a flow rate measuring device. The volumetric flow rate, q_n, is measured at the downstream end. Steady state is achieved when the upstream and downstream pressure and mass flow rate throughout the sample all become constant with time. Using gas as fluid phase has two main advantages over using a liquid. First, Nitrogen gas is chemically inert so the risk of interaction of rock/fluid is mitigated. Second, Gas is less sensitive to temperature change that may induce the error for permeability measurement compared to water. However, major caution should be taken when gas steady state is considered especially when gas slippage comes into effect. Klinkenberg (1941) discovered that permeability to gas is relatively higher than that to water, and he interpreted this phenomena as "slip flow" between gas molecules and solid walls. Gas molecules collide each other and to pore-walls during traveling through the porous medium. When the pore radius approaches to the mean free path of gas molecules, the frequency of collision between gas molecules and solid walls increases. This results in an additional flux due to the gas flow at the wall surface, which is called "slip flow".

Klinkenberg (1941) proposed a method in which gas permeability made at several different mean pore pressures can be extrapolated to infinite pore pressure where the gas behaves like a liquid. The extrapolated gas permeability known as Klinkenberg permeability, k_∞, is equal to the permeability obtained using non-reactive liquid such as clean, refined hydrocarbon. This can be written as,

$$k_g = k^\infty(1 + \frac{b}{p_m})$$

where $k\infty$, is the Klinkenberg corrected permeability; b is gas slippage factor; Pm is the mean pore pressure and k_g is the gas permeability.

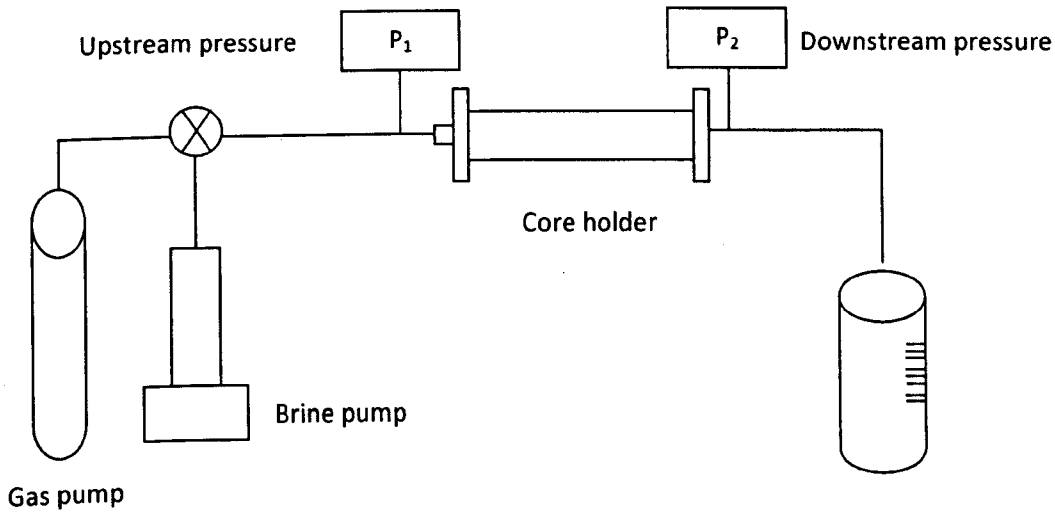

Figure 3.8 Gas and liquid steady state permeability setup.

3.3.2 Fluids displacement Test

Two types of displacement test were conducted in this thesis: spontaneous displacement and force displacement. **Figure 3.9** shows a schematic diagram of the spontaneous imbibition apparatus. This apparatus was designed for tests at room temperature and atmospheric pressure for immiscible oil and water systems. The forced displacements set up is shown in **Figure 3.10**. This apparatus, designed for either constant displacement rate or constant displacement pressure at room temperature and ambient pressure, consists of a fluid injection system, a transducer for pressure drop measurement, crude oil and brine reservoirs, confining pressure supply, core holder , and oil/water separator and collector.

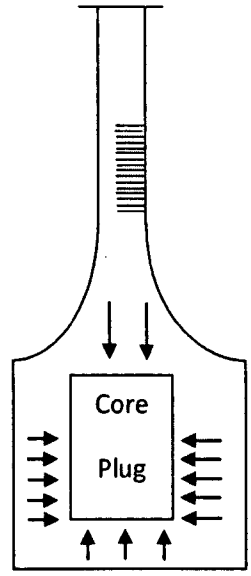

Figure 3.9 Spontaneous displacement setup in which brine freely imbibes to all faces of core plugs to displace oil.

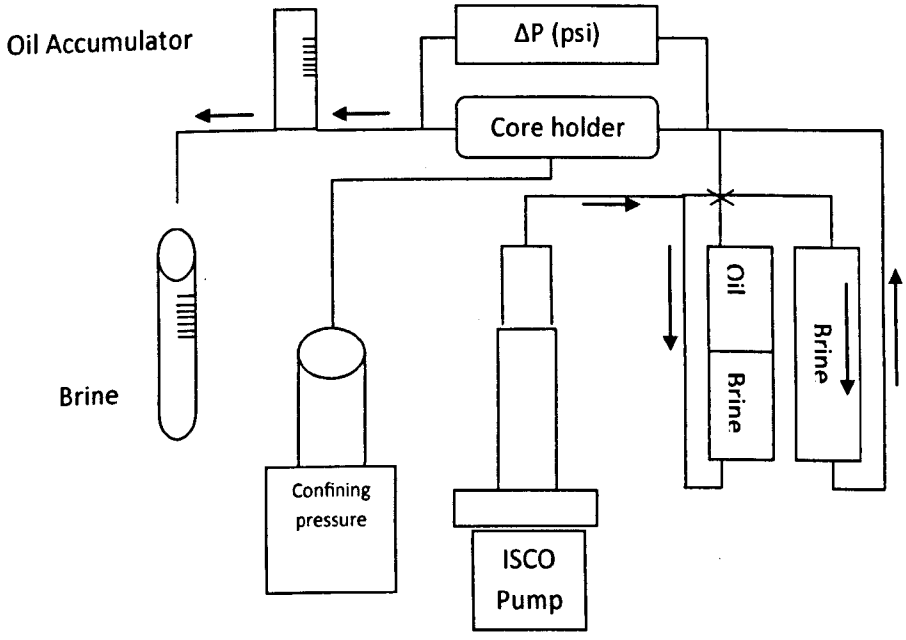

Figure 3.10 Force displacement setup.

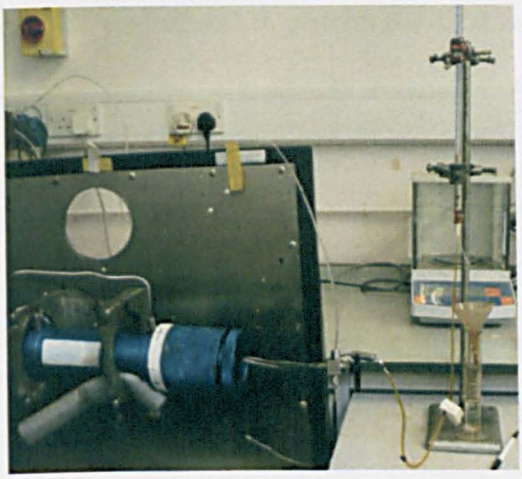

Figure 3.11 Core holder and force displacement set-up.

3.3.3 Nuclear Magnetic Resonance

NMR T_2 relaxation time measurement was performed in all the core samples. The measurements were taken at two different saturations: initial water saturation and residual oil saturation. The measurement of T_2 relaxation was performed as it is faster compared to T_1 and more comparable with data gathered by the new generation of NMR logging tools. The NMR T_2 measurements were performed on a Resonance Instruments MARAN 2 bench top spectrometer **Figure 3.12** at ambient pressure and 35°C, operating at 2 MHz. The pulse sequence is generated by Carr-Purcell-Meiboom-Gill (CPMG) to remove the effect of inhomogeneous field that emerge because of different parts of the sample may be subject to different magnetisations. The parameter setting for the CPMG pulse sequence are summarised in **Table 3.1**. The mapping of the decaying magnetization into relaxation time distribution was performed with the DXP programme, a software programme provided by Resonance Instruments as part of the MARAN 2 software.

The outcrop and reservoir samples were prepared for NMR measurements as follows:

i. The sample was first rolled gently across a piece of tissue paper to remove excess fluid on its surface. Then the sample was wrapped in cling-film to prevent fluid loss by evaporation.

ii. The sample was put into the MARAN 2 sample chamber to perform the NMR measurements.

iii. The CPMG pulse sequence was selected to perform the T_2 relaxation measurements. After finishing the measurement, the raw data and all parameters are automatically stored in computer files.

iv. The data were then fitted using the DXP programme. The DXP data-fitting algorithm was used in the interpretation of the raw relaxation data. After the use of the data-fitting algorithm, the T_2 distribution was obtained. The results were compared by normalising the T_2 signal amplitude using normalised amplitude:

$$NA = \frac{SA}{\sum SA}$$

The log mean of the T_2 distribution was also calculated. This is an average value of T_2 of the distribution and is given by

$$T_{2LM} = \exp\left(\frac{\sum(SA_i log T_2)}{\sum SA_i}\right)$$

Where, T_{2LM} is the T_2 logarithmic mean and SA is the signal amplitude.

ParameterID	Definition	Value
	Pulse parameters	
P90 (μs)	90° pulse length, duration of 90° pulse	15.9
P180 (μs)	180 pulse length, duration of 180° pulse	31.8
Dead1(μs)	Probe delay time, the time allows the probe to settle after pulse	60
TE	Echo spacing	200
RD (ms)	Recycle Delay, the time between successive scans	10000
SF (MHz)	Spectrometer Frequency	2.2
	Acquisition Parameters	

FW (Hz)	Filter width, applied to smooth the NMR signal and reduce the noise	1
DW (μs)	Dwell time, the time	1
NS	Number of scans, total number of scans per experiment	100
Nech	Number of echoes, number of echoes that will occur	8000

Table 3.1 *Parameters setting for T_2 measurements.*

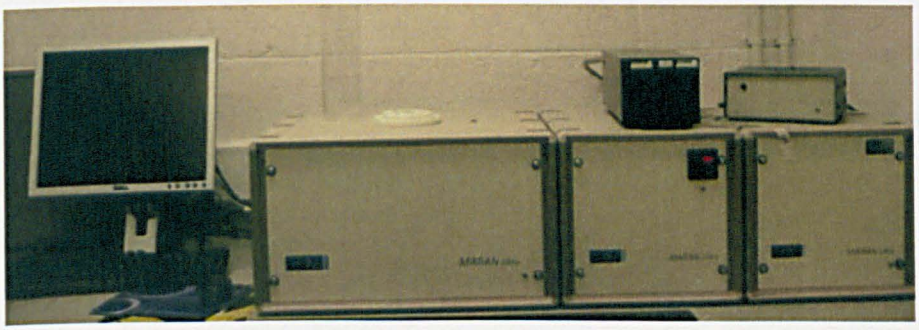

Figure 3.12 *The NMR spectrometer (MARAN2)*

3.4 Vertical scanning interferometry

Interferometry is the science and technique of combining two or more waves, to create an output wave that differs from the input waves. The combination of waves result in a set of dark and light bands known as fringes which can be translated into description of surface topography.

The behaviour of the two plane wavefronts and their interaction can be summarised as follows. The physical principles of optical interferometry exploit the wave properties of light. Light can be thought as electromagnetic wave propagating through space. If we assume that we are dealing with a linearly polarized wave propagating in a vacuum in z direction, electric field, E, can be represented by a sinusoidal function of distance and time.

$$E(x, y, z, t) = a\cos(\omega t - kz)$$

Where a is the amplitude of the wave, $\omega = 2\pi v$ is the circular frequency (v being the frequency of the light) and $k = \frac{2\pi}{\lambda}$ is the wave number (λ being the wavelength of the light). For more convenient mathematical manipulation, the previous equation can be expressed in complexed form as

$$E(x,y,z,t) = Re\{A\ exp(wt)\}$$

Where $A = a \exp(-i\emptyset)$ is the complex amplitude and $\emptyset = \frac{2\pi z}{\lambda}$.

Typically, in an interferometer a wave is split into two parts which travel different paths, and the waves are combined to create interference. The complex amplitude at any point in the image plane is the sum of complex amplitudes of the two interfering wave front (A_1 and A_2), such that

$$A = A_1 + A_2$$

Consequently, the intensity of the fringe at any point can be described as:

$$I = I_1 + I_2 + 2\sqrt{I_1 I_2} cos\Delta\emptyset$$

Where I_1 and I_2 are the individual intensities of the two wave component, and $\Delta\emptyset = \emptyset_1 - \emptyset_2$ is the phase difference. When a common source is used for the two wavefronts, the phase difference can be related to directly to the optical path difference (OPD):

$$OPD = (\frac{\lambda}{2\pi})\Delta\emptyset$$

When the paths differ by an even number of half wavelengths, the superposed waves are in phase and constructive interference is observed, increasing the amplitude of the output is observed. When they differ by an odd number of half wavelengths, the combined waves are 180° out of phase and destructive interference is observed, decreasing the amplitude of the output. The highest contrast fringe when the optical path difference (OPD) is zero. The fringes result from the interference of the field scattered from the test surface with that reflected from the reference surface **Figure 3.13**. As the surface is scanned relative to the reference surface, individual pixels within the image are seen to

brighten and darken as they meet the condition for constructive and destructive interference respectfully **Figure 3.14**. From the intensity of the fringes, surface elevation can be determined using the equation,

$$I_{x,y}(B) = I_o(B) + I_{AC}(B - h_{x,y})cos[K_0(B - h_{x,y})]$$

Where B is the height from the reference surface, $h_{x,y}$ are the surface height topography of the sample surface at the pixel location, I_o is a constant offset intensity term and I_{AC} is the slowly varying modulation envelope intensity. The spatial frequency, K_0 is related to the mean effective wavelength, λ_o, such that:

$$k_o = \frac{4\pi}{\lambda_o}.$$

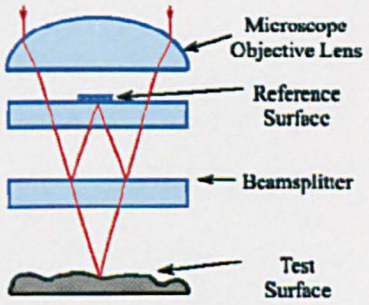

Figure 3.13 *Principle of white light wave reflection.*

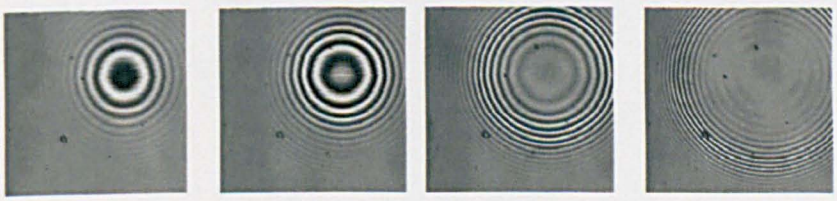

Figure 3.14 *Example of successive images and fringe patterns.*

By use of a Mirau Interferometric objective with a magnification of 50, a field of view of 250 μm by 500 μm per measurement is obtained. The systems vertical resolution is better than 2 nm if a white light source is used. Resolution improves to 0.7 Å if a narrow band of green light is used. Under these

conditions, the lateral resolution is about 0.5 μm. A single vertical scan of a 4 μm height difference takes less than 2 s (scan rate, 2.1 μm/s) and gathers as many as 100,000 height data at a time. Analysis of the surface topography was carried out by Talymap which is comprehensive 3D analysis software that facilitates a wide range of data manipulation.

Chapter 4
Wettability in Pure Surface Mineral

Contact angle is the universal measurement of wettability. In chapter 4, a practical approach of defining the reservior wettability as it developed during the oil drainage and water imbibition in the porous media. Role of water film, brine salinity, asphaltene content and asphaltene solvency investigated extensively. This chapter provides rapid screening criteria for the tendency of crude oils to alter the wettability of rock surface.

4.1 Introduction

The wettability of an oil reservoir has a fundamental control on petrophysical properties (capillary pressure, relative permeability and electrical conductivity) and has a significant impact on reservoir behaviour during production (Anderson, 1986 a-c). It is generally assumed that reservoirs are water-wet when they are first invaded by oil. However, over geological time, crude oil-brine-rock (COBR) interactions may alter the wettability of the reservoir (Morrow, 1991). There is also evidence that the wettability of a reservoir (or parts of a reservoir) may be altered during production as a result of changes in temperature, pressure or water chemistry (Al-Mjeni et al, 2011). For example, water salinity and temperature are both key controls on wettability alteration during production remain poorly understood. It is the basic aim of the current chapter to help fill some of these knowledge gaps by presenting results from a series of experiments conducted to identify the impact of these variables on wettability.

Based on previous work in wettability, Kovscek et al. (1993) outline pore scale events that illustrate how wettability generated by crude oil evolve in reservoir rock. Kovscek et al. (1993) construct their pore scale event relative to oil invasion into a water saturated porous media. As oil migrates into a reservoir, the capillary pressure eventually rises to maximum potentially causing the water thin film that separates the oil from the mineral surface to rupture. According to the picture of Kovscek et al.

(1993), the pore walls where the thin films break become oil wet, whereas the corners of the pores are water filled and remain water-wet. However, there remains uncertainty regarding the nature of governing factors that cause the pore walls to become oil-wet such as crude oil composition, brine chemistry and reservoir temperature. A key aspect of the work presented in this chapter is the use of a new experimental technique that was developed to create an analogue to the wettability evolution that occurs in reservoir rocks. In particular, a flat smooth mineral substrate is utilised as a pore wall to measure the contact angle behaviour in advancing and receding modes representing displacement process during waterflooding and oil drainage respectively. The contact angle method is usually applied to study the wettability of flat solid surfaces. In this chapter, the use of contact angle measurement is focused on wettability of solid surface resulting from deposition of crude oil.

Various methods are used for measuring the contact angle between two liquids and a solid surface (e.g. drop method, sessile drop method and capillary method). In the drop method, the contact angle is determined directly from the profile of a liquid drop on a plane solid surface (Fox and Zisman, 1950). The sessile drop method indirectly determines the contact angle by measuring light refection from the drop surface at the point of contact, or by measuring the drop dimensions from which the contact angle can be calculated from the drop height and the diameter of its base (DSA Manual, 2004). In the capillary method, contact angles are obtained from the balance between capillary and hydrostatic forces (Morrow and Nugyen, 1982; Li and Firoozabadi, 1998; Spildo and Buckley, 1999). This method requires the solid to be available as a closed capillary tube not as open flat surface. In this study, oil/brine/borosilicate glass combinations are used to investigate wettability alteration in the COBR systems. Silicate represents the dominant mineral in most sandstones with 78.5% in Berea sandstone (Ma and Morrow, 1994). For this reason, borosilicate glass is used as a model surface to study wettability alteration in reservoir rocks. Advancing, receding and static contact angles provide both dynamic and static definition of wettability. Despite the absence of rock morphology on the model surface, wettability will be still dependent on contact angle as mentioned by (Hirasaki, 1991).

4.2 Materials and experimental methods

4.2.1 Preparation of glass plates

Glass plates (1.0 x 0.5 cm) composed of borosilicate material were obtained from Fisher Scientific Ltd. Before use, they were carefully cleaned so to so that they were perfectly water-wet against air and against a pure alkane.

The plates were cleaned by four different solvents to simulate the core cleaning process and select the best cleaning agent for the silicate surface. Dichloromethane (DCM), toluene, decalin and water were used. The plates were immersed in the cleaning agents for 24 hours then the contact angle of water against air and alkane was measured. A contact angle close to zero was taken to indicate that water wet conditions had been established during the cleaning process. After deciding the best cleaning solvent, the glass plates were oven dried at 80°C for 2 hours.

4.2.2 Fluids used

4.2.2.1 *Crude oil*

Four types of crude oil with distinctive asphaltene contents were used in this study. The physical properties of the oils are shown in **Table 4.1** . The asphaltenes from these crudes were removed by de-stabilisation the asphaltene and then filtering to produce four types of de-asphaltene crude oils as discussed in the experimental material in Chapter 3. In this chapter total of 8 crude oil samples have been used (F-200, F-410,GN,S,) and deasphaltene of each previous crude oil. Also, Interfacial tension between crude oil and brine interface was measured using pendent drop technique.

Crude oils	Density (g/mL)	Interfacial tension (mN/m)	Viscosity (cp)	Asphaltene recovered (wt. %)
F-200	0.857	27.1	19.0	0.56 (n-heptane as precipitant)
F-410	0.835	26.5	27.0	0.34 (n-heptane as precipitant)
GN	0.865	25.0	150.0	0.78 (n-heptane as precipitant)
S	0.826	25.0	7.4	0.04 (n-heptane as precipitant)

Table 4.1 *Oil physical properties.*

The chemistry of the crudes was characterized using the SARA test and their acid and base number determined as described below.

SARA test:

Identifying crude oil composition can help to explain its physical and chemical properties (Mullins et al., 2007). One common method is to divide crude oil into four fractions: saturates, aromatics, resin and asphaltenes, which are referred to SARA test (Fan and Buckley, 2002). The precipitate obtained by creating a 1:40 mixture of crude oil and hexane is defined as asphaltene fraction of the oil. The remainder of the oil can be separated chromatographically on the basis of polarity. The saturate fraction consists of non-polar material such as linear, branched and cyclic saturated hydrocarbons. The aromatics are more polarisable which is hydrocarbons that contains one or more aromatic rings. The remaining fractions, resins consist of hydrocarbons with small percentages of polar heteroatom (mainly oxygen, nitrogen and sulfur). According to Fan and Buckley (2002), three main methods applied for separations in SARA test are (i) clay-gel adsorption chromatography, (ii) high-pressure liquid chromatographic (HPLC), and (iii) thin-layer chromatography (TLC). Here we used a clay-gel adsorption chromatography method to produce SARA test for our crude oil samples as shown in **Table 4.2**.

Crude oil	SARA			
	Saturates, %	Aromatics, %	Resins, %	nC7Asph. %
F-200	38.2	38.2	23.04	0.56
F-410	36.8	43.6	19.16	0.44
GN	41.1	34.8	23.4	0.70
S	55.6	23.3	21.06	0.04

***Table 4.2** Crude oil composition.*

Acid and base number

Acid number is defined by ASTM 664-89 as the amount of base, expressed in mg KOH, necessary for titration of 1 grams sample to a well-defined inflection point. The base number is similarly defined by ASTM 2896-88 as the amount of perchloric acid necessary for titration of 1 gram sample to a well defined infection point. Prior to the determination of acid and base numbers, all samples have been centrifuged to remove any particulate matters.

Crude oil	Acid number (mg KOH/g oil)	Base number (mg KOH/g oil)
F-200	0.15	1.7
F-410	1.20	1.5
GN	0.90	1.3
S	0.05	0.6

Table 4.3 Acid and base numbers of four crude oil samples.

4.2.2.2 *Probe oil*

As well as the eight crude oil, two refined oils, decane and multipar (H), were used in contact angle measurements; they are referred to as probe oils when used to test the wettability of plates treated with crude oil. The physical properties of the probe oils are listed in **Table 4.4**.

4.2.2.3 *Solvents*

Normal heptane was used as a precipitant of asphaltene solids from the crude oil. Toluene and decalin were used as a solvent to remove the bulk crude from the treated glass substrates. All the solvents listed were used as received. The physical properties of the solvents are listed in **Table 4.4.**

Oil	Density (g/ml)	Viscosity (cp)	Usage
Decane	0.731	0.920	Probe oil
Multipar H	0.759	1.80	Probe oil
Heptane	0.684	0.386	Precipitants

Toluene	0.867	0.590	Solvent
Dichloromethane	1.33	0.449	Solvent
Decalin	0.896	2.60	Solvent

Table 4.4 Probe oil and solvent physical properties.

4.2.2.4 *Brine*

The primary brine used most in this work was sodium chloride (NaCl). A range of concentrations between 3 M and 0 M NaCl were used for both contact angle and interfacial tension measurement.

4.2.3 Experimental procedures

4.2.3.1 *Adhesion test (Short time interaction)*

The adhesion test was originated by Morrow et al. (1986) to investigate wettability of pure minerals surfaces. The purpose of the test is to identify the conditions in which an oil drop rapidly adheres to a solid surface through the brine phase. A drop of oil is formed under water at the tip of either a microburette or syringe. The time for contacting the drop is 5 minutes. The main observation is whether or not the oil drop adheres to the solid surface. A map is then constructed to highlight how pH and NaCl brine concentration affect adhesion; this is referred to as an adhesion map. Two temperatures were used during the tests, 20°C and 60°C.

4.2.3.2 *Oil deposition test (Long time interaction)*

It was intended to use a direct approach to measure the contact angle of water drops surrounded by crude oil on the cleaned borosilicate glass slides. However, this approach proved impossible with the crude oil samples used in this study as their opacity prevented visualisation of water drops. The approach was augmented to make the crude oil drops attach by an inverted needle onto the underside of the glass substrate so that water is the surrounding phase. The static contact angle was monitored but the dynamic contact angle could not be maintained due to for formation of rigid films at the oil/brine interface. These suppressed the movement of the contact line, which makes measurements of the advancing and receding contacts inaccurate. The rigidity phenomena resulted in another approach

being developed in which the crude oil and brine interaction was part of surface preparation not surface measurement.

The approach begins by selecting a brine to equilibrate with the glass plates. Glass was immersed in the selected brine for 7 days. The rational of selecting 7 days is to make sure that surface charge reached equilibrium with the glass surface. Kulkani and Somasundarn (1973) noticed that surface charge changes rapidly during the first few hours and is more stable after two or three days. After equilibration, the glass plates were removed and immersed directly into a crude oil for different periods of times (2 hours, 5 hours, 7 hours, 12 hours, 1 day, 3 days, 6 days and 15 days). Temperature was varied at this stage to 20°C, 40°C and 60°C. Sealed bottles containing the slides were continuously weighed to confirm no losing of light end crude oil composition during high temperature by effect of evaporation.

After the glass plates have been treated by brine and crude oil, the bulk of crude oil, which is the non-deposited components, were removed by selective solvents. Decalin and toluene were used to assess their suitability to remove the bulk crude oil without affecting the oil components that adsorb during the aging process. The treated glass surface was only rinsed with each solvent. Advancing, receding and static contact angles are used to judge which solvent is suitable for removing the bulk crude oil that was used.

After removal of the bulk crude oil, the surface is ready to assess its wettability. Pure oil is used as the surrounding phase and a drop of water was used to measure the contact angle through it. Static and dynamic contact angles were determined. Static angle measurements were obtained by placing a 15 µl drop on glass plates that were immersed in water. Advancing angle measurements were obtained by enlarging the drop at constant rate (1 µl/s) whereas receding angle is obtained by retracting the drop at similar rate.

4.2.3.3 *Contact angle measurement*

Contact angles were measured using a KRUSS *EasyDrop,* which has a video camera, automatic dosing system and computer software "Drop Shape Analysis" (DSA). The software provides various

methods to fit the shape profile of the drop to calculate the contact angle. According to the Easy Drop Manual (2004), several profiles/methods can be used to assess contact angle:

Tangent method:

The complete profile of a sessile drop is fitted to a general conic section equation. The derivative of the equation at the baseline gives the slope at the three-phase contact point and thus the contact angle.

Height/width method:

This is a standard method in which it is assumed that the contact angle for small drops is not influenced by the absolute drop size. From the ratio of the maximum height and width of a sessile drop, conclusions can be drawn about the contact angle.

Young-Laplace method:

The drop contour can be mathematically described by adapting the Young-Laplace equation for curved boundary areas. This is based on a technique called Axisymmetric Drop Shape Analysis Profile (ADSA-P), which fits the measured profile of a drop to a Laplacian curve (Lahooti et al., 2010).

The Young-Laplace method was used during the current study to determine the contact angle. Three contact angle measurements were observed: advancing, receding and static contact angle. The advantage of ADSA-P over prior fitting is that it numerically fits the Laplace equation to the entire drop profile rather than obtaining shape information from a few drop dimensions, which can be difficult to identify. This serves to increase greatly the accuracy of the drop shape approach and makes it much easier to use.

4.2.3.4 *Interfacial tension measurement*

IFT was measured as a function of drop aging time using a KRUSS pendant drop apparatus with Drop Shape software. IFT was calculated from drop shape by fitting to the Young-Laplace equation. The pendant drop method of IFT measurement requires that a stable drop be formed.

4.3 Results

4.3.1 Oil/brine interface

Figure 4.1 shows the dynamic interfacial tensions with F200 crude oil for eight different brine salinities as a function of aging time. A significant lowering in interfacial tension is observed with range of 5 to 11 mN/m when the measurement of interfacial tension is started. All crude oil interfacial tension achieves a steady interfacial tension value after 15 min and remains constant for another 60 min, which indicates the oil/brine interface has reached equilibrium.

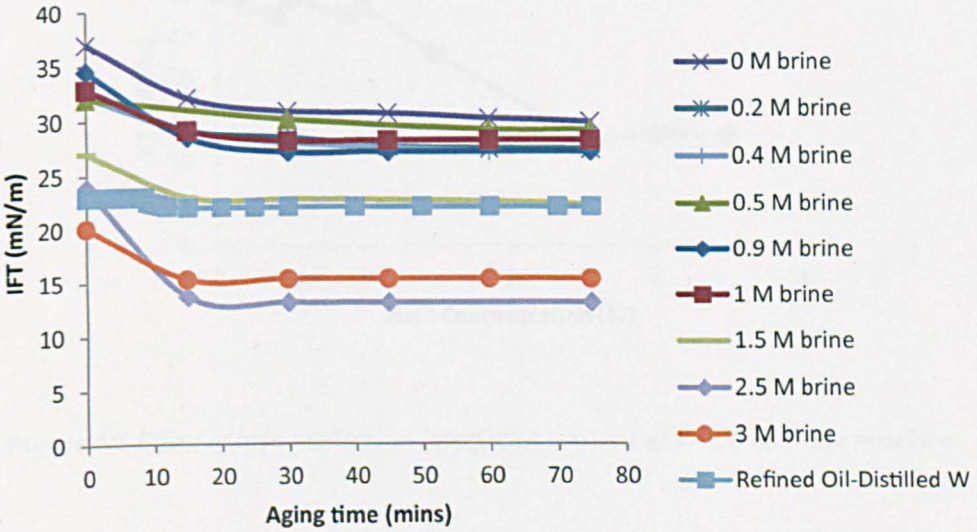

Figure 4.1 *Effect of time equilibration in interfacial tension for different brine composition and F-200 crude oil.*

Crude oil interfacial tension shows a distinct behaviour with brine properties as shown in **Figure 4.2** and **Figure 4.3**. At a pH of 3, the interfacial tension is the lowest at 3 mN/m. However, S-crude has a higher interfacial tension (12 mN/m) compared to the other crudes. The interfacial tension reaches its highest value at a neutral pH for all the crude oil samples. As the pH becomes alkaline, interfacial tension drops continuously from 22 mN/m at pH 7 to 19 mN/m at pH 9 for F-200 and S crude oils. However, the degree of reduction is more dramatic for crude oils GN and F-410, which drops to 7 mN/m at pH 7 and 3 mN/m at pH 9. Also, interfacial tension of crude oil varies with the ionic strength of the brine., Interfacial tension is independent of brine between 0 to 1 M NaCl;generally only a

change of 3 mN/m is observed. However, the oil/brine interfacial tension drops from 28 to 22 mN/m as brine salinity increases up to 1.5 M NaCl. The interfacial tension reaches a minimum of 13 mN/m at a brine salinity of 2.5 M NaCl. At 3 M and 3.5 M brine salinity, interfacial tension remains at around 13 mN/m. Conversely, the interfacial tension of refined oil does not depend on the ionic strength of the brine. Interfacial tension remains constant at around 22 mN/m for brine salinities ranging from 0 to 3.5 M NaCl brine **Figure 4.4**.

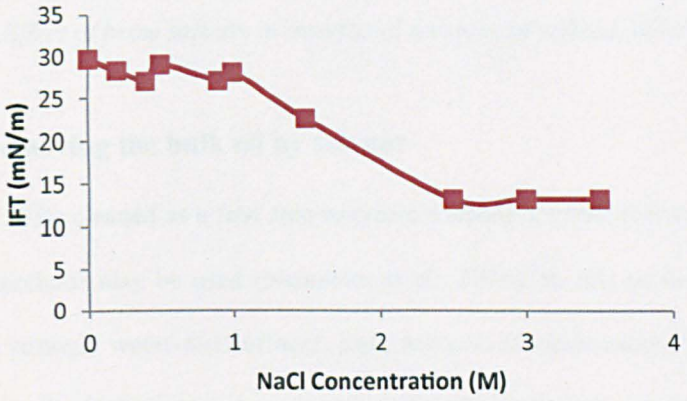

Figure 4.2 *Effect of brine salinity in interfacial tensions of F-200 oil/brine interface.*

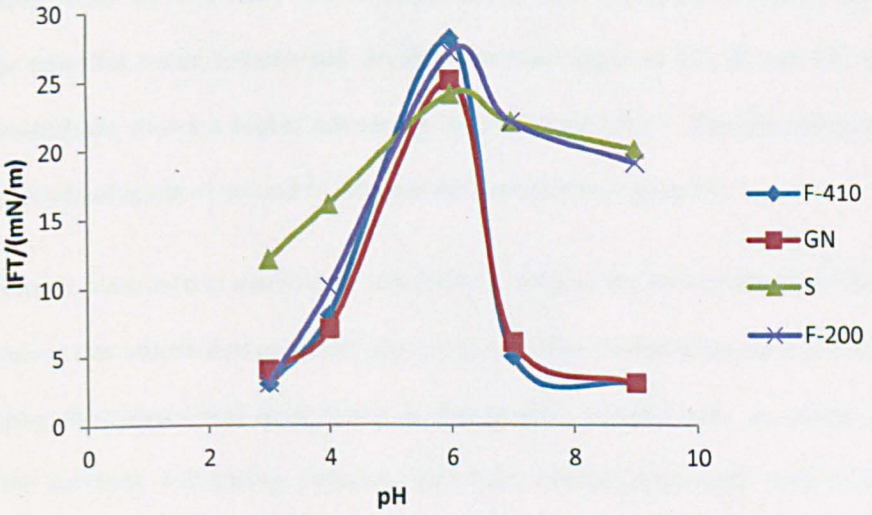

Figure 4.3 *Effect of brine pH in crude oil/brine interfacial tension.*

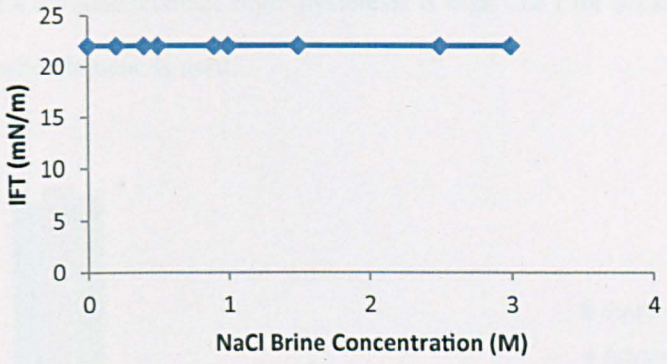

Figure 4.4 *Effect of brine salinity in interfacial tensions of refined oil/brine interface.*

4.3.2 Effect of removing the bulk oil by solvent

Glass surfaces need to be cleaned as a first step to create a strongly water-wet surface. Mechanical or chemical cleaning methods may be used (Neumann et al., 2010). In this section, chemical methods were used to create strongly water-wet surfaces. Four solvents (dichloromethane, water, toluene and decalin), which are used widely in cleaning of extracted rocks in special core analysis, were assessed to assessed to identify which was the most effective for cleaning the glass surfaces. **Figure 4.5** shows that all solvents give a very reproducible surface with static contact angle around 7° expect dichloromethane, which gives a static contact angle of 54°. Advancing contact angle measurements show a similar trend for water, toluene and decalin at contact angle of 12°, 8° and 10° respectively. Again dichloromethane shows a higher advancing contact angle of 57°. Decalin, toluene and water gave a receding contact angle of around 6° whereas dichloromethane gave 55°.

Decalin and toluene were used to assess their suitability to remove the bulk crude oil without affecting the oil components that adsorb during the oil deposition test. The treated glass surface was dipped in a bottle containing the solvent and then rinsed in the specific solvent until no colour change was observed in the solvents. Advancing, receding and static contact angles are used to judge which solvent was best suited for removing the bulk crude oil. The results show that the toluene caused a sharp reduction of static contact angle to 10° compared with 67° when decalin was used to remove the

bulk crude oil **Figure 4.6**. Also, contact angle hysteresis is high (52°) for decalin whereas there is a minor hysteresis (3°) when toluene is used.

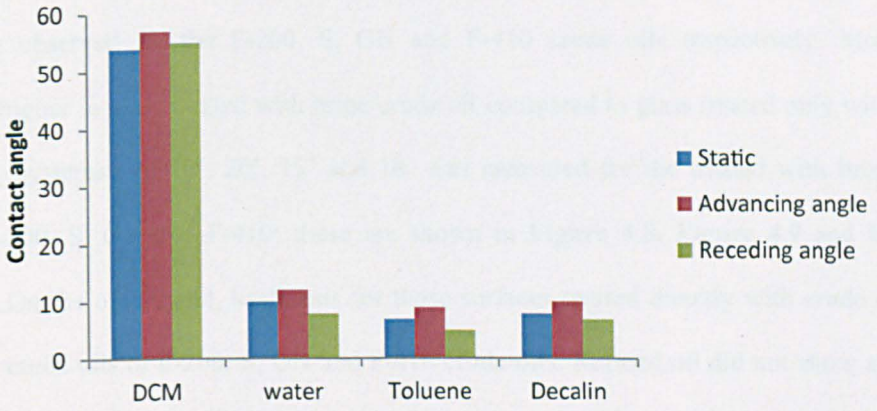

Figure 4.5 *Effect of solvent during silicate cleaning process. Silicate surface was cleaned by different solvent. Contact angle measurements used to assess the nature of surface wettability after cleaning.*

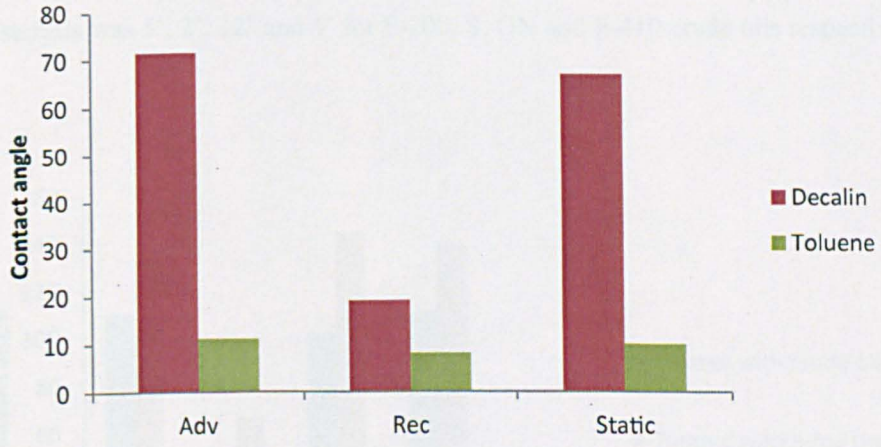

Figure 4.6 *Effect of solvent rinsing in treated glass surface.After long time deposition test, bulk oil has been removed from the treated glass surface to allow for direct measurement of contact angle in new oil treated glass surface.*

4.3.3 Effect of brine contact

Figure 4.7 shows the effect of the presence of brine on wettability alteration of glass surfaces by crude oil. Two sets of glass surface were prepared. One surface was pre-wetted with brine and aged in crude oil for 10 days; this is referred to as "*treated with brine/crude oil*". The other glass surface was immersed directly in crude oil without passing through brine; this is referred to as "*treated with crude*

oil". Four different crude oils were used to increase the validity of the results. All four crude oils show systematic increasing in the oil-wetness of the glass that was pre-wetted compared to those directly treated with crude oil. In particular, a systemic increase in advancing contact angles of 30°, 20°, 42° and 30° was observed for the F-200, S, GN and F-410 crude oils respectively. Moreover, the hysteresis is higher in glass treated with brine/crude oil compared to glass treated only with crude oil. In particular, hysteresis of 10°, 20°, 15° and 18° was measured for the treated with brine and then crude oils F-200, S, GN and F-410; these are shown in **Figure 4.8, Figure 4.9** and **Figure 4.10** respectively. On the other hand, hysteresis for those surfaces treated directly with crude oils was 2°, 1°, 1°, 1° for crude oils of F-200, S, GN and F-410 crude oils. Refined oil did not show any effect to brine contact. However, when the solid surface is treated by distilled water instead of brine and then with crude oil, the degree of water-wetness is increased more than the surface that was treated directly with crude oil. The incremental reduction advancing contact angle was 15°, 29°, 64° and 20° and the degree of hysteresis was 5°, 2°, 12° and 4° for F-200, S, GN and F-410 crude oils respectively **Figure 4.11**.

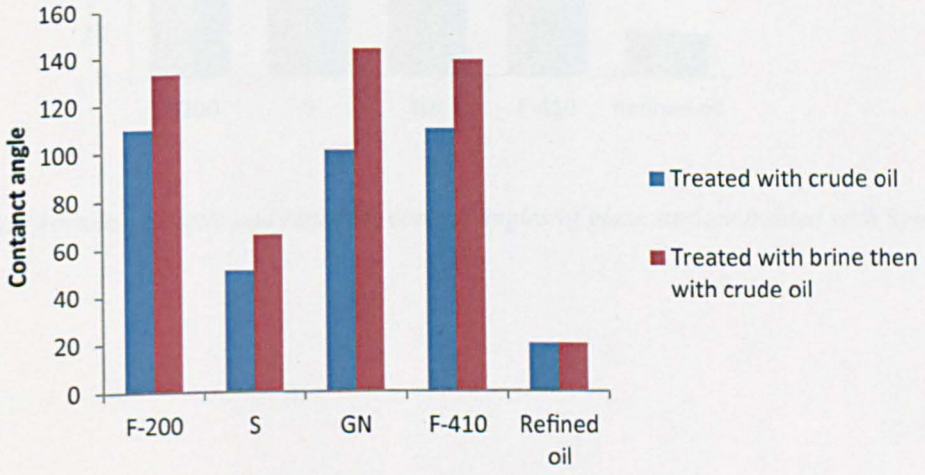

Figure 4.7 *Comparing between solid surface pre-wetted with brine and aged in crude oil with glass only aged in crude oil.The different behaviour in contact angle measurement shows the role of water film in promoting different wettability.*

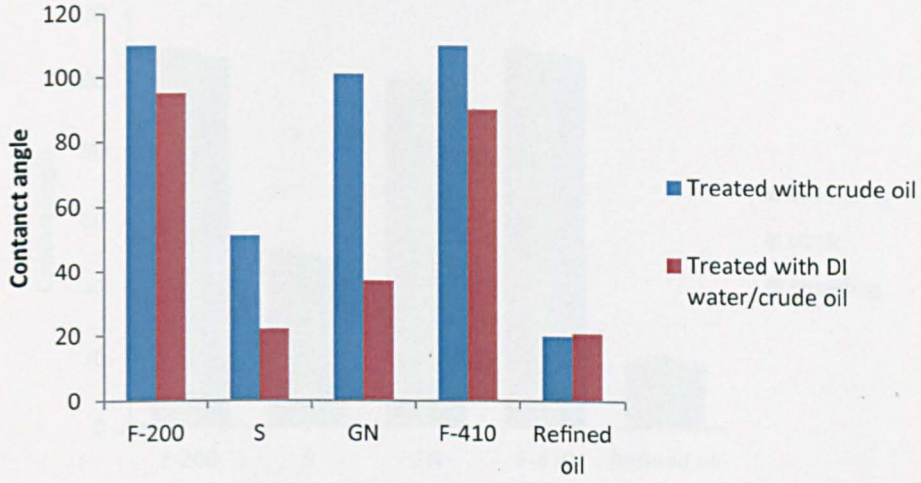

Figure 4.8 *Effect of presence of distilled water prior to oil deposition in solid surface.*

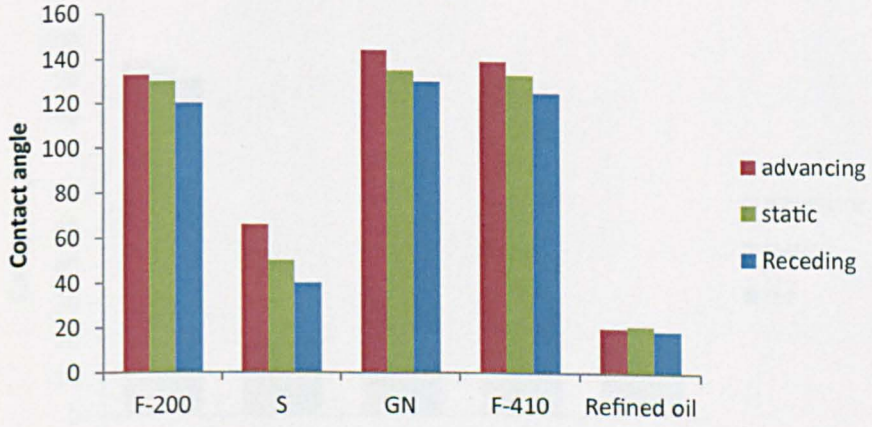

Figure 4.9 *Advancing, static and receding contact angles of glass surface treated with brine/crude oil.*

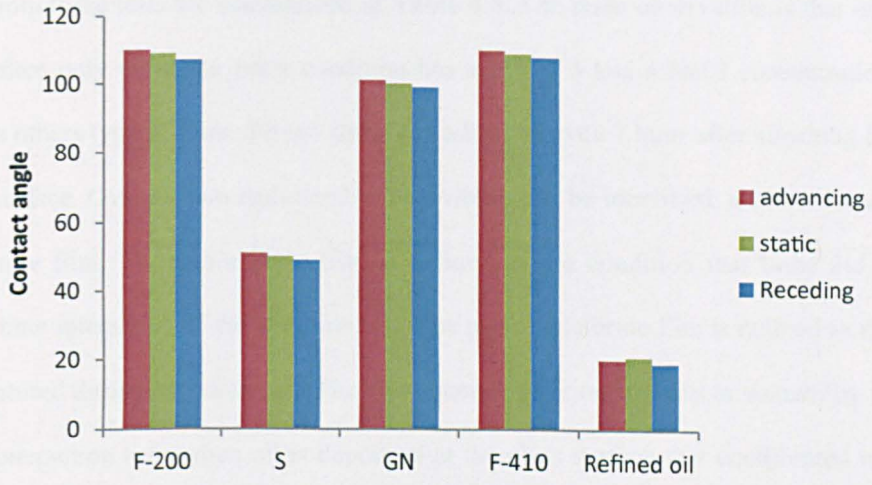

Figure 4.10 *Advancing, static and receding contact angles of glass surface treated only with crude oil.*

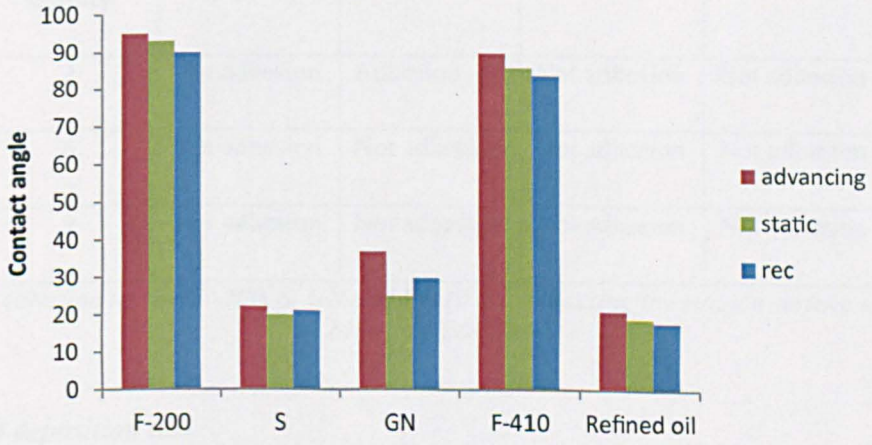

Figure 4.11 *Advancing, static and receding contact angles for glass surface treated with distilled water and crude oil.*

4.3.4 Effect of brine composition

4.3.4.1 *Adhesion test*

The purpose of adhesion test is to identify under which brine conditions the water film will be retained or ruptured when a drop of crude oil is attached to a solid surface that has been equilibrated in aqueous brine. Adhesion may be observed after only a short time period of exposure of solid surface to crude and is the basis of a qualitative test.

The results from these tests are summarized in **Table 4.5**. The main observation is that oil adheres to the glass surface only when the brine condition has a pH of 3 and a NaCl concentration of 0.1 M NaCl. All the others type of brine did not show any adhesion even 1 hour after attaching the crude oil to the solid surface. Overall, two end-member behaviours can be identified: a stable brine film and a non-stable brine film. The stable brine film is defined as the condition that brine did not rupture during short time interaction of the adhesion test. The non-stable brine film is defined as the condition that brine ruptured during adhesion test. The consequence of brine stability in wettability is studied in longer time interaction tests when oil is deposited at the glass surface that equilibrated in brine over 13 days. The longer time interaction of brine and crude oil is referred to as the "oil deposition test".

pH/brine salinity	0 M	0.1 M	0.5 M	1 M
3	Not adhesion	Adhesion	Not adhesion	Not adhesion
6	Not adhesion	Not adhesion	Not adhesion	Not adhesion
9	Not adhesion	Not adhesion	Not adhesion	Not adhesion

Table 4.5 *Adhesion test for F-200, S, GN and F-410 oil contacting the silicate surface at different brine composition*

4.3.4.2 *Oil deposition test*

After crude oil was allowed to interact with stable brine residing on the solid surface for a longer period of time, two main observations were noticed. First, there is no major change in advancing or static contact angle when a stable brine film was used compared to unstable brine film **Figure 4.12** and **Figure 4.13**. Second, a drastic change in receding contact angle is observed with brine film stability change from stable to non-stable. This large change in receding contact angle reflects quantitatively in the magnitude of hysteresis between advancing and receding contact angle when brine film stability is alternated from stable to non-stable. A stable brine film results in a hysteresis of 13°, 16°, 9° and 9° for F-200, S-crude, GN and F-410 respectively **Figure 4.14**. Conversely, the hysteresis is more than double to 42°, 35°, 47° and 59° for F-200, S-crude, GN and F-410 respectively

when an unstable brine film is used. An unstable brine film increases the hysteresis noticeably compared to when the surface is equilibrated in stable brine film.

Varying the brine salinity resulted in gradual decrease in advancing contact angle for F-200 and S-crude **Figure 4.15**. For example, the advancing contact angle dropped from 145° at 3 M to 133° at 0.5 M brine salinity. Further reduction to 95° occurred when distilled water was used. Similarly for S-crude, the advancing contact angle drop from 136° at 3 M to 65° at 0.5 M to reach 21° at 0 M brine salinity **Figure 4.15**. Hysteresis between advancing and receding contact angle was larger when brine salinity is at its highest (**Figure 4.16**, **Figure 4.17**, **Figure 4.18** and **Figure 4.19**). At 3 M brine salinity, the hysteresis was 15° and 17° for F-crude and S-crude respectively. At 0.5 M brine, the hysteresis was 13° and 16° for F-crude and S-crude respectively. At 0 M salinity, the hysteresis falls drastically to 5° and 1° for F-crude and S-crude respectively. The advancing contact angle or hysteresis is not affected by salinity when refined oil is used.

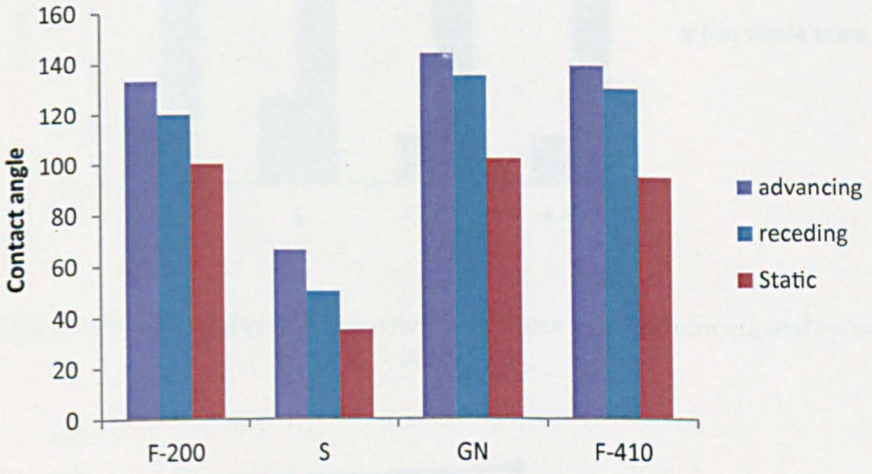

Figure 4.12 *Effect of stable brine film during oil deposition test.*

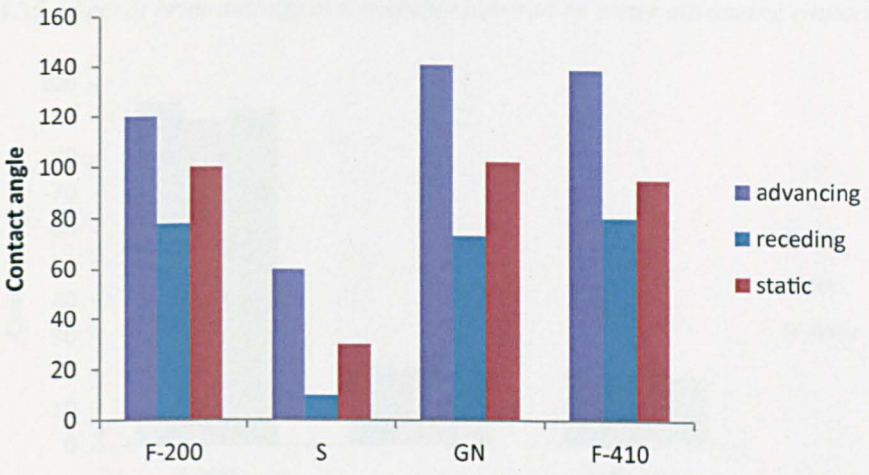

Figure 4.13 *Effect of instable brine film during oil deposition test.*

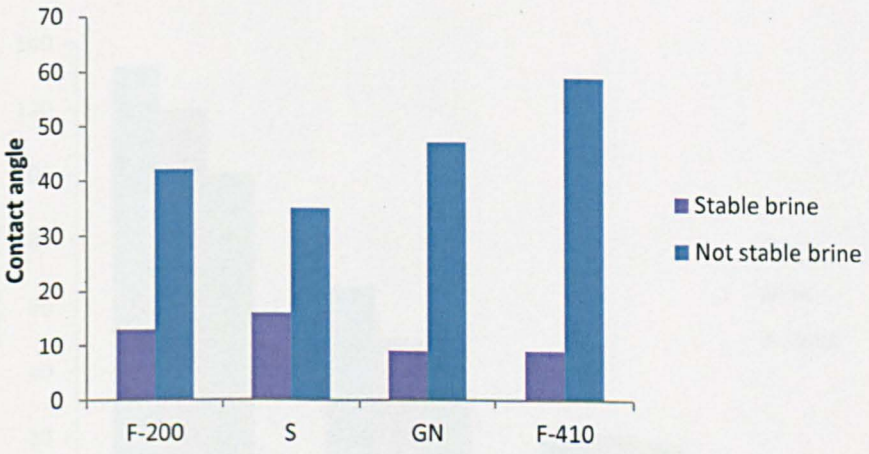

Figure 4.14 *Effect of brine stability film in hysteresis between water advancing and receding contact angle.*

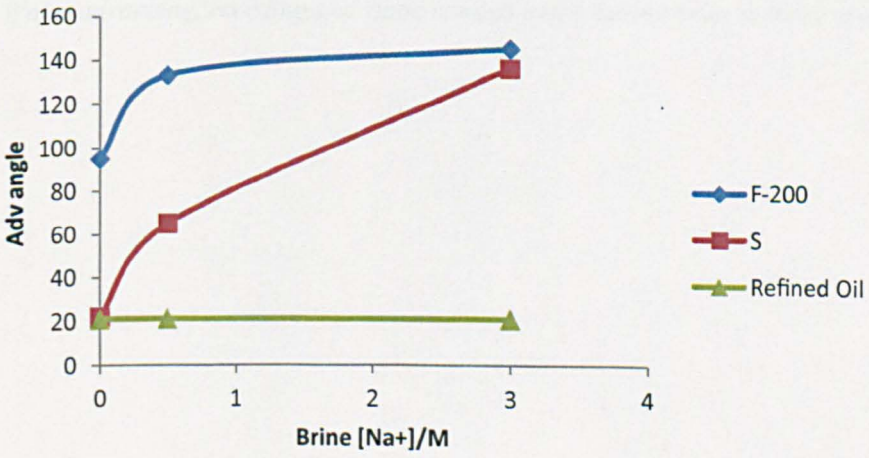

Figure 4.15 *Effect of brine salinity in wettability inferred by water advancing contact angle*

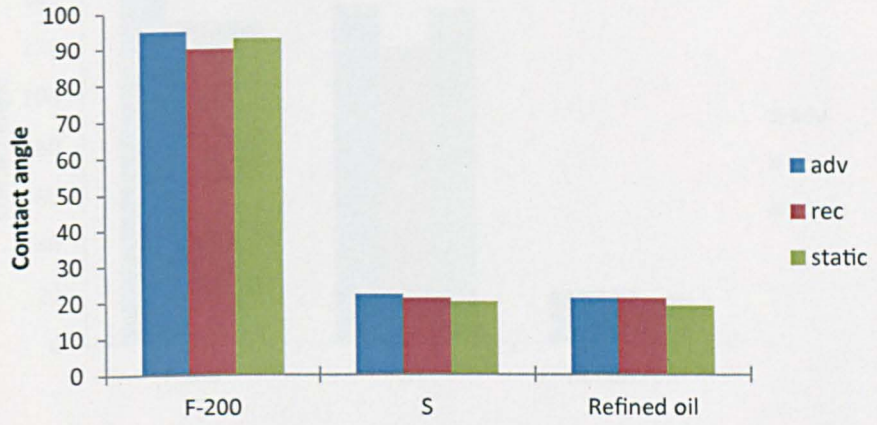

Figure 4.16 *Water advancing, receding and static contact angle during brine salinity of 0 M NaCl*

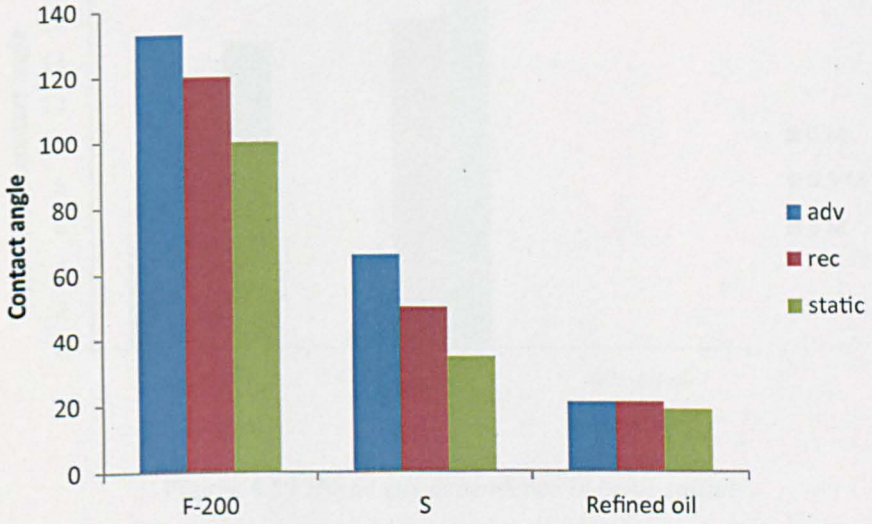

Figure 4.17 *Water advancing, receding and static contact angle during brine salinity of 0.5 M NaCl.*

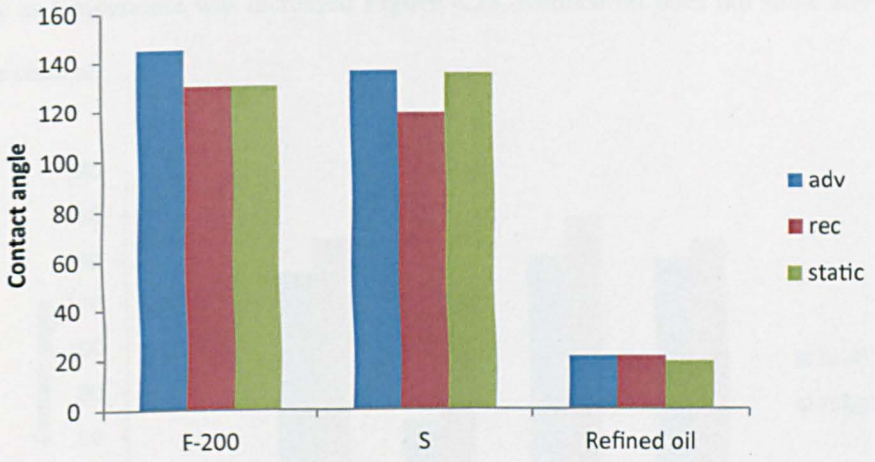

Figure 4.18 *Water advancing, receding and static contact angle during brine salinity of 3 M NaCl.*

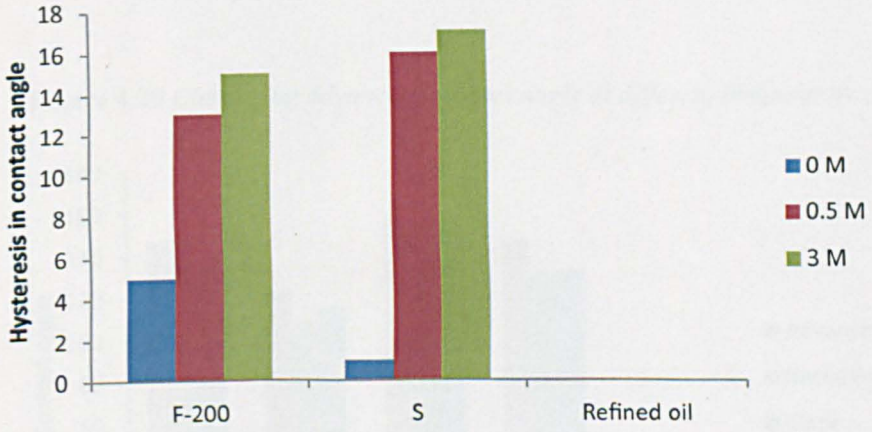

Figure 4.19 *Hysteresis dependence in brine salinity.*

4.3.5 Effect of temperature

After crude oil was allowed to interact with the silicate surface at 60°C, advancing contact angle increased by 15°, 57, 18° and 8° for F-200, S, GN and F-410 crude oils respectively **Figure 4.20**. Similar an incremental increase of static and receding angles were also observed. The hysteresis between advancing and receding contact angle shows a consistent decreasing trend as temperature increased to 60°C **Figure 4.21**. In particular, hysteresis was 13°, 16°, 9° and 9° for F-200, S, GN and F-410 respectively. The hysteresis dropped to 10°, 11°, 8° and 4° for F-200, S, GN, and F-410

respectively as temperature was increased **Figure 4.22**. Refined oil does not show any sensitivity to temperature change.

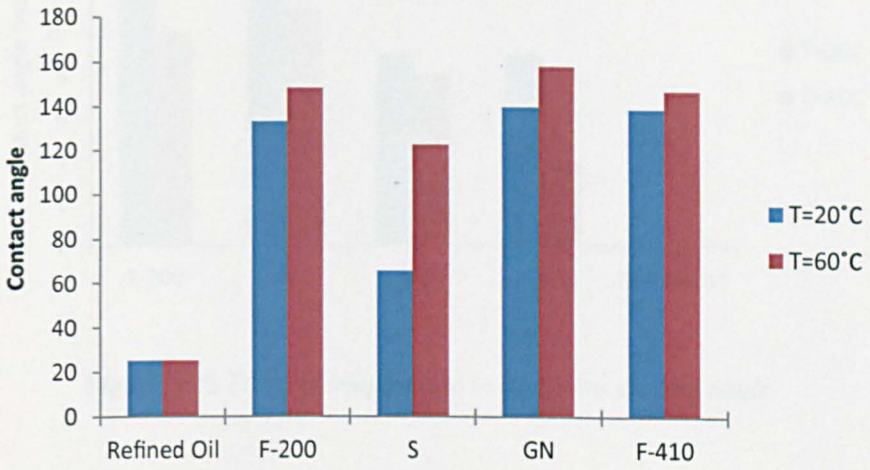

Figure 4.20 *Comparing advancing contact angle at different temperatures.*

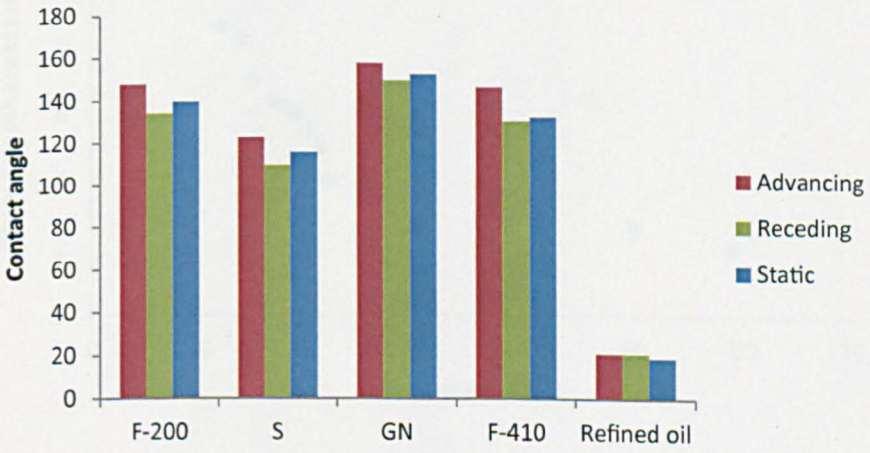

Figure 4.21 *Effect of temperature in solid surface treated with brine/crude at 60°C.*

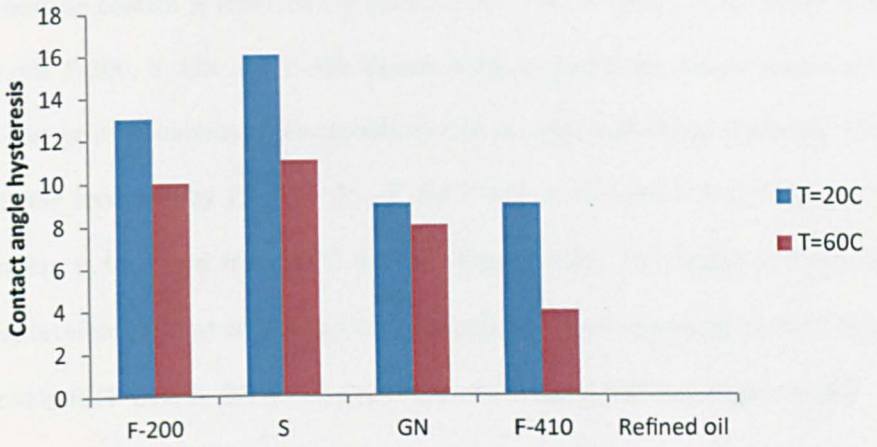

Figure 4.22 *Effect of temperature in hysteresis contact angle.*

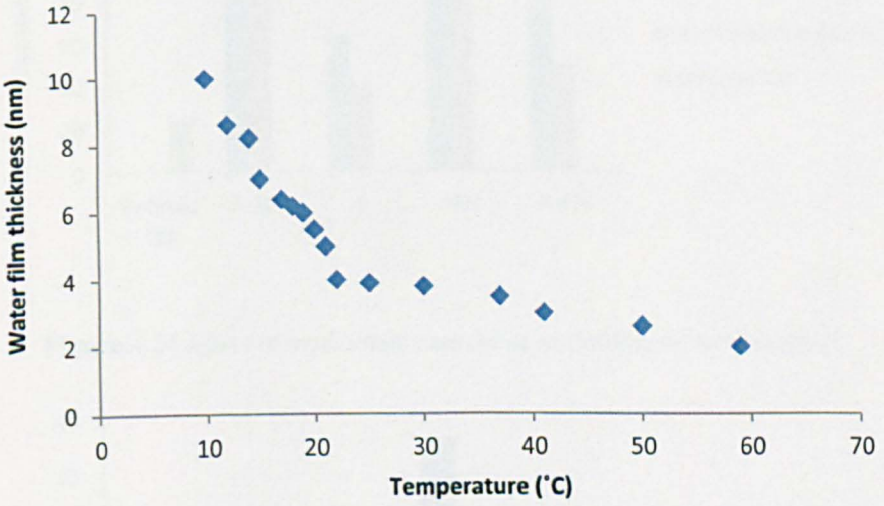

Figure 4.23 *The thickness of water film residing in fused silica as function of temperature after Derjaguin (1987).*

4.3.6 Effect of asphaltene content

Removing asphaltene from crude oils decreased the oil-wetness of the solid surface. In particular, the advancing contact angle drops by 33˚, 24˚, 38˚, 89˚ for F-200, S, GN and F-410 respectively **Figure 4.24**; similar reduction in receding and static contact angles. The result confirms that asphaltene content is a major crude oil component responsible for alteration of wettability of solid surface. The hysteresis between advancing and receding contact angle is increased noticeably to 30˚, 38˚, 26˚ and

24° when asphaltene content is removed compared to 13°, 16°, 9° and 9° when asphaltene content is still in crude oils F-200, S, GN and F-410 **Figure 4.25**. Furthermore, temperature does not induce such a major change in wettability of de-asphaltene oils as when asphaltene is present. The advancing contact angle only increased by 13°, 18°, 4°, 11° for F-200, S, GN and F-410 crude oils respectively when temperature is increased from 20°C to 60°C **Figure 4.26**. The degree of hysteresis between advancing and receding contact angles reduced compared to those measured at 20°C to reach 4°, 4°, 6°, 4° respectively for F-200, S, GN and F-410 crude oils (**Figure 4.27** and **Figure 4.28**).

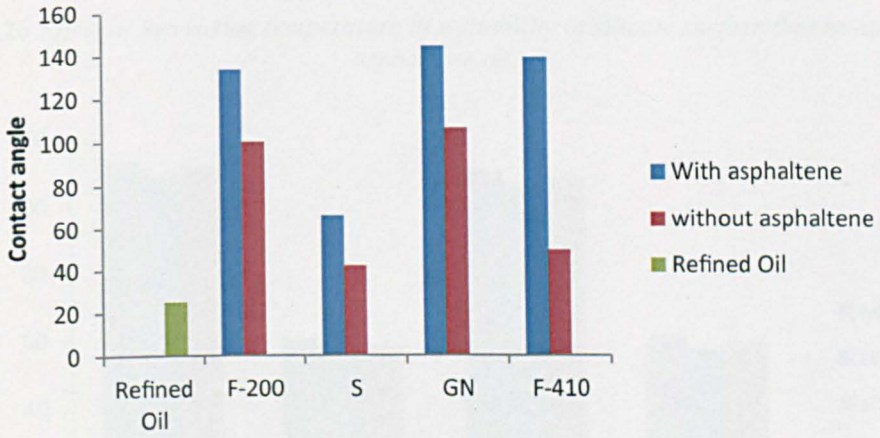

Figure 4.24 *Effect of asphaltene content in wettability of solid surface.*

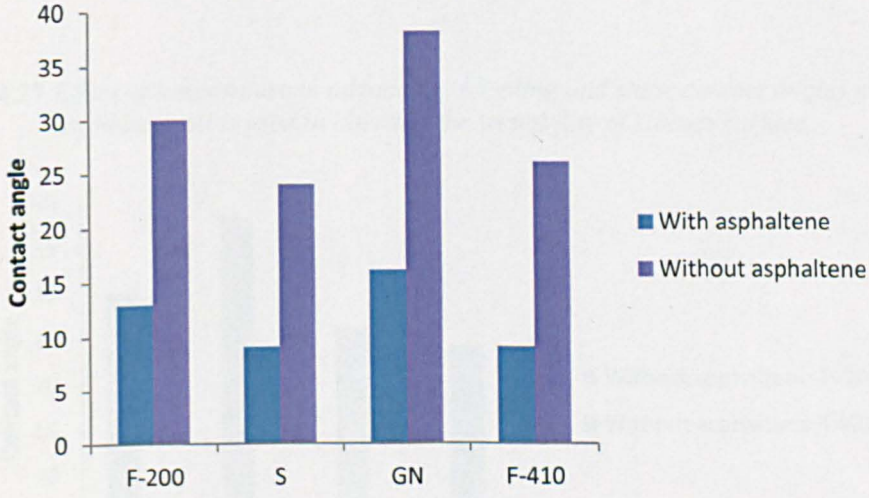

Figure 4.25 *Effect of asphaltene content in hysteresis between advancing and receding contact angle at temperature T=20°C.*

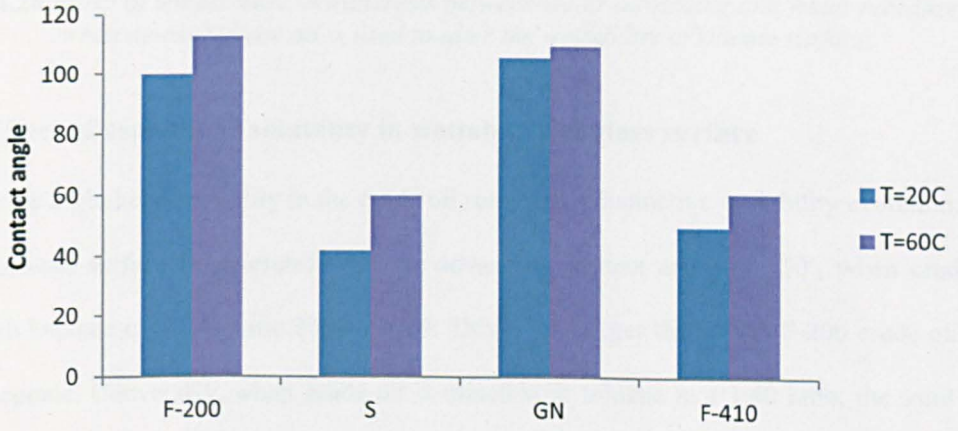

Figure 4.26 *Effect of increasing temperature in wettability of silicate surface that treated by de-asphaltene oil.*

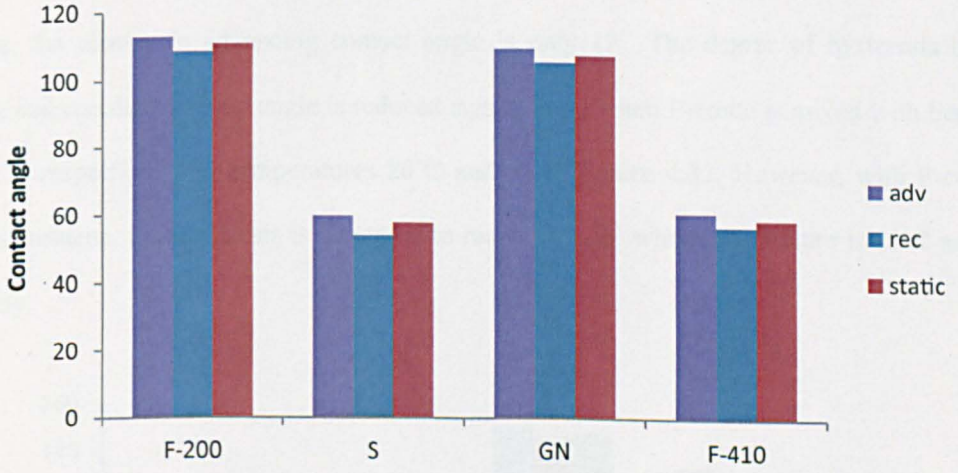

Figure 4.27 *Effect of temperature in advancing, receding and static contact angles when de-asphaltene oil is used in alterting the wettability of silicate surface.*

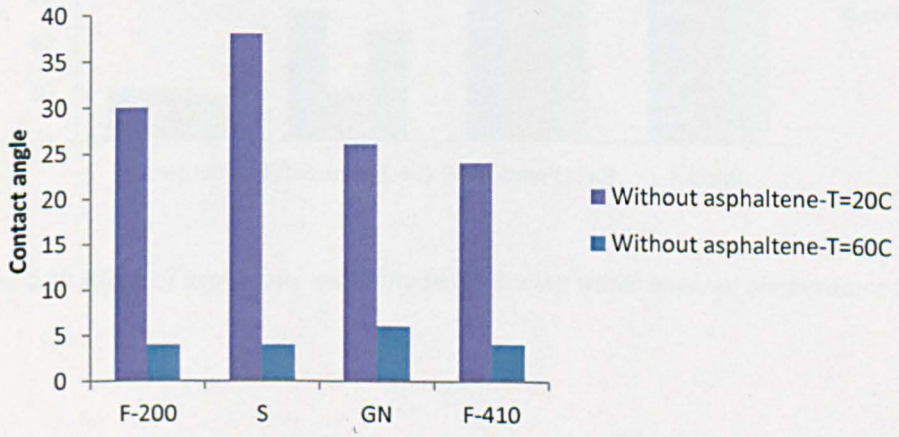

Figure 4.28 *Effect of temperature in hysteresis between water advancing and water receding angle when de-asphaltene oil is used to alter the wettability of silicate surface.*

4.3.7 Effect of asphaltene solubility in wettability of glass surface

Changing the asphaltene solubility in the crude oil results in a distinctive wettability evolution. A very strongly oil-wet surface is generated, with an advancing contact angle of 150°, when crude oil is mixed with heptane in a 1:40 ratio **Figure 4.29.** This is 17° larger than when F-200 crude oil is used without heptane. Conversely, when crude oil is mixed with toluene in a 1:40 ratio, the solid surface experiences a sharp reduction in its oil-wetness with advancing contact angle of 53°. An increase of advancing contact angle to 165° is observed for the mixture of crude oil:heptane when temperature is increased to 60°C **Figure 4.31**. However, when temperature is increased for a mixture of crude oil:toluene, the change in advancing contact angle is only 19°. The degree of hysteresis between advancing and receding contact angle is reduced significantly when F-crude is mixed with heptane to reach 5°, 3° respectively for temperatures 20°C and 60°C **Figure 4.32**. However, with F-crude oil mixed with toluene, the hysteresis is increased to reach 33°, 35° when temperature is 20°C and 60°C respectively.

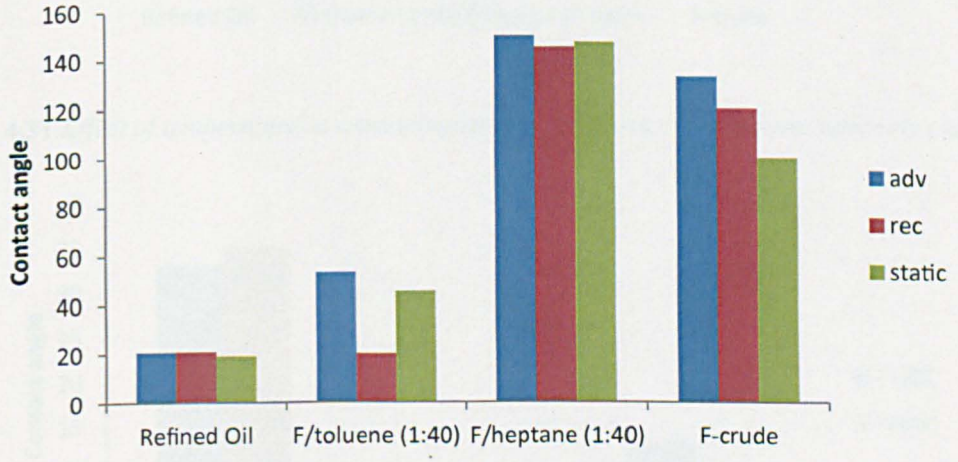

Figure 4.29 *Effect of asphaltene solubility in advancing water angle at temperature 20°C*

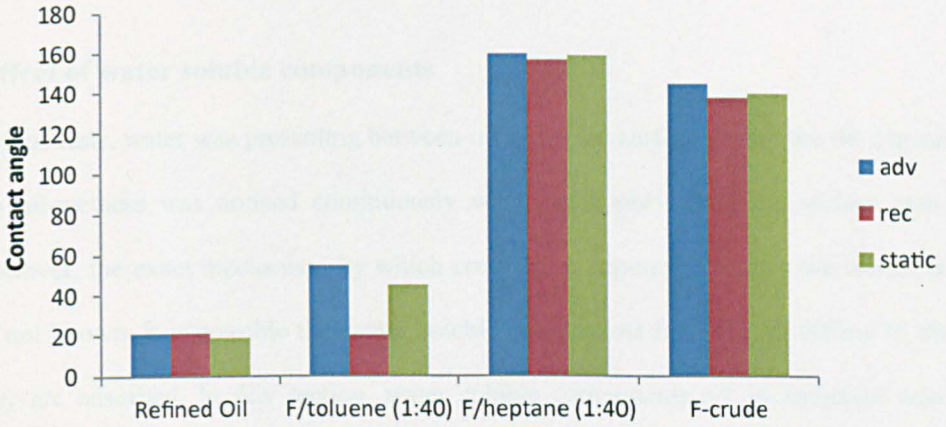

Figure 4.30 *Effect of asphaltene solubility in advancing water angle at temperature 60°C*

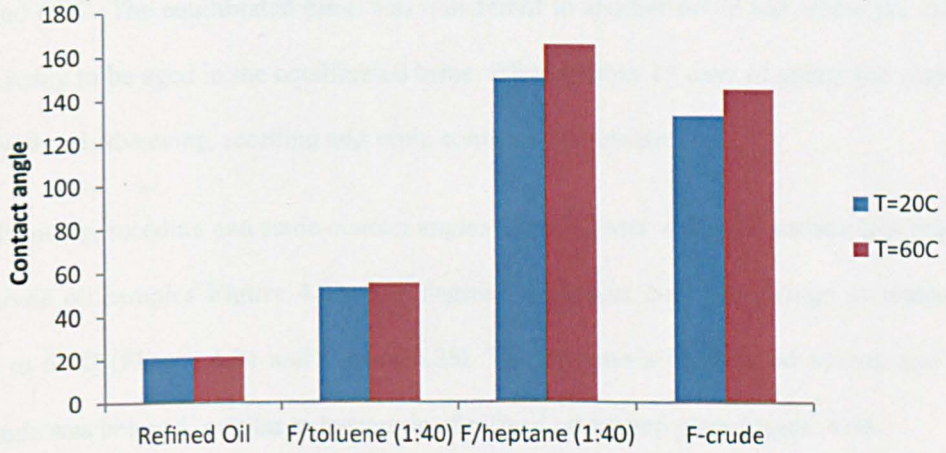

Figure 4.31 *Effect of temperature in advancing contact angle when asphaltene solubility changed.*

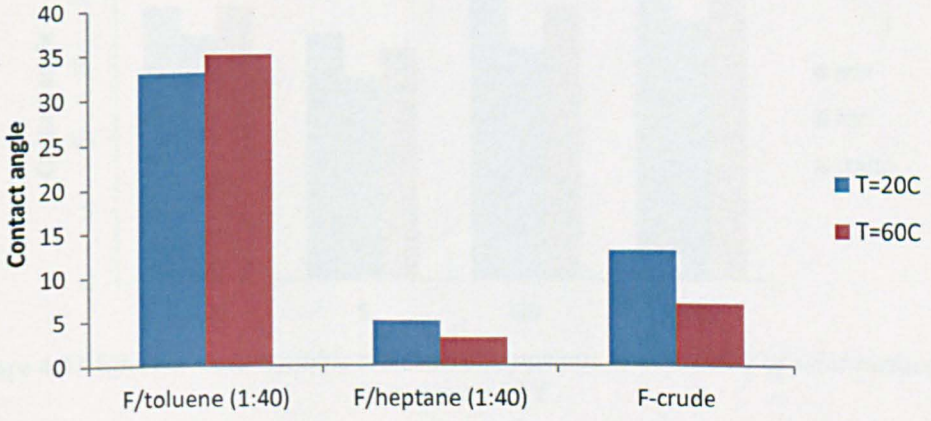

Figure 4.32 *Effect of temperature when in contact angle hysteresis when asphaltene solubility is changed.*

4.3.8 Effect of water soluble components

In all previous tests, water was presenting between oil and solid surface during the oil deposition test. Increasing oil-wetness was noticed continuously when brine pre-wetted the surface (see **Section 4.3.3**). However, the exact mechanism by which crude oil components change the wettability of the surface is not known. It is possible that water soluble components from the oil diffuse to the surface where they are adsorbed. In this section, water soluble components are investigated whether this mechanism contributes to the final wetting state of the solid surface. F-200, S, GN and F-410 crude oil components were initially selected to equilibrate with the brine phase for 13 days at temperatures of 20°C and 60°C. The equilibrated brine was transferred to another bottle test where the clean glass surface is ready to be aged in the equilibrated brine. After another 13 days of aging, the glass surface was removed and advancing, receding and static contact angle measured.

All the advancing, receding and static contact angles show a water-wet solid surface less than 20° for all four crude oil samples **Figure 4.33**. The degree of wetness does not change as temperature is increased to 60°C (**Figure 4.34** and **Figure 4.35**). The hysteresis between advancing and receding contact angle was below 5° similar to hysteresis of refined oil treated glass **Figure 4.36**.

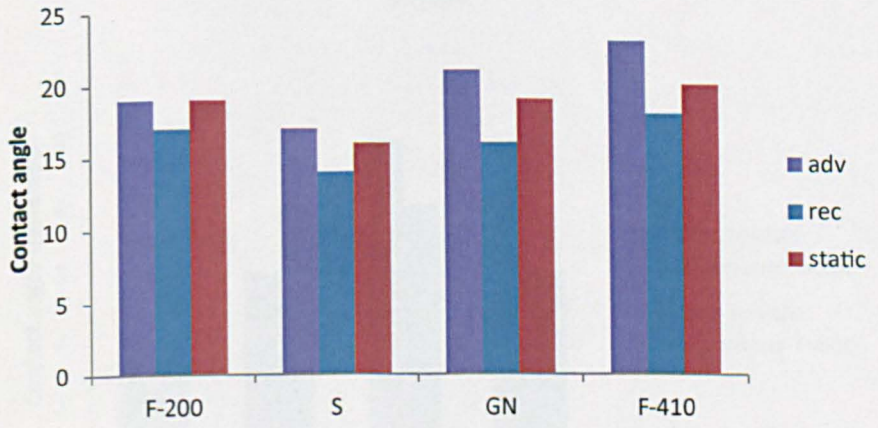

Figure 4.33 *Effect of water-soluble crude oil components in wettability of solid surface at temperature 20°C.*

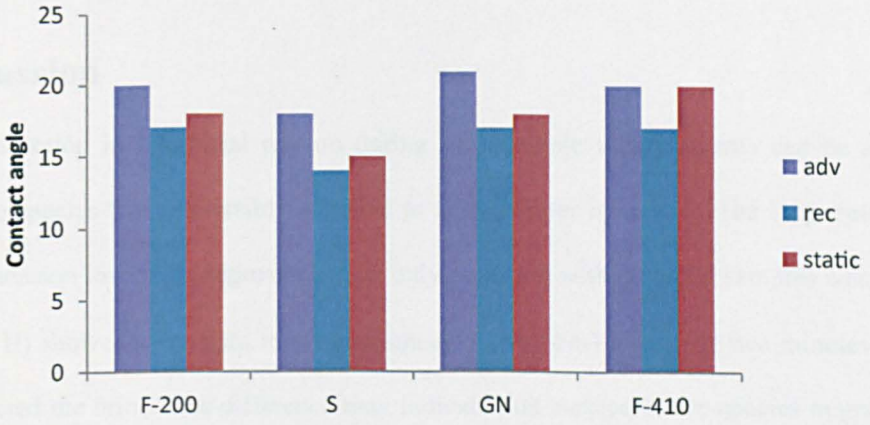

Figure 4.34 *Effect of Water-soluble crude oil components in wettability of solid surface at temperature 60°C.*

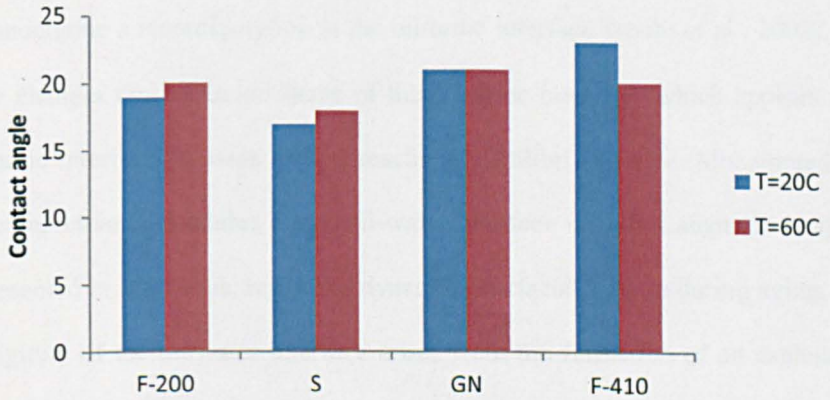

Figure 4.35 *Effect of temperature in water-soluble crude oil components in wettability of solid surface.*

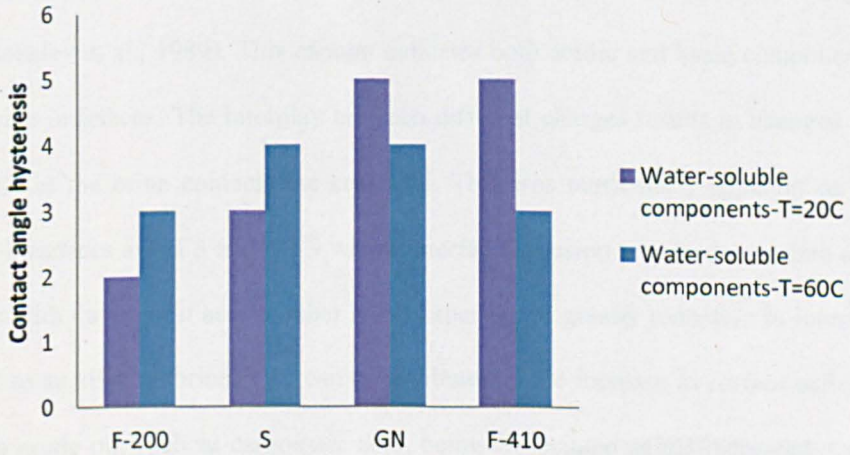

Figure 4.36 *Hysteresis effect when temperature is changed for water-soluble crude oil components in wettability of solid surface.*

4.4 Discussion

The larger reduction in interfacial tension during the dynamic measurements can be attributed to surface-active-species that irreversibly attached to the oil/water interface. The long time relaxation (75 min) for tension lowering (**Figure 4.1**) was only observed with crude oil samples whereas refined oil (multipar H) showed a constant interfacial tension (23 mN/m) after only two minutes from when the oil contacted the brine. The difference may indicate that surface-active-species migrate from the crude oil to reach the oil/brine interface and gradually reduce the interfacial tension until the oil/brine interface is saturated with the surface active components. Asphaltenes tend to diffuse through the bulk crude oil and undergone a reconfiguration at the oil/brine interface (Jeribi et al., 2002). This transfer in the interface changes the Laplacian shape of the oil-brine interface, which appears as a transient change in dynamic interfacial tension until it reachs its equilibrium value. Mohammed et al. (1993) measured the compressional modulus of the oil-water interface using a Langmuir trough. Similar to the findings presented in this thesis, regarding dynamic interfacial tension during aging, these authors conclude the rigidity of the oil/water interface arises from the formation of an asphaltenic network structure that strengthens with aging time. This supports the idea that reconfiguration of the asphaltene network is modifying the interfacial tension.

It is well known that the crude oil surface has a net positive charge at low pH and net negative charge at high pH (Buckley et al., 1989). This change indicates both acidic and basic components are active at crude oil/brine interfaces. The interplay between different charges results in changes of interfacial tension as soon as the brine contacts the crude oil. This was particularly apparent on more highly charged brine interfaces at pH 3 and pH 9 where interfacial tension was far lower than at neutral pH. The crude oils with the highest acid number (AN) experienced greater reduction in interfacial tension when exposed to an alkaline brine. This can be attributed to the increase in surface activity for acidic components in crude oil, such as carboxylic acid, being dissociated as pH increased. Comparing the reduction of interfacial tension of S-crude (AN=0.05) with reduction of interfacial tension of GN-crude (AN=0.90) is consistent with this explanation. At pH=9, interfacial tension of S-crude drops

only by 3 mN/m whereas the GN-crude interfacial tension drops by 18 mN/m. The sensitivity of interface activity to pH is very comparable to the sensitivity of stearic acid model oil and water interface as investigated by Cratin (1993). Similar behaviour is observed when brine is acidic at around pH = 3, the crude oils that have the highest base number experience more reduction in interfacial tension. All crude oils have a high base number except the S-crude, which has a base number of 0.6. S-crude shows a drastic reduction in interfacial tension from around 27 mN/m to 2.5 mN/m as pH decreases from 6 to 3. This is attributed to the increase in surface activity for base components in the crude oil, such as basic amines, being dissociated as pH decreased (Mullins et al., 2007). The interfacial tension tends to be similar for most salinities, however, the reduction in interfacial tension was noticed at salinities above 1.5 M. It is noteworthy that IFT passes through a minimum at specific brine concentration. This can be attributed to that polar components in crude oil aggregating at the brine/oil interface at specific concentrations above the so-called "critical micelle concentrations" (Rosen, 1989). The aggregation rate of crude oil micelles tends to increase as the brine concentration increases until the brine salinity reaches 2.5 M NaCl. More saline brines cause the aggregation rate to level out, which makes the interfacial tension constant at higher brine salinity. This explanation is consistent with the behaviour of refined oil interfacial tension, which shows no dependence on brine salinity concentration as a result of an absence of micelle aggregation at the oil/brine interface.

Toluene, decalin and water are all effective cleaning agents for silicate surfaces without affecting the nature of the surface as inferred from contact angle measurements. However, dichloromethane was shown to be an aggressive solvent that decreases the surface affinity to water five times more than the other cleaning agents. The combination of high dynamic contact angles and very low hysteresis of surfaces cleaned by dichloromethane suggests that a change of original wettability of silicate surface occurred (Brzoska et al., 1994). Although all solvents create a silicate surface that is in the water-wet region, dichloromethane was excluded in subsequent tests to prevent further complicated alteration of the silicate surface.

After oil deposition test, some of non-deposited bulk oil remains on the treated surface and it is an essential step to remove this before making the contact angle measurement over the treated surface. Washing the glass slide with toluene increased the affinity of the glass slide to water seven times more than decalin. Furthermore, washing with toluene makes the affinity of the treated glass surface to water the same as untreated glass **Figure 4.5**. This confirms that toluene removed all the crude oil components that were adsorbed on the surface during the oil deposition test. Previous observations indicate that decalin is a mild solvent that has lesser effect than toluene on crude oil adsorbed species. Therefore, decalin was selected to be used as a solvent to remove the bulk oil from the glass surface after the oil deposition test.

All the results suggest that the contact angles of dry glass surfaces are higher than for the pre-wetted glass surfaces when crude oil is used during the oil deposition tests. However, this is not observed when refined oil is used; here contact angles are the same for glass surfaces whether or not they were pre-wetted with brine. These results are consistent with the idea that water partially shields the surface from subsequent adsorption of crude oil components. Collins and Melrose (1983) measured asphaltene adsorption onto a solid surface and found the water pre-adsorbed on surface reduces the subsequent adsorption of asphaltenes compared to surfaces that do not have water residing prior to asphaltene adsorption. Furthermore, based on thermo-gravimetric analysis (TGA), Alipour Tabrizy et al. (2011) show that high humidity inhibits the adsorption of asphaltene. According to their work, the adsorption enthalpy of quartz that is initially wetted by water and modified being by asphaltene adsorption reduces by is 30 KJ/mol lower compared with quartz that does not have water residing in its surface. The reduction of the affinity of water by surfaces treated with brine and crude oil results from brine promoting adsorption of oil components on to the glass surface resulting in a more oil-wet state. The reason for enhanced adsorption is that brine film provides the medium for the electrical interaction between the oil and glass surface. This medium of electrolyte does not exist with the distilled water, which make the water film act as a barrier for oil adsorption. The crude oil components seem to adsorb to glass surface without the water film through van der Waals attraction force only (Hirasaki, 1991).

The presence of brine increases the degree of hysteresis between the advancing and receding water contact angle compared with surfaces that are treated directly by crude oil or surface treated with deionised water before crude oil deposition. This may be related to the so-called Dalmation wetting patterns previously reported by Kaminsky et al. (1994) and Ese et al. (2000), which arise from water pockets being trapped beneath the asphaltene coating on the solid surface. The Dalmation wetting pattern results in a heterogeneous adsorption of crude oil on mineral surfaces that are pre-wetted by brine. The effect of this wettability pattern is manifest in the large degree of hysteresis, which has not been observed when crude oil is directly adsorbed on the solid surface that has not been pre-wetted by brine.

The only brine condition that shows adhesion of oil droplets to a silicate surface after a short time adhesion test was with a low pH (pH=3) brine with a salinity of 0.1 M. Along with the negative nature of silicate surface, the attraction forces dominate over the brine, which results in destabilization of the brine film and adhesion of oil droplets. The longer-term oil deposition test reveals that hysteresis is more than double when an unstable brine film occurs between crude oil and the glass surface to when a stable film exists. The similarity in advancing contact angle despite the brine stability alternating suggests that adsorption of oil components onto the silicate surface has a different pattern. This results in a more heterogeneous wetting surface for the unstable brine film, which results in a large difference between advancing and receding angles. **Figure 4.37** is a schematic diagram of an unstable brine film present between the crude oil and silicate surface. The aggregation of crude oil components occurs in a way that they do not entirely cover the silicate surface. This increases the contact angle as it advances over oil-wet patches of macromolecules deposited on the surface. The water contact angle interacts with regions on the surface that are not fully covered by oil-wet patches and it recedes. This results in a lower receding contact angle, and high hysteresis. Conversely, aggregation of oil components seems to be somewhat more uniform when brine film is stable resulting in more coverage of the silicate surface and similar water advancing and receding contact angles. Lord and Buckley (2003) calculate the mean roughness using the atomic force microscopy (AFM) for surfaces treated by crude oil in presence of stable and non-stable brine film. The mean roughness, when stable brine was

present, was 36 times lower than when non-stable brine is used. Kumar and Fogden (2009) using field emission scanning electron microscopes (FESEM) to further illustrate the impact of brine film stability on the deposition of oil components on surfaces. In particular, their study showed that irregular branch deposits formed when unstable brine film is present whereas more continuous oil deposition existed if the brine film is stable.

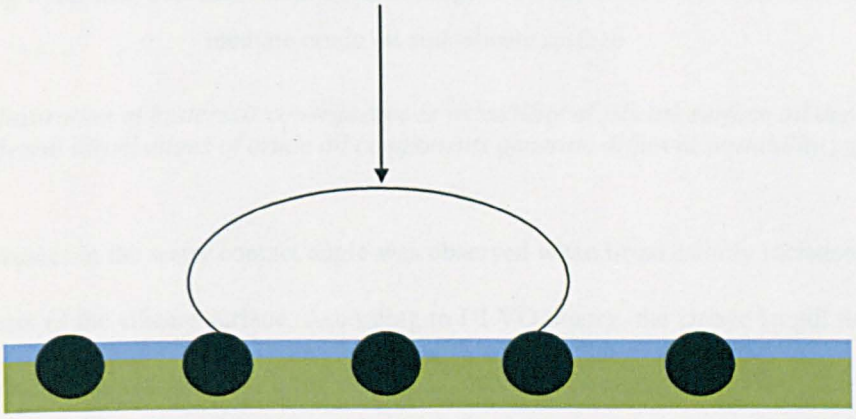

(a) Advancing water into a silicate surface that undergone oil deposition test with unstable brine that mediate crude oil and silicate surface

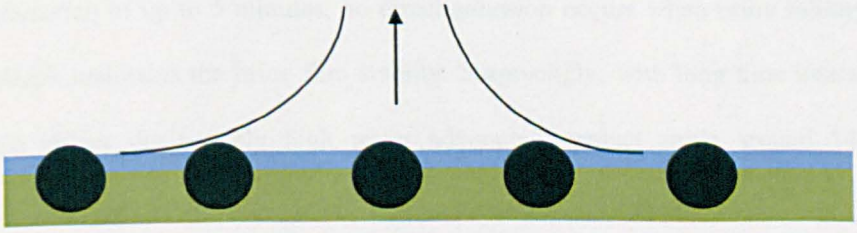

(b) Receding water into a silicate surface that undergone oil deposition test with unstable brine that mediate crude oil and silicate surface

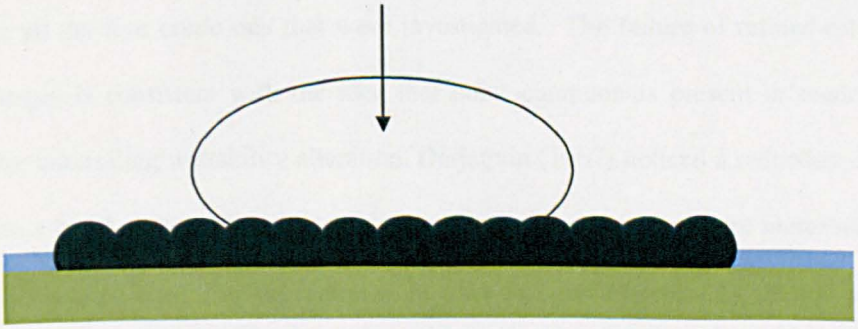

(c) Advancing water into a silicate surface that undergone oil deposition test with stable brine that mediate crude oil and silicate surface

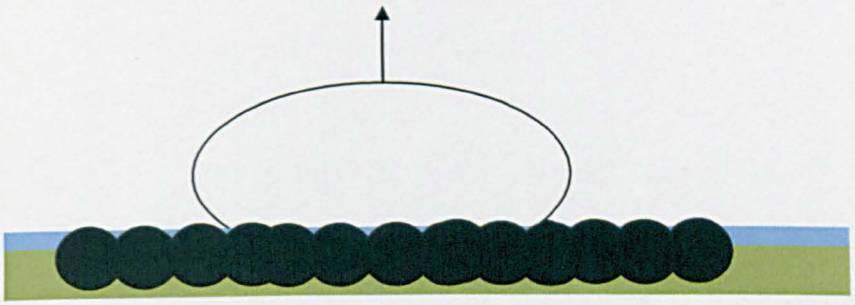

(d) Receding water into a silicate surface that undergone oil deposition test with stable brine that mediate crude oil and silicate surface

Figure 4.37 *Illustration of hysteresis consequence in wettability of silicate surface oil deposition test. Two different distributions of crude oil components generate different wettability pattern.*

Consistent increases in the water contact angle was observed when brine salinity increased promoting more oil-wetness of the silicate surface. According to DLVO theory, the Debye length decreases and the double layer is compressed when brine salinity is increased (Adamson and Gast, 2007). This will tend to destabilise the water film between the crude oil and solid surface, which gives the polar components in the crude oil an increased chance of adsorbing to the mineral surface. However, during short time interaction of up to 5 minutes, no direct adhesion occurs when brine salinity is varied at neutral pH, which maintains the brine film stablity. Surprisingly, with long time interaction, the oil deposition test shows distinctively high water advancing contact angle around 140°, which is consistent with adsorption of polar crude oil components onto the surface.

Increasing the temperature from 20°C to 60°C clearly induced a wettability alteration towards more oil-wetness for all the four crude oils that were investigated. The failure of refined oil to generate wettability changes is consistent with the idea that polar components present in crude oil are the governing factor controlling wettability alteration. Derjaguin (1987) noticed a reduction of water thin film residing on a fused silica surface as temperature increased. As temperature increased from 20°C to 60°C, the thickness of water film decreased from 5 nm to 2 nm **Figure 4.23**. Based on the results from oil deposition tests presented earlier, the polar components from crude oil have more chance to penetrate the thinner water films at 60°C than at lower temperatures, which provides more access to

the silicate surface than at 20°C. Consequently, the degree of water-wetness of the solid surface decreased further by increasing the temperature. The further reduction of hysteresis observed when the temperature is increased from 20°C to 60°C can be attributed to an increase of asphaltene multi-layers on the solid surface. Along with the brine film diminished, increasing asphaltene multilayers will give a more compact hydrophobic surface with less heterogeneous distribution. Golton et al. (1992) suggest that asphaltene tends to adsorb on the quartz surface in a multi-layer mode.

The type of crude oil polar components that penetrate the thin film are mainly asphaltene because when asphaltene is removed from the crude oil samples, major reduction in oil-wetness degree is observed **Figure 4.24**. Furthermore, when temperature is increased, it was clear that thinning of the brine film without the asphaltenes yields a very minor change in wettability of the solid surface. Moreover, the absence of asphaltene generates more hysteresis compared to when asphaltene is present. The reason for that can be ascribe to the type of coverage of adsorption components on the silicate surface. These findings are consistent with the AFM work of Ese et al. (2000), which found that asphaltene deposited on silicate surface has a closed packed structure with film material consisting of round disks or rod-formed units. Conversely, deposits formed from deasphaltene crude oil, have an open structures with a non-uniform pattern. The results from the experiments presented in this chapter can relate the higher degree of hysteresis with de-asphaltene oil to the non-uniform open structures deposit of de-asphaltene oil.

The presence of asphaltene in crude oil is also not sufficient to induce the wettability alteration towards oil-wetness. In other words, the condition that is required is asphaltene aggregation and subsequent precipitation on the solid surface. This discussion inferred from **Figure 4.29**, which shows when crude oil is mixed with known precipitant that make the asphaltene macro-molecules to destabilised in the mixture of heptane and crude oil. The result from oil deposition tests confirms the very high degree of oil-wetness that can be obtained when destabilisation of crude oil occurs. The high degree of oil-wetness seems to exist after asphaltene macromolecules aggregate and adsorb in the solid surface. Conversely, if the asphaltene have been stabilised by mixing in a good solvent such as toluene, the surface will retain its hydrophilicity. The correspondence between the existence of

asphaltene aggregation and low hysteresis was clearly evident and suggests that aggregation of asphaltene makes the adsorption on the surface more homogenous.

4.5 Conclusion

Studying the wettability of the COBR system using a smooth mineral surface provides a useful framework to understand the sensitivity of wettability to brine composition, crude oil composition and temperatures. Six main conclusions emerge from this study:

- Refined oil does not alter the wettability of silicate surface but crude oil can result in wettability alteration.
- Removing asphaltene from crude oil fractions makes the silicate surface less oil-wet. However, making the asphaltene stable by mixing the crude oil with toluene has a more profound effect on wettability; it can reduce the ability for crude oil to alter the wettability of the silicate glass surfaces.
- Crude oil components that are soluble in water only caused a very minor change in the wettability of silicate surfaces.
- Silicate surface contacting brine before aging in crude oil generates different wettability behaviour than silicate surface aged directly in crude oil; oil wettability was higher when brine is residing on the silicate surface.
- Increasing the temperature causes the wettability of silicate surface to become more oil-wet. Lack of wettability reversal as function of temperature, when asphaltene is absent from crude oil, indicate the presence of asphaltene in crude oil is a critical factor.
- Changing the salinity of brine induced a change in crude oil/brine/silicate contact angle.

Chapter 5
Micromodel Investigation of Brine Salinity and Temperature effect in Multiphase Flow

Understanding the microscopic displacement efficiency is a vital part of enhanced oil recovery design. In this chapter, a micromodel tool is utilised to visualise the movement of oil and brine into pore morphology that is representative of reservoir rock. Two main variables investigated are the brine composition and temperature. The visualisation of distinctive pore scale events is coupled with analysis of the relative permeability.

5.1 Introduction

Oil recovery is controlled by several parameters including, the size of the matrix block/fracture spacing, pore structure, fluid properties (density, viscosity and interfacial tension), wettability, thermodynamic conditions (temperature) and boundary conditions (Cuiec et al., 1994). Understanding the impact of wettability is of particular importance for designing EOR programmes (Al-Mjeni et al.,2011). Various approaches have been used to investigate *in situ* wettability ranging from core scale studies to field. However, sorting out the many factors that control multiphase flow is difficult when the only data available are changes in pressure and volumes of the produced phases as a function of time. The ability to visualise the movement of fluid interfaces makes it possible to distinguish between different flows mechanisms, which in turn allows different production behaviour to be explained.

Micromodels are two-dimensional (2-D) flow cells that have a network pattern of flow channels to represent idealized porous media. They offer a high resolution method to visualize the wetting film and fluid interfaces under a range of temperature and chemical conditions. The first report of micro-

scale observations of two-phase flow was from Chatenever and Calhoun (1952) who made packs from single layers of glass and Lucite beads and observed immiscible displacements with brine and crude oil. Later, improvements in photo-etching emerged. The first application of etched glass networks was to provide a better visualisation of displacement (Mattax and Kyte, 1961), which is the basis of most glass micromodels used in the literature nowadays. A major advantage of the glass etching procedure is that a variety of patterns including regular and repeating models can all be made in glass micromodels. Recent advanced in plasma etching allow the design of smaller pore-throat diameters than the micromodels that were prepared by chemical etching, which is more realistic to a real porous medium (Salimi et al., 2008). Although glass micromodels have many applications in understanding the physical phenomena of multiphase flow, there are some limitations that should be considered. The main limitation in the micromodel is its two dimensional nature compared to the three-dimensionality of real porous media. Also, they don't contain point grain-to-grain contacts and as a result cannot develop true pendular ring structures of wetting fluid. Nevertheless, it is believed that many of the phenomena observed in two dimensions also occur in three dimensional rocks and so micromodels can be used as a basis for the understanding fluid flow in a real porous media. Sun and Tang (2006) reported on use of the first sandstone micromodel that was imported directly from thin section cores to preserve the original mineral and pore structure. Clean cores are cut into small chips and combined together between two glass plates with cementing technique without filling the pore space.

Micromodels have proven useful for wide range of applications including surface phenomena (Dullien et al, 1986); pore scale distribution of fluids (Morrow et al., 1986); wettability alteration by additives such as drilling fluid surfactants (Ballard and Dawe, 1988); impact of wettability on imbibition (Rangel and Kovscek, 2006) and the consequence of heterogeneity on fluid flow (Dawe et al., 2011). The advantage that micromodels offer in studying wettability phenomena is that the fluid distribution can be seen before, during and after the displacement. In the previous chapter, it was demonstrated that wettability of crude oil/brine/mono-mineral flat surfaces is very sensitive to brine composition and temperature. In this chapter, the previous investigation is extended to include the

visualisation of dynamic behaviour that includes capillary forces between the immiscible fluids, which was not including in the previous chapter in studying the effective wettability of flat surface.

Generally, two main approaches have been taken in studying wettability phenomena in the glass micromodels. Donaldson and Thomas (1971) used a crude oil to establish the initial wettability of a micromodel packed with clean sand. Their micromodel application was to study the effect of surfactant in sweeping the oil that remains after waterflooding. Morrow et al. (1986) investigated the ability of Moutray crude to induce a wettability alteration. As part of their work, pore network micromodels were used in which the initial wettability was established by equilibrating the pore network micromodels with crude oil at irreducible water saturation (S_{wi}) for 24 hours. Similar methods were used to establish the initial wettability of micromodels for studying: (i) the impact of brine pH (Jerauld and Rathmell, 1997) (ii) the effect of Water Alternating Gas (WAG) (Sohrabi et al., 2001), and (iii) the effect of alkaline flood in heavy oil (Alireza et al., 2010). The second approach uses organic coatings on glass micromodel to create uniform hydrophobic wetting (oil-wet) surfaces. Early work by (Morris and Wieland, 1963) used a surface active additive such as octylamine to destroy the natural affinity of the glass surface to water. By varying the concentration of octylamine in oil, different spectrums of wettability ranging from intermediate wettability with $15x10^{-3}$ mole per litres to strongly oil wettability with $30x10^{-3}$ mole per litres. Yu and Wardlaw (1986) were among the first who created an oil-wet glass micromodel using a silicone agent. The micromodels were then used to study the critical aspect ratio and contact angle for snap off flow mechanism at two extreme wettability conditions. Caruana and Dawe (1996) studied the effect of heterogeneous wettability on formation of residual oil and recovery factor due to capillary trapping by using glass beads coated by water repellent dimethyldichlorosilane to produce oil-wet region and untreated glass beads to produce water-wet regions. By packing both glass beads at different patterns, the effect of heterogeneous wettability were directly visualised.

In this chapter, both approaches are used to produce three different types of wettability namely as water-wet, mixed and oil-wet. Transparent glass micromodels provide a visualisation tool which allows the fluid distribution and pore-filling sequence to be observed at various conditions, including

salinity and temperature. The wettability of the silica pore surfaces in the micromodels is altered by interaction with crude oil components at conditions that are similar to the interaction observed in monomineral surfaces in **Chapter 4**. The possibility of altering brine salinity and temperature to improve better sweeping efficiency is evaluated through quantitative measurements such as pressure response and volume analysis, which are the main sources of information about the progress of displacements in real reservoir. Calculation of relative permeability is achieved using previous pressure measurements. Conditions representing distinctly different wetting states on flat silicate surfaces in Chapter 4 have been selected to observe their effects in the flow behaviour using the micromodels. The nature of micromodel work requires details descriptions of complex flow behaviour. Chatizis et al. (1988) classify the shapes of fluid blobs in the context of the pore partitioning of the rock: sub-singlet, and singlet. For example, singlet blobs occupy one pore body and have sizes equivalent to a single pore. In this chapter, concept of singlets flow is used to describe the flow behaviour.

The main aim of this chapter is to answer the following questions:-

- What are the pathways the invader follows during the displacement?
- What are the mechanisms responsible for trapping residual oil?
- What is the structure of trapping oil?
- Finally, how much of trapping residual oil is affected by change of wettability, brine salinity and temperature?

5.2 Experimental procedure

Glass micromodels were treated by three methods, which can provide three distinctive wettability states: (i) treated with refined oil (decane), (ii) treated by S-crude oil, and (iii) treated with water-repellent material (dimethyldichlorosilane). The cleaning of micromodels is accomplished by flushing solvents through the micromodel. The washing solvents include: distilled water, isopropyl alcohol (IPA) and dichloromethane (DCM), see **Figure 5.1**. Toluene is used in the cases where asphaltene precipitation was observed in the micromodel.

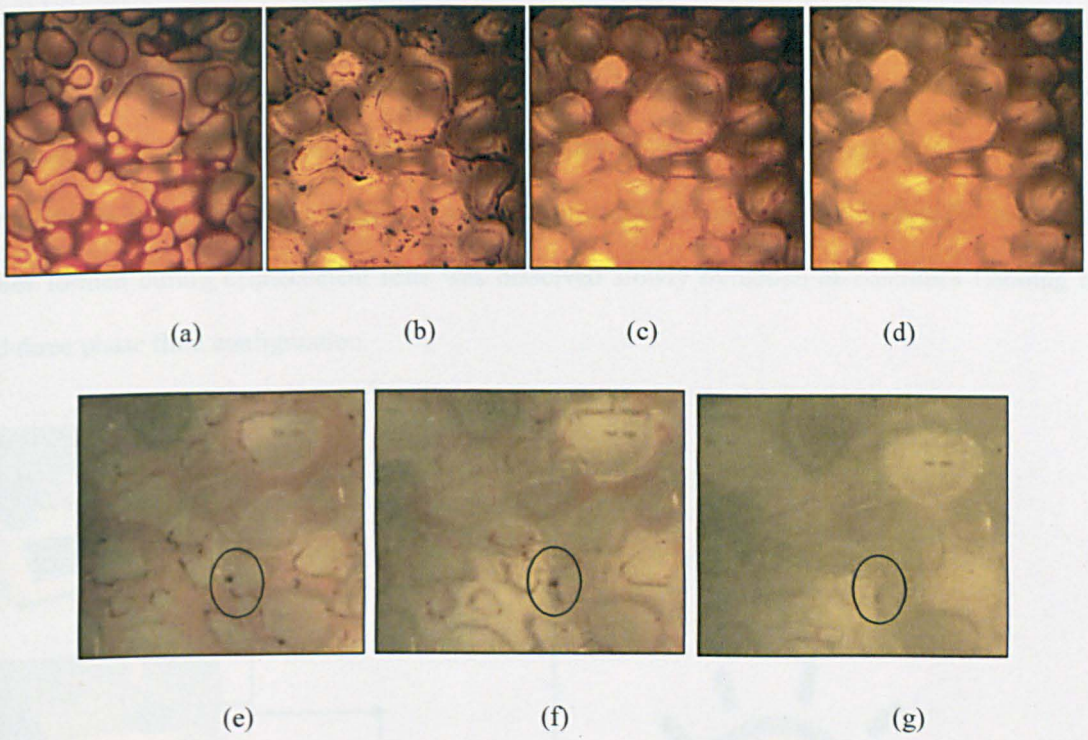

Figure 5.1 *Micromodel cleaning by different solvents. (a) Before cleaning; (b) After cleaning by IPA, 10 PV; (c) After cleaning by DCM, 20 PV; (d) After cleaning by DCM, 100 PV. (e) Special case when Asphaltene precipitation (inside circle). (f-g) flushing 10 PV toluene cleaning asphaltene.*

The wetting state of micromodels was confirmed to be water-wet by circulation of refined oil and water after every cleaning step, which shows water adhering to the glass surface and coating the grains, while oil occupies the centre of pores **Figure 5.2**.

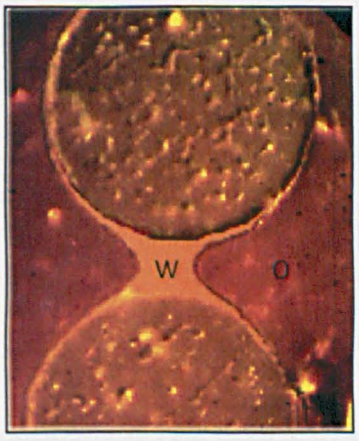

Figure 5.2 *After micromodel cleaning, pore throats are occupied by water which indicates the water-wetting state of micromodel. (Yellow=water, Brown=oil).*

Two main experiments were conducted in micromodels: steady state flow and slow rate imbibition. Injection of fluids in both experiments was controlled by microsyringe pump (World Precision Instruments, model number: (ALADDIN-1000) at constant rate of 1, 0.1 and 0.04 cc/min. The micromodel is maintained in a horizontal position to minimise the effect of buoyancy. Small air bubbles formed during displacement tests was dissolved slowly by action of continues flooding to avoid three phase fluid configuration.

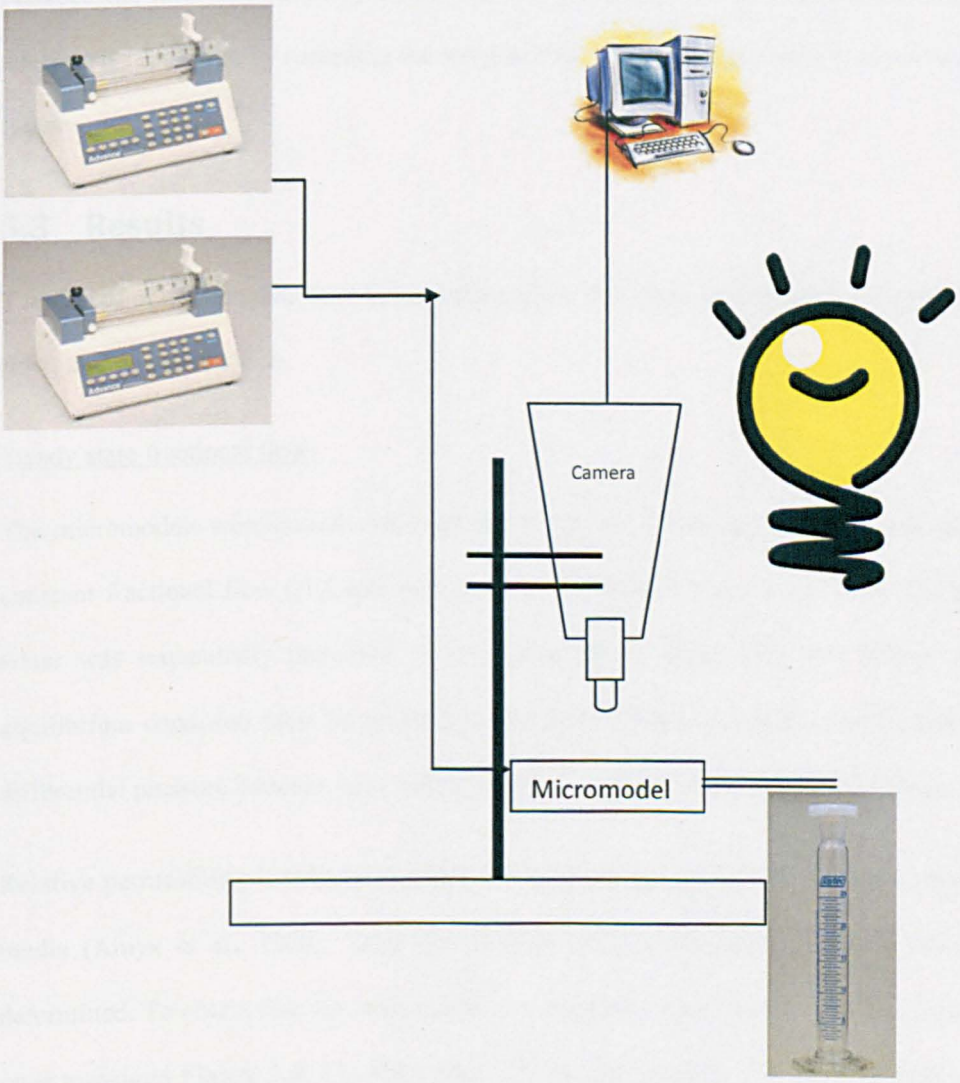

Figure 5.3 *Schematic diagram for micromodel. One pump is used for the waterflooding and both pumps for steady-state flow.*

In all micromodel experiments, three sources of data were collected: (i) fluid distribution, (ii) pressure response, and (iii) fluids volumes displaced. Fluids distribution is monitored by high-definition optical equipment for image capturing and analysis. Image analysis software was used to determine the saturations of oil and water at each fractional flow during steady state experiments. In image analysis, five rows next to each boundary of the micromodel are not taken into account to avoid end effects in determining the residual saturations. Pressure response is detected by a precise pressure transducer between the inlet and outlet of the micromodels. During slow rate imbibition experiments, volume analysis is monitored by recording the weight of the effluent versus time to determine the oil recovery factor.

5.3 Results

Two series of experiments have been conducted on 2-D glass micromodels: Steady state fractional flow, and water injection.

Steady state fractional flow:

The micromodels were initially fully saturated with oil. Water and oil was simultaneously injected at constant fractional flow (F_w) and total flow rate of 0.04, 0.1 and 1 cm^3/min. The fractional flow of water was sequentially increased in four steps (25%, 50%, 75% and 100%). At each ratio an equilibrium condition must be reached before the readings are taken. This is indicated by a stable differential pressure between inlet and outlet, and the fluid inflow and outflow ratios being the same.

Relative permeability is calculated based on the extended Darcy's law for two phase flow in porous media (Amyx et al., 1960). First, the absolute (base) permeability of each micromodel to oil is determined. To obtain this, the micromodel was saturated with oil and pressure drops at different flow rates measured **Figure 5.4**. The slope from differential pressure, ΔP, vs. flow rate, q, is a function of the absolute permeability:

$$k(abs) = \frac{L}{A} \times \frac{\mu}{Slope}$$

$$Slope = \frac{\Delta(\Delta p)}{\Delta(q)}$$

where, A is the cross sectional area, L is the length and μ is the viscosity.

Second, the effective permeabilities were then calculated by applying Darcy's law to oil and water individually at each fractional flow. Relative permeability for each phase is obtained by dividing the effective permeability to absolute permeability.

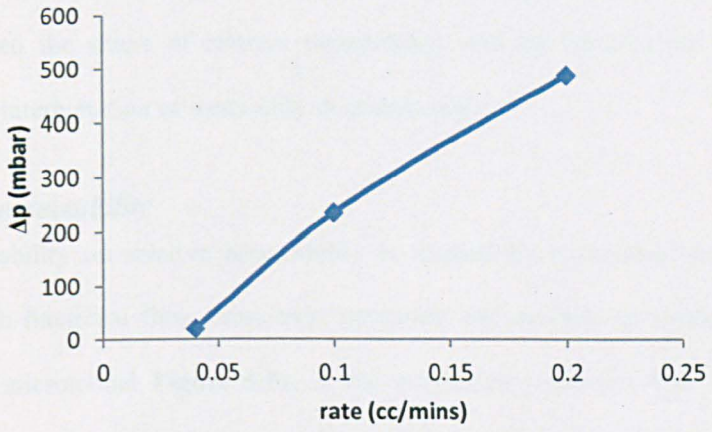

Figure 5.4 *Single phase flow in micromodel to determine the absolute permeability*

In summary, at each fractional flow rate the following procedure was followed;

- Set fractional flow rates,
- Monitor pressure until it stabilised,
- Photograph central portion of micromodel to obtain saturation data. Image J software was used to calculate the saturations of oil and water.

Waterflooding:

Waterflooding was performed with brine on the three wettability models treated by the same previous cases (refined, crude oil, silane). The rate of waterflooding is the minimum rate that can be offered by our microsyringe pump (0.01) cm^3/min for a micromodel initially saturated with oil.

5.3.1 Effect of wettability

Three wetting states were obtained in the micromodels according to method used to treat their internal glass surface: treatment by refined oil, treatment by crude oil and treatment by Repelcote (dimethyl di-chlorosilane). From the previous chapter, fluid system of refined oil and water provide a water-wet state for silicate surface compared to crude oil. Thus, water-wetness is achieved by saturating the model with brine and decane. A mixed-wet condition is achieved by aging the micromodel in crude oil for one day. Uniform oil-wetness is achieved by treating glass models with Repelcote. The combination between the shape of relative permeability and the microscopic flow visualisation provide the tool for interpretation of wettability in micromodels.

5.3.1.1 *Relative permeability*

The effect of wettability on relative permeability is studied by measuring the oil/water relative permeability at each fractional flow, cross-over saturation and residual oil saturation. Starting with refined oil treated micromodel **Figure 5.5a**, at the imbibition fractional flow of 25%, the water relative permeability (k_{rw}) does not change as rate increased from 0.04 cc/min to 0.1 cc/min in which 0.12 and 0.08 k_{rw} is attained respectively. Further increasing the rate to 1 cc/min doubles the k_{rw} to 0.23. Similar behaviour for k_{rw} is observed as water fractional flow is increased to 50%. In particular, k_{rw} does not show a significant increasing as rate increases from 0.04 cc/min to 0.1 cc/min. However, at 1 cc/min the k_{rw} becomes the double that observed at rates of 0.04 cc/min and 0.1 cc/min. Increasing flow rate results in an increase in k_{rw} when the imbibition fractional flow is changed to 100%. In particular, relative permeabilities of 0.44, 0.60 and 0.69 result from flow rates of 0.04, 0.1 and 1 cc/min. Less than 10% change in oil relative permeability (k_{ro}) was observed during the imbibition experiments at fractional flows of 25% and 50%. In particular, the k_{ro} changed from 0.26 and 0.17 when the rate increased from 0.04 cc/min to 1 cc/min. Increasing the rate to 1 cc/min causes the k_{ro} to increase 22% compared with a rate of 0.04 cc/min. At imbibition fractional flow of 50% and 75%, minor change is occurred less than 10% between all the rates that investigated. At fractional flow of 100%, the oil is totally trapped despite the change in rates. The residual oil saturation (S_{or}) appears independent of flow rate. In particular, flow rates 0.04, 0.1 and 1 cc/min result in S_{or} values of

0.10, 0.09 and 0.07 respectively . The cross-over saturation is 0.82, 0.78 and 0.85 for flow rates at 0.04, 0.1 and 1 cc/min. In other words, cross over saturation varies by less than 10%. The behaviour of differential pressure shows a consistent increasing without fluctuation in first 10 min then a period of stabilisation is attained in range of 10 min for all rates that applied 0.04 cc/min, 0.1 cc/min and 1 cc/min **Figure 5.6**.

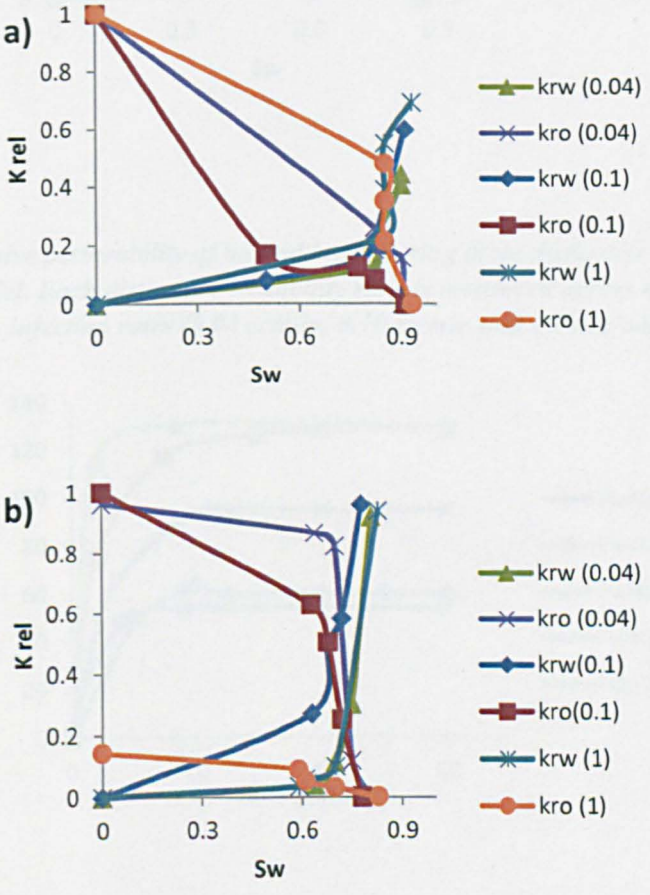

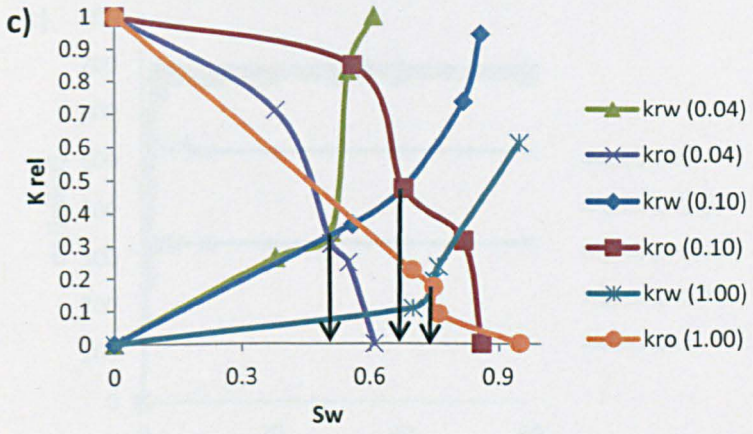

Figure 5.5 ***Relative permeability of oil and brine during three distinctive wettability states of glass micromodel. Each distinctive wettability state is measured across three different fluid injection rates (0.04 cc/min, 0.10 cc/min and 1.00 cc/min).***

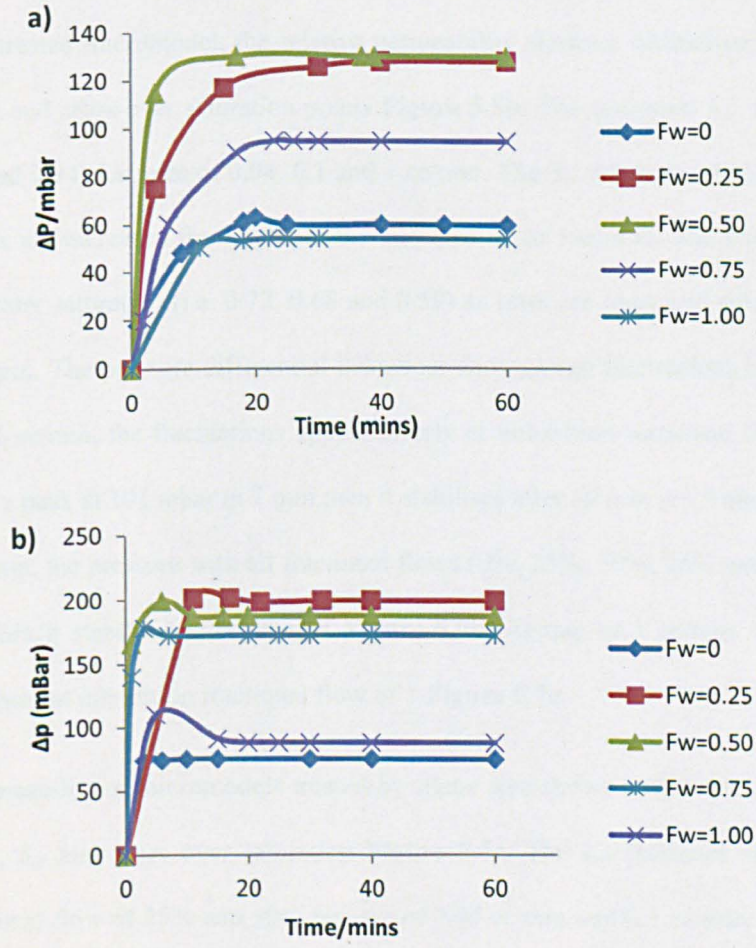

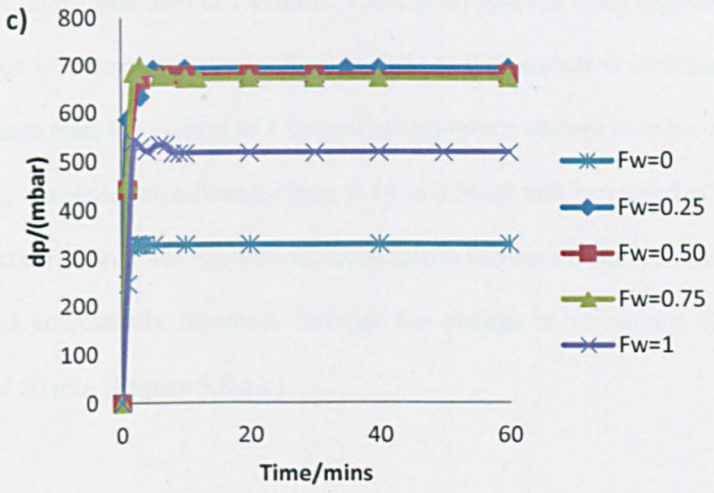

Figure 5.6 *Differential pressure across glass Micromodel that treated by refined oil at different fluid injection rates (a) 0.04, (b) 0.1 and (c) 1 cc/min.*

In the crude oil treated micromodel, the relative permeability shows a distinctive shape in terms of end-point k_{rw}, S_{or} and cross-over saturation points **Figure 5.5b**. The end-point k_{rw} is almost identical (i.e. 0.93, 0.94 and 0.94) for rates of 0.04, 0.1 and 1 cc/min. The S_{or} decreases slightly (i.e. 0.81, 0.78 and 0.75) as rates are increased from 0.04, to 0.1 and then up to 1 cc/min. The cross-over saturation shifts to lower water saturation (i.e. 0.72, 0.68 and 0.59) as rates are increased from 0.04, to 0.1 and then up to 1 cc/min. The pressure differential behaviour shows large fluctuations before it stabilizes. At a rate of 0.04 cc/min, the fluctuations appear clearly at imbibition fractional flow of 1 in which pressure reaches a peak at 101 mbar in 7 min then it stabilises after 50 min at 17 mbar **Figure 5.7a**. At a rate of 0.1 cc/min, the pressure with all fractional flows (0%, 25%, 50%, 75% and 100%) fluctuates significantly before it stabilises after 40 min **Figure 5.7b**. At rate of 1 cc/min, the fluctuations in pressure only appear at imbibition fractional flow of 1 **Figure 5.7c.**

The relative permeability of micromodels treated by silane also shows a characteristic shape in terms of end-point k_{rw}, S_{or} and cross over saturation **Figure 5.5c**. The k_{rw} increases significantly during imbibition fractional flow of 25% and 50% for rate of 0.04 cc/min and 0.1 cc/min. Conversely, a rate of 1 cc/min tends to increase k_{rw} at lower fractional flow of 25% and 50% only. Increasing fractional flow to 100% causes the end-point k_{rw} to decreased systematically (i.e. 0.99, 0.94, 0.61) as rates are

increased from 0.04, to 0.1 and then to 1 cc/min. There is no specific trend regarding the k_{ro} with rate. Cross-over saturation is increased systemically from 0.51 to 0.66 as rate is increased from 0.04 cc/min to 0.1 cc/min. Increase from 0.1 cc/min to 1 cc/min causes minor change in cross-over saturation from 0.66 to 0.71. The S_{or} decreases significantly from 0.40 to 0.86 as rate increased is from 0.04 cc/min to 0.1 cc/min. A reduction of only 4% is observed when rate is increase from 0.1 cc/min to 1 cc/min. The pressure differential consistently increases through the change in imbibition fractional flow with stabilisation time of 20 min (**Figure 5.8 a-c**).

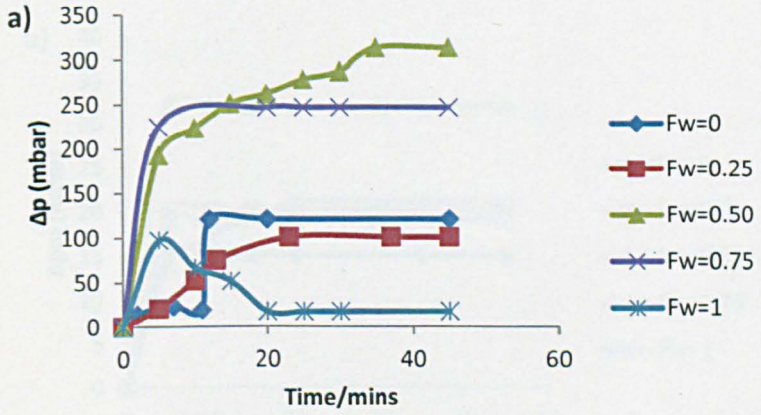

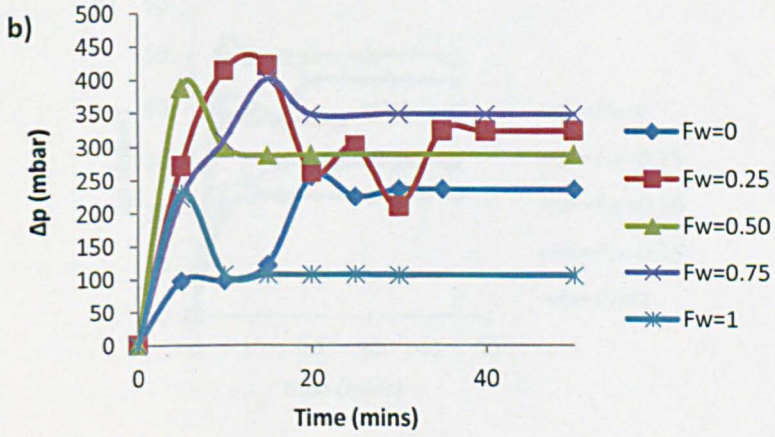

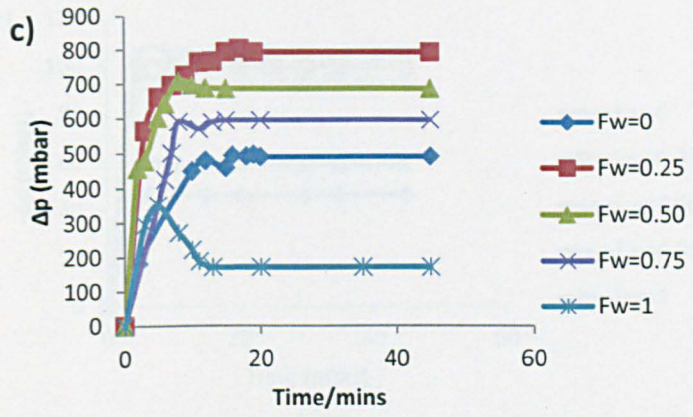

Figure 5.7 *Diffierntial pressure across the mixed-wet glass micromodel at different fluid injection rate of (a) 0.04,(b) 0.1 and (c) 1 cc/min.*

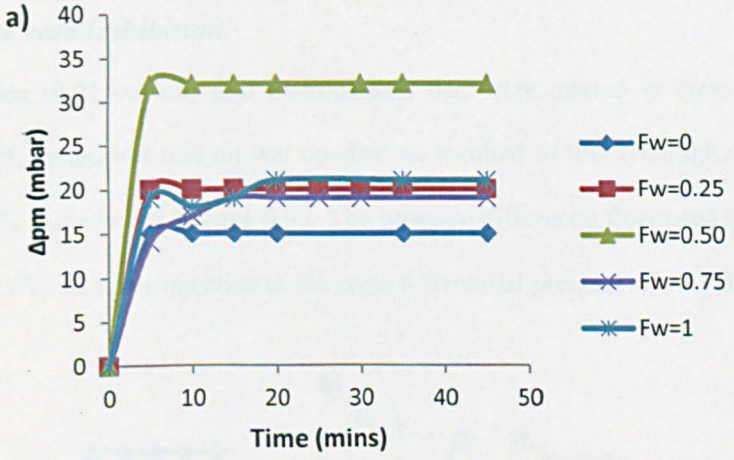

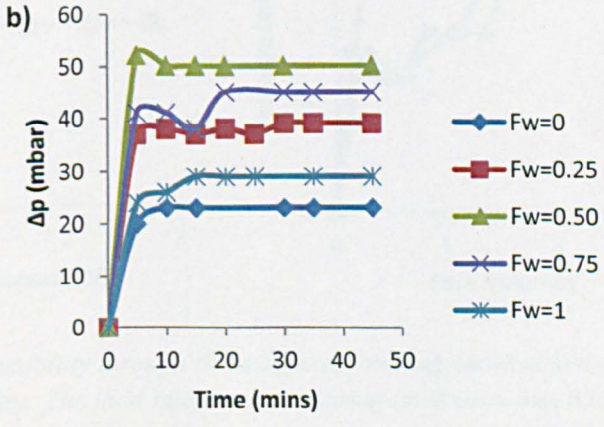

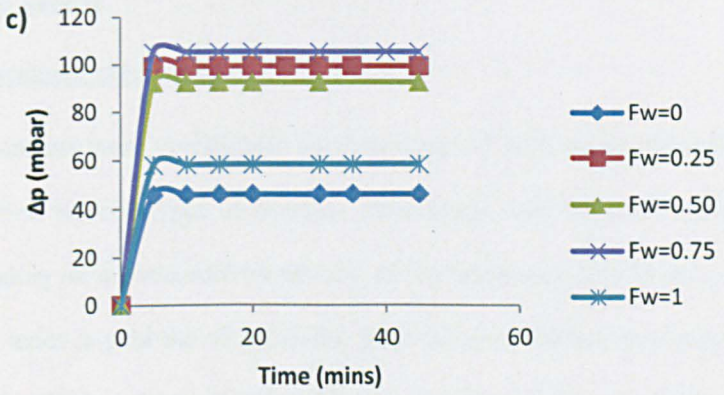

Figure 5.8 *Differential pressure across the oil-wet glass micromodel at different fluid injection rate of (a) 0.04,(b) 0.1 and (c) 1 cc/min.*

5.3.1.2 *Low rate imbibition*

Low rate imbibition (0.01 cc/min) into micromodels that were treated in three different ways to produce water-wet, mixed-wet and oil-wet conditions, resulted in breakthrough recovery factors of 90%, 74% and 55% respectively **Figure 5.9a**. The pressure difference fluctuated significantly before it stabilised with 2 PVs of water injection at the same differential pressure of 12 mbar **Figure 5.9b**.

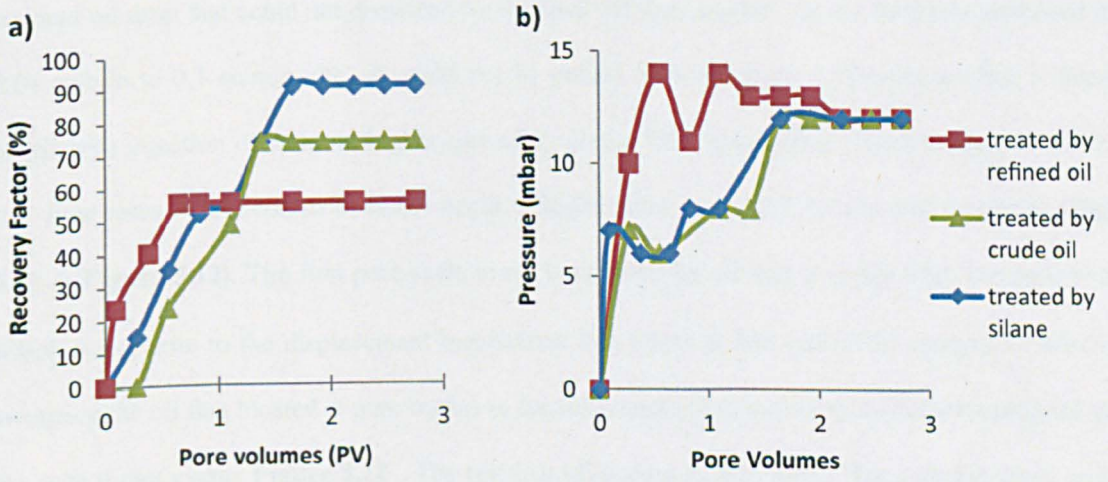

Figure 5.9 *Effect of wettability through three different wetting states achived by refined oil,crude oil and silane. The fluid injection rate during imbibition was 0.01 cc/min.*

5.3.2 Pore scale events

Microscopic displacement efficiency

Imbibition displacements were investigated by displacing oil with water through micromodels with differing wettabilities. Several types of interface movements were observed inside pore bodies and pore throats depending on micromodel wettability. In the water-wet micromodel, the water, which is the wetting phase, tends to peel the oil gradually from the grain surface until a layer of water totally surrounds the grain (**Figure 5.10a-c**). The water lens starts to grow gradually in the pore throat **Figure 5.10e** until it closes the oil path of the pore throats. This causes the oil to break and snapped off, which leaves residual drops in the middle of the pore body **Figure 5.10f**. The water then moves to another grain surface through the pore throat and forms a continuous film that transfers from grain surface to others **Figure 5.10g**. This mechanism of "grains jumps" is only observed in the water-wet micromodel. The residual oil in the micromodel tends to be trapped in the pore bodies rather than in the pore throats (**Figure 5.10h-k**). A second flow regime is initiated when continuous films of water are formed by water starting to spread out from the small pore throat to invade the pore bodies in a manner of continues displacement. This is known as "frontal displacement"; it reduces the size of the residual oil drop that could not displaced by the snap off flow regime. As the flow rate increased from 0.04 cc/min to 0.1 cc/min, the oil could not be peeled from the grain surface even after 3 hours of continuous injection of water at higher rate of 1 cc/min. The "grain jump" mechanism that occurs at low flow rates (0.04 cc/min) does not occur at higher flow rates (0.1 cc/min and 1 cc/min) (**Figure 5.11 & Figure 5.12**). The first pore scale event is initiated by oil that is swept from the pore bodies, which is opposite to the displacement mechanism that exists at low rate (0.04 cc/min) in which the sweeping the oil that located at pore bodies is the subsequent pore scale event after sweeping the oil in the pore throat events **Figure 5.11**. The residual oil occurs as thin layers that coat the grain surface. These vary in thickness between 51.4 μm and 36.7 μm for flow rates of 0.1 cc/min and 1 cc/min respectively **Figure 5.13**. The structure of residual oil at high rate is totally different from that created at at low rate (0.04 cc/min). In particular, at high flow rates the oil occurs mainly as isolated sub-singlets in the pore bodies.

In the mixed-wet micromodel, the snap-off mechanism observed in the water-wet micromodels is suppressed. In **Figure 5.14**, the water invades the pore throat without connecting the grain surface where the oil film still resides. The interface of the water that invades the pore throats tends to be more flat as it advances from pore throats to pore bodies compared with the interface in the water-wet micromodel. The water does not maintain its continuity as it invades the pore throat because the oil lens in the pore throats starts to grow and causes the water to break up **Figure 5.14**. Increasing the rate to 0.1 cc/min and 1 cc/min did not change the flow regime from frontal advance of water **Figure 5.15**. However, the oil thin film that coats the grain surface undergoes a continuous change from 47.4 μm at 0.04 cc/min to 18.2 μm at 0.1 cc/min to 14.7 μm at 1 cc/min **Figure 5.16**. The residual oil tends to be thinned into the pore throats as the water advances with a piston front into the pore throats. Residual oil remains in some pore throats, which blocks the water causing it to seek other available pore throats. This residual oil that tends to hang between grain surfaces was not observed in the water-wet micromodels **Figure 5.15**.

In the oil-wet micromodel, the ability of oil to flow via the snap off mechanism is suppressed compared with the water-wet micromodel. The invading water only maintains to sweep the oil from the pore bodies as water invades the pore throat before the water broken into drops. The oil flow regime is maintained through the continuous oil film through pore throats only **Figure 5.18**. Increasing the rate from 0.04 cc/min to 0.1 cc/min tends to thin the oil that coats the grains from 36.9 μm to 18.4 μm **Figure 5.19**. Further increasing the rate to 1 cc/min causes a reduction of the oil film to 14.7 μm. The micromodel experiments also showed that the water that sweep the oil tends to be continuous through a maximum of one pore throat before it divides into two broken drops when the rate is 0.04 cc/min **Figure 5.18**. As rate increased to 0.1 cc/min, the water tends to be continuous over 5 adjacent pore throats before it breaks. As the rate increase more to 1 cc/min, the water tends to be continuous more over 10 pore throats before it breaks.

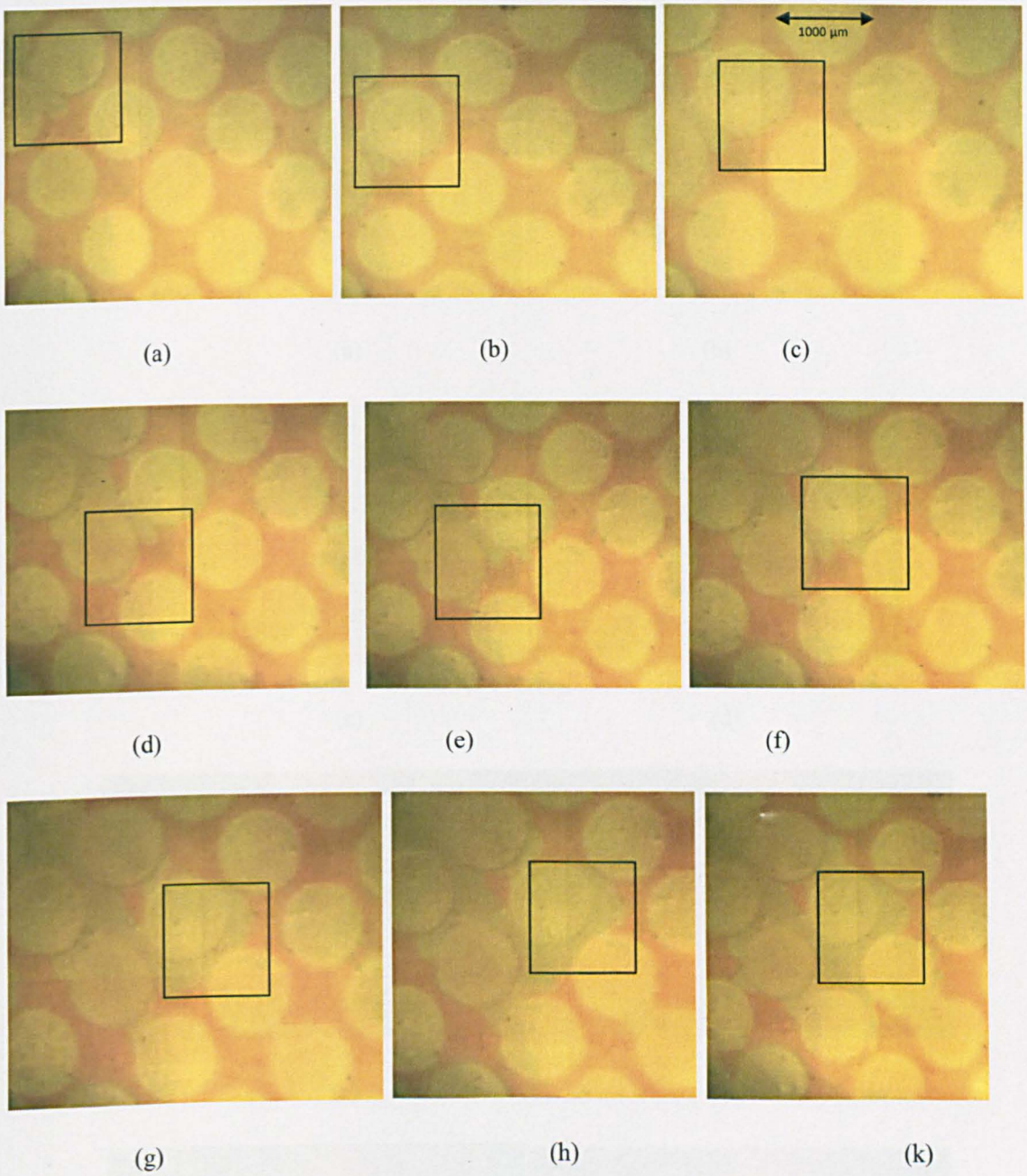

Figure 5.10 *Flow regime of steady state of water and oil during water-wet micromodel at very low rate of fluid injection 0.04 cc/min.*

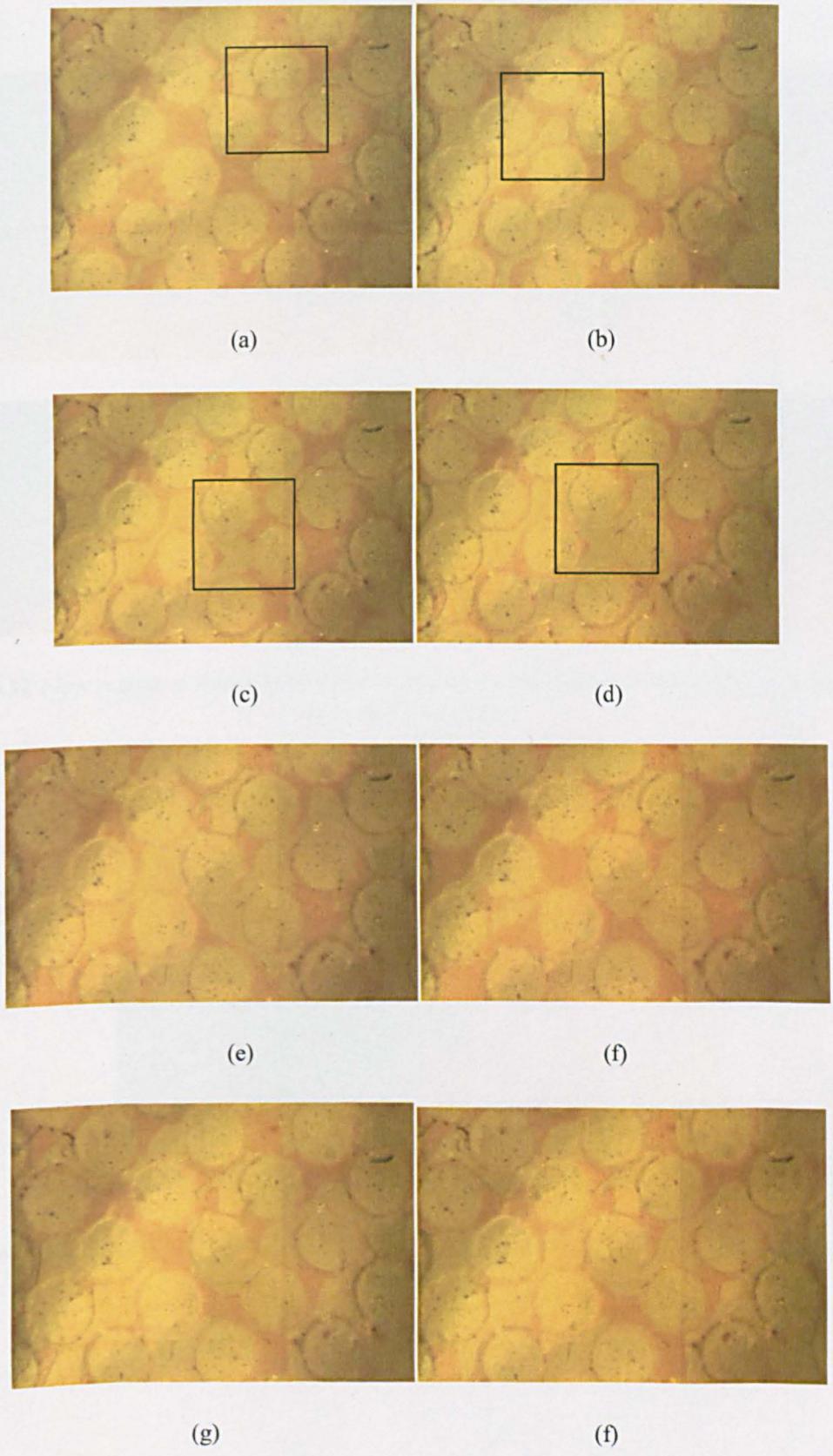

Figure 5.11 *Flow regime of steady state of water and oil during water-wet micromodel at very low rate of fluid injection 0.10 cc/min.*

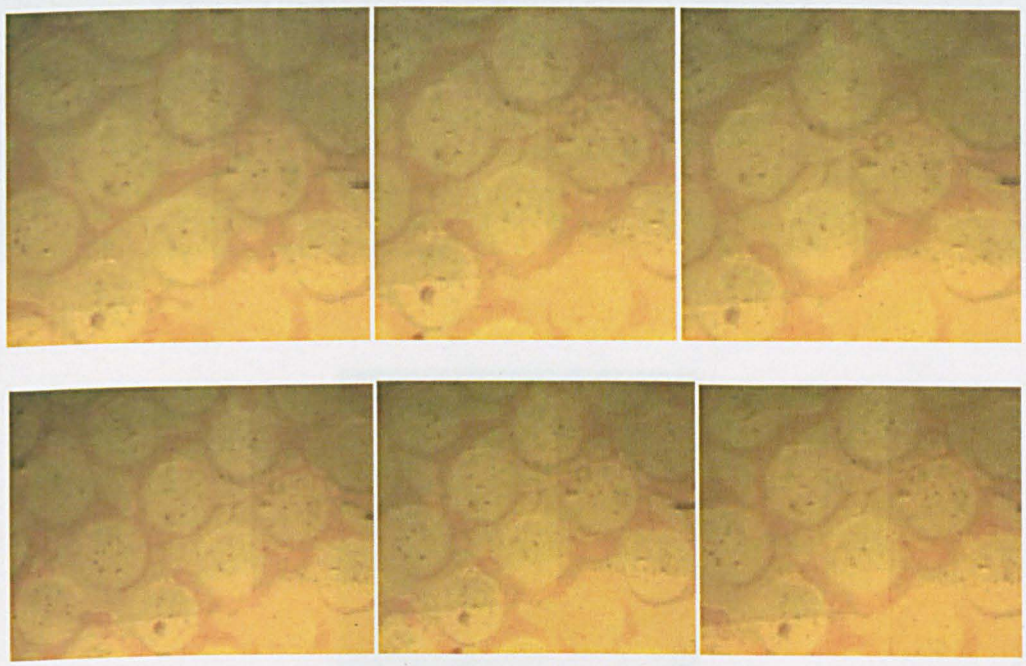

Figure 5.12 *Flow regime of steady state of water and oil during water-wet micromodel at rate of fluid injection 1.00 cc/min.*

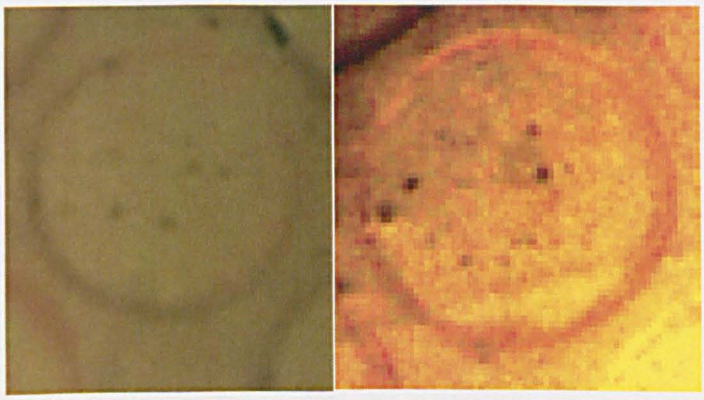

(a) Oil thin film 0.1 cc/min (b) Oil thin film 1 cc/min water-wet micromodel

Figure 5.13 *Structure of residual oil saturation in the end of steady state flow during water-wet micromodel.*

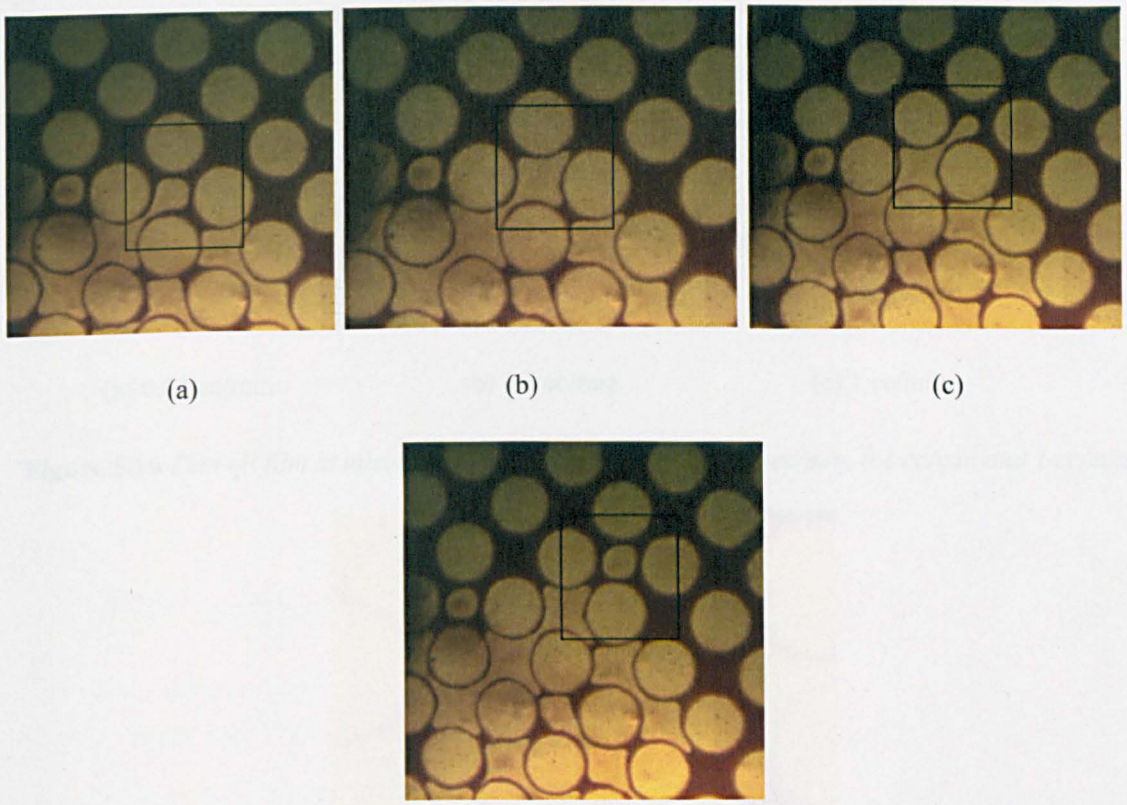

(a) (b) (c)

(d)

Figure 5.14 *Flow regime of steady state of water and oil during mixed-wet micromodel at very low rate of 0.04 cc/min.*

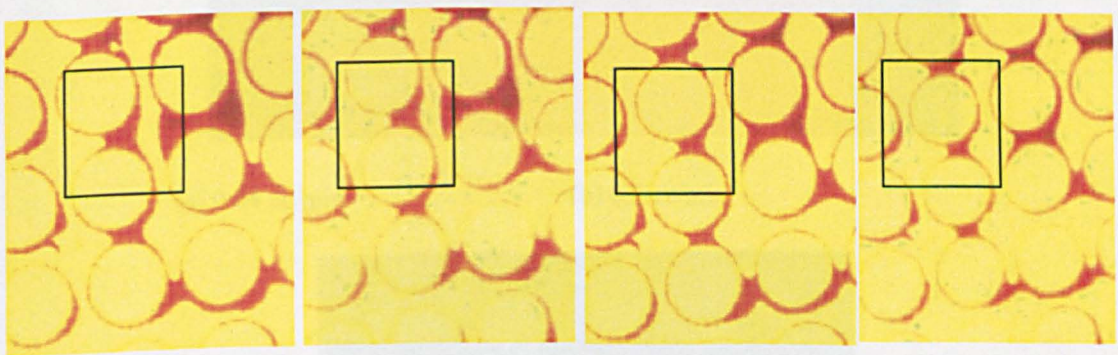

(a) 0.1 cc/min (b) 0.1 cc/min (c) 0.1 cc/min (d) 0.1 cc/min

Figure 5.15 *Flow regime of steady state of water and oil during mixed-wet micromodel at rate of 0.1 cc/min.*

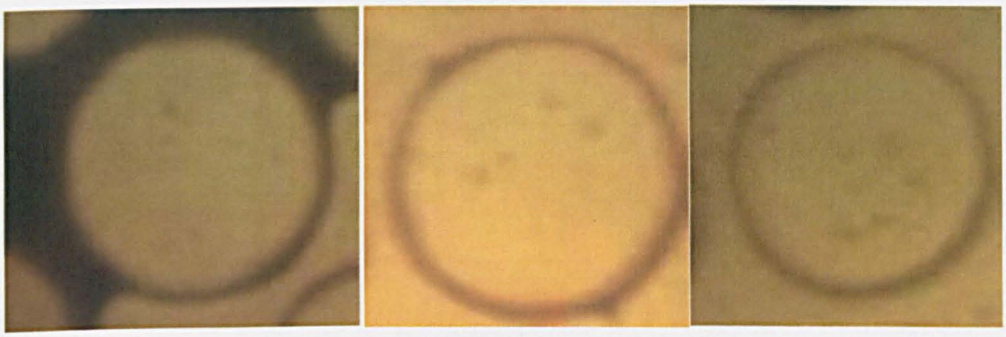

(a) 0.04 cc/min (b) 0.1 cc/min (c) 1 cc/min

Figure 5.16 *Thin oil film at mixed-wet at different flow rates 0.04 cc/min, 0.1 cc/min and 1 cc/min.*

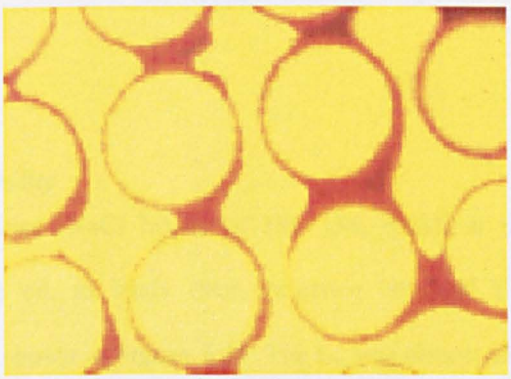

Figure 5.17 *Structure of residual oil saturation in mixed-wet micromodel.*

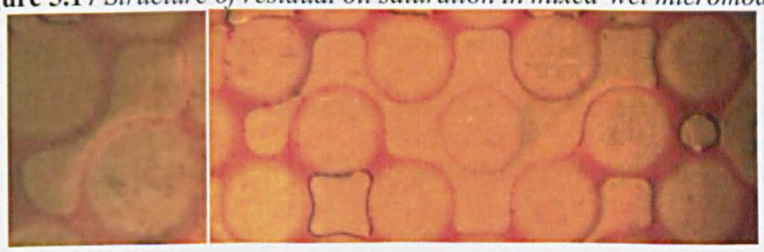

(a) 0.04 cc/min (b) 0.1 cc/min

(c) 1 cc/min

Figure 5.18 *The water blobs length in oil-wet micromodel as rate increased from 0.04 to 1 cc/min.*

(a) 0.04 cc/min (36.9 μm) (b) 0.1 cc/min (18.38 μm) (c) 1 cc/min (14.7 μm)

Figure 5.19 *Thin oil film at end of the fractional flow at three different rates 0.04, 0.1 and 1 cc/min in oil-wet micromodel.*

5.3.3 Effect of salinity

5.3.3.1 *Relative permeability*

Three different brine salinities (NaCl brines of 3M, 1M, 0.1M) at neutral pH were used, in a micromodel aged in crude oil, to study their influence on fluid flow behaviour and relative permeability; the results are shown in **Figure 5.20**. The k_{rw} was almost identical for all brine salinities for fractional flows of 25%, 50% and 75%. At 100% fractional flow, the end point k_{rw} varied with salinity. In particular, the end point k_{rw} was 0.14, 0.20 and 0.31 for 3 M, 0.1 M and 1 M NaCl respectively. During the initial step imbibition fractional flow of 25%, the degree of reduction in k_{ro} at 3 M brine is higher by double (0.41) compared to 1 M brine (0.77) and 0.1 M brine (0.67). A steep reduction in k_{ro} by 40% occurred during tests with fractional flows of 50% and 75% for brine 1 M NaCl and 0.1 M NaCl. The k_{ro} dropped from 0.77 to 0.30 and from 0.67 to 0.30 for NaCl salinities of 1 M and 0.1 M respectively. The S_{or} shows a continuous decrease as the salinity decreases from 3 M to 0.1 M. At 3 M, the S_{or} was 47%, 36% with brine 1 M and 25% with brine 0.1 M. The water saturation of cross over point was 49%, 66% and 66% for salinities of 3 M, 1 M and 0.1 M NaCl respectively.

It is noteworthy that the pressure during the fractional flow step change fluctuated significantly during the steady state flow of 3 M NaCl brine/crude oil **Figure 5.21**. During the first 20 min, the pressure difference monotonic increases to reach 126, 90, 230 and 117 mbar for fractional flow 25%, 50%,

75% and 100%. After 80 min, the differential pressure become more stable at 198, 203, 230 and 116 mbar for fractional flow 25%, 50%, 75% and 100%. The degree of fluctuation in differential pressure that was observed in the 3 M NaCl brine was not observed for 1 M NaCl brine and 0.1 M NaCl brine. The differential pressure for 1 M NaCl reaches a maximum at 5 min for all fractional flow steps 0, 0.25, 0.50, 0.75 and 1. After 80 min, the differential pressure stabilises at 84, 109, 188, 153 and 54 psi for fractional flows of 0, 0.25, 0.75 and 1 respectively. Similarly, at a salinity of 0.1 M, the differential pressure stabilises after 80 min at 77, 125, 187, 154 and 77 psi for fractional flow 0, 0.25, 0.50, 0.75 and 1 respectively without a distinctive maximum pressure at first 10 min as observed for brine 1 M NaCl.

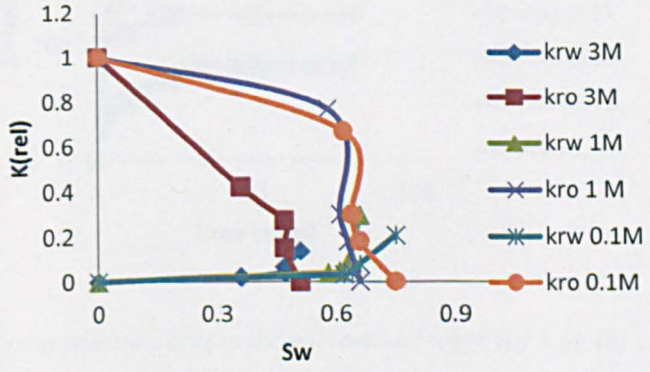

Figure 5.20 *Effect of brine salinity in imbibition steady state flow of oil and water relative permeability.*

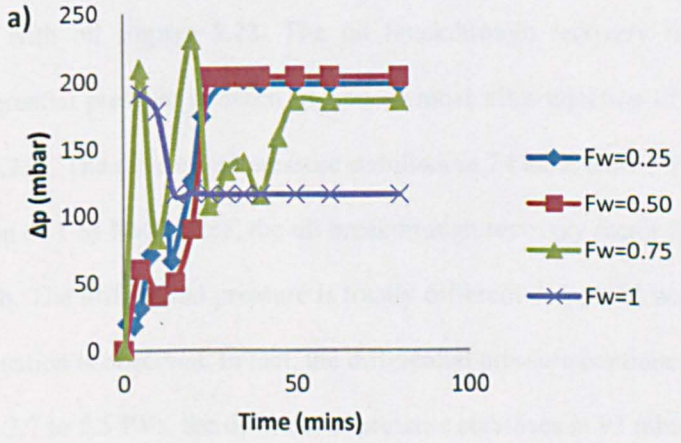

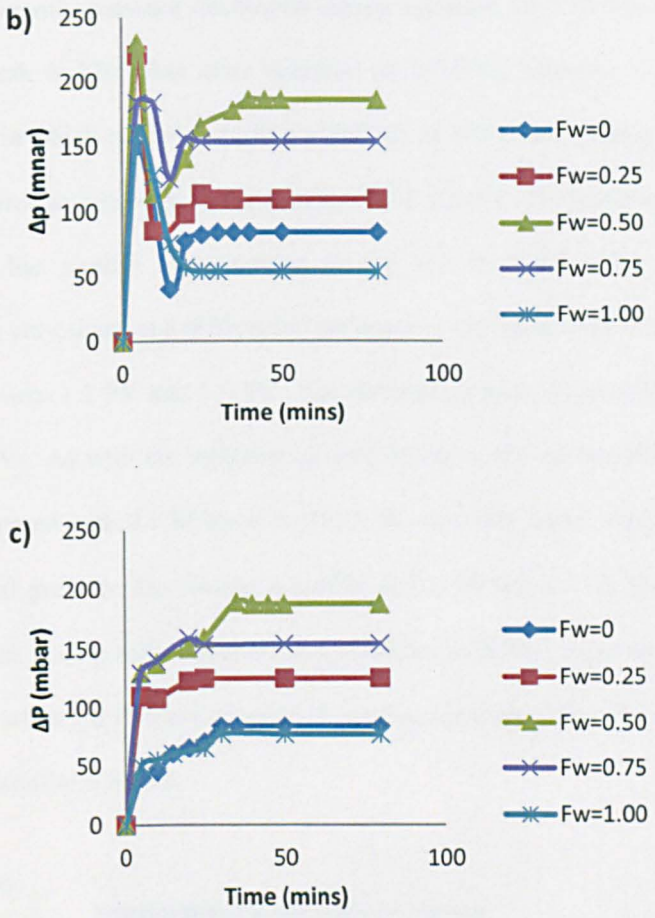

Figure 5.21 *The differential pressure across the micromodel when (a) 3 M, (b) 1M and (c) 0.1 NaCl brine salinity is used.*

5.3.3.2 *Low rate imbibition*

Recovery factors increase as salinity is reduced during very low rate (0.01 cc/min) to a micromodel that fully saturated with oil **Figure 5.22**. The oil breakthrough recovery factor is 57% with a fluctuation in a differential pressure between 21 and 74 mbar after injection of 1 and 3 PVs of 3 M NaCl brine **Figure 5.23a**. The differential pressure stabilises at 74 mbar after 3 PVs injection until 5.6 PVs. During injection of 1 M NaCl brine, the oil breakthrough recovery factor is increased from 57% to 72% **Figure 5.23b**. The differential pressure is totally different compared with 3 M NaCl brine in which no sharp fluctuation is observed. In fact, the differential pressure continues to increase up to 2.7 PVs injection. From 2.7 to 5.5 PVs, the differential pressure stabilises at 93 mbar. During injection of 0.5 M NaCl brine, the recovery factor increased from 72% to 74% **Figure 5.23c**. The differential

pressure behaves differently pressure developed during injection of 1 M and 3 M NaCl brine. The pressure reaches a peak at 120 mbar after injection of 1.7 PVs, however, a continuous drop then occurs up to 3.8 PVs in which the pressure then stabilises at 100 mbar. During the injection of 0.1 M brine, the oil breakthrough recovery factor reaches 92% after 1 PV injection **Figure 5.23d**. The differential pressure has similar characteristic to the 0.5 M NaCl brine injection experiment. Although, the peak is very sharp at a differential pressure of 150 mbar with a narrow interval of pore volume injection between 1.1 PV and 1.9 PV. The differential pressure is stabilised around 80 mbar after injection of 6 PVs. As with the injection of 0.01 M brine, the oil breakthrough recovery factor did not increase compared with 0.1 M brine in which the recovery factor stays stable at 92% **Figure 5.23e**. The differential pressure has similar a profile as 0.5 M and 0.1 M NaCl brine in which the pressure reaches a peak during early injection then stabilises at further injection. The pressure reaches the peak at 190 mbar when 1.4 PVs are injected. A continuous drop is then observed until the pressure is stabilised in 70 mbar after 6.8 PVs.

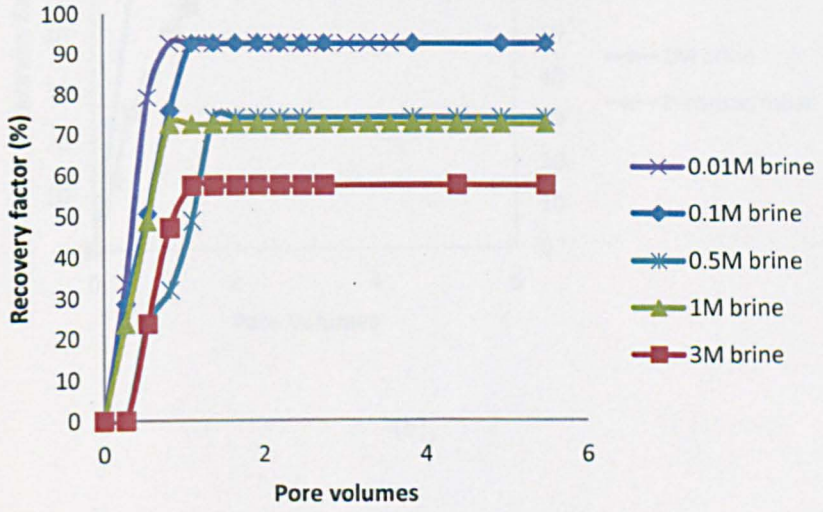

Figure 5.22 *Effect of brine Salinity in sweeping the crude oil from micromodel which is fully saturated with crude oil. The fluid injection rate is 0.04 cc/min,.*

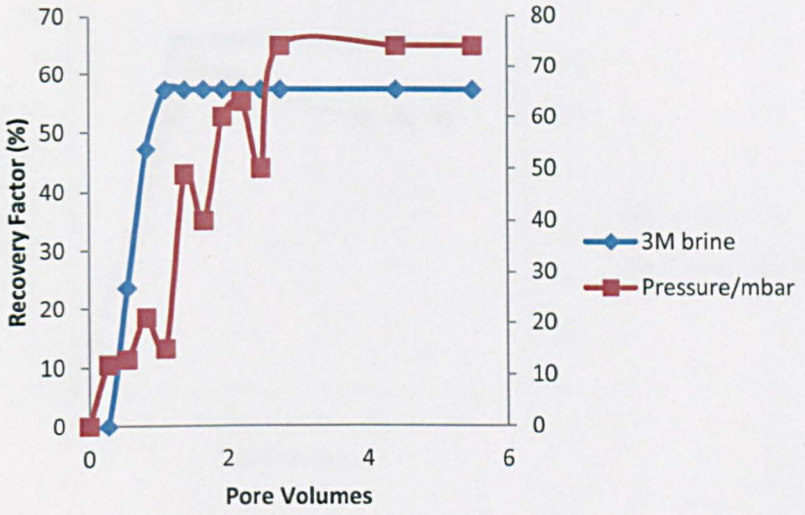
Recovery Factor (%)
Pore Volumes
3M brine
Pressure/mbar

(a)

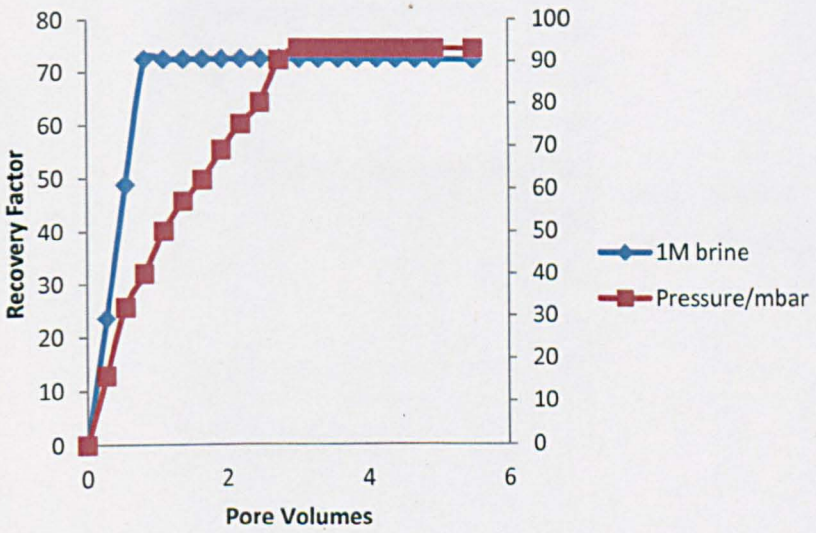
Recovery Factor
Pore Volumes
1M brine
Pressure/mbar

(b)

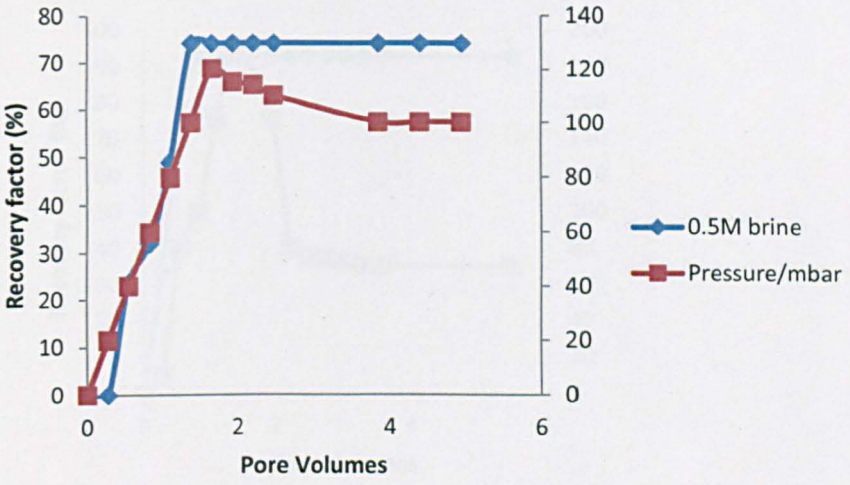
Recovery factor (%)
80
70
60
50
40
30
20
10
0
140
120
100
80
60
40
20
0
0
2
4
6
Pore Volumes
0.5M brine
Pressure/mbar

(c)

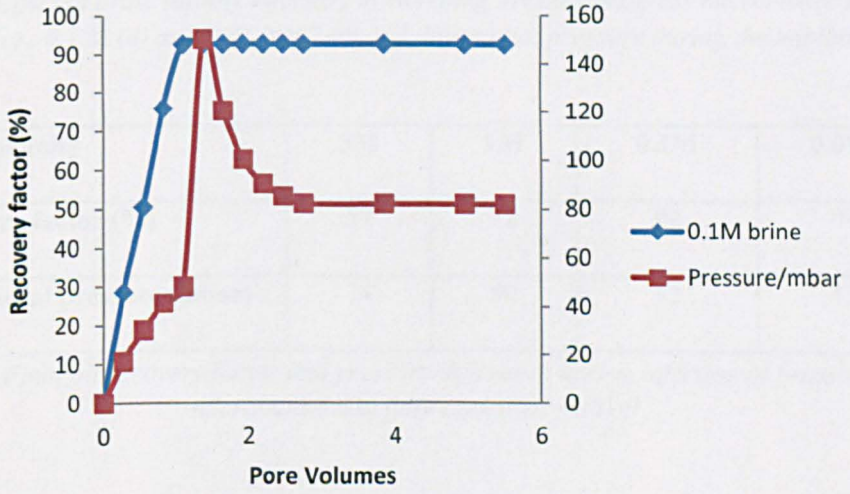
Recovery factor (%)
100
90
80
70
60
50
40
30
20
10
0
160
140
120
100
80
60
40
20
0
0
2
4
6
Pore Volumes
0.1M brine
Pressure/mbar

(d)

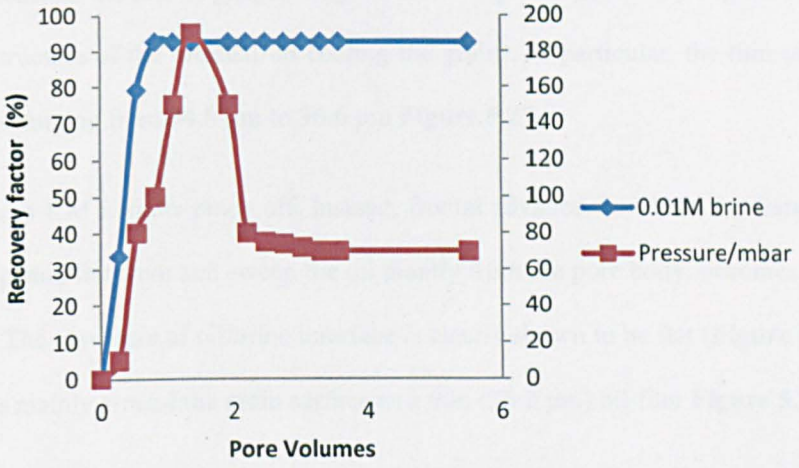

(e)

Figure 5.23 *Effect of brine salinity injection in sweeping the oil from glass micromodel 3 M (a) ,1 M (b) ,0.5 M (c) , 0.1 M (d) and 0.01 NaCl (e) and differential pressure during the imbibition brine.*

Brine salinity	3M	1M	0.1M	0.01M
Recovery factor (%)	57	72	92	70
Differential pressure (mbar)	74	90	82	5.5

Table 5.1 *Final oil recovery factor and pressure difference during injection of brine salinity to micromodel that fully saturated with oil.*

5.3.3.3 *Pore scale events*

The effect of salinity on oil displacement efficiency was studied qualitatively by observing the oil/brine interface under three different injection schemes. For each displacement scheme, the micromodel was fully saturated with oil. At 3 M NaCl brine, a "pinch-off" mechanism by which the oil and water were discontinuous to sub-singlets. By this mechanism, mobile water/oil ganglia are broken up into smaller segments. In **Figure 5.25**, the ganglion constricts until it pinches off and divides into two smaller droplets. No indication of snap off was observed during the pinch off flow regime. In fact, a coalescence of water ganglia is observed because the stable oil lamella that separated the two brine sub-singlets is pinched off. However, the size of the sub-singlets water does

not developed to reach to the size of ganglia singlets that occupied a pore body **Figure 5.27**. Pinch off flow affects the structure of the residual oil coating the grains. In particular, the thin oil film has an irregular thickness ranging from 54.8 μm to 36.6 μm **Figure 5.27.**

Diluting the brine to 1 M inhibits pinch off. Instead, frontal advance, in which the water invades the pore throats with piston flat front and sweep the oil mainly from the pore body, becomes the dominant flow mechanism. The curvature of oil/brine interface is clearly shown to be flat (**Figure 5.28a-b)**. The residual oil occurs mainly around the grain surface as a thin (26.2 μm) oil film **Figure 5.28c.**

Diluting the brine to 0.01 M NaCl changes the flow behaviour from piston frontal advance to a mechanism where water tends to strip the oil from the grain surface as water invading the pore throats. This results in a water collar film growing in the pore throats and results in the formation of lenses that are prone to snapped off. Due to difference in the interfacial curvature, oil is driven by interfacial tension into the growing collar at the pore throat **Figure 5.29a**. Eventually, sufficient brine collects in the collar so that it becomes unstable and rearranges itself to form a brine lens. The snap off is following by frontal advance with very sharp curvature between brine and oil that sweeps the residual oil resulting from the first pore scale event of snapped off. The final residual oil tends to occur as a very discrete thin oil film that coats less than 25% of the grain surface whereas the other 75% of the grain surface is stripped out by 0.01 M brine **Figure 5.30**.

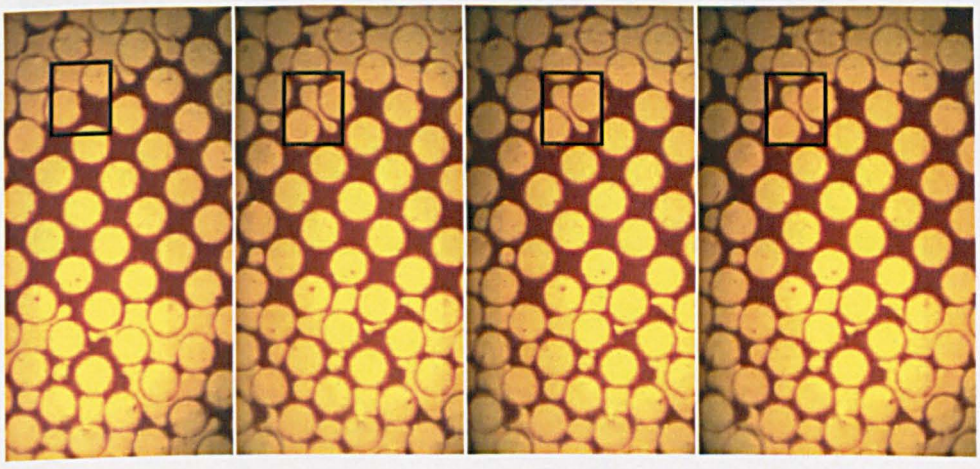

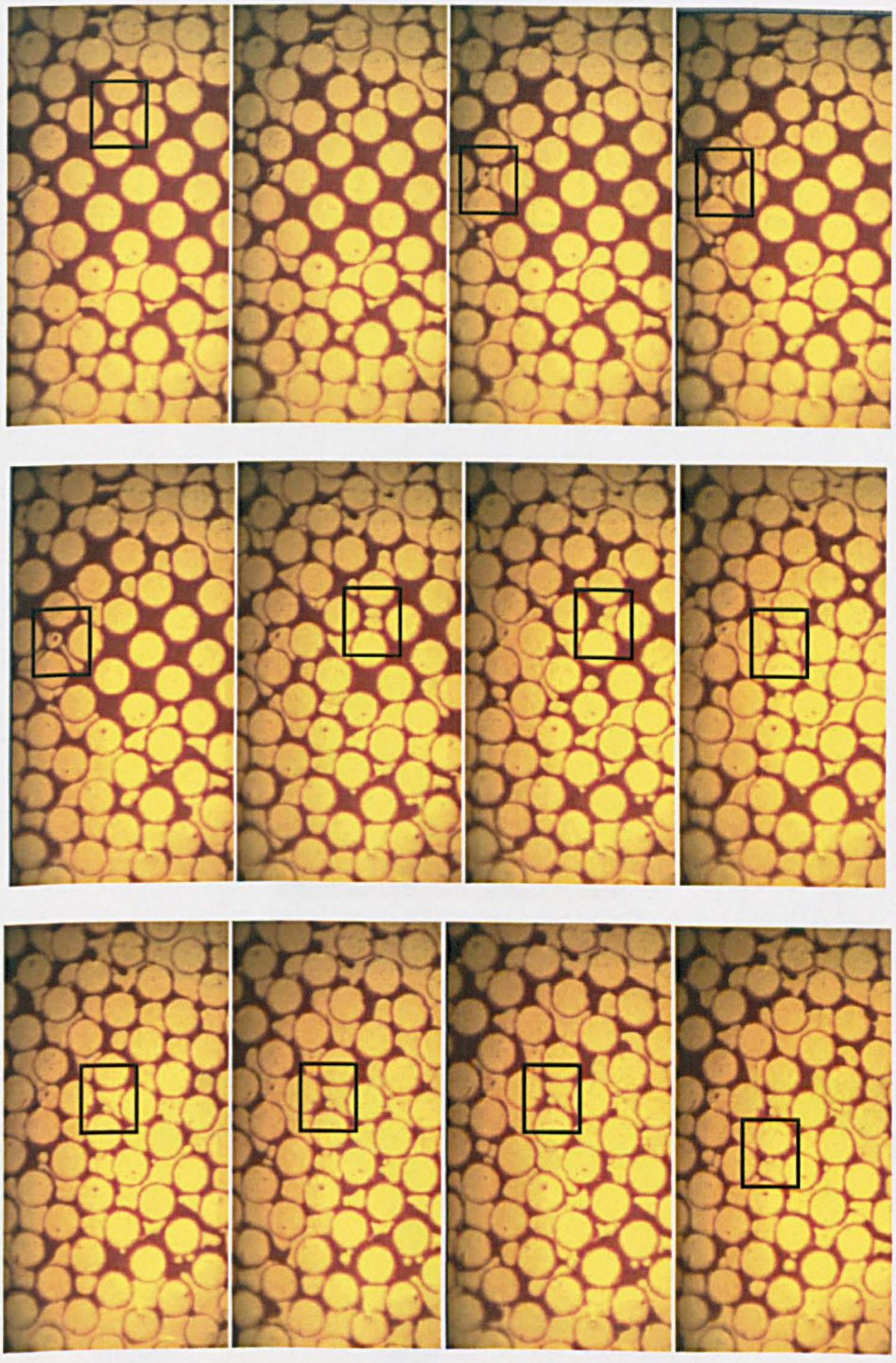

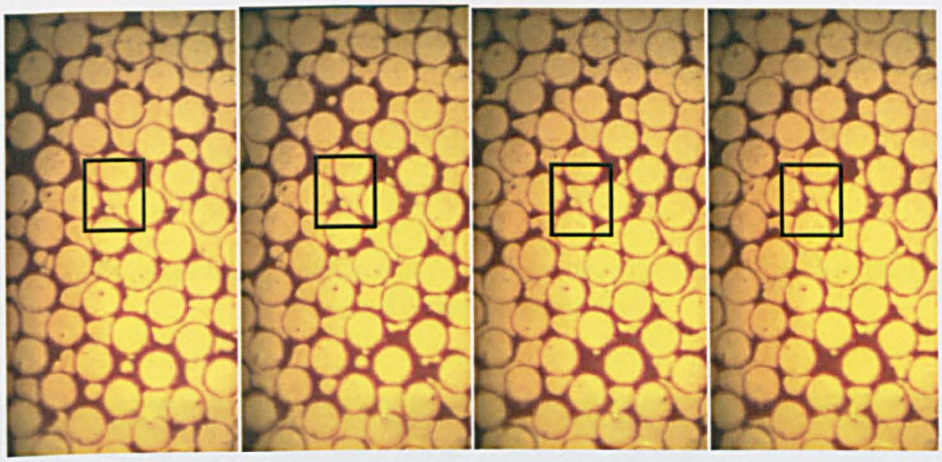

Figure 5.24 *Flow regime of steady state of 3M NaCl brine salinity and oil during mixed-wet micromodel.*

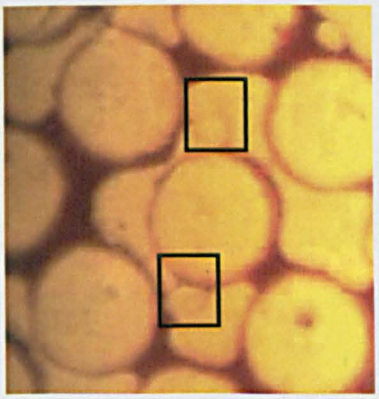

Figure 5.25 *Distinctive flow regime known as "Pinch off mechanism" during steady state flow of 3 M NaCl brine salinity and oil during mixed-wet micromodel.*

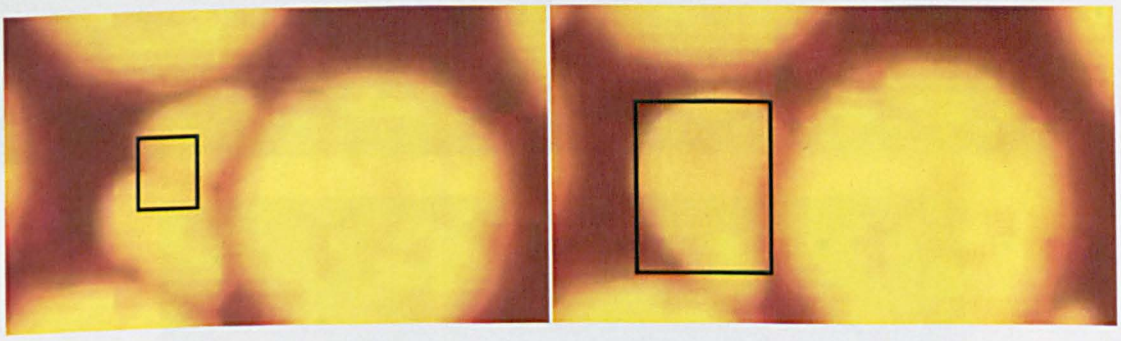

Figure 5.26 *Distinctive flow regime known as "coalescence mechanism" during steady state flow of 3 M NaCl brine salinity and oil during mixed-wet micromodel.*

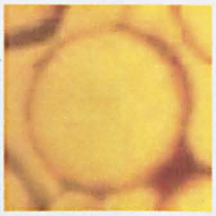

Figure 5.27 *Thickness of residual oil film that surrounding the grain surface during steady state flow of brine 3 M NaCl and crude oil.*

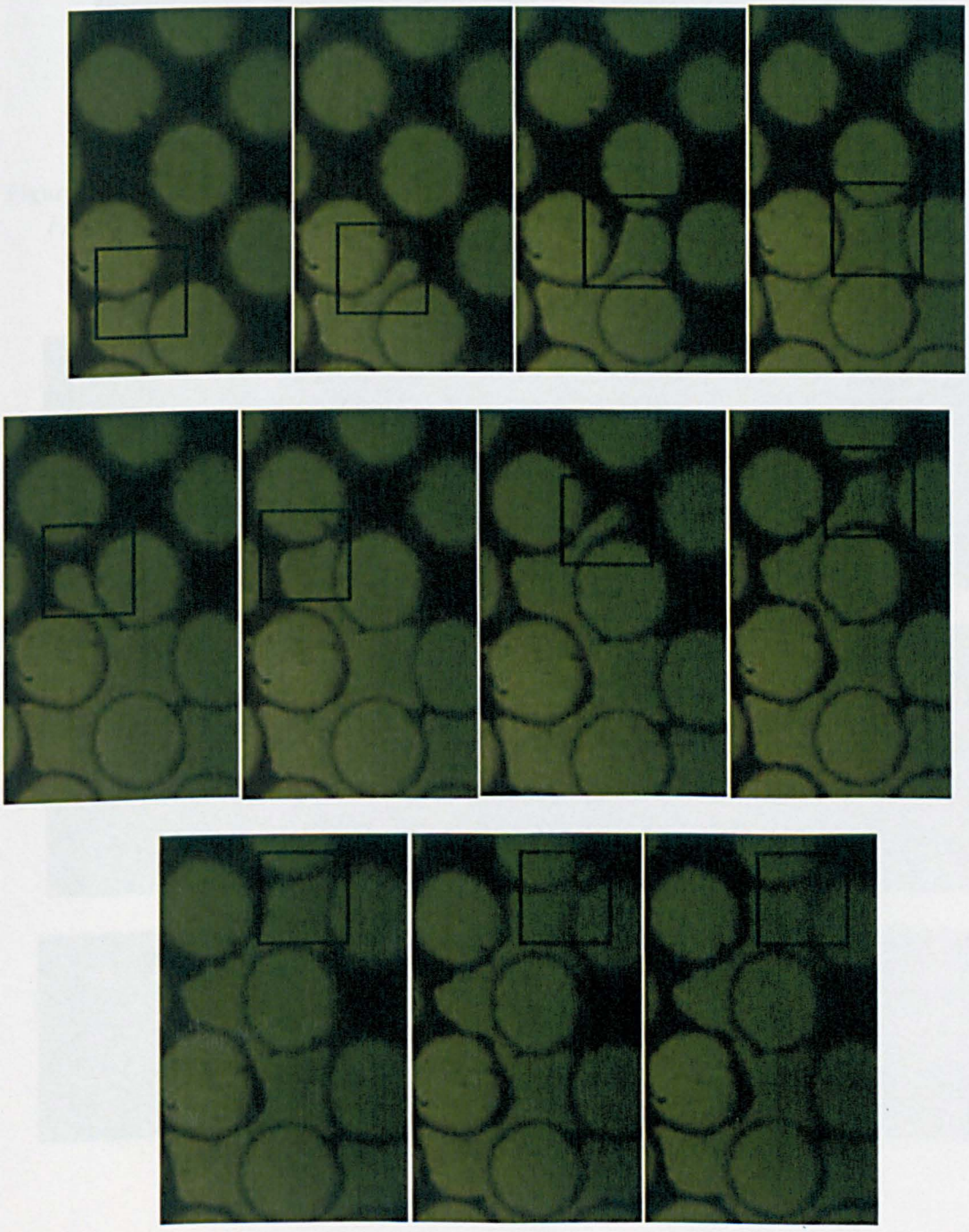

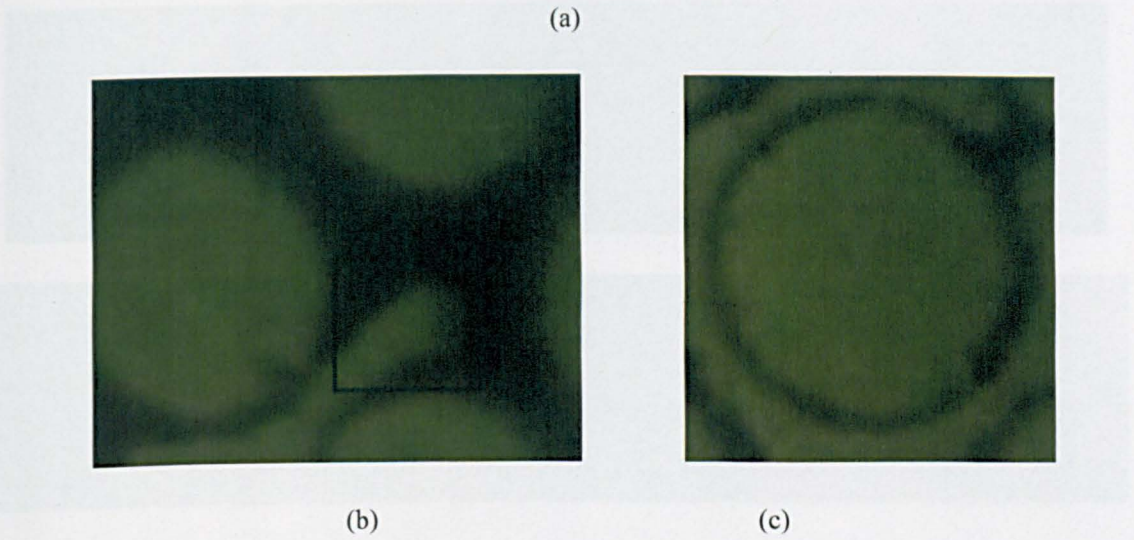

Figure 5.28 *Steady state flow of 1 M NaCl brine salinity and crude oil. (a) Distinctive flow regime (b) Flat frontal interface between oil and brine and (c) Structure of residual oil saturation.All the previous micromodel was mixed-wet.*

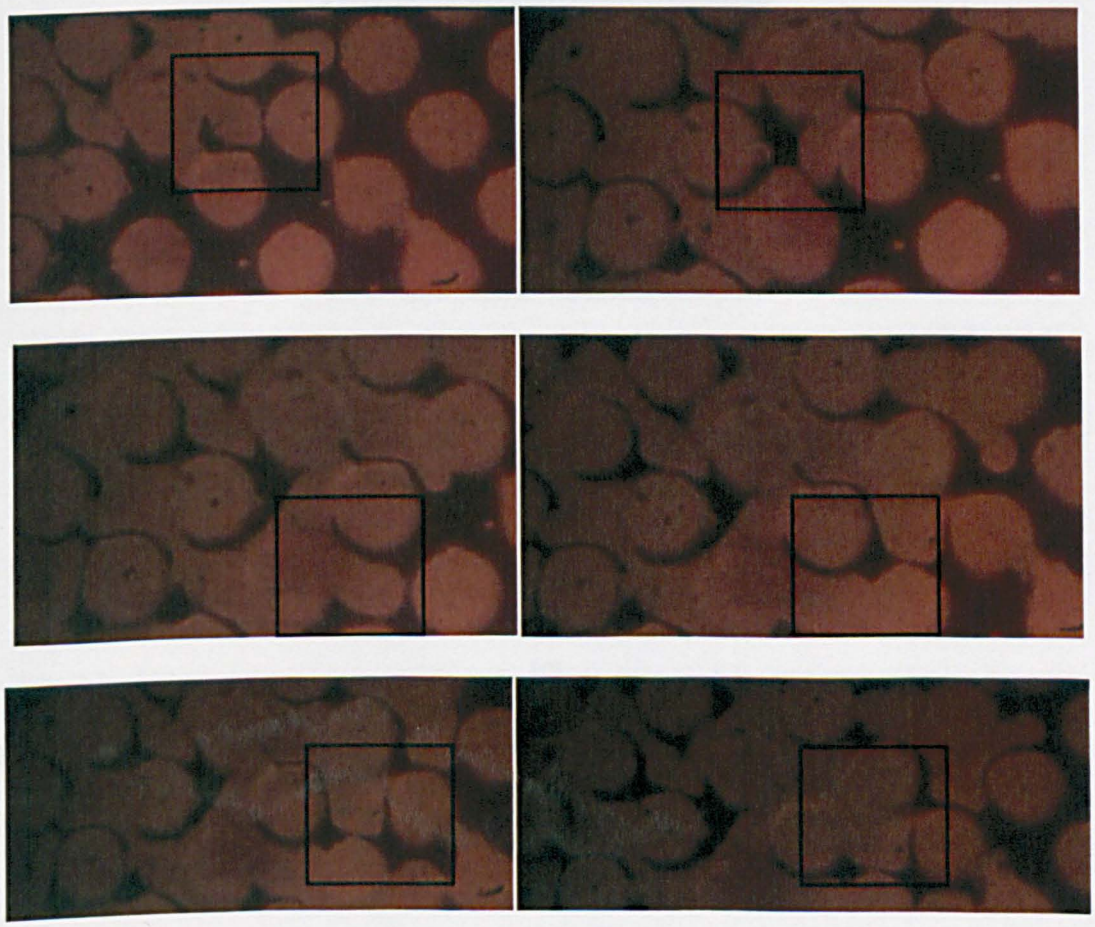

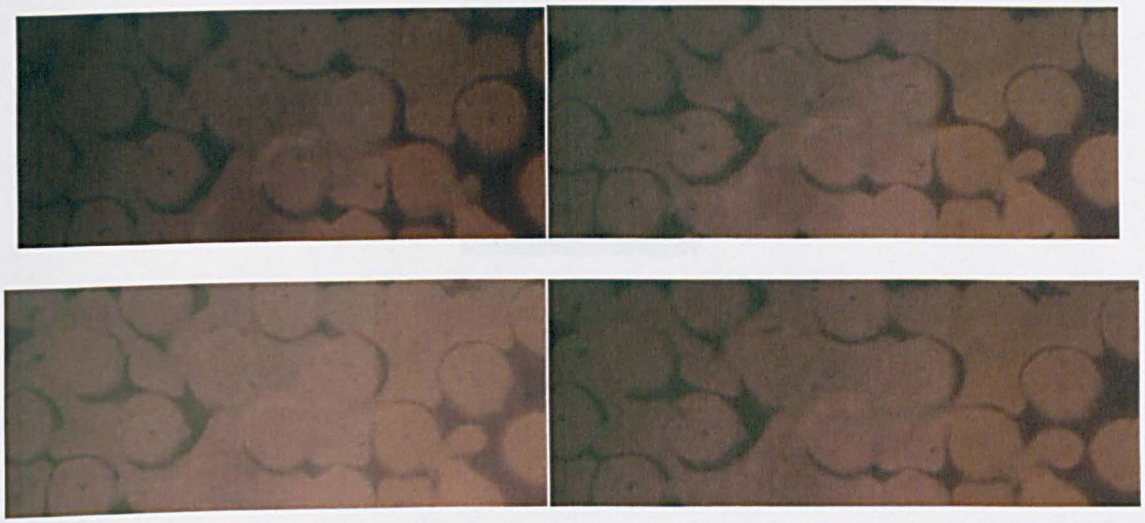

(a)

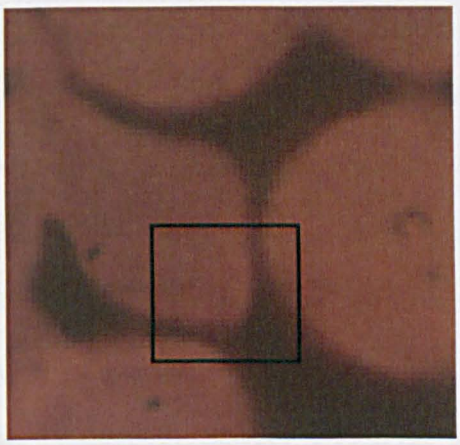

(b)

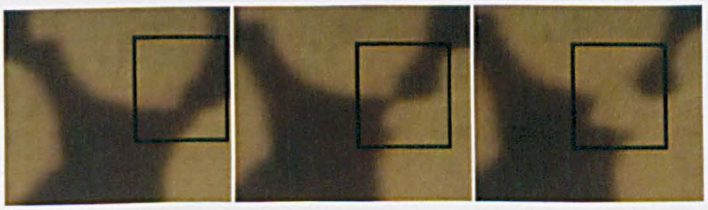

(c)

Figure 5.29 *Steady state flow of 0.01 M NaCl brine salinity and crude oil in mixed-wet micromodel: (a) Flow regimes (b) sharp frontal advance of oil and water interface. (c) Collar grow of water between grain surface.*

Figure 5.30 *Structure of residual oil in the end of steady state flow of 0.01 M NaCl brine salinity and crude oil in mixed-wet micromodel.*

5.3.4 Effect of temperature

5.3.4.1 *Relative permeability*

During the steady state relative permeability, the effect of temperature is found to be profound as the fractional flow step increased **Figure 5.31**. Between 0 and 25% fractional flow, the difference in k_{rw} between a temperature of 20°C and 60°C is 0.27 and 0.23 respectively. As the fractional flow increased up to 50%, the k_{rw} is dropped from 0.50 at temperature of 20°C to 0.32 at temperature of 60°C. Further increasing in fractional flow to 75% causes more dramatic reduction in k_{rw}; it drops from 0.58 at temperature of 20°C to 0.40 at temperature of 60°C. Similar behaviour is observed as fractional flow step increased to 100%, the end point k_{rw} drop by 52% as temperature increased from 20°C to 60°C. Regarding the k_{ro}, a continuous reduction is observed as temperature increased during different fractional flow. At 25% fractional flow, k_{ro} is decreased from 0.63 to 0.54 as temperature increased from 20°C to 60°C. At 50% fractional flow, k_{ro} is decreased from 0.50 to 0.32 as temperature increased from 20°C to 60°C. Further increasing in fractional flow to 75% makes the k_{ro} to decrease from 0.25 to 0.17. The most striking observation is the temperature tends to decrease both water and k_{ro} at all fractional flows, however, the degree in reduction of k_{rw} is more severe than the degree of reduction in k_{ro} with temperature.

At 20°C, the differential pressure profile across the micromodel tends to have a peak value before it is stabilised after a period of time of up to 100 min. This is illustrated for all differential pressures at fractional flow 0%, 25%, 50%, 75% and 100% **Figure 5.32**. However, at 60°C, the differential pressure across the micromodel did not have the observed sharp peak pressure profile present at 20°C.

At 20°C, the peak pressure is observed at 261 mbar after 20 min, 241 mbar after 15 min, 387 mbar after 5 min, 400 mbar after 15 min and 230 mbar after 5 min for fractional flow 0%, 25%, 50%, 75% and 100% respectively. All the previous fractional flows stabilised at a lower differential pressure than the peak differential pressure after 100 min at 235 mbar, 322 mbar, 287 mbar, 347 mbar and 106 mbar at fractional flow 0, 25%, 50%, 75% and 100% respectively. Increasing the temperature to 60°C flattens or totally reduces the peak pressure profile compared to 20°C before the differential pressure reaches its stabilisation state. In **Figure 5.33**, the pressure profile during the 0% fractional flow is totally flat and stabilises at 226 mbar after 25 min. Further increasing the fractional flow to 25% and 50% causes the pressure to stabilise after 60 min around 375 mbar and 500 mbar respectively. Increasing the fractional flow to 75% and 100% flattens the peak pressure profile at 600 mbar and 700 mbar after 30 min to 60 min.

The S_{or} at the end of the steady-state experiment tends to be insensitive to the temperature; a S_{or} of 0.22 is reached at both 20°C and 60°C. The saturation at the relative permeability cross over tends to decreases from 0.68 to 0.63 as the temperature is increased from 20°C to 60°C.

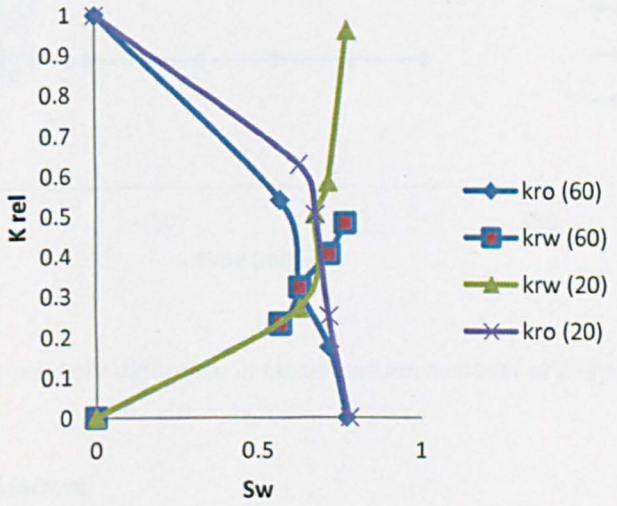

Figure 5.31 *Effect of temperature on relative permeability in micromodel treated by crude oil.*

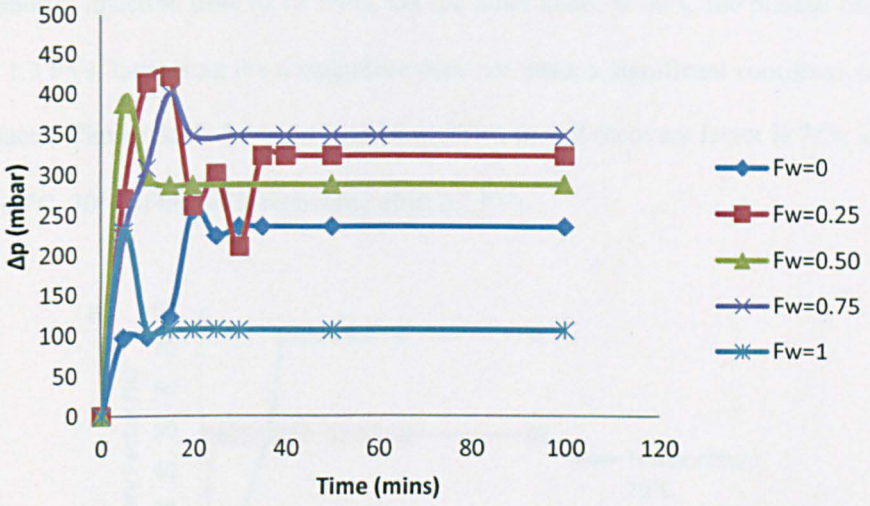

Figure 5.32 *The pressure difference in mixed-wet micromodel at temperature of 20°C.*

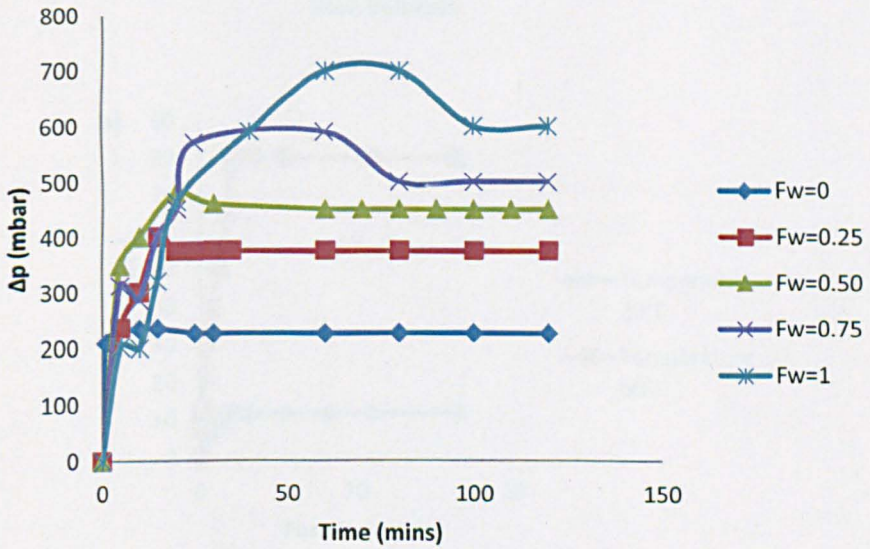

Figure 5.33 *The pressure difference in mixed-wet micromodel at temperature of 60°C.*

5.3.4.2 *Low rate imbibition*

The temperature has a profound effect in the imbibition recovery factor. At 20°C, the recovery factor is 74% compared with 49% when aging temperature is changed to 60°C **Figure 5.34**. The higher temperature of 60°C creates a higher pressure differential by 68 mbar when the brine imbibes into the micromodel. It is noteworthy that the higher temperature micromodel reaches its plateau oil recovery

in relatively shorter injection time (0.18 PVs). On the other hand, at 20°C the plateau oil recovery is reached after 1.3 PVs. Increasing the temperature does not make a significant contribution to the final oil recovery factor **Figure 5.35**. As water invades at 20°C, the oil recovery factor is 73% after 1.4 PVs injection. At 60°C, 70% of the oil is recovered after 2.7 PVs.

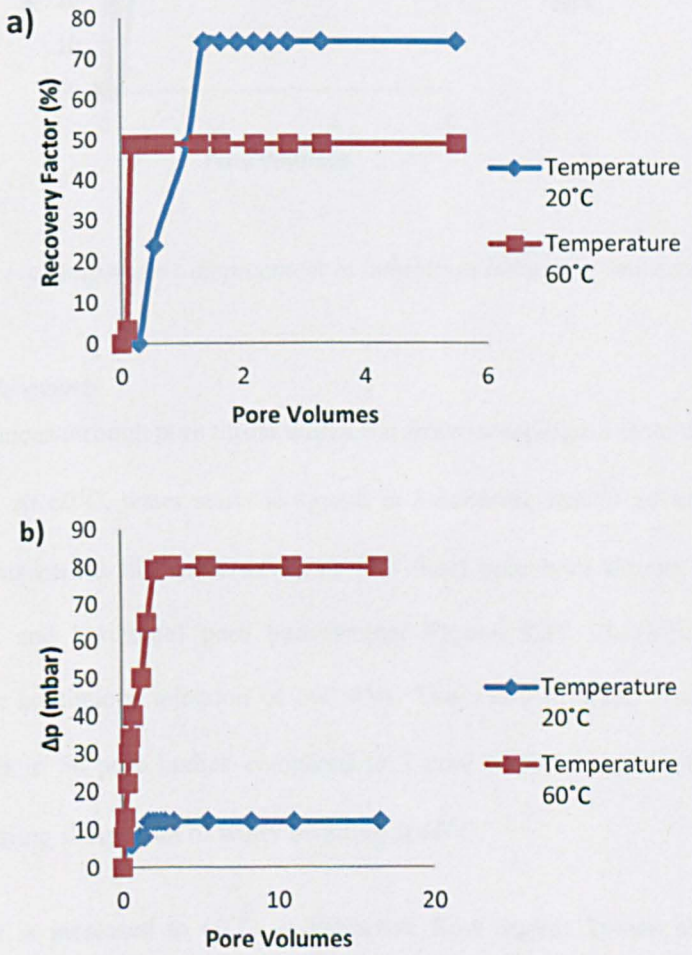

Figure 5.34 *Effect of aging temperature in imbibition of water to fully saturated micromodel by crude oil (a) Oil Recovery factor (b)Pressure response.*

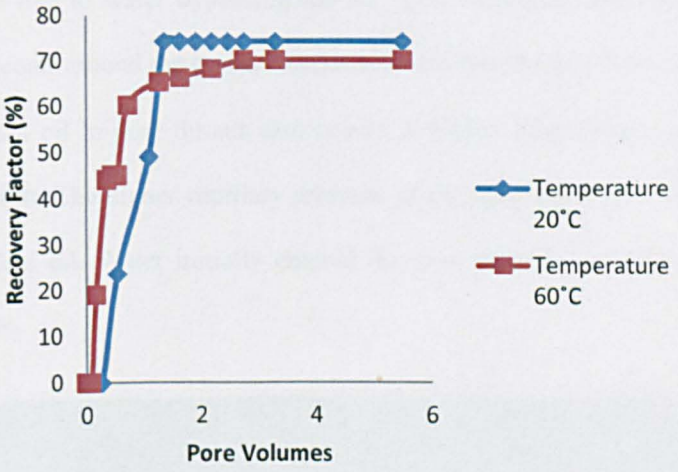

Figure 5.35 *Effect of temperature displacment in imbibition behaviour in mixed-wet micromodel.*

5.3.4.3 *Pore scale events*

At 20°C, water advances through pore throat with a flat front sweeping oil from the middle of the pore throat **Figure 5.36**. At 60°C, water starts to spread in a dendritic frontal advance rather than a flat frontal advance. This means the water advances into front pore body/throats instead of spreading equally to vertical and horizontal pore body/throats **Figure 5.37**. Dendritic frontal advance is observed even after continuous injection of 600 PVs. The width of water front that penetrates the micromodel extends to 50 pore bodies compared to 3 pore bodies at ambient temperature (20°C), which indicates a strong sharp front of water invading at 60°C.

As the temperature is increased to 60°C, a distinctive flow regime known as "sub-singlets flow" occurs. Water invades the pore bodies with smaller ganglia than at 20°C **Figure 5.38**. Due to the small size of sub-singlets of water drops, the water passes through pore throats without break-up into two sections as observed at 20°C.

Furthermore, the structure of residual oil varies with temperature. At 20°C, the oil tends to be trapped in circular thin (63.4 μm) oil films around the grains **Figure 5.16b**. At 60°C, the residual oil occurs as an irregular lamella that extend between more than one grain surfaces **Figure 5.40a**. The extension of lamella among several grain surfaces provide continuous residual oil films. This structure of residual

oil saturation trapped due to water bypassing the oil. This behaviour may reflect the presence of thicker (97.3 μm) oil coats around the grains compared to the thinner (63.4 μm) coats formed at 20°C. Entrainment of residual oil in pore throats also occurs at higher temperature, which restricts water movement **Figure 5.40b**. The higher capillary pressure in the pore throat may be responsible for the structure of the residual oil. Water initially entered the pore body but could not continue its path through the pore throat.

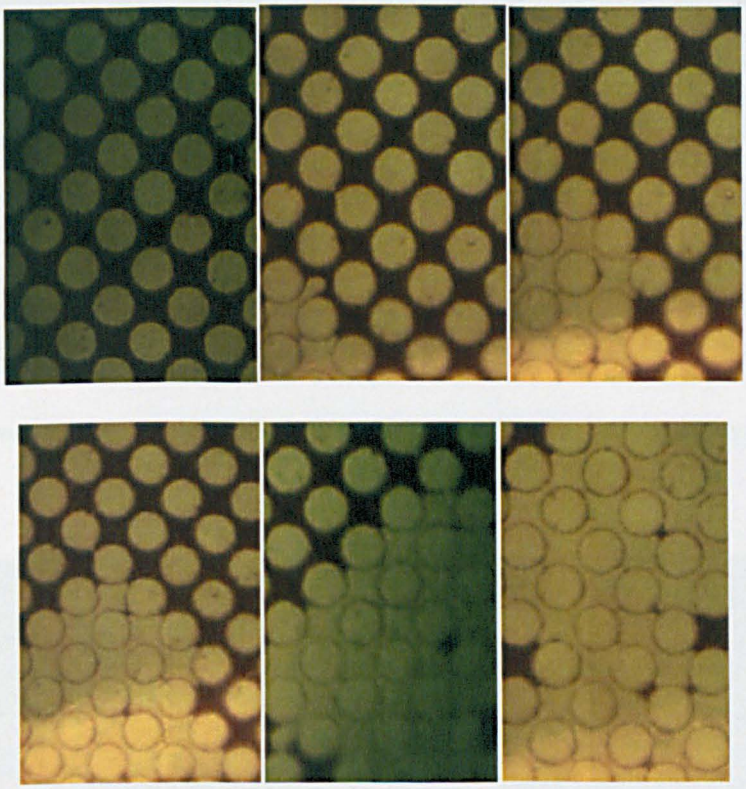

Figure 5.36 *Frontal advance flow regime of steady state flow of oil and water at temperature 20°C.*

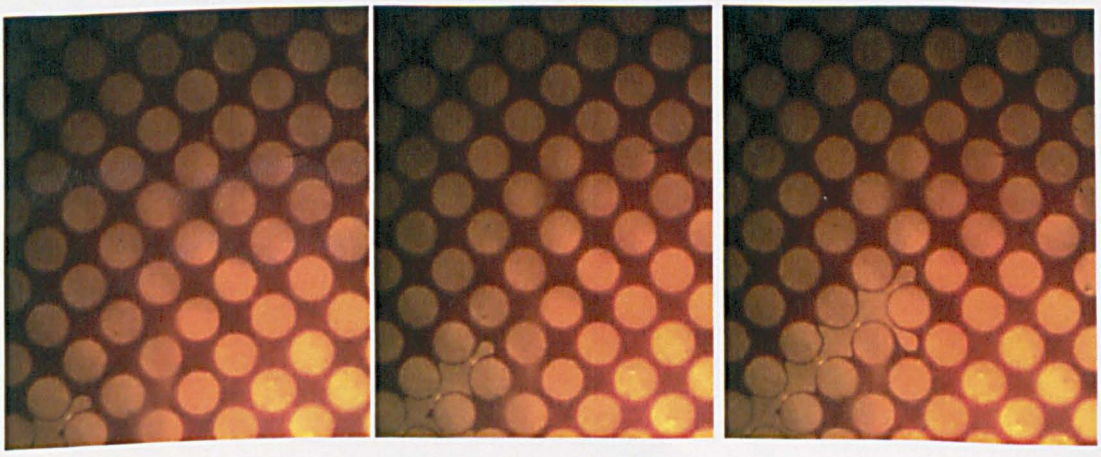

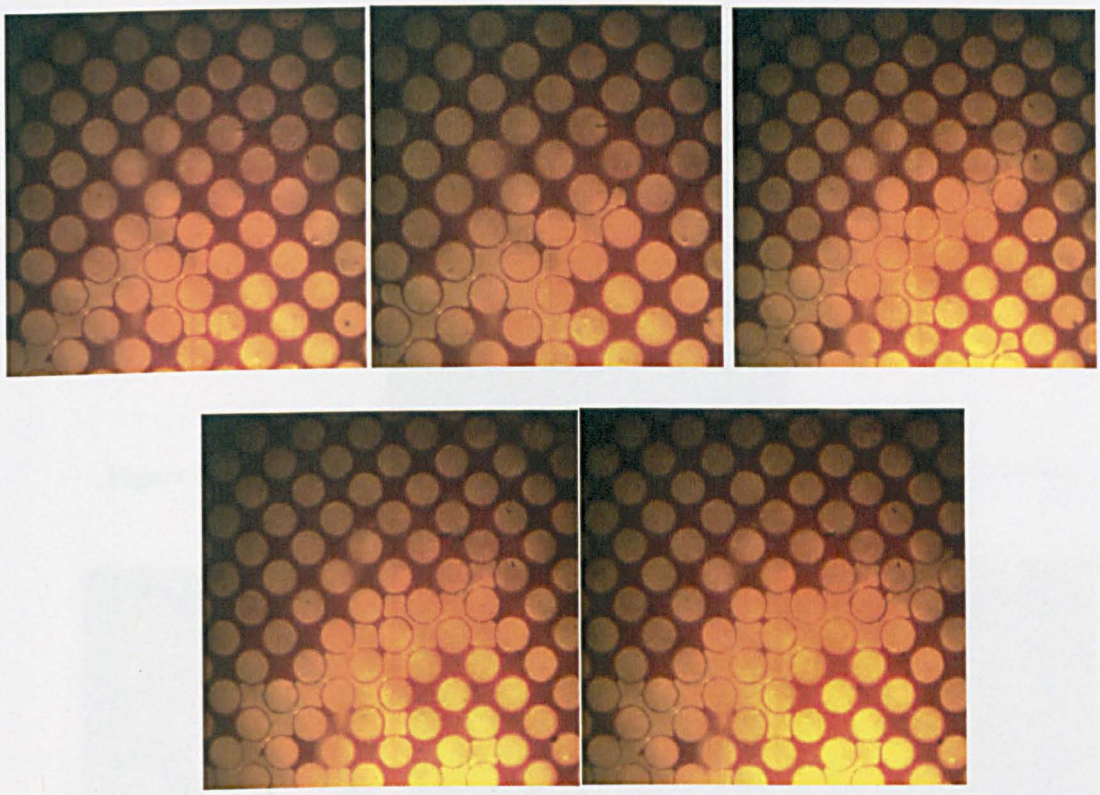

Figure 5.37 *Frontal Dendritic advance flow regime of steady state flow of oil and water at aging temperature 60°C .*

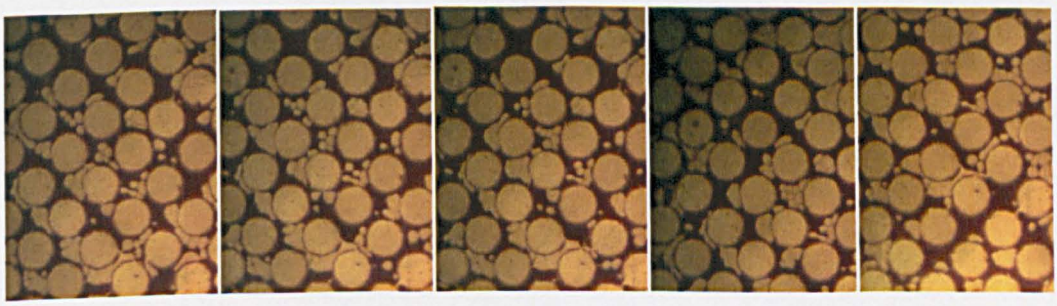

Figure 5.38 *Sub-singlet flow regime of steady state flow of oil and water at displacement temperature 60°C.*

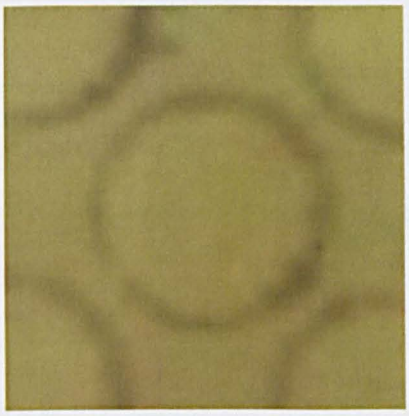

Figure 5.39 *Structure of residual oil saturation when temperature is 20°C (63.4 um).*

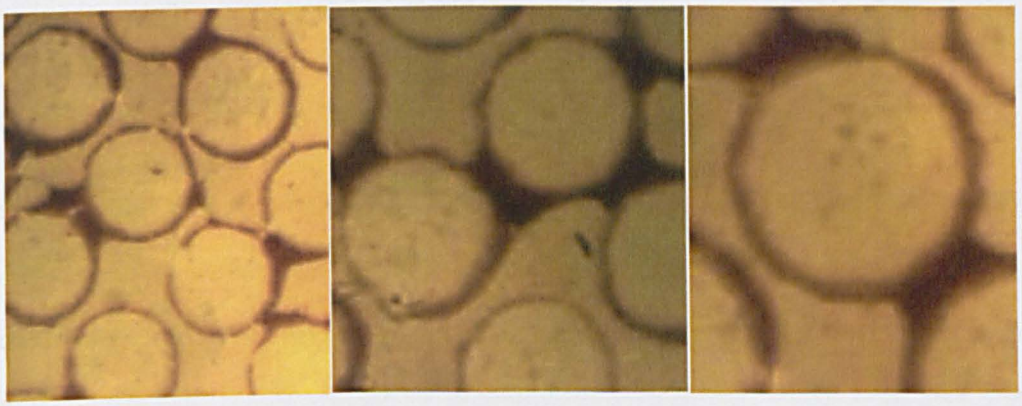

(a) (b) (c)

Figure 5.40 *Structure of residual oil a aging temperature 60°C: a) Lamella structure and (b) Entrainment residual oil saturation (c) Oil thin film (97.3 μm).*

5.4 Discussion

5.4.1 Effect of wettability

In water-wet micromodels, two distinctive pore scale flow mechanisms were observed during imbibition fractional flow at two rates: grain jump at flow rates of 0.04 cc/min and frontal imbibition at flow rates of 0.1-1 cc/min. Grain jump was observed when water was transferring through pore throats by jumping from grain to grain. Frontal flow initiated when water displaced oil mainly through pore bodies. When water film accumulates in the wetting layer, as a result of a reduction in the capillary pressure, it prevents oil being the continuous phase. The subsequent pore scale flow mechanism is frontal flow, which starts when further reduction in capillary pressure occurs, which

allows further invasion of water to the pore body. As a consequence of grain jump, the snap off oil occurs when the swelling of water no longer be accommodated in thin films. The occurrence of snap off at very low rates (0.04 cc/min) means that a long displacement time is an essential requirement to make the snap off occur. As the time increases, the water interface grows until it closes the path of oil which confirms why the snap off does not exist when displacement time is relatively short at higher rates (0.1 and 1 cc/min). This distinctive behaviour reflects clearly in the difference of 25% water end point relative permeability between rates of 0.04 cc/min and 1 cc/min. Although this distinctive pore scale events exists, the S_{or} changes by less than 5%, which indicates the action of grain jump during low rates mechanism contributes very little to the final S_{or}. Even though the structure of residual oil at low rate tends to be sub-singlets compared with thin oil layers that coat grain surfaces at high rates, the final difference in S_{or} was less than 5%.

The impact of these results, which show distinctive flow behaviour as a function of rate in the water-wet micromodel, contributes further undertanding relevant to dynamic pore scale modelling. Previous work on dynamic pore scale models (e.g. Mogensen and Stenby, 1998; Lenormand et al., 1983) focus only on single rate experiments, and only show snap off and piston-type motion. The work presented above shows that snap off is a function of rate; it is observed only at 0.04 cc/min and not at 0.1 cc/min and 1 cc/min. This means the dynamic pore scale modelling can enhance understanding of snap off only at specific rates not by extending the pore scale visualisation at single rate to be representative of a wide set of displacements rates. The experimental evidence of high resolution water/oil brine interface movement between pore bodies and pore throats is the first of its type that distinguish between flow behaviour as a function of rate in water-wet micromodels. These results contradict the work of Avraam and Payatakes (1995) and Valavanides and Payatakes (2001) who studied two-phase flow behaviour in imbibition and found disconnected ganglion dynamic is the main mechanism of the flow behaviour at low capillary numbers. In fact, the ganglion dynamic is observed in other types of wettability rather than the water-wet micromodels.

In the mixed-wet micromodel, snap off, that appears in water-wet micromodels at 0.04 cc/min, is suppressed. This suppression increased the end point k_{rw}, to 0.93 compared with 0.48 in the water-wet

micromodel at a rate of 0.04 cc/min. However, increasing the injection rate in the mixed-wet micromodel does not result in any major change in end point k_{rw}. This reflects a similar flow regime occurring at three rates (0.04, 0.1 and 1 cc/min). Although the thickness of the oil layers that surround the grains is reduced from 47.4 μm to 14.7 μm, the total S_{or} changes only by 6%. This indicates that residual oil in the mixed-wet micromodel is trapped mainly in pore throats, which contribute more to the final S_{or} rather than the isolated oil thin layers around the grains. This supports theoretical calculation (e.g. Sorbie et al., 2011) in which residual oil is modelled as films that are connected though pore throats across the porous media.

In the oil-wet micromodel, a sharp drop (39%) in end point k_{rw} is observed as the rate is increased to 1 cc/min from 0.04 cc/min. This was accompanied by a change in flow mechanisms in which the size of water blobs at 1 cc/min is five times larger than those that occur at 0.04 cc/min. This increase in size causes a high pressure across the blobs, which are translated into lower end point k_{rw}. According to Morrow et al. (1979), there is a tendency for blobs to become relatively more difficult to mobilise by viscous forces as they increase in size. The grain jump mechanism observed in the water-wet micromodel was not observed in the oil-wet models due to the low affinity of the grain surfaces to water. This hydrophobicity causes the water to seek alternative flow paths through pore bodies, which are wider than the pore throats. As a consequence, end point k_{rw} tends to increase more compared to the water-wet model. The S_{or} shows a clear dependence on the total rate between the 0.04 cc/min case and the (0.1 and 1 cc/min) case. In particular, at a rate of 0.04 cc/min the residual oil occurs as a 36.9 μm layer that coats the grains; which is the main governing contribution to the final residual saturation since there are no residual oil blobs in pore throats. On the other hand, at rates of 0.1 and 1 cc/min, S_{or} is reduced by 34%-35% corresponding to a reduction in thickness of the oil layer by 29.2 μm-32.7 μm. This means the ability of oil-wet grains to retain the oil is affected largely by rate. Compared with the mixed-wet case, S_{or} is less dependent on the rate increasing during mixed-wet model. This reflects the oil in the mixed wet model hangs between pore throats which become attached not only physically by hydrodynamic force, in fact is attached chemically through surface active components. These surface active components start anchoring in the grain surface that resist the

increasing rate more than the oil attached by hydrodynamic force in case of oil-wet model case. This indicates the existence of a critical capillary number in which S_{or} is reduced sharply. Chatzis and Morrow (1983) suggested this only occurs where uniform extreme wetting is applied. The critical capillary number does not exist in the mixed-wettability micromodels at any of the rates tested **Figure 5.41**.

Criags' rule (Criags, 1970) used to distinguish the wettability as dicussed in literature review (Chapter 2). However, Criags' rule proves a method to distinguish the wettability for all rates with some exception at high rate of 1 cc/min (**Table 5.2, Table 5.3** and **Table 5.4**). At 0.04 cc/min, residual oil saturation S_{or} was the least (20%) for decane treated micromodel, which is water-wet model. The S_{or} is the highest (39%) for silane treated micromodel, which is oil-wet model. In between extreme wetting models, the crude oil treated micromodel has an intermediate S_{or} (22%). Similarly there is a systemic decrease in relative permeability cross-over saturation as oil-wetness degree increases. The end point k_{rw} increases noticeably (by 48%) only when wettability treatment changes from decane to crude oil. A minor increase (7%) occurs when the micromodel treatment changes from crude oil to silane. At 0.1 cc/min, S_{or} does not agree with Criags' rule; achieving the highest (22%) among all three distinctive treatments **Table 5.3**. The reason for that might be that the residual oil hangs in the pore throats **Figure 5.40**. This type of structure persists even though flow rate is increased. As a result, the residual oil saturation is not striped easily compared with residual oil in micromodels treated of decane and silane. In fact, as rates increase to 1 cc/min, Criags' rule shows the extreme wetting created by treatment with decane and silane, is insensitive to residual saturation **Table 5.4**. Also, it shows the micromodel treatment by crude oil to hold residual oil by 30%. Nevertheless, these findings confirm the results of Blunt (1997) and Kumar et al. (2009) who found that S_{or} is extremely sensitive to changes in wettability. The anomalous behaviour in the silane micromodel, which shows a drastic reduction in end point k_{rw} from 0.99 during 0.1 cc/min to 0.60 during 1 cc/min can indicate the water continuity reduction is attributed to larger pressure increasing during 1 cc/min by large blob size of water compared to other pore scale events.

Micromodel treatment	Decane	crude oil	Silane
Relative permeability cross over saturation,%	77	68	68
Residual oil saturation, %	13	22	14
Maximum water Kr	0.60	0.99	0.94
Tendency in wettability based on Craig's wettability	W-W	O-W	O-W

Table 5.2 *Criags' rule of wettability used to define wettability class of micromodel treated by different agent at rate of 0.04 cc/min.*

Micromodel treatment	Decane	crude oil	Silane
Relative permeability cross over saturation,%	82	72	56
Residual oil saturation, %	20	22	39
Maximum water Kr	0.44	0.92	0.99
Tendency in wettability based on Craig's wettability	W-W	O-W	O-W

Table 5.3 *Criags' rule of wettability used to define wettability class of micromodel treated by different agent at 0.1 cc/min.*

Micromodel treatment	Decane	S-crude	Silane
Relative permeability cross over saturation,%	85	61	70
Residual oil saturation, %	7.00	30.0	5.00
Maximum water Kr	0.69	0.94	0.60
Tendency in wettability based on Craig's wettability	WW	OW	OW

Table 5.4 *Criags' rule of wettability used to define wettability class of micromodel treated by different agent at 1 cc/min.*

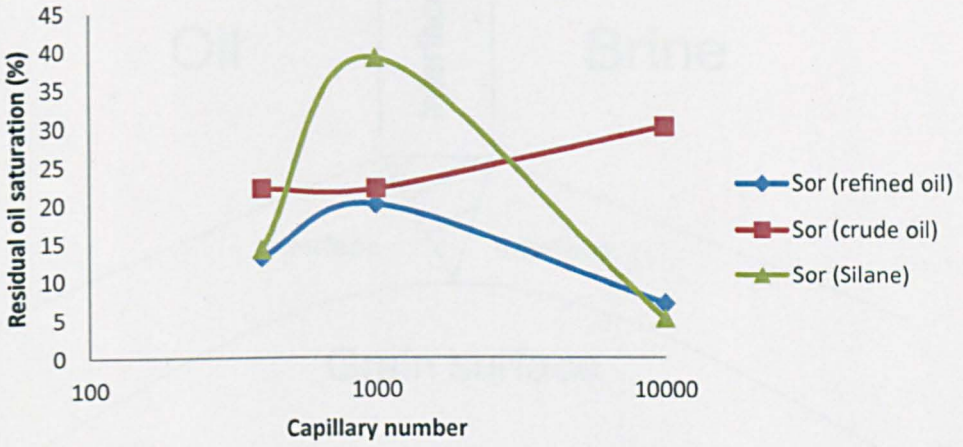

Figure 5.41 *Effect of capillary number on residual oil saturation through different wetting state (water-wet, mixed-wet and oil-wet).*

5.4.2 Effect of salinity

Three main flow behaviours that emerge from diluting the brine are pinch off in 3 M brine, piston frontal advance in 1 M brine, and striping oil with sharp frontal advance in 0.1 M brine. Since the change in end point k_{rw} is less than 10% with all brines, the alteration of flow behaviours does not seem to influence the shape of k_{rw} curve **Figure 5.20**. However, pinch off is the reason that causes the drastic drop in k_{ro} in 3 M brine compared with two other brines. The piston frontal advance and sharp frontal advance during the 1 M brine and 0.1 M brine did not cause a large difference in the k_{ro}. This means the distinctive difference in the shape of oil/brine curvature, which was observed with the 1 M and 0.1 M brine, does not influence the k_{ro}. Thus, the contribution of 3D line tensions, which locate around the three-phase confluence zone, is the governing factor in the process of displacement by brine **Figure 5.42**.

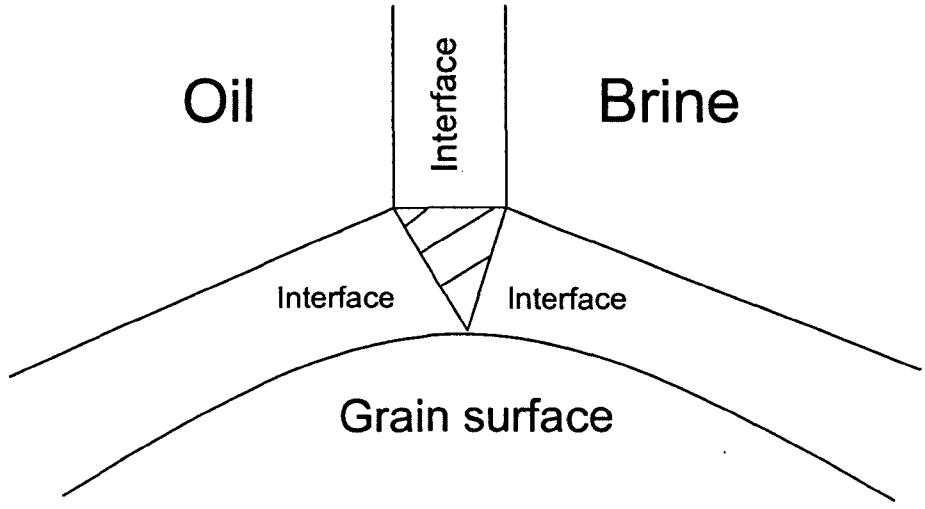

Figure 5.42 *Three dimensional line tensions which locate around the three-phase confluence zone influence during the flow of oil and brine interfaace.*

It is noted that the instability of pressure was accompanied with pinch off when approaching steady state flow. The instability of pressure totally disappears with sharp frontal advance type flow. This instability in pressure is caused by virtually chaotic passage of oil ganglia through most regions of the pore network. Coalescence during pinch off in 3 M brine can be explained through differences in pressure inside brine bubbles and oil wall formed by thin film. Due to high pressure inside brine bubble, migration of relatively high salinity brine increases until it displaces the thin oil film that separated the bubbles resulting in coalescence. Coalescence does not develop further to form continuous water drops that occupy pores. In other words, coalescence events are limited to small sub-singlet pores. The question remain to be answered what does it make coalescence to be inhibited at larger size drop when it involves a reduction in surface area which make overall energetically-favoured process? (Stover et al., 1998). Capillary flow, which encourages coalescence, can be retarded when other factors, such as brine salinity, are present in solution. Surface adsorption changes the interfacial flow at the oil-brine interface **Figure 5.43**. As liquid is carried away from the centre of a planar film during oil film drainage, any surface active components at the interface are transported towards the edge of the film. The stretching of the oil film surface, located between two brine bubbles, lowers the surfactant concentration at the centre of the film and raises its local interfacial

tension. The Gibbs adsorption isotherm, Γ, describes how the interfacial tension is related to the surface excess:

$$\Gamma = \frac{-C}{KT}\partial\frac{IFT}{C}$$

where c is concentration, K is Boltzmann's constant, IFT is interfacial tension and T is temperature. A local variation in surface excess across the surface of oil film drives a local variation in interfacial tension. The consequent restoring force against non-equilibrium surface concentration gradients is known as the Marangoni effect (Starov et al., 2007). These phenomena act to retard the oil film drainage, hence, inhibit the rupture of the oil film. The Marangoni effect is the reason for the emulsion-like flow behaviour that is observed during imbibition displacement by high salinity (3 M) NaCl brine. Furthermore, the deformation of the film surface during oil film squeezed between brine bubbles leads to increased interfacial elasticity. Gibbs elasticity of an interface, E, is a measure of the response of the interface to mechanical disturbance. It is proportional to the square of interfacial tension gradient, $(\frac{\partial IFT}{\partial c})$:

$$E = \frac{4c[\frac{\partial IFT}{\partial c}]^2}{kTD}$$

Here c is concentration, $(\frac{\partial IFT}{\partial c})$ is the change in interfacial tension with brine concentration, k is Boltzmann's constant, T is temperature and D is a measure of interfacial thickness (Christenson and Yaminsky, 1995). The impact of salinity on interfacial tension is too small between 0 M to 1 M; the interfacial tension changes by < 3 mNm^{-1} M^{-1}. Therefore the relative change of interfacial tension at the relevant concentration of brine is <10%. However the change in interfacial tension between 1 M to 3 M is 7.5 mNm^{-1} M^{-1}. Therefore the change is interfacial tension at relevant concentration of brine is <60%. This means the Gibbs elasticity is increased six times in the case of 3 M brine, which implies the oil film is more difficult to rupture during the collision.

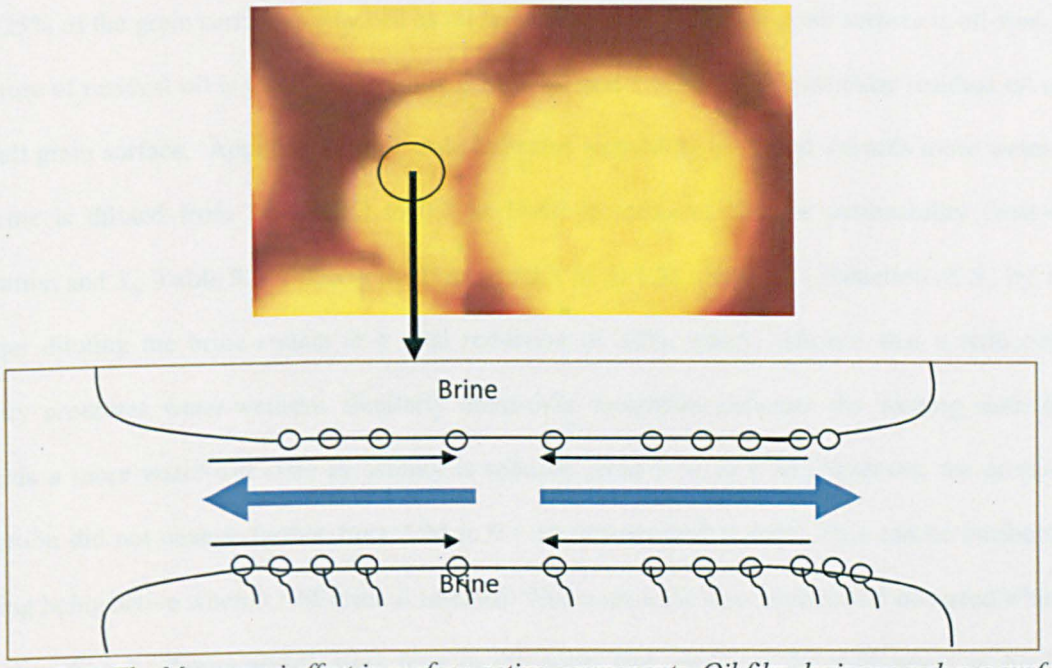

Figure 5.43 *The Marangoni effect in surface active components. Oil film drainage reduces surface concentration in the film centre. As a result, a non-equilibrium surface tension gradient is induced and opposed hydrodynamic oil film drainage which freeze the interface mobilised. This phonemena promote pinch off mechanism during 3 M NaCl brine and oil.*

Pinch off is not very effective in sweeping the oil as indicated by higher residual oil entrapment compared to frontal advance and striping with sharp frontal advance. The inefficiency of pinch off as an oil sweeping mechanisms is that the only way oil is transported between sub-singlets is via thin oil lamella. Avraam and Payatakes (1995) reported that the flow behaviour of non discrete connected oil pathway is aided by the fact that it leads to much smaller mechanical energy dissipation than discrete ganglion dynamics. The reduction of oil saturation in the experiments presented above is enhanced by the energy that is utilised to strip the oil from grain surface. In contrast, this energy is dissipated as occurred in the action of collision during 3 M brine.

The stripping of oil coats from grain surfaces proved to be the most effective sweeping mechanism, which decreased the S_{or} by 22% compared with pinch off. The shape of oil/brine interface into 0.1 M experiment is sharp whereas it is flat during 1 M brine experiment. Despite the existence of a sharp oil/brine interface in 0.1 M brine, there is no more residual saturation left behind the front movement compared to flat piston oil/brine interface during 1 M brine. It is the oil sweep by the strip off mechanism that compensates for any loss that can happen by sharp oil/brine interface. After strip off,

only 25% of the grain surface is attached as oil layer whereas 75% of the grain surface is oil-free. The structure of residual oil is totally different in 3 M brine and 1 M brine. In particular residual oil coats the full grain surface. Applying Criags' rule indicates wettability is shifted towards more water-wet as brine is diluted from 3 M NaCl to 0.1 M NaCl in terms of relative permeability cross-over saturation and S_{or} **Table 5.5**. Diluting the brine from 3 M to 1 M results in a reduction of S_{or} by 11%. Further diluting the brine results in a total reduction of 22%, which indicates that a reduction of salinity promotes water-wetness. Similarly cross-over saturation indicates the wetting state shifts towards a more water-wet state as salinity is reduced from 3 M to 1 M. However, the cross-over saturation did not change further from 1 M to 0.1 M; it remained at 66%. This can be attributed to striping being active when 0.1 M brine is injected. This pore scale flow mechanism occurred when k_{rw} is higher than k_{ro} during steady state flow in the pores and results in the differences in final S_{or}. However, when k_{rw} is equal to k_{ro} the stripping mechanism still does not act, which explains why the cross-over saturations are the same. These results do not support the proposed mechanism of oil recovery by low salinity flooding, which state that the presence of clay is an essential requirement to promote incremental oil recovery (Tang et al., 1999; Morrow and Buckley, 2011). In the micromodel, the type of mineral is pure silicate that does not contains any other minerals lining the pore walls, which indicates the existence of silicate negative surface is a sufficient condition to promote oil release by lower salinity displacement.

Micromodel treatment	**S-crude**	**S-crude**	**S-crude**
Brine condition	**Brine: 3M**	**Brine: 1M**	**Brine: 0.1M**
Relative permeability cross over saturation,%	49	66	66
Residual oil saturation, %	47	36	25
Craig's wettability	Weak W-W	W-W	Stronger W-W

Table 5.5 *Verification of the impact of brine salinity on wettability alteration.*

5.4.3 Effect of temperature

Increasing temperature results in a significant fall in end point k_{rw} in crude oil/brine/glass interaction, the relative permeability shows a drastic drop with water end point relative permeability by 48% during the steady state relative permeability. This drastic drop can be explained through dendritic advance flow behaviour **Figure 5.37**. This dendritic flow behaviour is totally different from the frontal advance flow behaviour that is active at 20°C. It is possible that dendritic flow occurs at 60°C due to the formation of a rigid oil skin at pore throat which blocks water. Water tends to seek another weaker oil skin to penetrate and allow the water to pass through without restriction. The 48% reduction of k_{rw} can be the result of rigid oil restriction to water flow compared to less restrictive frontal advance flow that occurs at 20°C **Figure 5.36**. S_{or} appears insensitive to temperature even though the residual oil shows an increase in layer thickness by 33.9 µm as temperature increased to 60°C **Table 5.2**.

Increasing the displacement temperature results in a small drops of flow behaviour defined as sub-singlet in which the water transfers into very small sizes while invading the micromodel. This sub-singlet flow does not influence the final residual oil saturation, S_{or}. In sub-singlet flow, the size of water interface is very small to carry out the oil, which makes the S_{or} insensitive to temperature.

Applying Criags' rule to distinguish the effect of aging temperature on wettability was inconclusive for two reasons: i) insensitivity of residual saturation to temperature, and ii) the contradiction between relative permeability cross over saturation values and end point k_{rw}. The shift of cross over saturation supports the promotion the oil-wetness due to reduction of cross over saturation from 0.68 to 0.63 as temperature increased from 20°C to 60°C respectively. However, the drastic drop of end point k_{rw} as temperature increases is consistent with the notion that oil-wetness decreases as temperature increases. Visualising residual oil during aging at 60°C reveals the presence of irregular lamella that extends between more than one grain surfaces. Such lamella resist the streaming of water into the pore

throat, which reduces the end point k_{rw}. As a result, Craig's rule of wettability can be misleading in tracking the wettability progress as temperature change **Table 5.6**.

Micromodel treatment	Crude oil	Crude oil
Temperature aging condition	20°C	60°C
Relative permeability cross over saturation,%	68	63
Residual oil saturation, %	22	22
Water relative permeability at maximum water saturation	1	0.48
Craig's wettability	Oil-wet	Strongly oil-wet

Table 5.6 *Verification of effect of aging temperature in wettability alteration.*

5.5 Conclusion

2D glass micromodels were utilised to investigate the effect of wettability, brine salinity, temperature and injection rate through visualising the fluid interfaces and quantifying the relative permeability of each fluid and the residual oil saturation. Several conclusions emerge during this study:

- Depending on the dynamic rate and wetting contact angle, flow imbibition behaviour can be classified into two main flow regimes. First, at very low rate (0.04 cc/min), grain jump, a flow mechanism in which water peels off the oil from grain surfaces and pore throats, is dominant. Increasing the rate to 0.1 cc/min and 1 cc/min converts the flow behaviour to frontal advance regime in which oil is mainly swept from pore bodies. Moreover, the existence of snap off at very low rates (0.04 cc/min) means that a long displacement time is an essential requirement for snap off to occur. The long displacement time comes from the action of growing water interface until it closes the path of oil. This confirms why snap off does not exist when displacement time is relatively short at higher injection rates of 0.1 and 1 cc/min. Increasing the contact angle to 60° and 170° using crude oil and silane agent respectively does not show a

sensitive rate effect in the flow behaviour. S_{or} is clearly dependent on wettability especially at high capillary number $\geq$ 1000.

- Three salinity-dependent flow regimes where identified in micromodels whose wettability had been altered using crude oil. Pinch off flow dominates when 3M NaCl is injected due to the Marangoni effect that maintains the thin oil lamella between brine bubbles. Diluting the brine to 1 M NaCl results in a change in flow behaviour to the frontal advance flow regime with brine maintain its continuity phase. Further diluting the brine to 0.1 M NaCl induces oil to be stripped from grain surfaces. S_{or} shows to be the maximum in the case of pinch off flow behaviour whereas it minimise in the case of stripping off oil flow behaviour.
- Existence of specific type of mineral in grain surface, such as clay, is not a requirement to have a successful low salinity EOR. The distinctive stripping off mechanism that exists in pure glass grain surface supports this conclusion. Thus, identifying clay content as screening EOR criteria in low brine salinity should be revisited.
- Temperature plays a major role in controlling the flow regimes in terms of static and dynamic modes. Increasing the temperature through static aging results in dendritic flow as a result of oil blocking the streaming water through pore throat which create an early sharp water front. Increasing the temperature during dynamic displacement create a sub-singlet water flow behaviour which inhibited any snap off flow behaviour.

Chapter 6
Effect of Salinity and Temperature in Wettability-Core Scale experiment

Pore geometry, type of minerals and geological heterogeneity are important factors that should be considered during EOR implementation. Investigation of the effect of brine salinity and temperature in reservoir cores is the central focus of this chapter. A novel experimental technique, which couples the NMR and displacement tests, is utilised to track the wettability alteration. The results are discussed in the context of field application to aid the fundamental understanding of effect of wettability alteration in petroleum recovery.

6.1 Introduction

Field development planning is critical in the development of successful EOR programmes. Various types of information are required from reservoirs regarding the interaction of the COBR system so as to optimize the EOR process. Core analysis studies are central to gathering the information needed for optimizing EOR. Core-scale experiments yield critical data that assists the reservoir engineer in executing the right decision during EOR implementation in specific reservoirs. For example, laboratory core tests are commonly made to evaluate the displacement efficiency of various EOR techniques. To mimic the reservoir conditions, reservoir wettability should be replicated in the tests. There are three approaches taken to replicate reservoir wettability. First, preserved core can be used that has been extracted from the reservoir without altering wettability (Wunderlich, 1991). Second, wettability of cleaned cores can be restored by saturating with reservoir brines and crude and the "aging" the core for a suitable length of time. Third, *in situ* reservoir conditions, such as high pressure and temperature, are used in the core tests.

The oil in the reservoir is always accompanied by a small amount of water. This water, which was deposited during the rock sediments in prehistoric times or introduced as a result of fluid flow over geological time, is known as connate water. Several factors control the interaction between crude oil, brine and the rock surface (e.g. type of rock minerals and aquifer composition). The understanding of these factors is enormously important for developing a rigorous knowledge about the reservoir play. Temperature and brine salinity are both critical factors that control COBR interactions (Al-Mjeni et al., 2011) but their impact is still poorly understood. Thus, this chapter aims to increase understanding by using core-scale experiments to study the effect of brine salinity and temperature on COBR interaction in outcrop and reservoir samples. Mixed wettability is recognised as the most widely accepted model of reservoir wettability (Salathiel, 1973; Morrow et al. 1986; Kovscek et al., 1993; Masalmeh, 2003; Tie and Morrow 2005). Previous core scale experiments are discussed in detail in the literature review (**Chapter 2**). The new contribution in the current work is that it provides a novel approach in combining experimental techniques: displacement tests, which is dominated by capillary imbibition, and non destructive, nuclear magnetic resonance (NMR), to track the effect of brine salinity and temperature in the COBR system. For the first time, this combination of techniques is applied in core scale experiments. Furthermore, the emphasis of rock interaction as a function of brine salinity and temperature was investigated by tracking the relative permeability behaviour during forced displacement experiments in a viscous dominated regime. Integration of the results from these experiments provides a framework for understanding COBR interaction in terms of wettability in static and dynamic displacements.

6.2 Experimental material and methods:

6.2.1 Experimental material:

6.2.1.1 *Core samples*

Three main core plugs used in the experimental section are an outcrop sandstone, a reservoir sandstone and a reservoir carbonate. The outcrop sample is the Berea sandstone extracted from Cleveland Quarries (Ohio in United States). The Berea sandstone has been used as a type material for experiments on porous media for almost 50 years due its homogenous petrophysical properties. The

mineralogical composition of Berea sandstone consists of quartz (78.5%), feldspar (6.0 %),Chert (1.6%), dolomite (2.5%), rock fragments (8.6%) and kaolinite (2.8%) (Ma and Morrow, 1994). The reservoir sandstone was extracted from Amal field in southern Oman. It is a medium grained, moderately sorted sandstone. The mineralogical composition consists mainly of quartz (71.0%), chert (26.0%), K-feldspar (3.0%), and heavy minerals (0.67%). The Amal sandstone differs from the Berea in two ways. First, the Amal reservoir sandstone does not contain kaolinite. Second, the pore structure in Amal reservoir sandstone is tighter than the Berea sandstone. The third type of core plug used in this study is a carbonate from Fahud field in Northern Oman. It is composed of calcite (86.4%), dolomite (5.9), quartz (2.0%), pyrite (1.2%) and gypsum (4.5%).

Mineral type	**Mineralogy composition (%)**	
	Berea sandstone	**Amal reservoir sandstone**
Quartz	78.5	71.0
Chert	1.6	25.0
Feldspar	6.0	3.0
Heavy minerals	0.0	0.67
Kaolinite	2.8	0.0
Sedimentary	0.0	0.38
Dolomite	2.5	0.0
Rock Fragments	8.6	0.0
Total	100	100

Table 6.1 *Berea sandstone and Amal sandstone cores mineral composition. Berea data is from Ma and Morrow (1994).*

Mineral type	Mineralogy composition (%)
	Fahud reservoir core
Calcite	86.4
Dolomite	5.91
Quartz	2.02
Pyrite	1.20
Gypsum	4.47

Table 6.2 *Fahud reservoir cores mineral composition.*

Sample ID	Length (cm)	Formation	Diameter (cm)	He Permeability (md)	Porosity (%)
B4	6.64	Berea sandstone	3.78	111.3	19.42
B5	6.64	Berea sandstone	3.75	69.6	20.10
B6	6.61	Berea sandstone	3.75	106.8	20.88
B7	6.60	Berea sandstone	3.78	129.8	20.54
B7a	6.62	Berea sandstone	3.80	129.8	25.71
B7b	6.59	Berea sandstone	3.79	67.4	25.34
B7c	6.65	Berea sandstone	3.78	97.5	26.56
B7d	6.63	Berea sandstone	3.80	67.6	26.43
B7e	6.60	Berea sandstone	3.79	125.7	26.16
B7g	6.62	Berea sandstone	3.80	88.6	26.27
B8	6.62	Berea	3.79	70.5	25.77

		sandstone			
B9	6.60	Berea sandstone	3.79	64.0	23.16
B10a	6.63	Berea sandstone	3.78	111.0	24.98
B10b	6.64	Berea sandstone	3.79	129.0	25.82
B10c	6.64	Berea sandstone	3.79	126.0	26.23
B10d	6.57	Berea sandstone	3.80	71.6	24.71
B10db	6.61	Berea sandstone	3.79	81.3	25.45
B11	6.62	Berea sandstone	3.80	57.6	21.38
B12	6.62	Berea sandstone	3.79	51.7	24.19
B13	5.15	Berea sandstone	3.78	50.0	27.04
B14a	5.03	Berea sandstone	3.75	50.8	29.48
B15	4.98	Berea sandstone	3.77	70.8	25.52
B16	4.80	Berea sandstone	3.77	60.9	26.20
C13	3.95	Carbonate	3.50	3.35	32.75
C14	4.07	Carbonate	3.78	1.23	25.84

Table 6.3 *Petrophysical properties of core plugs.*

6.2.2 Fluids

An asphaltic crude oil is used in this study that sampled from Fahud crude oil reservoir. **Table 6.4** and **Table 6.5** list its physical and chemical properties measured by methods discussed in Chapter 3. Prior to use, the crude oil was filtered to remove particulate matter and then left under vacuum for 2 hours

at room temperature to minimize the possibility of gas production during the course of displacement. NaCl brines were used in all experiments. The brine was degassed by vacuum. The viscosity of the brines were all 0.90 cp at 20°C. The density of the brine is 0.998 g/cc.

Crude oils	Density (g/mL)	Interfacial tension (mN/m)	Viscosity (cp)	Asphaltene recovered (wt%)
F-200	0.857	27.1	19.00	0.56 (n-heptane as precipitant)

Table 6.4 *Crude oil physical properties.*

Crude oil	SARA			
	Saturates (%)	Aromatics (%)	Resins (%)	nC7Asph. (%)
F-200	38.2	38.2	23.04	0.56

Table 6.5 *Crude oil chemical properties.*

6.2.3 Core preparation

6.2.3.1 *Core cleaning*

Three main methods are commonly used in core cleaning for wettability restoration: Dean-Stark, Soxhlet (distillation-extraction), flow of solvents and gas-driven solvent extraction. Here, core plugs were cleaned by Dean-Stark extraction using dichloromethane (DCM) until no change in the colour of effluent fluids was observed.

6.2.3.2 *Establishing initial water saturation*

The cores were saturated with NaCl brine and held for 3 days at room temperature in sealed cups to establish ionic equilibrium. The cores were placed in a stainless steel pressure vessel and pressurised to 1000 psi to ensure the water saturated 100% of pores. A comparison between pore volumes calculated by weight method and helium porosimeter confirmed that the cores were fully saturated.

Initial water saturation, S_{wi}, was established by flooding the saturated cores with oil until water was no longer produced.

6.2.3.3 *Aging in crude oil*

After establishing S_{wi}, the core were removed from core holder, submerged in the crude oil in a pressure vessel, and aged at 20°C for 10 days. The selection of the aging time is justified by the results in **Chapter 4**.

6.2.3.4 *Displacement test*

The current study concentrated on two tests: spontaneous imbibition and waterflooding. After aging, the core was removed from the core holder and then placed in an imbibition cell filled with brine. The volume of the oil expelled from the core was recorded versus time. Oil recovery by spontaneous imbibition, R_{im}, was calculated using equation:

$$R_{im} = \frac{V_{o,im}}{V_{o,s}} \times 100$$

where R_{im} is oil recovery by spontaneous imbibition (% OIIP); $V_{o,im}$ is volume of the oil expelled from the core (cc); $V_{o,s}$ is volume of saturated oil (cc).

Scaling of spontaneous imbibition provides a technique for evaluating the wettability of reservoir rocks and provides a comparison of rock wettability from one system to another. This technique was used before in tracking the wettability change of sandstone and carbonate (Tang et al., 1999; Tong et al., 2005; Nasiri et al., 2009).

$$t_D = C\sqrt{\frac{k}{\emptyset}} \times \frac{\sigma}{\sqrt{\mu_o \mu_w}} \frac{t}{{L_c}^2}$$

where t_D is dimensionless time; C is a constant (0.018); k is gas permeability (md); ø is porosity (fraction); σ is interfacial tension (dyne/cm); μ_o is viscosity of oil (cp); μ_w is viscosity of brine (cp); t is imbibition time (min) and L_c is the characteristic length (cm). The curve of spontaneous imbibition, R_{im}, against t_D was plotted for each imbibition test.

After the spontaneous imbibition ceased, a forced imbibition was undertaken by flooding the core with brine at constant rates steps 0.04, 0.1, 0.15 and 0.2 cc/min to attain the final residual oil saturation. A core holder is used with an oil confing pressure of around 500 psi. The oil volume produced under spontaneous imbibition, Vo, imb, and force imbibition ,V_{of}, was used to obtain the water Amott index, I_w.

$$I_w = \frac{Vo, imb}{Vo, imb + Vo, f}$$

The cores were then placed under spontaneous imbibition and forced imbibition by oil in a similar manner of previous steps to calculate the oil Amott index, I_o. The subtraction of both indices yields Amott-Harvey index, I_{AH}, which is a standard wettability indicator (Morrow, 1990).

6.2.3.5 *Nuclear Magnetic resonance measurements*

NMR surface relaxation is utilised for the first time to investigate the role of brine salinity and temperature in wettability alteration. Previous work (e.g. Chen et al., 2006) showed that NMR is a sensitive indicator for wettability alteration by synthetic oil-based mud (OBM). Several NMR wettability indicies have been proposed. In this work, an NMR index formulated by Al-Mahrouqi et al. (2006) was used. This index was selected because it is less time consuming than the Fleury et al., (2003) wettability index, which requires four measurements of surface relaxation at four saturation points. The Al-Mahrouqi index only requires two measurements: surface relaxation at end points initial water saturation, $T_{2LM,Swi}$, and residual oil saturation, $T_{2LM,Sor}$, without the necessity of cleaning the core plugs. For the 25 core plugs described in this chapter, the NMR wettability index, I_{NMR}, is selected as following.

$$I_{NMR} = \left(\frac{T_{2LM,Swi}}{T_{2LM,Sor}}\right) - 1$$

6.2.3.6 *Unsteady state relative permeability*

Unsteady-state relative permeability experiments were used to investigate the impact of brine salinity and temperature during dynamic interaction of COBR. The method is based on JBN calculation

(Johnson et al., 1959) during waterflooding at rate 0.04 cc/min. The unsteady state displacement test setup is shown in **Figure 6.1**. The core plugs were confined under a pressure of 500 psi to mimic the reservoir overburden pressure. The core plugs were first fully saturated by brine and displaced by oil to attain S_{wi}. The pressure differential, ΔP, across the core was measured using a differential pressure transducer. The slope of ΔP vs. flow rate, q, is a function of the absolute and relative permeability. Next, a waterflood displacement test was carried out at 0.04 cc/min. Oil production was measured using an inverted burette, which acted as a separator/accumulator. The volume of oil produced was recorded at different time intervals. The breakthrough time was recorded using a stopwatch when the first droplet of water appeared at bottom of the inverted burette.

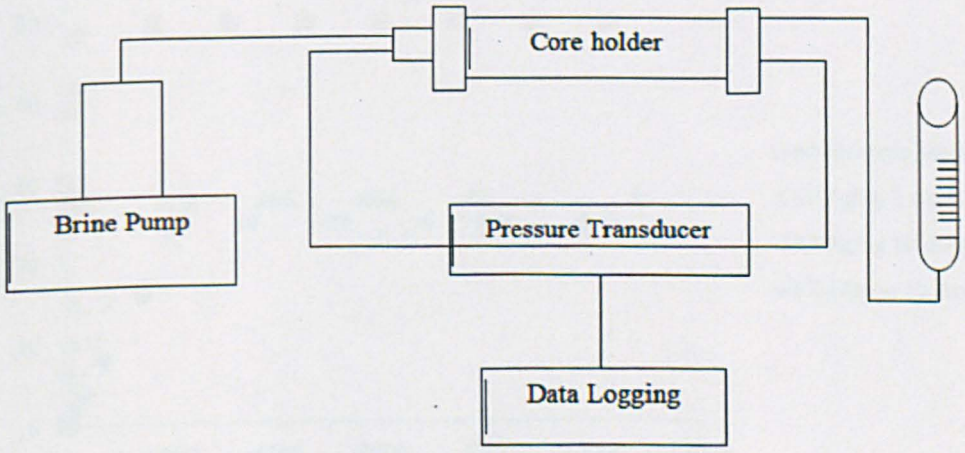

Figure 6.1 *Unsteady state relative permeability set-up.*

6.3 Results:

6.3.1 Displacement test

6.3.1.1 *Effect of aging time*

Imbibition behaviour is discussed in terms of imbibition rate and extent **Figure 6.2** as well as the Amott-Harvey wettability index, I_{AH}. For the core plug that was saturated with refined oil, the imbibition rate was very sharp, with 48.2% oil recovery in 220 min. Free imbibition for another 30 days only resulted in a total recovery 49.5%. Oil recovery rate was significantly slower from the core

plug that was aged with crude oil for 2 days. In particular, only 27.6% oil was recovered after 30 days, which is virtually the same as that recovered after breakthrough (27.1%). Increasing aging time to 10 days resulted in a further reduction in the imbibition rate, with 14.7% recovered after 1.5 days and 23% after 30 days. A distinctive feature with cores saturated with crude oil is the induction time period (t_D= 8.27x10^2) before oil production started compared with core plugs that were saturated with refined oil. Increasing the aging time to 25 days does not make any significant change in the rate except the minor reduction in the extent of oil recovery from 24.6% to 23%. The forced imbibition cycles of water and oil shows I_{AH} changes dramatically from 0.96 for cores that aged at two days to 0.38 for cores that aged for 25 days **Table 6.6**. I_{AH} is 0.36 for an intermediate aging time of 10 days.

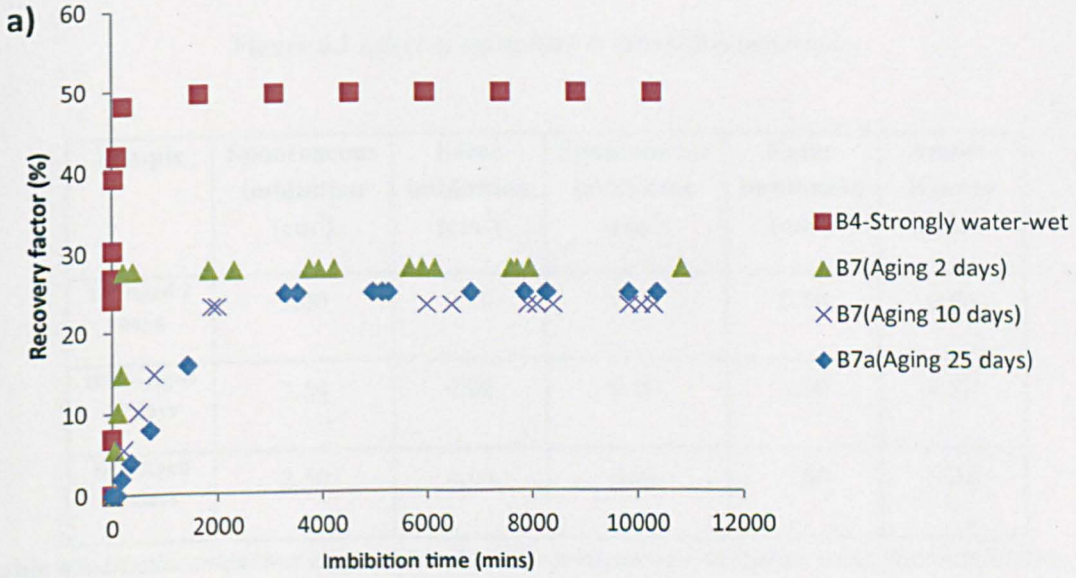

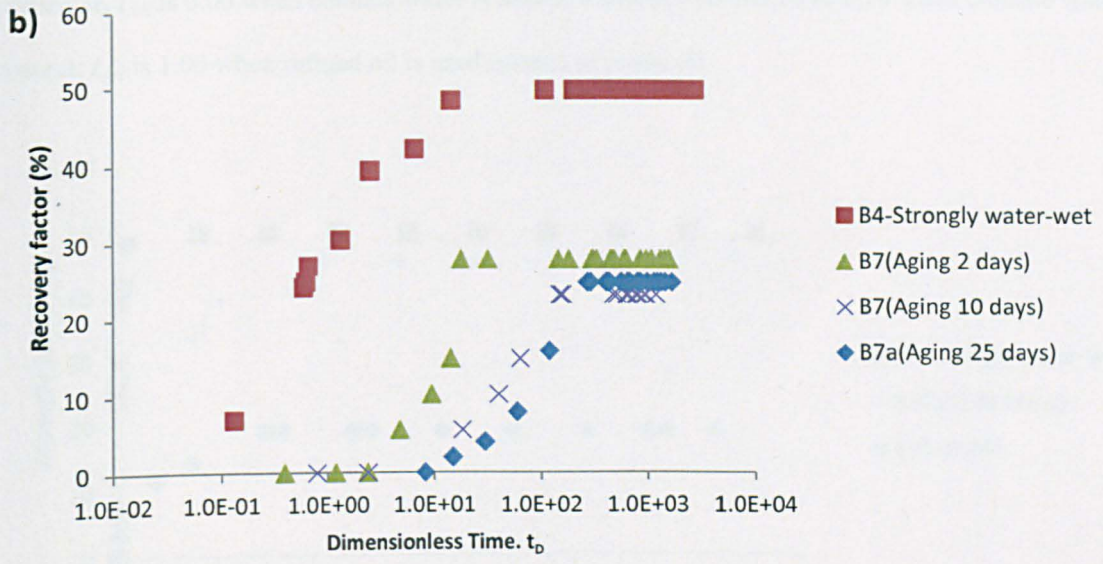

Figure 6.2 *Effect of aging time in imbibition behaviour.*

Sample	Spontaneous imbibition (cm^3)	Force imbibition (cm^3)	Spontaneous imbibition (cm^3)	Force imbibition (cm^3)	Amott-Harvey index
B7-Aged 2 days	3.00	0.10	0.00	0.10	0.96
B7a+-Aged 10 days	2.54	4.00	0.00	1.00	0.39
B7a-Aged 25 days	2.50	4.00	0.00	1.00	0.38

Table 6.6 *Displacement test experiment of water spontaneous imbibition, water force imbibition, oil spontaneous imbibition and oil force imbibition.*

6.3.1.2 *Impact of connate water*

The imbibition rate when connate water is absent is higher than in cores containing connate water. This behaviour can be observed between dimensionless time of 1 and 100 **Figure 6.3**. Around 46% of oil is recovered when connate water is absent compared with 19% when connate water is present. It is noteworthy that both cores show an induction time period before oil production breakthrough whether connate water is present or not. The presence of connate water has a distinct influence on I_{AH}. In

particular, I_{AH} is 0.00 when connate water is absent **Table 6.7** compared to 0.19 when connate water is present. I_{AH} is 1.00 when refined oil is used instead of crude oil.

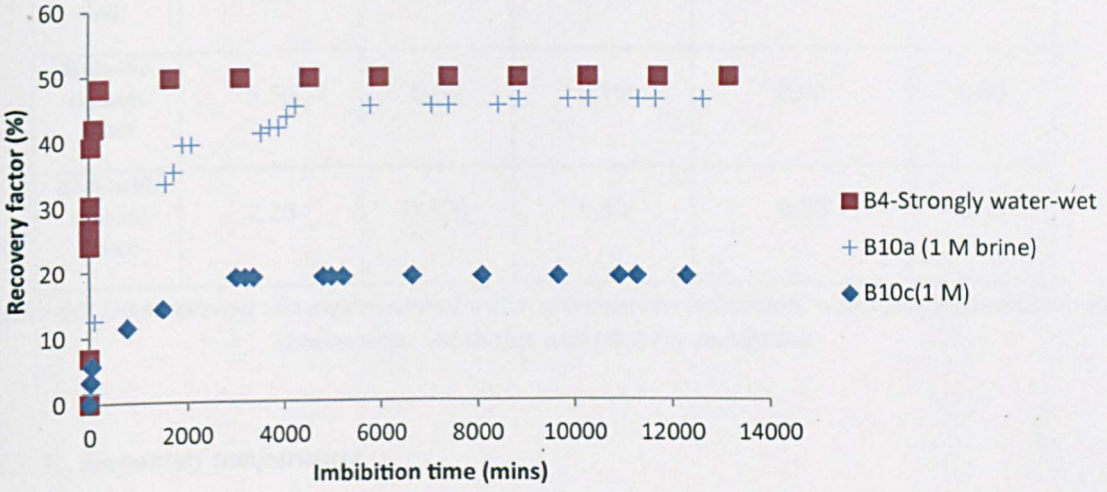

(a)

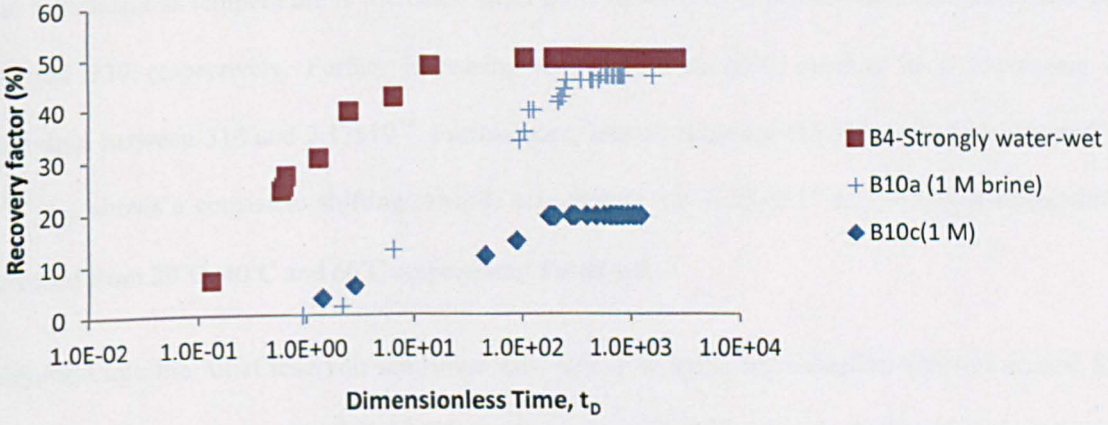

(b)

Figure 6.3 *Effect of connate water on imbibition behaviour.*

Sample	Spontaneous imbibition (cm^3)	Force imbibition (cm^3)	Spontaneous imbibition (cm^3)	Force imbibition(cm^3)	Amott-Harvey index
B4-refined oil	7.20	0.00	0.00	0.10	1.00
B10a-No connate water	5.50	0.00	0.10	0.00	0.00
B10c-with connate water	2.20	0.500	0.50	0.30	0.19

Table 6.7 *Displacement test experiment of water spontaneous imbibition, water force imbibition, oil spontaneous imbibition and oil force imbibition.*

6.3.1.3 *Impact of temperature*

Minor reduction in the imbibition rate was observed between dimensionless time of 10 and 500 as temperature was increased from 20°C to 40°C **Figure 6.4**. Moreover, the extent of oil recovery is reduced from 24.6% to 21.7% as temperature increased from 20°C to 40°C. The induction imbibition time is reduced as temperature is increased from 20°C to 40°C in which the dimensionless time was 830 and 330 respectively. Further increasing temperature to 60°C resulted in a lower rate of imbibition between 313 and $2.13x10^{+4}$. Furthermore, less oil recovery (15.5% total) was observed at 60°C. I_{AH} shows a consistent shifting towards oil-wetness (i.e. 0.38, 0.17 and -0.10) as temperature increased from 20°C, 40°C and 60°C respectively **Table 6.8**.

Imbibition into the Amal reservoir sandstone was very slow with long induction times of around 530 **Figure 6.5**. The recovery of oil is 12.5% at temperature of 20°C whereas 2.40% at temperature of 60°C. The induction imbibition time was $8.18 \times 10^{+4}$, which is clearly two fold higher than at room temperature. I_{AH} is 0.22 and -0.80 for temperatures of 20°C and 60°C respectively **Table 6.8**. The rate of imbibition in the carbonate core was very low compared with previous samples. It is clear that increasing the temperature slightly shifts the rate higher to reach 3.2% of oil recovery compared to no oil production when the temperature is 20°C **Figure 6.6**. I_{AH} shifts from -0.89 to -0.85 as temperature is increased from 20°C to 60°C respectively.

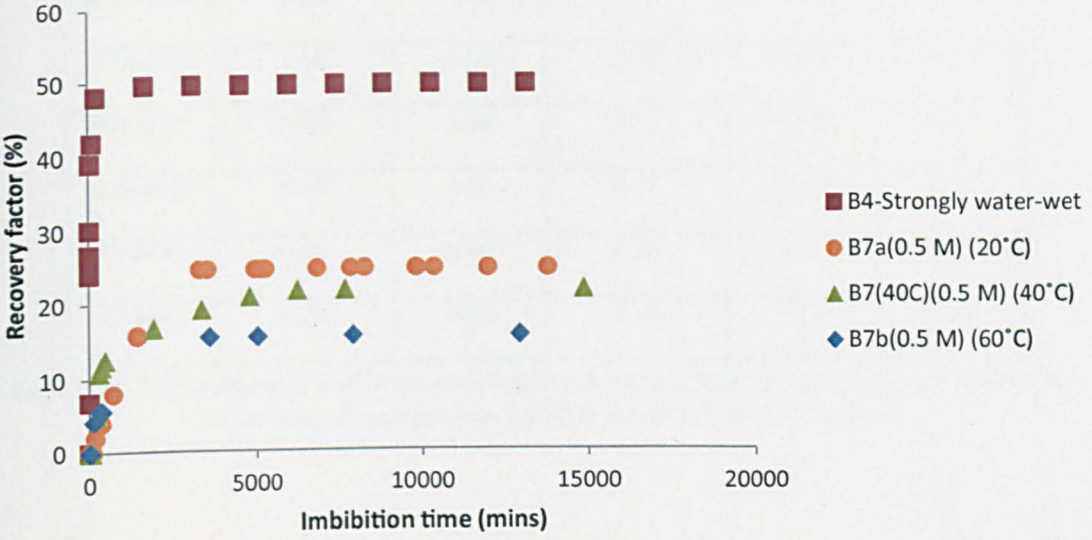

(a)

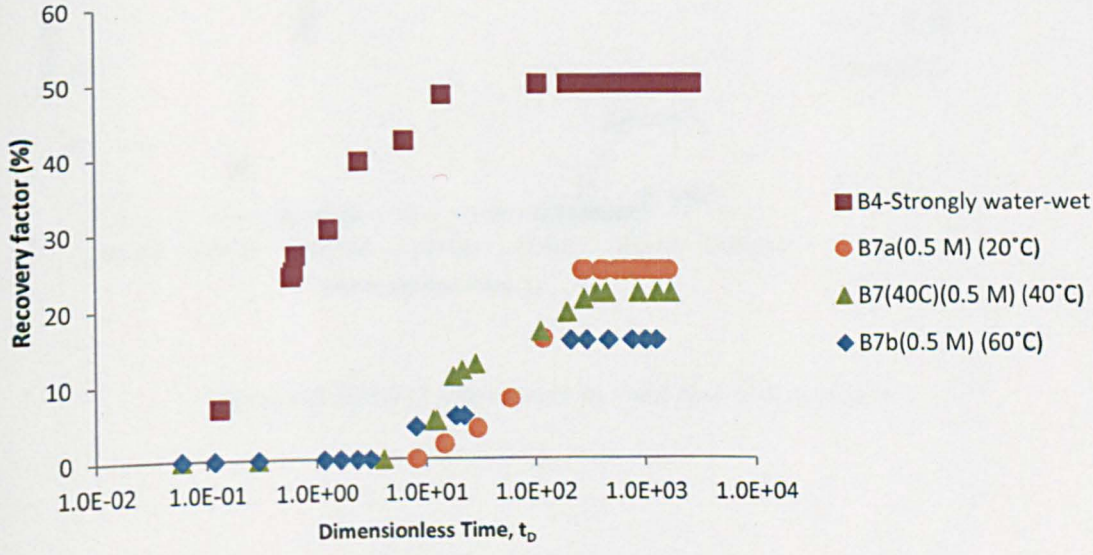

(b)

Figure 6.4 *Effect of temperature in imbibition of water.*

Sample-Temp	Spontaneous imbibition (cm^3)	Force imbibition (cm^3)	Spontaneous imbibition (cm^3)	Force imbibition (cm^3)	Amott-Harvey index
B7a-20°C	2.50	4.00	0.00	1.00	0.38

B7a+-40˚C	2.00	10.00	0.00	1.00	0.17
B7b-60˚C	1.10	4.00	0.50	1.00	-0.10
B13-20˚C	0.90	2.00	0.10	1.00	0.22
B14-60˚C	0.10	3.00	0.70	0.50	-0.55
F1-20˚C	0.00	6.00	4.00	0.50	-0.89
F2-60˚C	0.20	6.00	4.00	0.50	-0.85

Table 6.8 *Displacement test of temperature effect of water spontaneous imbibition, water force imbibition, oil spontaneous imbibition and oil force imbibition.*

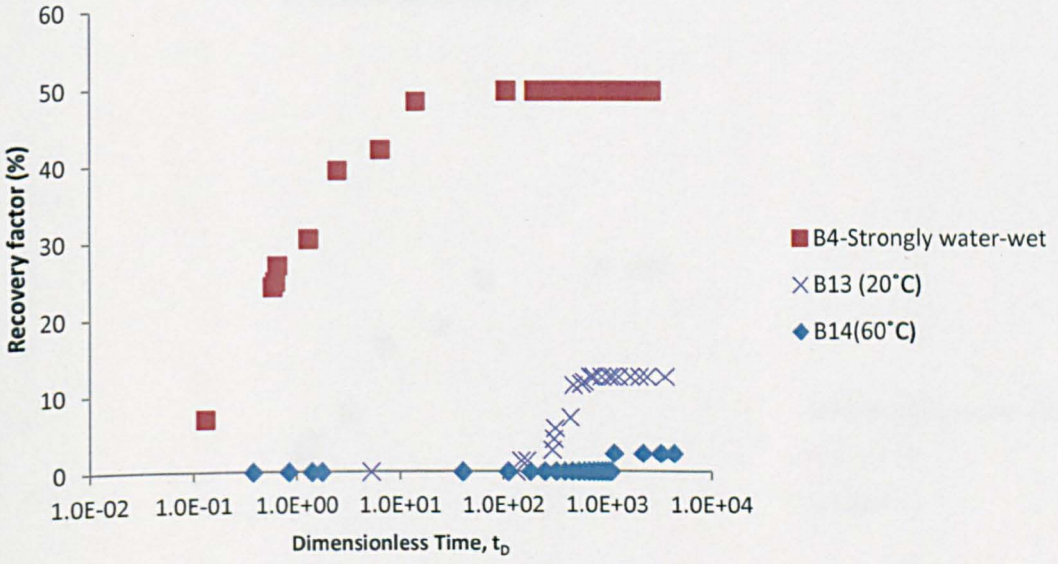

Figure 6.5 *Effect of temperature in Amal reservoir sandstone.*

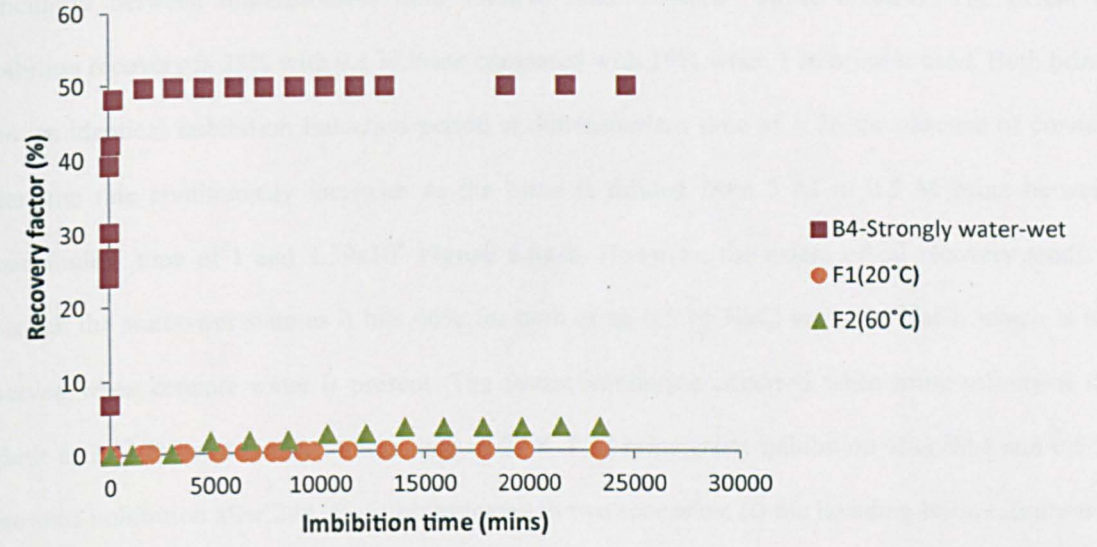

(a)

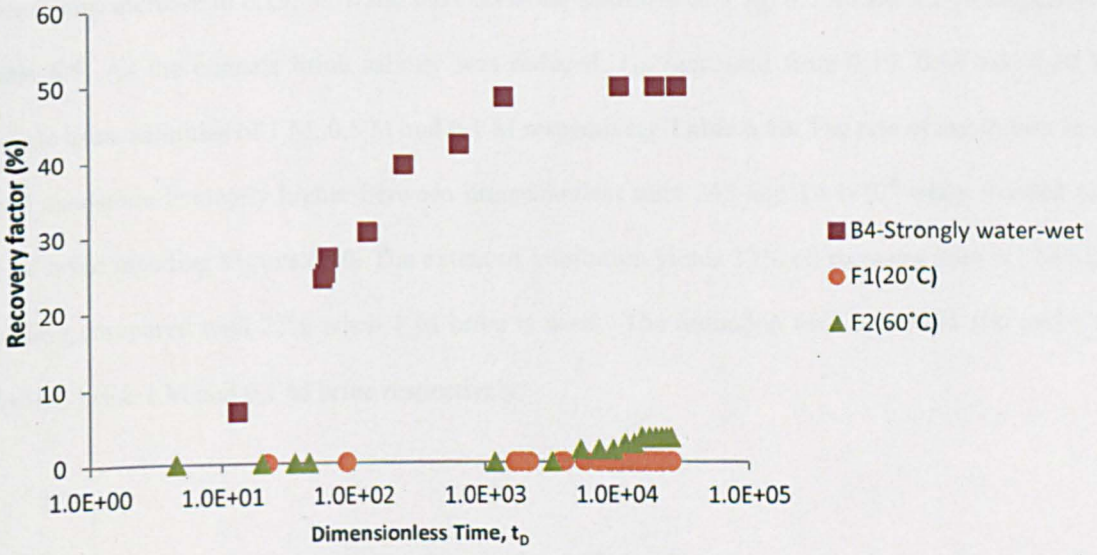

(b)

Figure 6.6 *Effect of temperature in Fahud reservoir sandstone.*

6.3.1.4 *Impact of brine salinity*

The impact of brine salinity is investigated through two different COBR interactions with connate water and without connate water. In the case of connate water, samples with 0.1 M NaCl brine experienced a higher rate of spontaneous imbibition compared with those with 1 M NaCl brine;

particularly between dimensionless time $1.49x10^4$ and $8.94x10^3$ **Table 6.10a-b**. The extent of imbibition recovery is 25% with 0.1 M brine compared with 19% when 1 M brine is used. Both brines show an identical imbibition induction period at dimensionless time of 1. In the absence of connate water, the rate continuously increases as the brine is diluted from 3 M to 0.5 M brine between dimensionless time of 1 and $3.39x10^4$ **Figure 6.8a-b**. However, the extent of oil recovery tends to approach the water-wet state as it hits 46% for both brine 0.5 M NaCl and 1 M NaCl, which is not observed when connate water is present. The fastest imbibition occurred when brine salinity is the highest in 3 M brine at dimensionless time of 27.8, 1 M brine starts imbibition after 92.8 and 0.5 M brine start imbibition after 248. I_{AH} is investigated in two scenarios: (i) the invading brine salinity was varied while the salinity of the connate brine was initially constant, and (ii) the connate brine salinity was varied while the brine salinity was held constant. As invading brine salinity is reduced, I_{AH} shows a consistent increase to 0.19, 0.51 and 0.81 for brine salinities of 1 M, 0.5 M and 0.1 M respectively **Table 6.9**. As the connate brine salinity was reduced, I_{AH} increased from 0.19, 0.38 and 0.50 for connate brine salinities of 1 M, 0.5 M and 0.1 M respectively **Table 6.10**. The rate of imbibition in the Amal sandstone is clearly higher between dimensionless time 245 and $1.84x10^4$ when flooded with 0.1 M brine invading **Figure 6.10**. The extent of imbibition yields 33% oil recovery with 0.1 M brine invading compared with 22% when 1 M brine is used. The induction time is around 100 and 3 for invading brine 1 M and 0.1 M brine respectively.

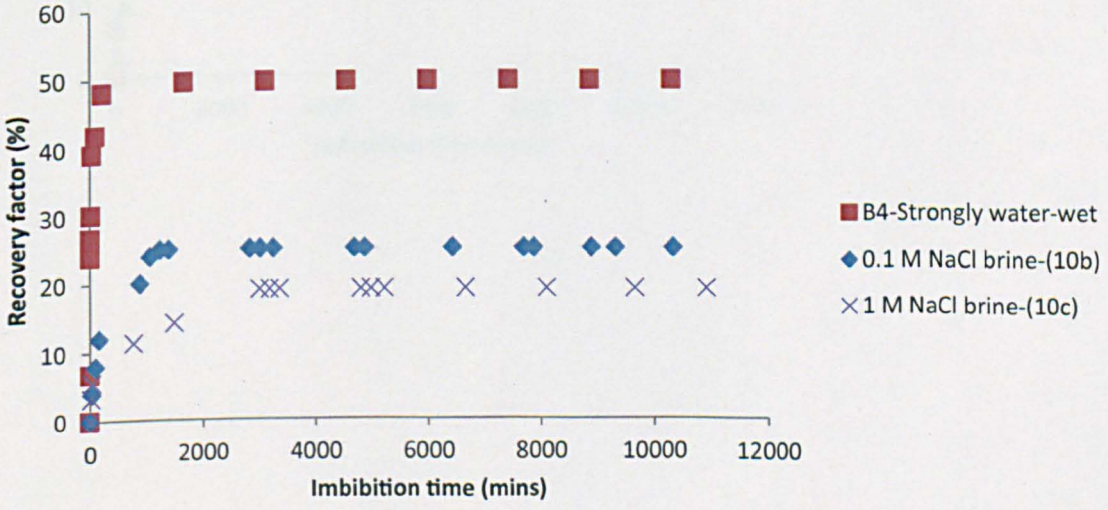

(a)

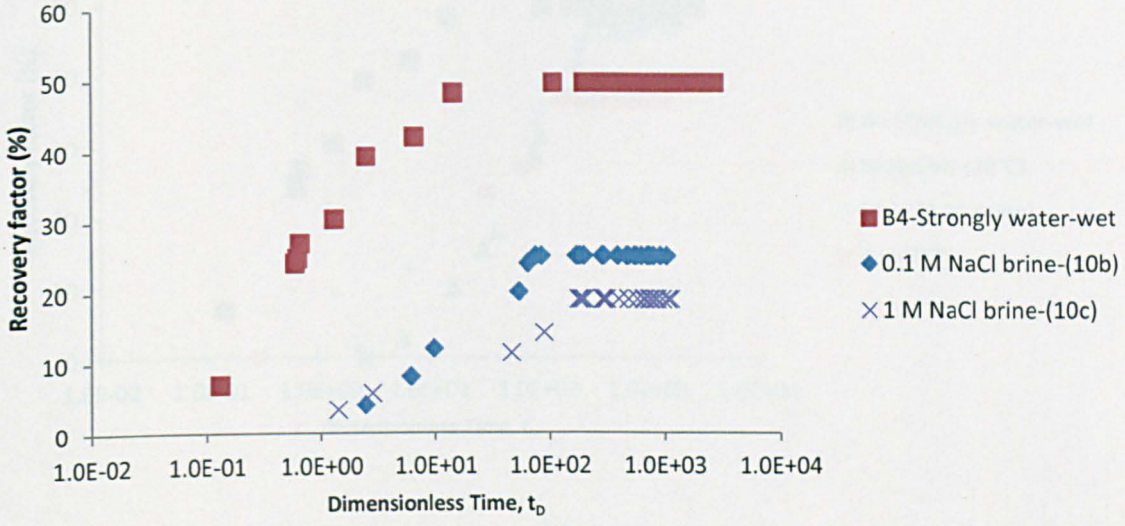

(b)

Figure 6.7 *Effect of brine salinity in imbibition of core with connate water.*

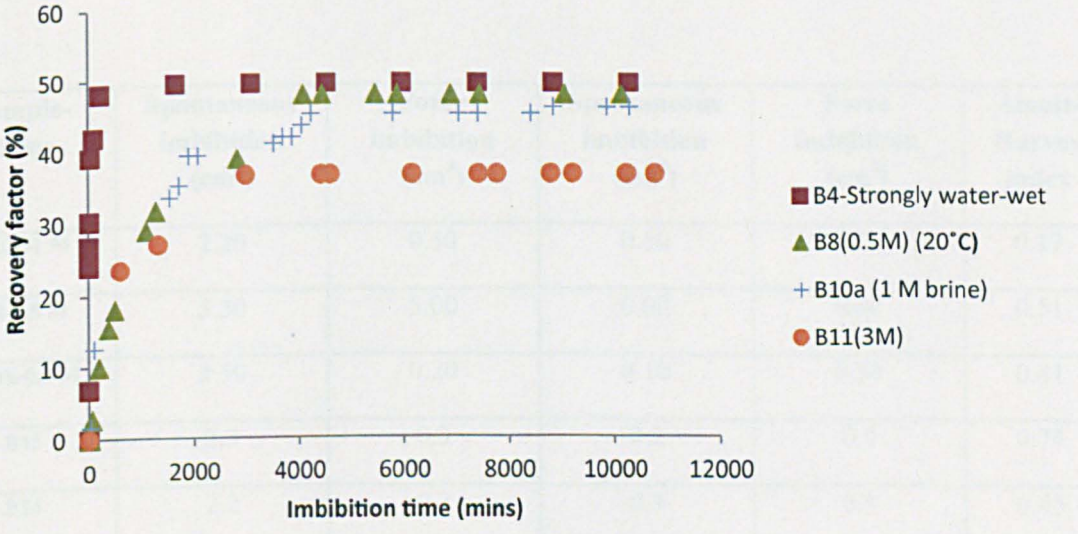

(a)

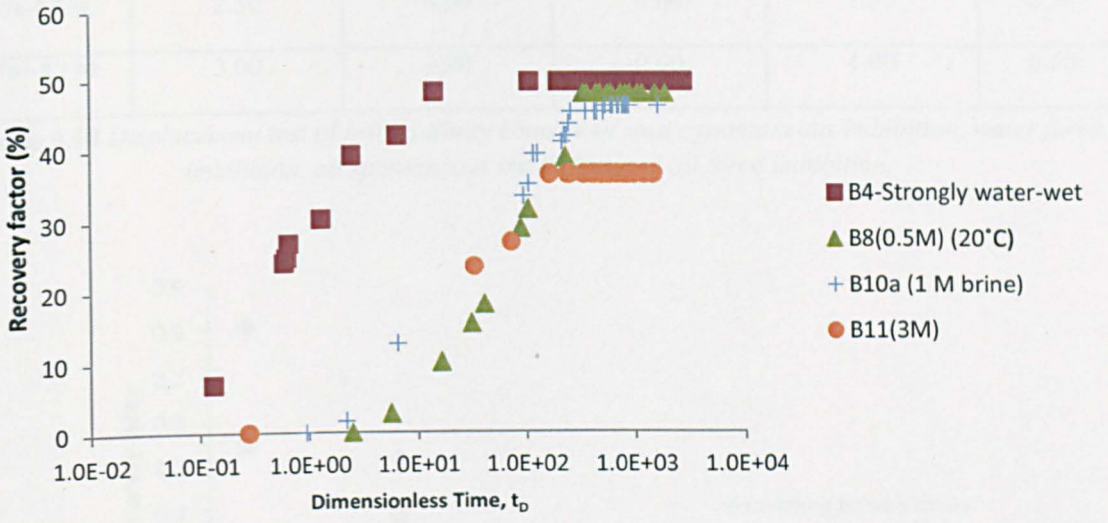

(b)

Figure 6.8 *Effect of brine salinity in imbibition of core without connate water.*

Sample-Brine	Spontaneous imbibition (cm^3)	Force imbibition (cm^3)	Spontaneous imbibition (cm^3)	Force imbibition (cm^3)	Amott-Harvey index
B10c-1 M	2.20	0.50	0.50	0.30	0.19
B8-0.5 M	5.30	5.00	0.00	6.00	0.51
B10b-0.1 M	2.50	0.20	0.10	0.80	0.81
B15	3.3	0.3	0.2	0.9	0.74
B16	2.2	0.2	0.3	0.5	0.45

Table 6.9 *Displacement test of brine salinity invading of water spontaneous imbibition, water force imbibition, oil spontaneous imbibition and oil force imbibition.*

Sample-Brine	Spontaneous imbibition (cm^3)	Force imbibition (cm^3)	Spontaneous imbibition (cm^3)	Force imbibition (cm^3)	Amott-Harvey index
B10c-1 M	2.20	0.50	0.50	0.30	0.19

B7a-0.5 M	2.50	4.00	0.00	1.00	0.38
B7b+-0.1 M	3.00	4.00	0.00	1.00	0.50

Table 6.10 *Displacement test of brine salinity connate of water spontaneous imbibition, water force imbibition, oil spontaneous imbibition and oil force imbibition.*

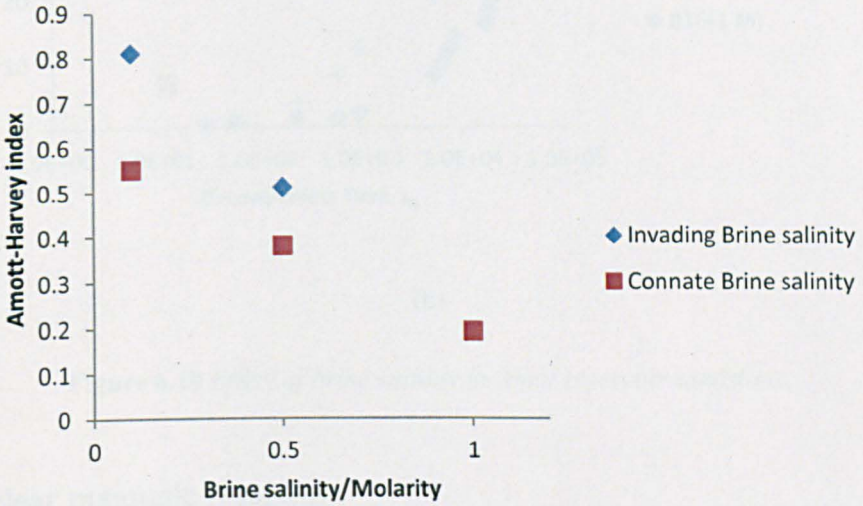

Figure 6.9 *Amott-Harvey index as brine salinity variation of invading and connate in COBR interaction.*

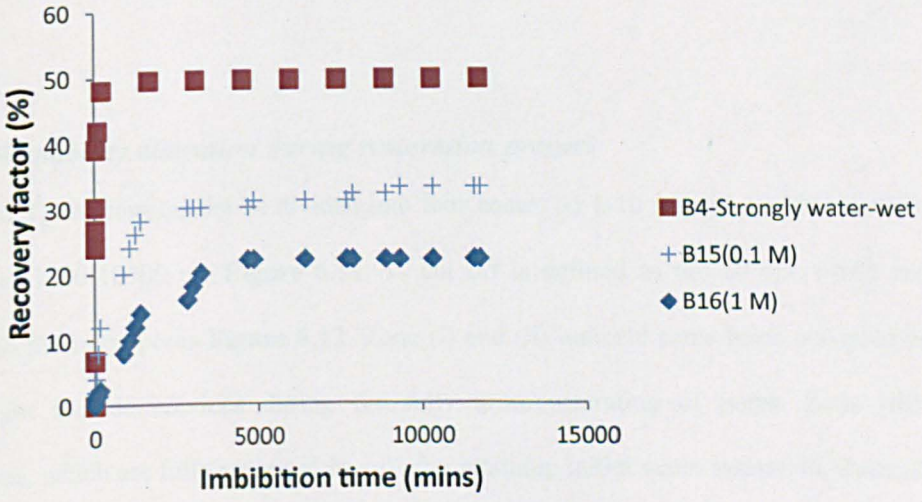

(a)

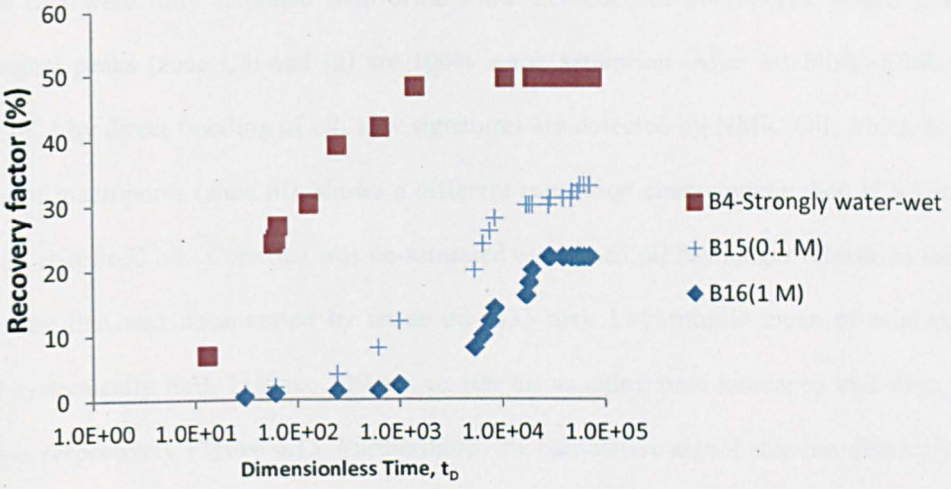

(b)

Figure 6.10 *Effect of brine salinity in Amal reservoir sandstone.*

6.3.2 Nuclear magnetic resonance

In this section, NMR time relaxation is measured at two different conditions: initial water saturation and after spontaneous imbibition. Time relaxation in NMR comes as a result of three different mechanism bulk relaxation, surface relaxation and diffusion relaxation as discussed in details in Chapter 2.

6.3.2.1 *Wettability alteration during restoration process*

Signals and T_2 distribution can be divided into four zones: (i) 1-10 ms, (ii) 10-100 ms, (iii) 100-1000 ms and (iv) 1000-10000 ms **Figure 6.11**. T_2 cut off is defined as the 20 ms, which means water occupies all the micropores **Figure 6.12**. Zone (i) and (ii) indicate some brine occupied micropores, which might include crevices during the fully brine saturating of pores. Zone (iii) indicates macrospores, which are fully saturated by oil after attaining initial water saturation. Zone (iv) indicate oil that is residing in the centre of pores without touching the rock surface. The changes in oil/water/rock surface by interpreting T_2 rate and signals amplitude through the four zones are described below. The factors that we have investigated on oil/brine/rock configuration are: crude oil and aging time.

First cores that were fully saturated with brine show existence of micropores, which inferred by multiple signal peaks (zone i, ii and iii) are 100% water saturation. After establishing initial water saturation (S_{wi}) by direct flooding of oil, new signatures are detected by NMR. Oil, which is detected in the area of macropores (zone iii), shows a different relaxation characteristic than if S_{wi} is attained by crude oil or refined oil. Core that was de-saturated by refined oil has longer relaxation time (1418 ms) than core that was de-saturated by crude oil (533 ms). Logarithmic mean of relaxation time decreased systemically from 116 ms, 109 ms, to 109 ms as aging time increased to 2 days, 10 days and 25 days respectively **Figure 6.13**. Furthermore, the cumulative signal size has distinctive values in the high time distribution whereas the cumulative signal is less varied between un-aged and aged samples in low time distribution window of < 19 ms **Figure 6.14**.

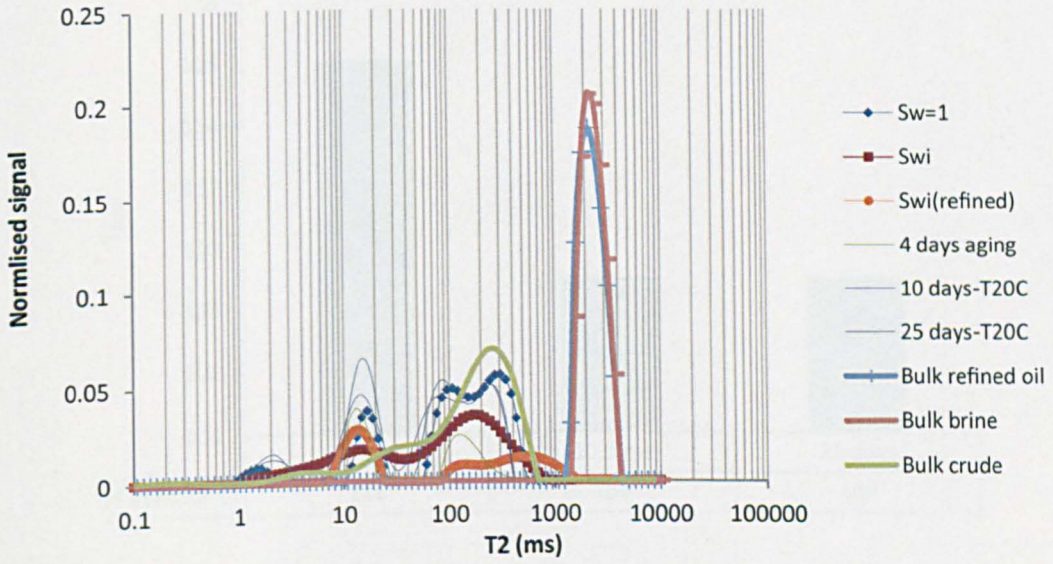

Figure 6.11 *T_2 NMR distribution as function of aging time in crude oil.*

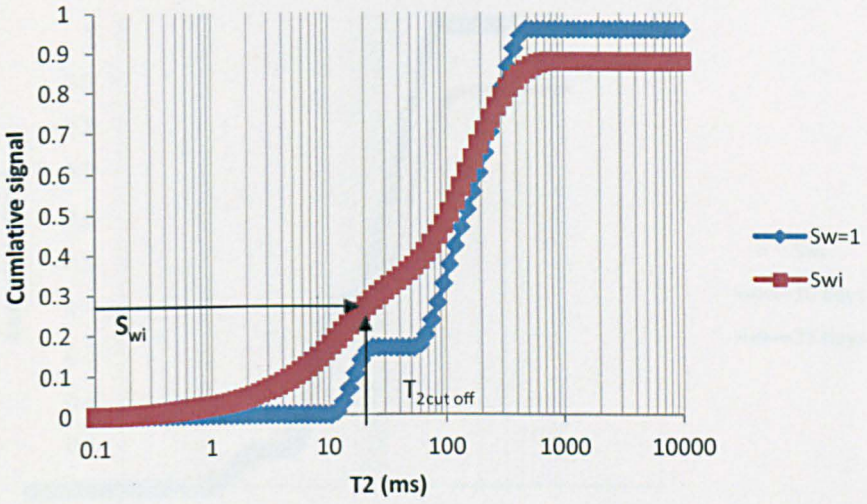

Figure 6.12 *T2 cut off of Berea sandstone which shows the micropores and macropores.*

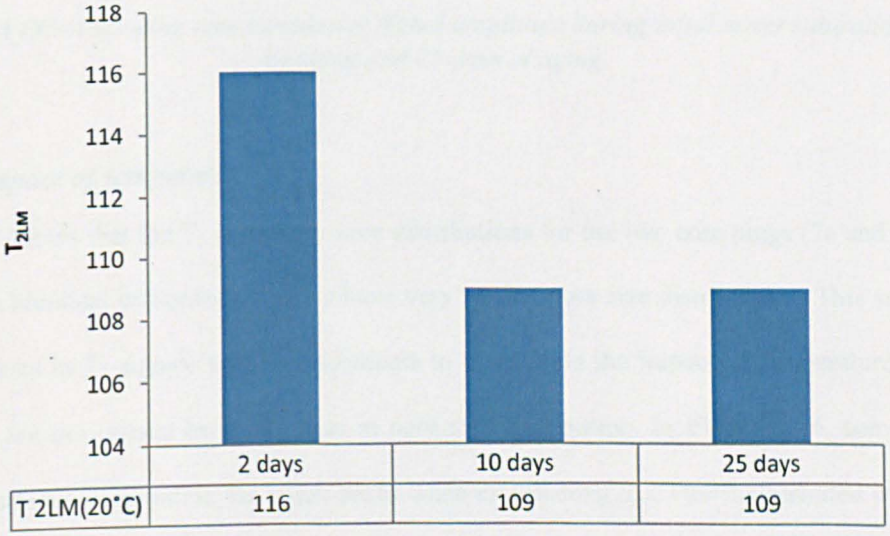

Figure 6.13 *Effect of aging time in T_{2LM}.*

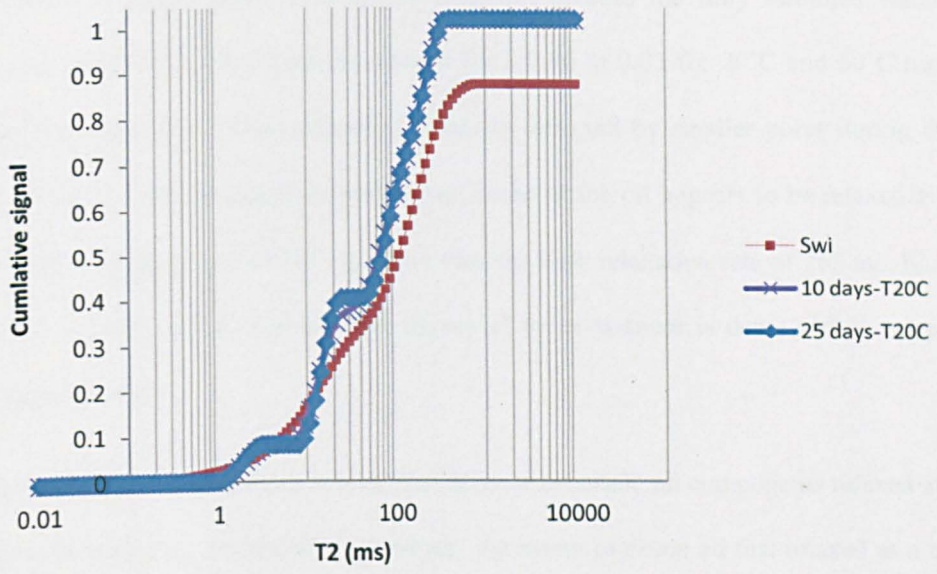

Figure 6.14 *Effect of aging time cumulative signal amplitude during inital water saturation,10 days of aging and 25 days of aging.*

6.3.2.2 *Impact of temperature*

Figure 6.15 shows that the T_2 relaxation time distributions for the two core plugs (7a and 7b) at S_w = 1 are almost identical indicating that they have very similar pore size distributions. This suggests that any differences in T_2 signals in the experiments to investigate the impact of temperature on COBR interactions are not caused by differences in pore size distribution. In **Figure 6.16**, some of the oil relaxes at surfaces surrounding the larger pores when establishing S_{wi}. This is illustrated when surface relaxation is hitting 315 ms, which exceeds the bulk relaxation rate at 265 ms. Increasing temperature from 20°C to 60°C shortens the relaxation time from 350 ms to 315 ms at similar aging time of 25 days **Figure 6.17.**

However, none of the water relaxes at the centre of pores during oil flooding to establish S_{wi}. This can be shown through relaxation of water is all below the water bulk rate of 2154 ms. There is no distinct difference in the signal peaks at S_{wi} between relaxation time 43 ms and 315 ms in which both of the normalised signals achieved 0.05 despite the change in temperature from 20°C to 60°C (**Figure 6.16** and **Figure 6.17**). However, at a relaxation time of 20 ms and below, corresponding to micropores, a

large distinction of signal peaks is observed when oil invades the fully saturated water core. In particular, the normalised signal peak is reduced from 0.06 to 0.03 for 20°C and 60°C respectively. This means the interplay of fluid saturation is mainly affected by smaller pores during the change from 20°C to 60°C. After spontaneous imbibition, some of the oil appears to be relaxed at centre of pores since the relaxation time is 315 ms larger than the bulk relaxation rate of 265 ms. I_{NMR} is 0.2 at 20°C and 0.1 at 60°C, which indicates the degree of water-wetness is decreased as temperature is increased **Figure 6.18**.

In the case of the Amal sandstone, it is clear that none of the crude oil components relaxed at centre of pores after establishing S_{wi} **Figure 6.19**. However, the extent of crude oil that relaxed as a bulk crude oil is higher in outcrops than in the reservoir sandstone, which indicates the outcrop samples might be less oil-wet than the reservoir sandstone due to oil coating the surface of rock. After spontaneous imbibition, the water does not relax at bulk rate, which indicates the water still exists as the wetting layer. Increasing the temperature of the Amal reservoir sandstone to 60°C does not change the surface relaxation during the initial water saturation, which means that T_{2LM} is constant at 20.3 ms **Figure 6.20**. However, T_{2LM} increased from 79.0 ms to 82.0 ms.

In the case of the carbonate reservoir samples F1 and F2, the fully saturated brine samples show a T_2 signature that is unimodal with a single peak (**Figure 6.21** and **Figure 6.22**). Both of the samples show some of oil to be relaxed as a bulk crude oil at 351 ms when aged at 20°C. Relaxation time increases further to reach 370 ms at 60°C. After the spontaneous imbibition, both residual oils relaxed at 231 ms and 114.9 ms for 20°C and 60°C respectively. Since these relaxation times are less than bulk crude oil (265 ms), these results suggest that the residual oil relaxed on the carbonate surface after brine invasion despite the effect of temperature. I_{NMR} decreased from -0.60 to -0.50 as temperature increased from 20°C to 60°C. This means the degree of oil-wetness decreased as temperature increased.

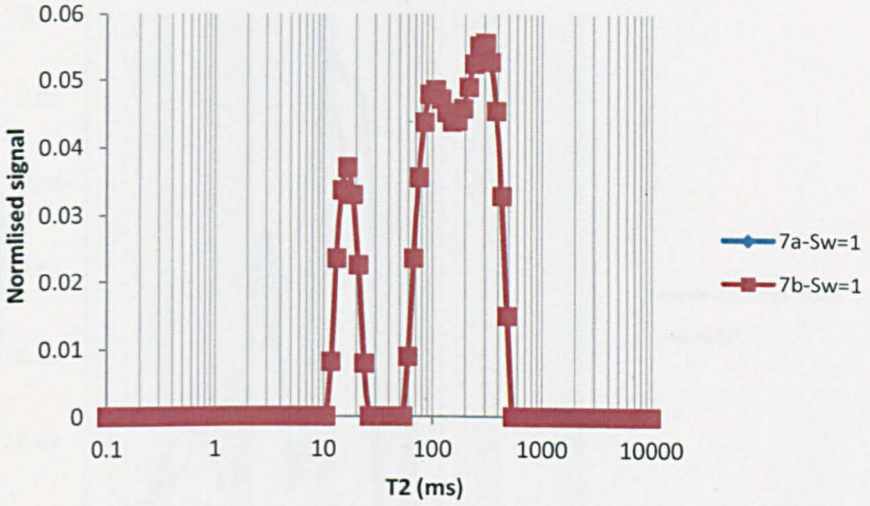

Figure 6.15 *T2 distribution at 100% water saturation for different core plugs. The identical time relaxation confirm the identical pore size distribution.*

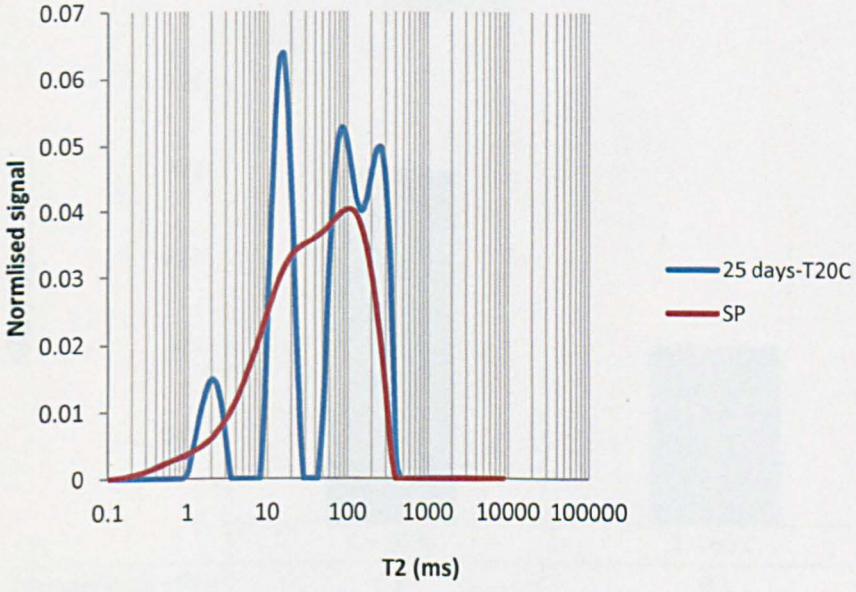

Figure 6.16 *T2 distribution at initial water saturation and after spontaneous imbibition during 20°C temperature.*

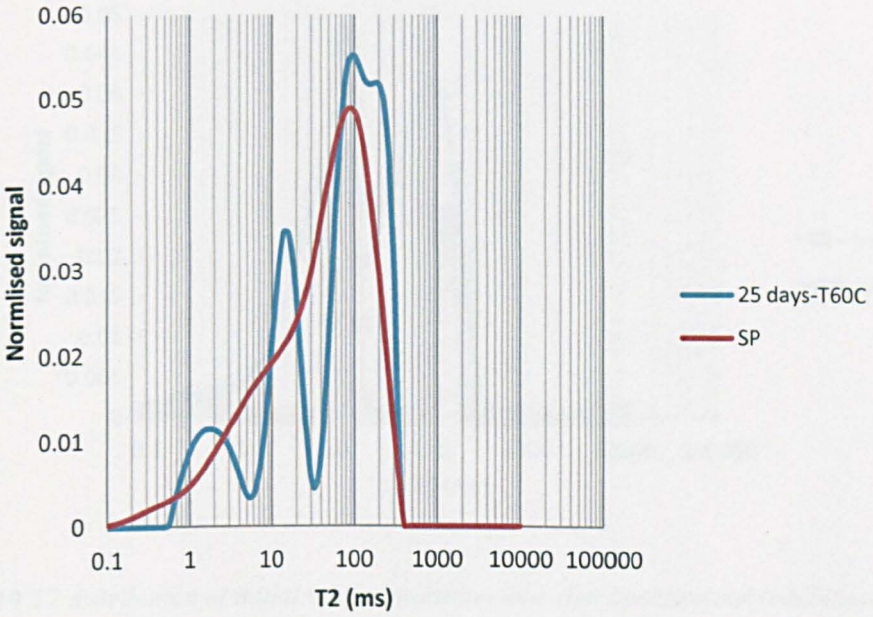

Figure 6.17 *T_2 distribution at initial water saturation and after spontaneous imbibition during 60°C temperature.*

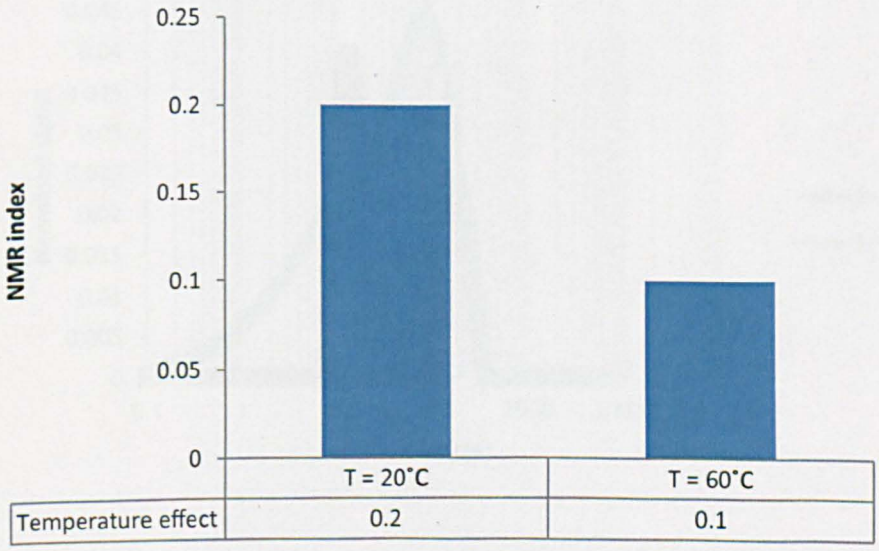

Figure 6.18 *NMR wettability index as function of temperature.*

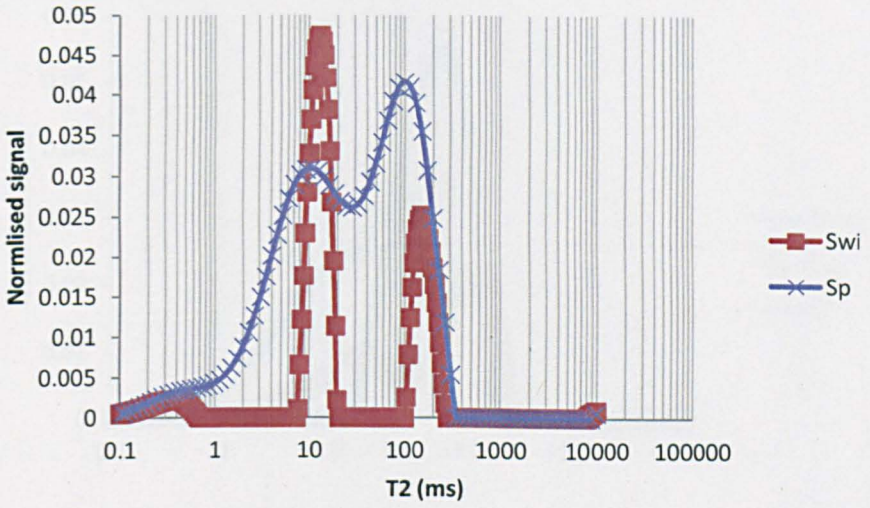

Figure 6.19 *T2 distribution at initial water saturation and after spontaneous imbibition during 20°C temperature at Amal reservoir sandstone.*

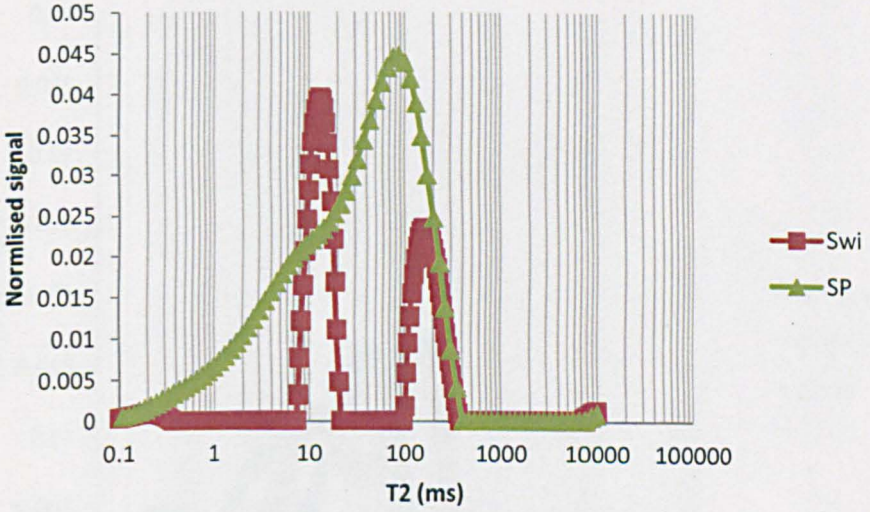

Figure 6.20 *T_2 distribution at initial water saturation and after spontaneous imbibition during 60°C temperature at Amal reservoir sandstone.*

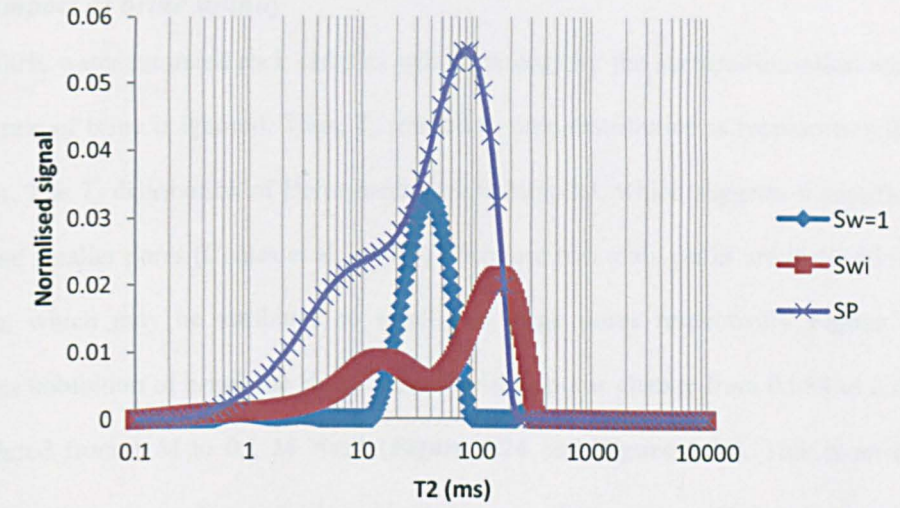

Figure 6.21 *T2 distribution at initial water saturation and after spontaneous imbibition during 20°C temperature at Fahud carbonate reservoir.*

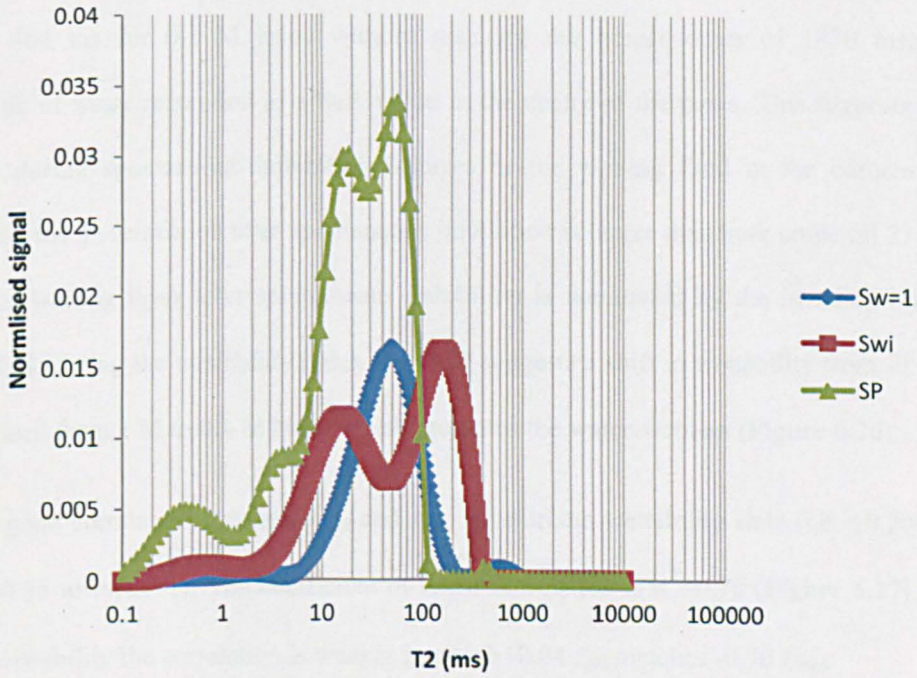

Figure 6.22 *T_2 distribution at initial water saturation and after spontaneous imbibition during 60°C temperature at Fahud carbonate reservoir.*

6.3.2.3 *Impact of brine salinity*

Brine in 100% water saturated rock samples will relax only by the surface-relaxation when the bulk relaxation rate of brine is ignored. Thus, T_2 relaxation time distribution is representing the pore-size distribution. The T_2 distribution of Berea sandstone is bimodal, which suggests a significant amount of larger and smaller pores (Coates et al., 1999). There are two main peaks are at 10-40 ms and zone 50-600 ms, which may be attributed to small and large pores respectively **Figure 6.23**. After spontaneous imbibition of brine, the signal from the large pores change from 0.054 to 0.053 as brine salinity diluted from 1 M to 0.1 M NaCl (**Figure 6.24** and **Figure 6.25**). This is an insignificant change and indicates the volume of oil does not change in larger pores. The clear interplay between brine and oil is occurring in smaller pores, which indicates more water is imbibed as the signal size increases from 0.044 to 0.049 as brine is diluted from 1 M to 0.1 M. The signals of T_2 relaxations peaks in large pores after spontaneous imbibition show distinctive T_2 relaxation at 553 ms for 1 M brine and 464 ms for 0.1 M brine without reaching the longer times of 1870 ms, which is characteristic of water relaxation as a bulk phase in the centre of the pores. This suggests that water introduced during spontaneous imbibition behaves as the wetting fluid in the corners of pores. Furthermore, the T_2 relaxation after spontaneous imbibition is larger than bulk crude oil 231 ms. This suggests the wetting layer after spontaneous imbibition is dominated by the invading brine not by crude oil. Calculating the wettability index by NMR suggests a shift in wettability from -0.1 to 0.1 as brine is diluted from 1 M to 0.1 M NaCl which promotes the water-wetness **(Figure 6.26).**

There is a good correlation between I_{NMR} and I_{AH} at extreme wettability state (i.e. +0.20 towards 1 and from -0.55 towards -1). The coefficient of linear correlation is R^2=0.70 (**Figure 6.27**). However, at neutral wettability the correlation is weaker in which -0.04 I_{AH} matches -0.70 I_{NMR}.

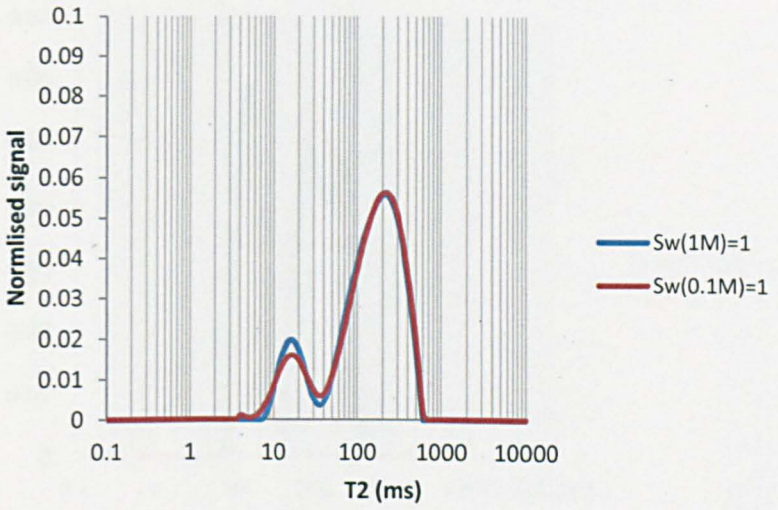

Figure 6.23 *T_2 distribution at 100% water saturation for different core plugs.The identical T_2 relaxation shows similar pore thorat distrubtion is exist at both core plugs.*

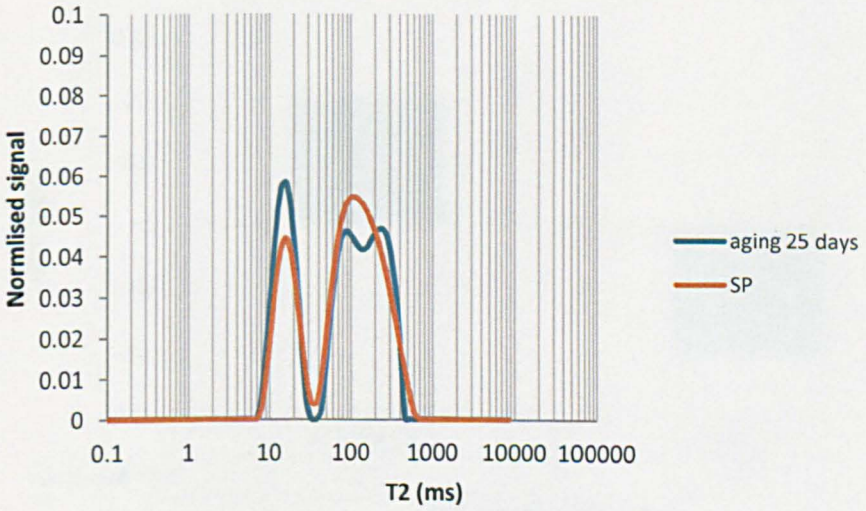

Figure 6.24 *T_2 distribution during initial brine 1 M saturation and after spontaneous brine imbibition.*

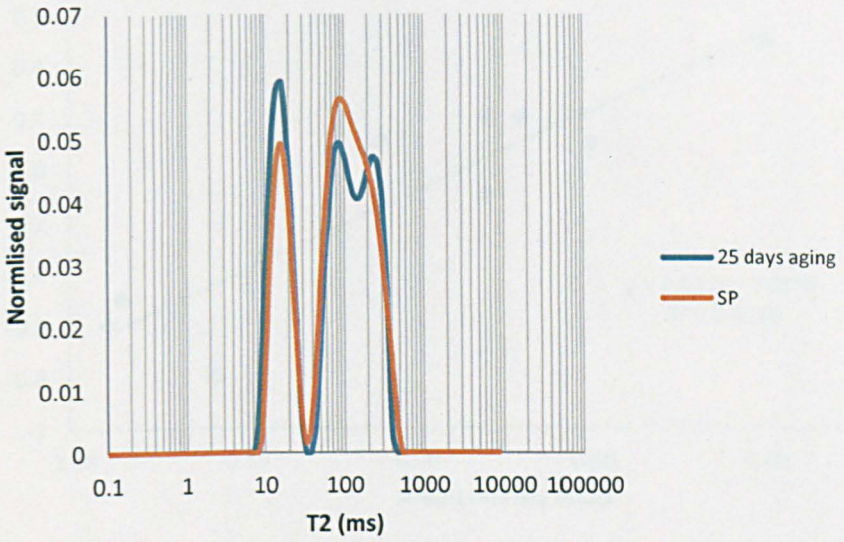

Figure 6.25 *T_2 distribution during initial brine 0.1 M saturation and after spontaneous brine imbibition.*

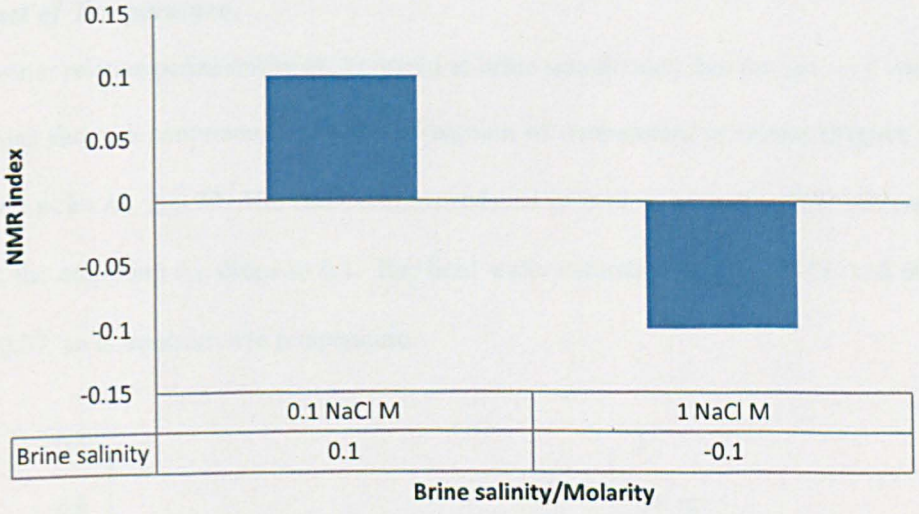

Figure 6.26 *NMR wettability index as function of invading brine salinity.*

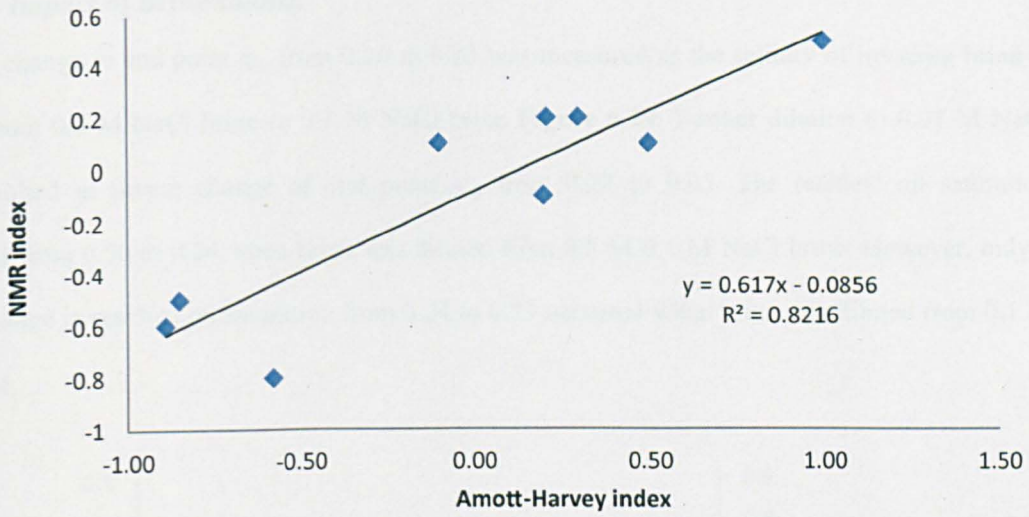

Figure 6.27 *Correlation between I_{AH} and NMR wettability index.*

6.3.3 Relative permeability:

6.3.3.1 *Impact of Temperature:*

The end point water relative permeability (k_{rw}) created as brine was flooded into the core at a very low rate (0.04 cc/min) shows a continuous decrease as function of temperature increased (**Figure 6.28**). At 20°C, the end point k_{rw} is 0.20. The end point k_{rw} reduces to 0.13 as temperature is increased to 40°C. At 60°C, the end point k_{rw} drops to 0.1. The final water saturation at 20°C, 40°C and 60°C is 0.58, 0.56 and 0.57; so is insensitive to temperature.

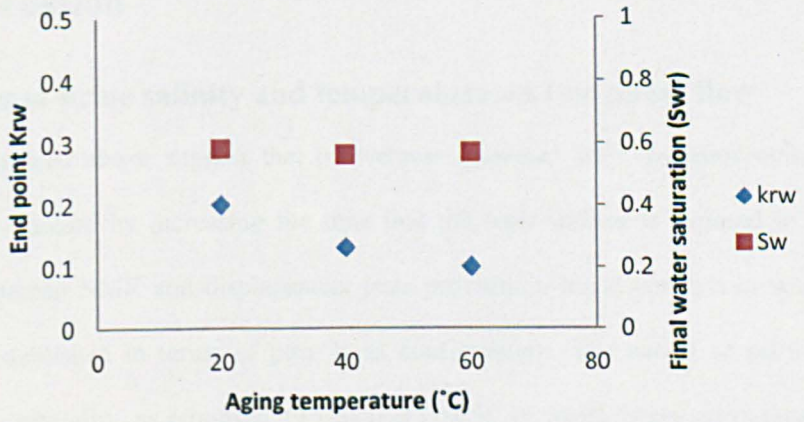

Figure 6.28 *Water end point relative permeability as function of temperature.*

6.3.3.2 *Impact of Brine salinity*

A minor change in end point k_{rw} from 0.20 to 0.23 was measured as the salinity of invading brine is diluted from 0.5 M NaCl brine to 0.1 M NaCl brine **Figure 6.29**. Further dilution to 0.01 M NaCl brine resulted in severe change of end point k_{rw} from 0.23 to 0.05. The residual oil saturation decreased from 0.50 to 0.24 when brine was diluted from 0.5 M 0.1 M NaCl brine. However, only a minor change in residual oil saturation from 0.24 to 0.23 occurred when brine was diluted from 0.1 M to 0.01 M.

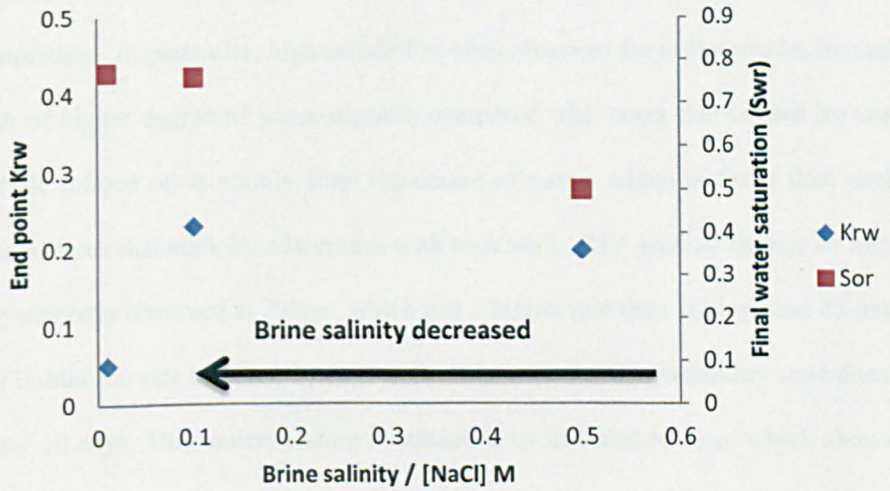

Figure 6.29 *Effect of brine salinity in water end point relative permeability during force displacement test.*

6.4 Discussion

6.4.1 Impact of brine salinity and temperature on two phase flow

The results presented above suggest that oil-wetness increases with increased aging time; this is probably simply caused by increasing the time that the rock surface is exposed to crude oil. The combination between NMR and displacement tests provided a novel analysis in which the type of wettability is established in terms of pore level configuration. The nature of oil-wetness is more towards mixed wettability, as proposed by Salathiel (1973), in which larger pores tend to be lined by crude oil components rendering them oil-wet. On the other hand, grooves and crevices, which form micropores, are not affected by the crude oil components. The high capillary force and thick water

film in micropores prevent the crude oil accessing the rock surface, which preserves the initial state wettability in the micropores. Furthermore, the nature of surface active components in crude oil is the main factor that promotes oil-wetness. This was inferred from the large difference of surface relaxation for refined oil, which is free of surface active components, and crude oil, which contains surface active components. The crude oil shows faster surface relaxation than refined oil, which suggests that crude oil is adhering to rock surface whereas refined oil relaxes at the centre of pores away from the rock surface. Assessing the wettability of cores using imbibition rate with dimensionless time modified by Ma et al. (1997) and Wickramathilaka et al. (2011) explains the nature of wettability. In particular, high imbibition rates observed for rock samples treated by refined oil is a result of higher degree of water-wetness compared with cores that treated by crude oil. The sweeping of the refined oil is mainly from the centre of pores, which is faster than peeling off the crude oil components that stick by adsorption with rock wall. The gradual change of imbibition rate during aging was only observed at 2 days, which has a higher rate than 10 days and 25 days. The lack of change of imbibition rate between 10 days and 25 days means the wettability state does not change after aging for 10 days. This understanding is enhanced by calculating T_{2LM}, which shows the drastic reduction in time surface relaxation that occurs after 2 days in which T_{2LM} drops from 116 to stay around 109 after 10 days and 25 days. This suggests the wettability is altered more towards oil-wet as aging time increased. Moreover, the distinctive difference in the NMR cumulative signal at high time distributions indicates that larger pores become oil-wet before the smaller pores.

The experimental results suggest that the existence of connate water is a critical factor in determining final oil recovery. In particular, the samples containing connate water yield less oil recovery during imbibition cores without connate water. The difference in oil recovery between the two cases may reflect the connate water being mobilised after imbibition of brine, which makes the connate water bank ahead of the oil. Unlike in water-wet core, not all connate water in mixed wet porous media is present as a continuous thin film (Masalmeh and Oedai, 2009). If some of the connate water blobs are not continuous, it is very possible that it acts as a discontinuous barrier in the front of residual oil. The banking of connate water ahead of oil movement results in increased oil trapping, which reduces the

oil recovery to 19% compared to 46% in cores without connate water. This understanding also is enhanced by the relatively slower oil production and increased water production during force imbibition cycle to obtain I_{AH}. The higher water/oil ratio that is observed with less than 0.4 pore volumes of water injection compared with the case without connate water indicates that the delay of oil production will not occur unless a bank of water exists. Similar observations were also reported in Kralik et al. (2000) in a study of preserved core in which the initial produced brine was found to contain iodide ion (I^-) whereas analysis of injected brine found no detectable iodide. This indicates that connate water banking occurs in both naturally and restored wetting systems. Connate water banking was also detected using radioactive tracer profiles in porous media made from Ballotoni glass, which is considered to have identical pore structure to sandstone (Sorbie et al., 1987). Furthermore, imbibition rate and I_{AH} indicates that the porous media with connate water is more water-wet than samples without connate water. This suggests that connate water may help screen the grain surfaces from surface active components within the crude oil.

Despite the different mineralogy between outcrop and reservoir sandstone, the effect of temperature on wetting is clearly evident in terms of reduction of imbibition rate as function of dimensionless time as well as the reduction of I_{NMR} and I_{AH}. Temperature increases the surface active components aggregation onto the rock surface, which increases the oil-wetness of sandstone rock surface. The shortening of NMR surface relaxation time from 350 ms to 315 ms as temperature increased from 20°C to 60°C indicates that increasing the temperature enhances the adherence of oil to the rock surface, which makes the NMR relaxation time faster. This change tends to decrease I_{NMR} from -0.7 to -0.8, which means oil-wetness increases with temperature.

Further evidence of the aggregation of surface active components is the systematic change of induction time of water imbibition into the rock as temperature is changed. The carbonate samples show a very minor change of wettability towards water-wet as temperature is increased from 20°C to 60°C as indicated from I_{AH} and imbibition rate. This might indicate the temperature window of 20°C to 60°C might not be sufficient to induce wettability alteration that increases the oil recovery significantly. One of the possible reasons for increasing the water-wetness of carbonate as

temperature is increased is the decarboxylation of the acidic material in crude oil at high temperatures due catalytic effect of $CaCO_3$. Using gas-liquid chromatography, Shimoyama and Johns (1972) showed that the degradation of fatty acids to alkenes is a slow reaction that is promoted by the presence of $CaCO_3$. The results in the current study agree with Rao (1999) who suggested that high temperature carbonate reservoirs appeared more water-wet than low temperature reservoirs.

Diluting NaCl brine influences the imbibition rate and the extent of oil recovery for both the Berea and Amal sandstone. This means that even though there is no kaolinite in the Amal reservoir sandstone, the brine salinity influences the wettability. Previous work by Tang and Morrow (1999) postulated that the existence of kaolinite is a necessary condition for obtaining an incremental oil recovery by reducing salinity. The work presented in this chapter suggests that the existence of negatively charged silica surface without clay is enough to promote a wettability modification during invading lower brine salinity. This result also confirms recent results by Cissokho et al. (2010) when using outcrop sandstone without kaolinite, in which an increase in oil recovery was observed as brine is diluted.

I_{AH} and I_{NMR} show a significant agreement at all wetting states scale as appeared from the correlation cofficent (R^2=0.83). This agreement of the correlation shows that I_{NMR} can be a useful tool in assessing wettability alteration following experiments on core.

The continuous drop of k_{rw} as temperature increased indicates temperature enhances the adsorption of oil onto the rock surface to the extent that the mechanical force initiated by the viscous force of water decreases since the restriction of water flow is increased. This can be explained through the schematic diagram in **Figure 6.30**. The mechanical force initiated by viscous flooding will be opposed by capillary force initiated from the adhesion of crude oil into the rock surface. The higher the temperature tends to aggregate crude oil components into pore throats which reduces the accessible pathway of water driven by mechanical force. This restriction of water movement causes a reduction in the k_{rw}.

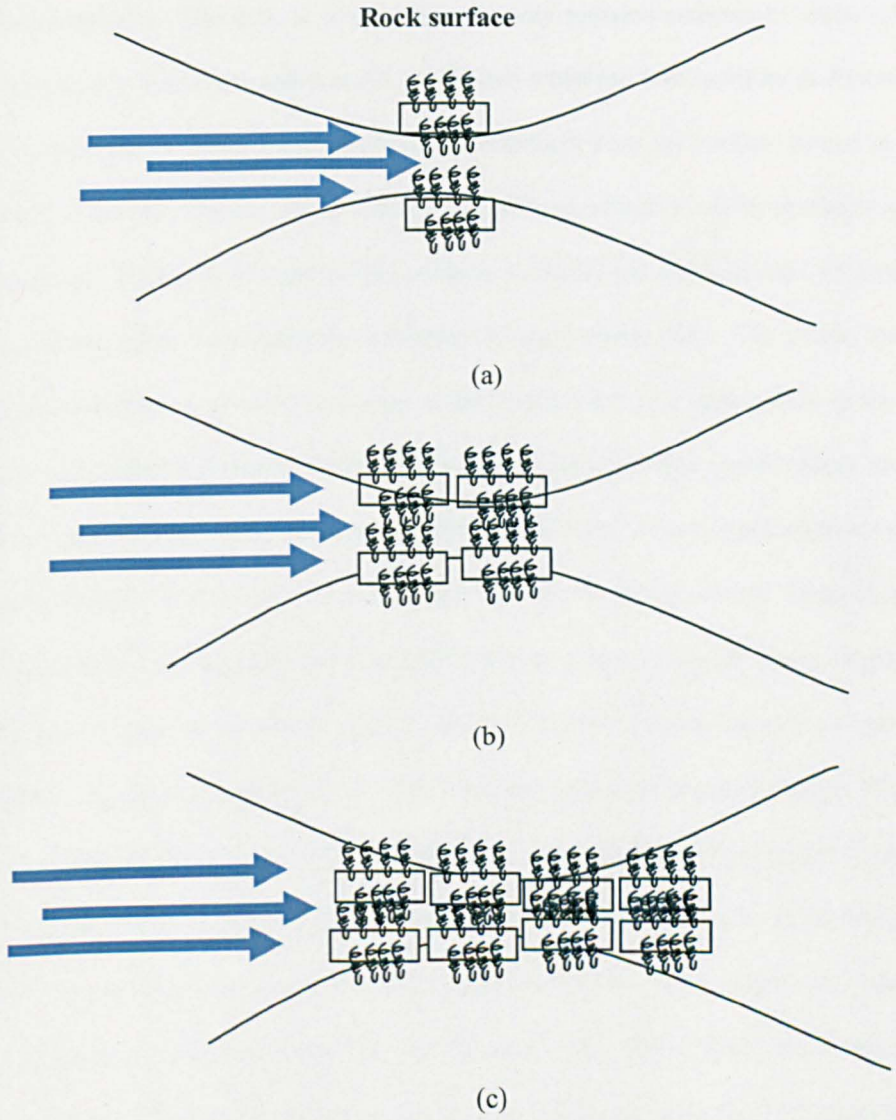

Figure 6.30 *Schematic diagram of effect of temperature in aggregation of surface active components into pore throats.*

Monitoring of end point k_{rw} as function of brine salinity reveals two important points. First, the ability of sweeping residual oil saturation is limited from 0.5 M to 0.1 M NaCl brine in which there is no change in S_{or}. As there is almost no change of residual oil saturation after diluting from 0.1 M to 0.01 M brine, the residual oil that is stripped from the grain surface of oil is limited by the ability of adhesive forces that does not appear to change very much from 0.1 M brine to 0.01 M brine. Therefore, the ability of viscous force to strip residual oil at 0.1 M brine and 0.01 M brine is almost the same and results in similar residual oil saturations. Second, two main injectivity patterns emerged

from the experiments. The first, is where the injectivity remains constant between 0.5 M and 0.1 M brine. The second, where the injectivity is totally lost when the brine salinity is diluted from 0.1 M to 0.01 M. The possible reason is that kaolinite is detached from the surface of grains and blocks the pore throats. Blockage of pore throats reduces the passage of water, which results in severe reduction of end point k_{rw}. Khilar and Fogler (1984) observe a critical salt concentration for kaolinite release in Berea sandstone when brine salinity is diluted in single phase flow. The results presented int this chapter indicate the critical salt concentration also exists when two phases flow in the sandstone. The reason for this behaviour can be attributed to competition between major forces that hold the clay particles to rock surface. Clay minerals are generally known to have a net negative charge, which is balanced by cations held weakly at the surface by van der Waals forces (Denicol and Jing, 1998). Electrochemical theory suggests that the surface of clay minerals carries excess negative charges as a result of the substitution of certain positive ions by others of lower valancy in a process known as isomorphous substitution; this results in a clay surface with a net negative charge. When the clays are brought in contact with an electrolyte with positive ions (e.g. Na^+), these negative charges attract the positive ions and repulse negative ions present in the solution. As a result, an electrical double layer is generated. The perturbation of the double layer by diluting the brine salinity can cause the repulsion force to weaken and releasing fines that line the rock walls. The hydrodynamic force initiated by the differential pressure would transfer these fines to the upstream until they are trapped in pore throats. Lever and Dawe (1987) provide a visual observation that proves a mechanism of clay bridges, which developed as a result of fine particles aggregating around the pore throats. This phenomenan might be the reason for increasing the upstream pressure, which is translated to a drastic reduction of water end point relative permeability during 0.01 M NaCl brine.

6.4.2 Implications of results for EOR

It is important to discuss the implications of the results presented above for petroleum production. Around 50% of oil is produced by waterflooding (Donaldson et al., 1985). In late stage life of a field, high water-to-oil ratios reduce profitability eventually to an extent where further production is uneconomic. This is very evident in Amal field which is a sandstone reservoir located in south central

Oman. The water cut reached above 85% between 2002 and 2007 with normal waterflooding, which reduced oil recovery to only 50 m^3/day **Figure 6.31**. The experimental work in this chapter shows a great potential for increasing the oil recovery factor by lowering brine salinity. Based on the core scale results, changing the scheme of water injection could potentially increase oil recovery. This can be designed by selecting a producing well to inject portions of multiple pore volumes of high salinity brine into the oil targeting zone. After plateau production is reached the injection fluid could be switched to lower salinity brine. Our results indicate the shifting of brine salinity from 3 M to 0.5 M brine can release more oil. The remaining oil saturation could be monitored using the log inject log tests technique (Webb, 2005).

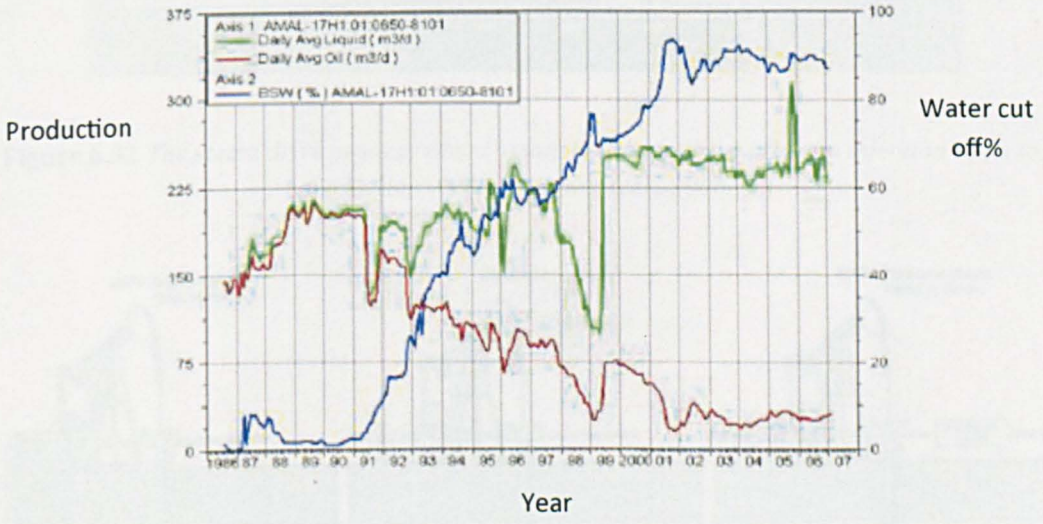

Figure 6.31 *Amal well production under normal waterflooding (PDO, 2008).*

The pattern of steam injection into the reservoir is very critical in terms of wettability and oil recovery. Two main techniques of heating the reservoir are steam flooding **Figure 6.32** or huff and puff modes **Figure 6.33**. In a steam flood, the displacement temperature is high and injection/production process occurs at the same time. The huff and puff technique involves injecting a slug of steam into the reservoir for 7 days after which the well is re-opened for production at normal temperature. This process of huff and puff is repeated in cyclic manner. The results presented in this chapter imply application of the huff and puff technique would decrease oil recovery from the sandstone reservoir. As a result, huff and puff should be avoided in Amal sandstone reservoir.

Furthermore, the potential of temperature application to carbonate reservoir is not economic since the oil recovery is only changed in the range of 3%.

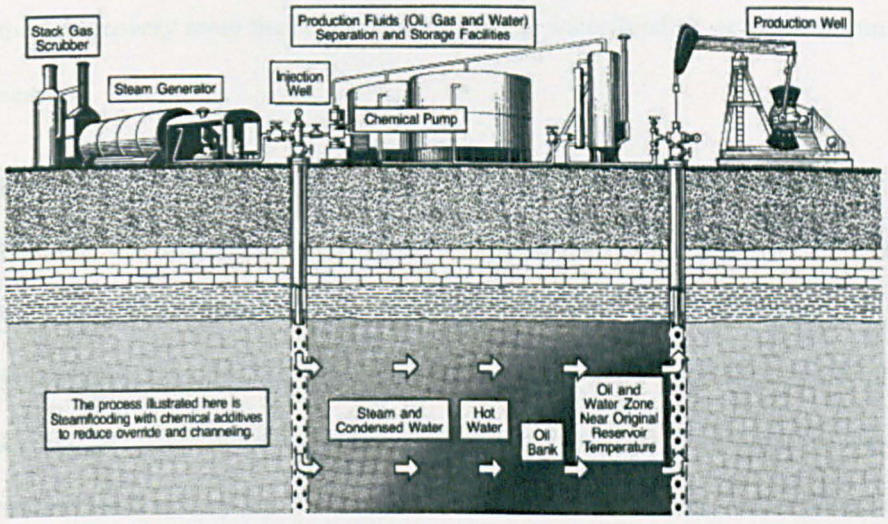

Figure 6.32 *The steam drive process where steam is used to drive oil from injection wells to production wells (from Kovscek, 2006).*

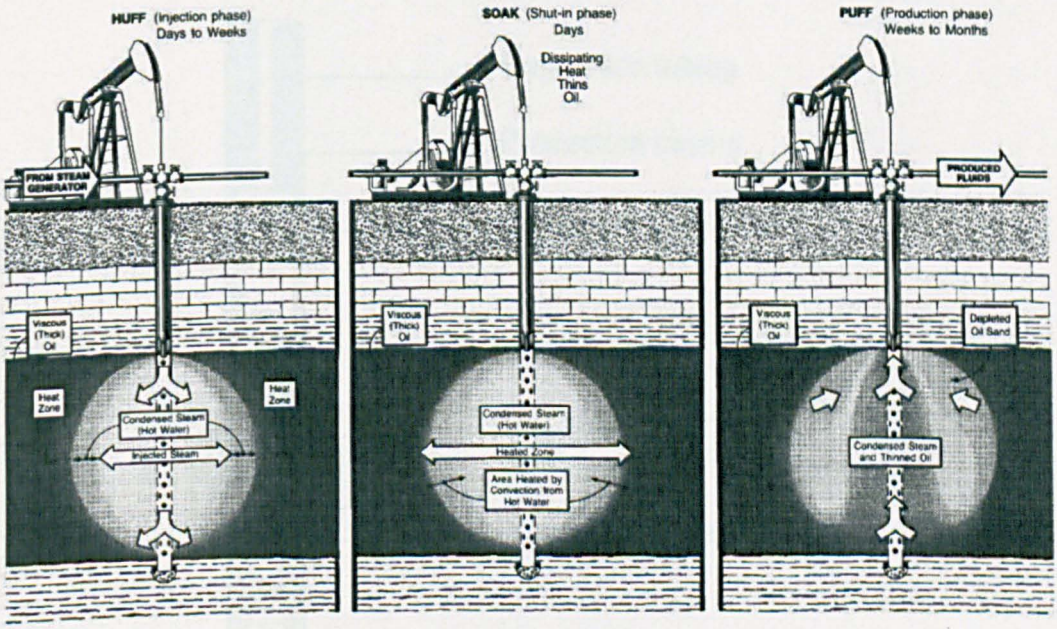

Figure 6.33 *Huff and puff steam injection mode (from Kovscek, 2006).*

Furthermore, if the crude oil is heavy in the reservoir, there is a great potential of using a hybrid process in which waterflooding and steam injection are alternated. This hybrid process combines the

advantage of temperature to lower the viscosity and the imbibition of condensed steam into a matrix of reservoir to displace the oil. The condensate steam is free of salt which could mobilize the residual oil saturation that trapped after waterflooding. The diluting process of condensate steam is expecting to enhance the oil recovery more than only applying single waterflooding or single steam flooding in heavy oil reservoir.

A major caution should be taken to sand control management during low brine salinity injection in sandstone reservoir. Our experimental investigation indicates a critical salt concentration that might cause a loss of injectivity during viscous flooding. From production technology point of view, collapsing the wellbore can close the perforation tunnel which will impact the well productivity. To mitigate this risk, it recommended using gravel pack completion strategy instead of normal completion if low brine salinity injection selected as EOR option for the field development. Gravel packing involves the complete placement of selected gravel across the production interval to prevent the production of formation fines or sand (**Figure 6.34** and **Figure 6.35**).

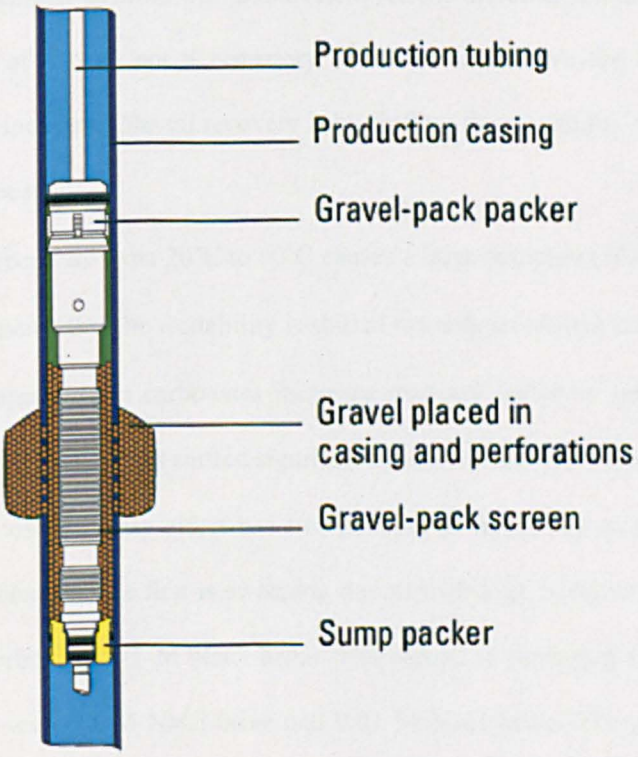

Figure 6.34 *Overall well completion*

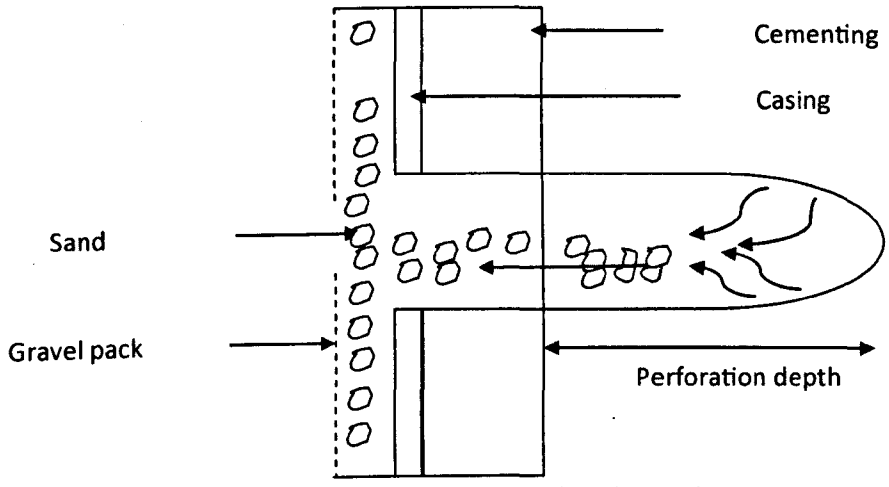

Figure 6.35 *Gravel pack completion*

6.5 Conclusion

The work in the core-scale chapter has produced five main conclusions:

- The combination of non destructive I_{NMR} and displacement I_{AH} provides an independent approach of tracking wettability modification as a function of brine salinity and temperature.
- Reducing the salinity of brine with monovalent cations increases the oil recovery in sandstones. The presence of clay is not a necessary condition to observe the low salinity effect. The mechanism of increasing the oil recovery is by shifting the wettability of rock surface towards a more water-wet state.
- Increasing temperature from 20°C to 60°C causes a large decrease (50%) of recovery factor, I_{AH} and I_{NMR} suggesting that the wettability is shifted towards an oil-wet state.
- Increasing temperature in carbonates increases recovery factor by less than 4%. I_{AH} and I_{NMR} indicate the wettability is not shifted significantly towards an water-wet state.
- The dynamic viscous force effect has two patterns of injectivity to sweep the residual oil as brine salinity change. The first is sweeping the oil with high injectivity, which occurs between 0.5 M NaCl brine and 0.1 M NaCl brine. The second is sweeping the oil with loss of water injectivity between 0.1 M NaCl brine and 0.01 M NaCl brine. The potential reason of losing injectivity is attributed to a detachment of the clay that coats the grains leading to a blockage of pore throats.

Chapter 7
Application of surface analytical techniques to wettability alteration

The microscopic wettability of reservoir rock controls the movement of fluids on uneven rock surfaces. To test the microscopic wettability phenomena, a nanoscale resolution study has been carried out. In this chapter, vertical scanning interferometry is utilised for first time to understand the effect of asphaltene in adsorption morphology. The role of brine salinity, temperature and oil solubility is extensively investigated through 2D and 3D surface analysis.

7.1 Introduction

Until recently, most of what is known about crude oil/brine/rock (COBR) interactions has been inferred from contact angle measurements, which are considered to be macro physical parameters. There is little direct information about the complex morphology of adsorbed and deposited crude oils that cause the wettability alteration. The advancement in surface topography measurement techinques that can characterise nano-scale structures is motivating us to probe the nano-scale structures of the COBR system. Probing these fine details was a long-standing source of curiosity to researchers in finding out the structure of residing oil as a function of solution properties (solubility, salinity and pH) and boundary conditions (temperature and rate). The breakthrough of scanning electron microscopy (SEM) and atomic force microscopy (AFM) have facilitated a substantial increase in the knowledge of nano-structures of COBR interaction.

SEM is a robust micro-analytical tool. It can provide images of the sample surface resolving surface features and micro-topography significantly smaller than could otherwise be resolved using a conventional light optical microscope. In the COBR interaction application, SEM has been used to image the oil and brine distribution at the micro-scale. Robin et al. (1995) successfully observed the distribution of fluids in pores media with a 0.1 μm resolution. This high resolution reveals a strong

correlation that realised between the type of mineral surface such as kaolinite and the structure of high trapped residual oil saturation in micropores. Environmental SEM (ESEM) is a recent technological breakthrough that circumvents the necessity of coating the sample and does not require a high vacuum to operate. Kowalewski et al. (2003) utilised the ESEM for studying the dynamic water imbibition into sandstone samples and provided the first observation of liquid trapping in low permeability cores due to capillary trapping. Although SEM and ESEM reveal into important aspects of pore characterisation and wettability of fluids inside the pore morphology, there is a need for a higher resolution that can characterise the nature of oil film thickness in more detail than is possible using SEM.

AFM serves as an analytical surface technique for high-resolution imaging of adsorption growth and dissolution. This is achieved through the use of a stylus, or tip, to sense mineral-surface topography **Figure 7.1**. As the extremely sharp tip is scanned across the sample surface by a piezoelectric scanner, the topography of the surface causes the tip to deflect as the force between the tip and sample changes. These deflections are monitored by a laser beam that is focused at the end of the cantilever holding the tip. The x, y, and z displacement of the piezoelectric scanner that is required to maintain constant force between the surface and the tip are converted into a topographic map of the surface by a computer. The application of AFM attracts different researchers from petroleum recovery community to study COBR interactions (e.g. Toulhoat et al., 1994; Yang et al., 1999; Ese et al., 2000; Lord and Buckley, 2002; Buckley and Lord, 2003; Karoussi et al. 2008; Kumar et al., 2008).

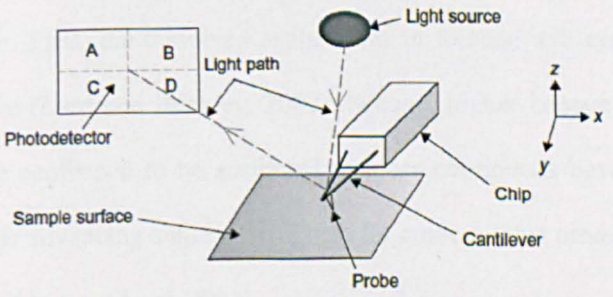

Figure 7.1 *Basic AFM set-up. A probe is mounted at the apex of a flexible Si cantilever. The sample surface is mounted on a piezocrystal with allows the position of the probe to be moved in relation to the surface. The deflection of the probe as it moves through topography of the surface is monitored by light reflection into photodetector (Bowen and Hilal, 2009).*

First use of AFM in characterising the surface topography of COBR interaction was by (Toulhoat et al., 1994). Adsorption of asphaltene from solution into mica surface was monitored over time using AFM contact mode. Their work shows the first observation of the aggregation of asphaltene as granular structure; with elementary grains have an average diameter of about 150 nm. Yang et al. (1999) utilised higher resolution AFM to show the first evidence of mixed-wet model surface, which exists at nano-scale of rock surface. The areal dimension of 200 nm shows patches of bare mica and patches of asphaltene appearing simultaneously, which gives the first nano-scale confirmation of the wettability pattern on rock surfaces. Ese et al. (2000) extended the application of AFM to study the topography of asphaltene and resin fractions exclusively. A monolayer consisting of pure asphaltenes fractions provides a rigid film with a close-packed structure, while the resins build up a continuous open network after adsorption on the silica mineral surface. According to Ese et al. (2000), the distinctive surface topography of asphaltene and resin explains their previous result in which a high compressibility properties inferred from Langmuir blodgett film observed for pure resin fractions is attributed to the nature of open film nano structure topography observed with AFM. Karoussi et al. (2008) used AFM to investigate for the first time the physical properties of calcite surface after exposure to fatty acid oil at different brine pH. Kumar et al. (2008) utilised the AFM to study the effect of cationic and anionic surfactant in removing the adsorbed oil components from mica surfaces. By using AFM, the anionic surfactant proved to be superior in reducing the adsorption oil thickness compared to cationic surfactant.

Two main contributions to knowledge in wettability literature have emerged from utilising AFM to study the COBR system. First, the dissolved asphaltenes in toluene will not prevent adsorption of asphaltene on the surface (Lord and Buckley, 2002). Second, higher contact angles on mica treated surface by crude oil are confirmed to be attributed to more continuous coverage of the surface by organic adsorption. Water advancing angles are highest for crude oil that produces the thickest coating layers in the surface (Buckley and Lord, 2003).

All the previous studies of AFM application to oil-treated substrates proved successful in providing a qualitative and quantitative understanding of the the various aspects of petroleum recovery at a scale

that never probed previously. However, the limitation in studying the COBR interaction by AFM is the nature of the imaging mode in which the tip remains in contact with the sample at all times. The contact mode is often used due to its simplicity of operation. However, there are several drawbacks reported in the literature regarding the contact mode including the lateral forces that can occur when the probe traverses steep edges on the sample. As a result, a decrease of the resolution of images due to the "stick-slip" movement for the probe tips over the surface (Bowen and Hilal, 2009). In addition, the relatively high force during contact mode cause a deformation in deposited material at the surface leading to an underestimation of the height of surface features.

Coherence scanning interferometry (CSI) is a non-contacting measurement technique that uses a white light source, and combines vertical (z-axis) scanning techniques with optical interferometry techniques, to achieve a 3D surface measurement. To understand the above concepts an understanding of optical interferometry is desirable. Interferometry is the science and technique of superposing two or more waves, to create an output wave that differs from the input waves (Petzing et al., 2010). Interferometry is based on the idea that two waves with the same frequency that have the same phase will add constructively whilst two waves that are out of phase by 180° will destructively cancel each other. This wave property is known as superposing and results in a set of dark and light bands known as fringes. The light from the broadband light source is directed towards the objective lens (**Figure 7.2 & Figure 7.3**). The beam splitter in the objective lens splits the light into separate beams. One beam is directed towards the sample and one beam is directed towards an internal reference mirror. The two beams recombine and the recombined light is sent to the detector. The detector measures the intensity of the light as the optical path is varied in the vertical direction (z-axis) and finds the interference maximum. Each pixel of the camera measures the intensity of the light and fringe envelope obtained can be used to calculate the position of the surface.

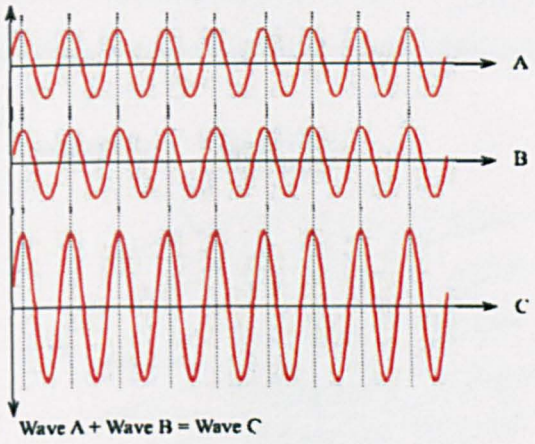

Figure 7.2 *Graph of amplitude against time showing constructive interference.*

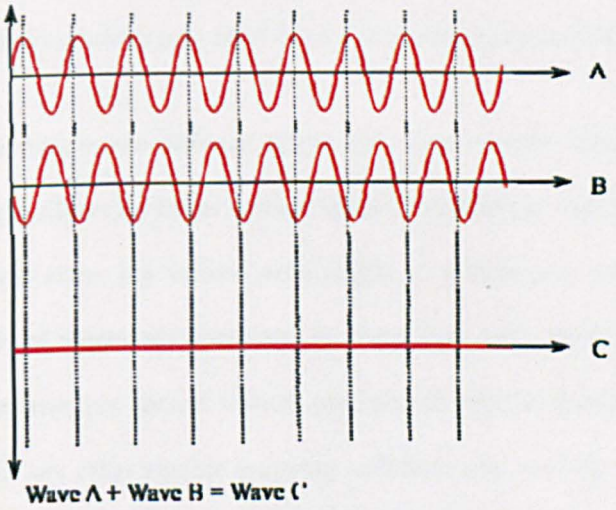

Figure 7.3 *Graph of amplitude against time showing destructive interference.*

To extract surface topography information from interference patterns, careful interpretation of the fringes pattern is required. Surface topography is deduced from the interference fringes that are observed as the object is scanned in a vertical direction. The fringes result from the interference of the light scattered from the object with that reflected from the reference surface **Figure** 7.3. As the object is scanned relative to the reference surface, individual pixels within the image are seen to brighten and darken as they meet the conditions for constructive and destructive interference respectfully. This information can be used to build up a three-dimensional map of the surface. Analysis of the data can

be considered on a pixel basis, identifying intensity changes for each pixel on a plane by plane basis, i.e. vertically drilling down through the multiple planes of data **Figure 7.4**.

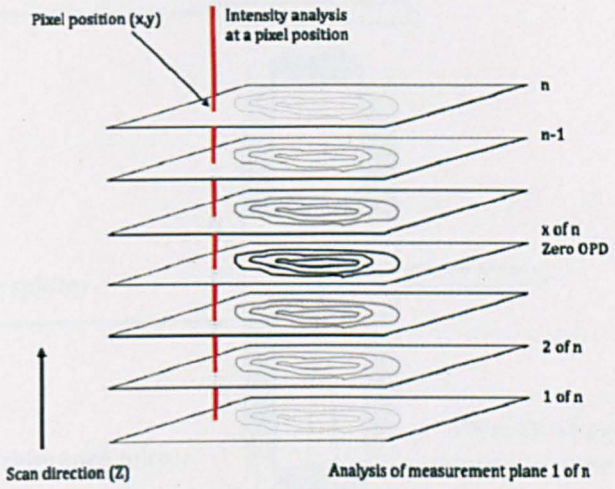

Figure 7.4 *Intensity analysis on a pixel basis which carried as vertical scanning occurred.*

CSI is capable of operating in two different modes: (a) using a narrow band of green light (b) using a white light. White light allows for larger vertical scans up to 100 nm with better than 2 nm precision. The use of green light allow the vertical scan height to a maximum of 4 μm, but improves the precision by an order of magnitude compared to white light, and provides angstrom scale vertical resolution. The two micron per second vertical scan rate allows the acquisition of the data orders of magnitude faster than any other surface mapping technique can provide. As an example, a surface area of almost 1 mm^2 and up to 20 μm of surface elevation can be quantified in less than 10 seconds.

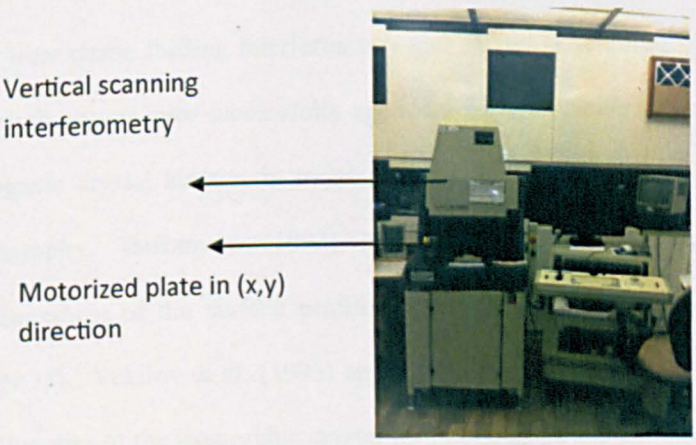

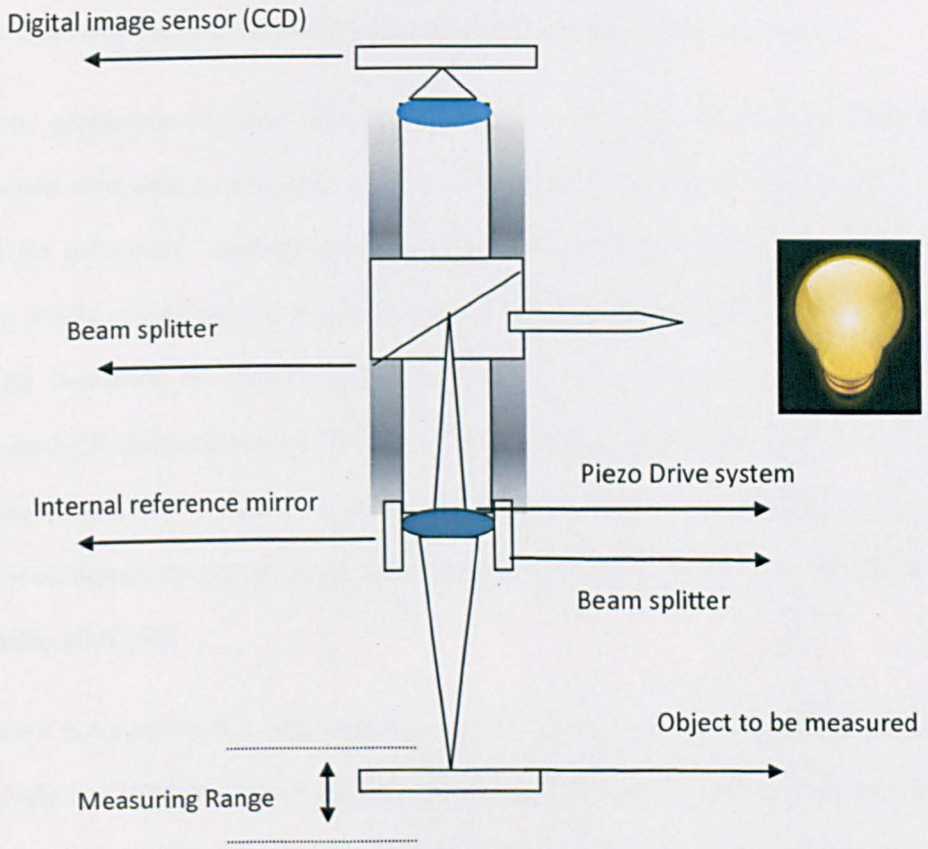

Figure 7.5 *Vertical scanning interferometry showing the light path in the Mirau interferometer and to the sample surface. (a) VSI overview. (b) Details section inside VSI.*

Interferometry has been successfully applied to a wide range of problems in crystal growth and dissolution kinetics. In addition to VSI, related techniques include laser Michelson interferometry, real-time phase shifting interferometry and in situ differential phase shifting interferometry. Several research groups have successfully applied a variety of interferometry techniques to study organic and inorganic crystal kinetics in terms of growth and dissolution by monitoring the change in surface topography. Tsukamoto (1993) employed real-time shift interferometry for time dependent measurement of the surface profile or growth rate of a dislocation-free surface of barium nitrate $(BaNO3)_2$. Vekilov et al. (1995) applied Michelson interferometry to study the growth morphology and kinetics of the isomorphic crystal face adsorption/deposition in aqueous solution. Yokoyama et al.

(1998) extend the previous technique by using sequence microscopic interferograms to analysis the concentration distribution that develops during the growth of crystal. Luttge et al. (1999, 2004) introduced VSI to study the dissolution kinetics of anorthite, calcite, dolomite and barite .

In contrast, the application of white light interferometry to study the COBR interaction has been relatively limited compared to previous works in rock/water hydrothermal application. Kao et al. (1988) used the differential interference method (DI) and reflected light interferometry (UI) to determine the profile of the crude oil droplet at solid/air and solid/micellar interface during surfactant adsorption. By measuring the distance between the fringes, the shape of oil droplet surface is obtained. Recently, Kumar and Fogden (2009) use phase shifting interferometry (PSI) to investigate the wettability pattern that induced by crude oil deposition through varying the brine salinity. Assessment of oil deposit through different brine salinity was assessed by two dimensional root mean square roughness (*Rq*) only.

At first glance it is surprising that analytical techniques based on interferometry have not been used more extensively in COBR process in mineral surface. Our approach in this chapter is to utilise the power visualisation of VSI to build a nano resolution of wettability that established by COBR interaction. The understanding of effect of water film beneath oil adsorption, oil adhesion, brine film salinity, temperature, asphaltene content and oil solvency during interaction of crude oil into mineral surface is investigated extensively. Assessment of the deposited oil was quantified through measurement of layer thickness. Furthermore, a detailed analysis is carried in two dimensional profile of adsorption and three dimensional of adsorption surface topography which is generated from optical fringes. The measurement of oil adsorption thickness is achieved through utilising the bare mineral surface and the oil-treated surface to be scanned by VSI simultaneously which can later subtracted to calculate the incremental increasing in surface profile which is equivalent to adsorption thickness in the crude oil treated surface. The two dimensional analysis is achieved through calculating the surface profile parameters and spacing parameters that have been standardized by ISO 4287 (2000) including *Rq*, skewness of assessed profile (*Rsk*),kurtosis of the assessed profile (*Rku*) and peak counting (*Rpc*). For the first time, the three dimensional areal characterisation is applied in studying the topography of

adsorption of crude oil into mineral surface. These included the root mean square value of the ordinates (*Sq*), skewness of topography height distribution (*Ssk*), kurtosis of topography height distribution (*Sku*),texture aspect ratio of the surface (*Str*) and mass of adsorption ($\Delta\Gamma$).

7.2 Materials and Preparation

7.2.1 Preparation of glass plates

Borosilicate glass plates (1.0 x 0.5 cm) were obtained from Fisher Scientific. The plates were used as a mineral surface substrate that represents the rock surface to characterise the adsorption morphology under various conditions of brine, oil and temperatures. Before use, the glass surface was carefully cleaned by acetone to obtain a perfectly bare glass surface without contamination. The roughness (*Rq*) of glass surface is 0.008 μm which gives a reference point to start compare the roughness of adsorption morphology when various conditions of brine, oil and temperature is applied.

7.2.2 Oil deposition test

Glass slides were immersed in brine for equilibration for 24 hours before immersion in crude oil closed cups. The bulk of crude oil, which is the non-deposited components, was then removed by rinsing in decalin until a colourless solution was obtained (Fogden, 2009). The treated surface was then analysed using VSI.

7.3 Experimental procedure

The present generation of VSI, like the MicroXAM MP8 (ADE-phase shift, Tucson), provides a high vertical resolution (0.1 – 1 nm) and a lateral resolution of about 500 x 500 nanometer (with a Nikon 50x Mirau objective). The lateral resolution of the system depends on the wavelength of the light source and the aperture of the Mirau objective. The MicroXAM MP8 has field of view of up to 845x630 μm^2. This range is large compared to the range provided typically by an AFM which is at maximum 100x100 μm^2 (Barron, 2009). The advantage of a larger field of view is to the ability to compare two separate substrates: untreated and the crude oil treated at the same scanning process. The high vertical resolution of VSI is achieved by moving the sample surface through the focal plane of the Mirau objective **Figure 7.5.** Only those parts of the surface that are exactly in the focal plane of

the objective produce interferograms. So the CCD camera images only a partial interferograms at each scan step unless the sample surface is perfectly levelled and atomically flat **Figure 7.6.** The vertical movement of the sample is achieved by a piezoceramic (PZT). **Figure 7.5** shows a photograph of the MicroXAM MP8 and schematic sketches of some the principles of white light VSI. Commercially available state of the art software packages (Talymap Gold Release 2.0) in combination with automated sample positioning stage allow the VSI to stitch several scans together. Field stitching is the process whereby a matrix of images are joined or stitched together. Field stitching is necessary especially when analysis is required over an area larger than field of view of the lens (at any resolution). The motorized horizontal translation stages allow the Talymap software to accurately adjust the surface position, so that each image is correctly positioned and there is consistent overlap of images. Overlap of the image is important because it allow the software to compare neighbouring images, and correctly correlate lateral position and consistent vertical range values. Software options will allow overlap typically ranging from 0% to 25%. Field stitching with a 10% overlap an image is a common option, this being a compromise between data integrity and speed of large area data acquisition and analysis. This means in case of the two scans that contain 100,000 pixels (i.e. height data) each, 10,000 pixels per scan are identical and can be used to match the two scans. In this way, large data sets can be produce that cover most or the entire surface (Petzing et al., 2010). VSI measures the topography to a precision height of up to 1-2 nm with later resolution up to 150 nm (Barron , 2009).

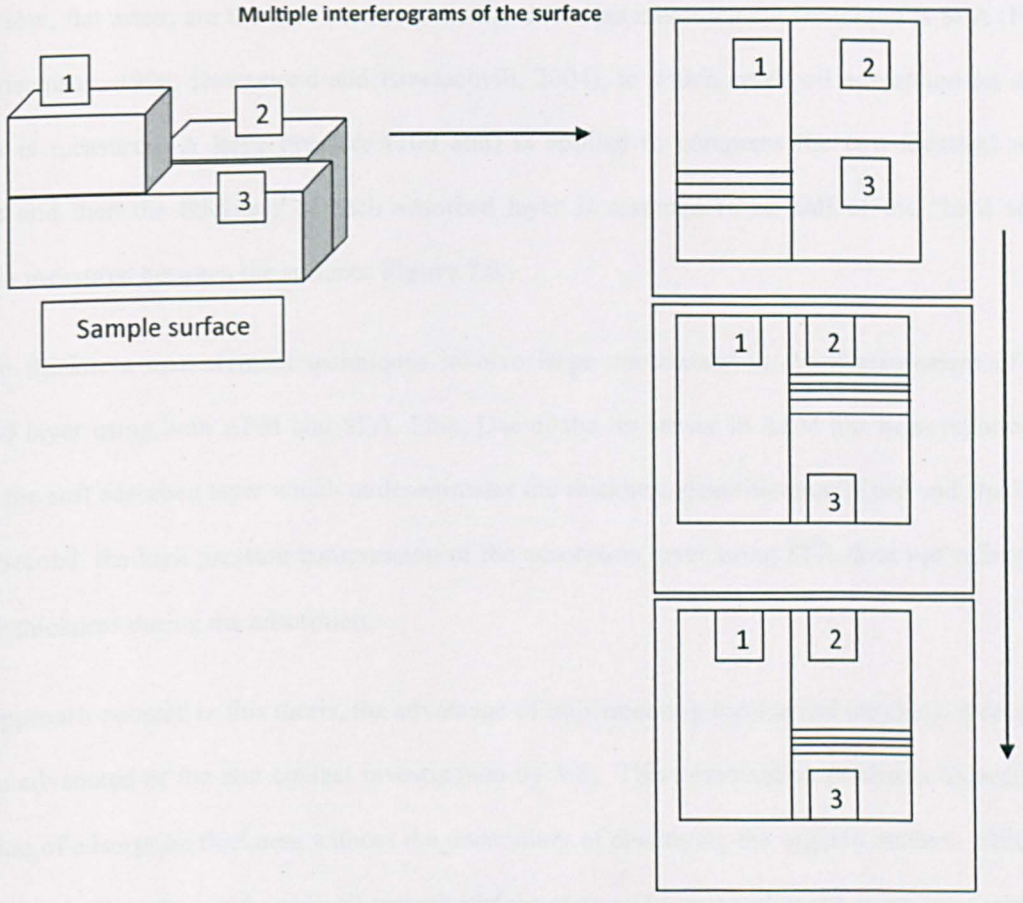

Figure 7.6 *Sketch illustrating the basic idea of white light scanning interferometry: The sample is continuously moved along the vertical axis in order to scan the surface topography. A series of interferograms is taken during the scan process. Due to the complex focal conditions for white light, there is only a small range of fringes observable at any time unless the sample surface is extremely flat and exactly levelled. All interferograms are automatically overlayed using Talymap system software. From the "stack" of interferograms the topographic information is extracted resulting in a height field representing the topography of the surface*

7.3.1 Statistical analysis

7.3.1.1 *Thickness measurement*

Previous works in measuring the thickness of adsorption crude oil into mineral surface was mainly centred on AFM and surface force apparatus (SFA). Lord and Buckley (2002) and Kumar et al. (2005) estimate the thickness of adsorption crude oil by using AFM tip to scrape the soft organic coating. Their field of view is focused over a small section of an AFM scan area (12.5 μm x 12.5 μm) and (50 μm x 50 μm) respectively. Estimates of film thickness is measured based on the assumption

that the low, flat areas, are the bare surface. Another thickness measurement technique is SFA (Fang and Christenson, 1990; Drummond and Israelachvili, 2004), in which crude oil adsorption on mica surfaces is measured. A large pressure (100 atm) is applied to compress the two identical mica surfaces and then the thickness of each adsorbed layer is assumed to be half of the "hard wall" thickness measured between the surfaces **Figure 7.8**.

The two thickness measurement techniques involve large uncertainty in the measurement of the absorbed layer using both AFM and SFA. First, Use of the tip sensor in AFM has been reported to destroy the soft adsorbed layer which underestimates the thickness quantification (Lord and Buckley, 2002). Second, the high pressure compression of the adsorption layer using SFA does not reflect the absolute thickness during the adsorption.

In the approach adopted in this thesis, the advantage of implementing mechanical stitching is coupled with the advantage of the non contact investigation by VSI. This combination produces an accurate estimation of adsorption thickness without the uncertainty of destroying the organic matters. Utilising a reference clean surface and crude oil treated surface glass to be scanned at the same time without any sort of contact or high pressure compression (**Figure 7.7-Figure 7.8**). A precise non-contact measurement of the thickness of adsorption oil is obtained by comparing the both topographic surface resulting from interferometry.

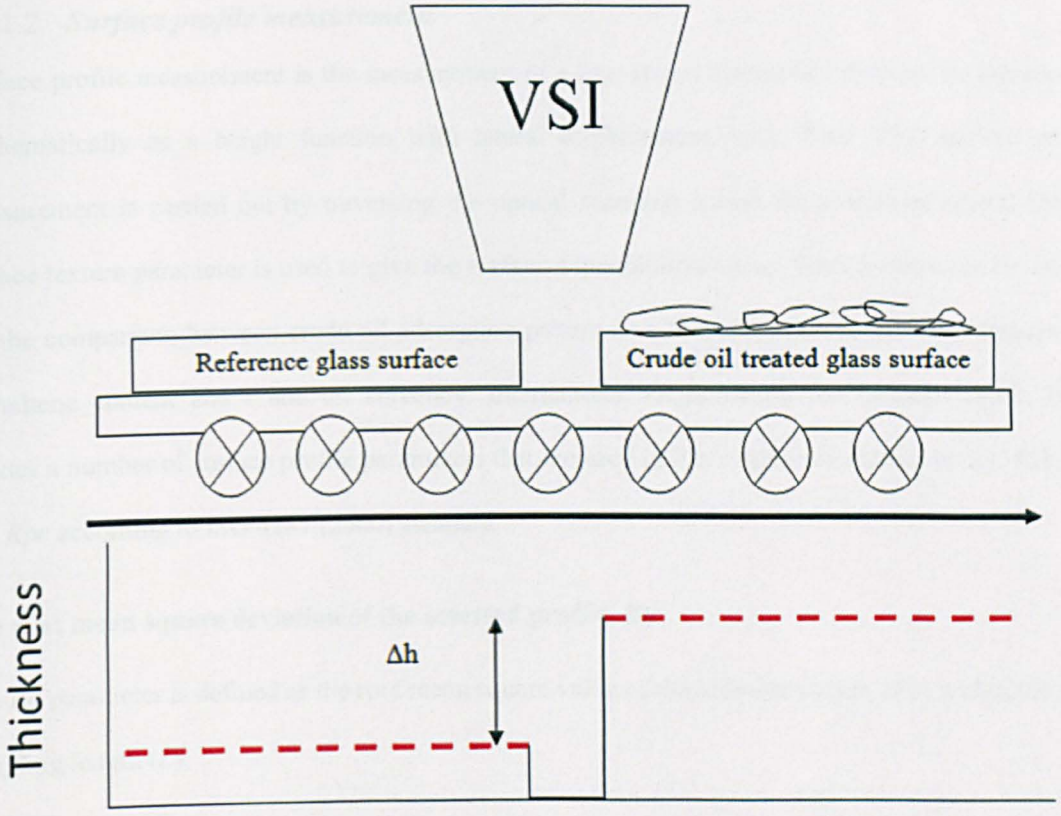

Figure 7.7 *Non-contact white light interferometry measurement technique for adsorption thickness.*

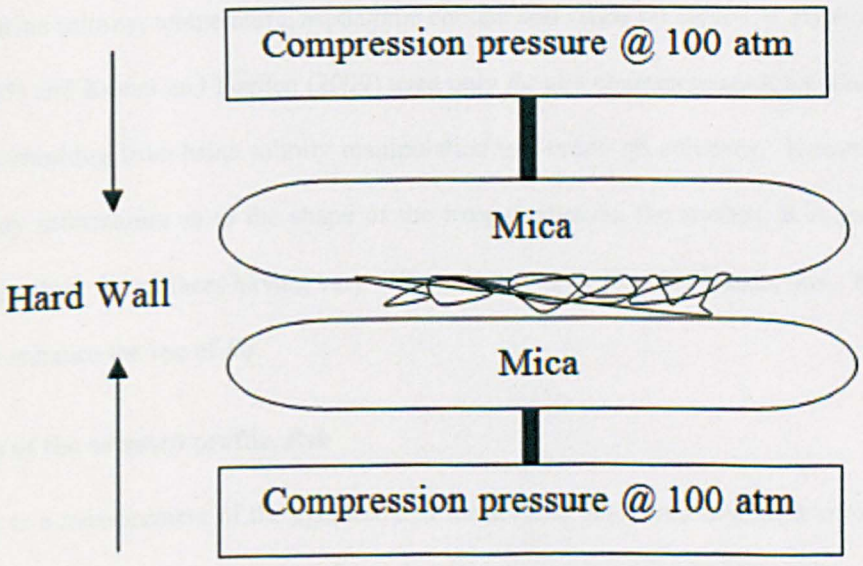

Figure 7.8 *Measurement of adsorption thickness by surface force apparatus.*

7.3.1.2 *Surface profile measurement*

Surface profile measurement is the measurement of a line across the surface that can be represented mathematically as a height function with lateral displacement, *z(x)*. With VSI, surface profile measurement is carried out by traversing the optical scanning across the sample at central line. A surface texture parameter is used to give the surface a quantitative value. Such a value can be used to aid the comparison between crude oil adsorption pattern as a function of brine salinity, temperature, asphaltene content and crude oil solvency. International Organization for Standardization (ISO) defines a number of surface profile parameters that are used in this chapter including the *Rq*, *Rsk*, *Rku* and *Rpc* according to ISO 4287 (2000) standard.

The root mean square deviation of the assessed profile, *Rq*

The *Rq* parameter is defined as the root mean square value of the ordinate values, *z(x)*, within the sampling length (*L*),

$$Rq = \sqrt{\frac{1}{L}\int_0^L z^2(x)dx}$$

Assessing the crude oil adsorption through roughness provides a quantitative approach to explain the effect of brine salinity, temperature, asphaltene content and crude oil solvency. Previous work Kumar et al. (2005) and Kumar and Fogden (2009) used only *Rq* as a characterisation for adsorption of crude oil profile resulting from brine salinity manipulation and crude oil solvency. However, *Rq* does not provide any information as to the shape of the irregularities on the surface. It is possible to obtain similar *Rq* values for surfaces having very different structures. For this reason, *Rsk*, *RKu* and *Rpc* are utilised to enhance the use of *Rq*.

Skewness of the assessed profile, *Rsk*

Skewness is a measurement of the symmetry of the surface deviations about the mean reference line and is the ratio of the mean cube value of the height values and the cube of *Rq* within a sampling area,

$$Rsk = \frac{1}{Rq^3}\sqrt{\frac{1}{L}\int_0^L z^3(x)dx}$$

Rsk describes the shape of the topography height distribution. For a surface with a random height distribution that has symmetrical topography, the skewness is zero. The skewness is derived from the amplitude distribution curve; it is the measure of the profile symmetry about the mean line. This parameter represents the degree of cavities and crevices after the oil adsorption profile, either as peaks shapes or valleys shape **Figure 7.9**. The direction of the skewness is dependent on the bulk of the adsorption is whether it is predominates peaks adsorption shape ($Rsk>0$) or it predominate by valleys adsorption shape ($Rsk<0$).

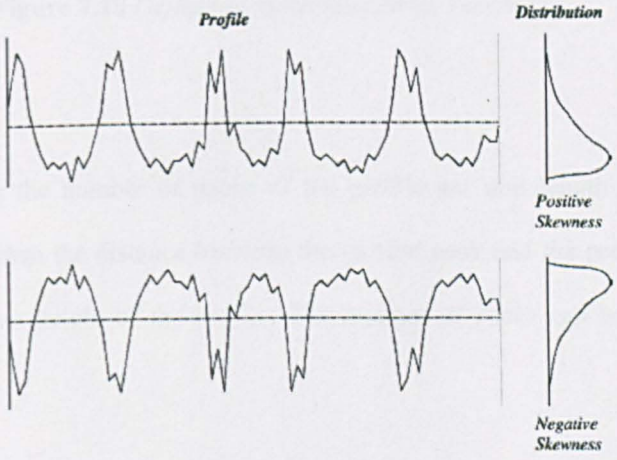

Figure 7.9 *Definition Rsk and the amplitude distribution curve according to ISO 4287 (2000).*

Kurtosis of the assessed profile, *Rku*

It is a measure of the sharpness of the surface height distribution and is the ratio of the mean of the fourth power of the height values and the fourth power of *Rq* within the sampling area,

$$Rku = \frac{1}{Rq^4}\sqrt{\frac{1}{L}\int_0^L z^4(x)dx}$$

Rku characterises the spread of the height distribution. According to ISO 4287 (2000) standard, a surface with normal height distribution has a kurtosis value of three, a spiky surface will have a high kurtosis value ($Rku > 3$) and a bumpy surface will have a low kurtosis ($Rku<3$) values **Figure 7.10**.

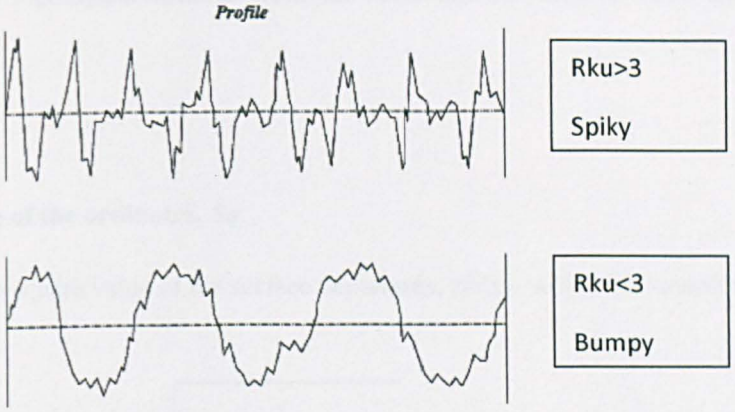

Figure 7.10 *Definition of kurtosis (Rku) parameter.*

Peak counting, *Rpc*

This parameter calculates the number of peaks of the profile per unit length (centimetre or inch). Peaks are counted only when the distance between the current peak and the preceding one is greater than 10% of the maximum height of the profile. The number of peaks can be calculated from the following equation:

$$\mathrm{Rpc} = \frac{1}{L}\sum_{i=1}^{n} Rpc\ (i)$$

7.3.1.3 *3D areal characterisation*

There are limitations with surface characterisation using only 2D surface measurement. A fundamental problem is that 2D profile itself does not contain enough information relating to surface topography in the xy areal view. Hence, three dimensional areal parameters can serve to provide a more detailed information regarding the oil adsorption pattern on mineral surface different conditions. All the areal standard parameters that used in this section are according to ISO 25178 (2007). There are two main classes of areal parameters: field parameters and feature parameters. Field parameters which are defined from all the points on scale limited surface which includes the root mean square value of the ordinates,*Sq*), skewness of topography height distribution, *Ssk*, kurtosis of topography height distribution, *Sku*, and texture aspect ratio of the surface, *Str*. Feature parameters are defined

from a subset of predefined topological features from the scale-limited surface, which including volume of oil adsorption.

7.3.1.4 *Field parameters*

The root mean square value of the ordinates, *Sq*

Sq is defined as the root mean square value of the surface departures, z(x,y), within the sampling area,

$$Sq = \sqrt{\frac{1}{A}\iint_A Z^2(x,y)dxdy}$$

where *A* is the sampling area, xy.

Skewness of topography height distribution, *Ssk*

Skewness is the ratio of the mean cube value of the height values and the cube of *Sq* within a sampling area,

$$Ssk = \frac{1}{Sq^3}\left[\frac{1}{A}\iint_A Z^3(x,y)dxdy\right]$$

Kurtosis of topography height distribution, *Sku*

Sku is the ratio of the mean of the fourth power of the height values and the fourth power of the *Sq* within the sampling area,

$$Sku = \frac{1}{Sq^4}\left[\frac{1}{A}\iint_A Z^4(x,y)dxdy\right]$$

Texture aspect ratio of the surface, *Str*

Str describes the characteristic of isotropy and long-cretness of surfaces. According to ISO 25178 (2007) a larger value of *Str* (> 0.5) indicates that a surface is isotropic, while a smaller value of *Str* (<0.5) indicates that the surface is long-crested or has anisotropy with significant texture.

Str can be defined as the ratio of the fastest to slowest decay to correlation length, 0.2, of the surface using an auto correlation function (ACF). The basic concept behind ACF can be found in Dong et al. (1995) and Leach (2010).

7.3.1.5 *Feature parameters*

Traditional surface texture parameters, such as the profile parameters and the areal field parameters, use a statistical basis to characterise the cloud of measured points derived from fringes analysis as described in section (7.3.1.1, 7.3.1.2 and 7.3.1.3). Pattern features such as hills and dales, and the relationships between them are terms feature parameters (Paul, 2009). Feature parameters apply statistics from a sub-set of pre-defined topographic features which consist of five steps: (i) selection of the type of texture features (hills, dales), (ii) segmentation, (iii) determining significant features, (iv) selection of feature attributes, and (v) quantification of feature attribute statistics. According to feature parameters that defined in the international standards ISO 25178 (2007), volume feature parameters is utilised to describe the crude oil adsorption features under different conditions. From the presented values of volumes, the adsorption mass per planar area, $\Delta\Gamma$, in ng/cm^2, can be calculated via multiplication by crude oil density (0.857 g/cc).

7.4 Results

As mentioned previously, the bare surface of glass provide a very low roughness value (0.008 μm) which serves as a starting point to compare the effect of COBR through different conditions of brine salinity, temperature and asphaltene content.

7.4.1 Thickness of adsorption layer

The thickness of adsorbed oil shows a clear trend of layer reduction as brine is diluted from 3 M NaCl brine to 0 M NaCl brine **Figure 7.11**. The adsorption thickness is 129 μm at 3 M NaCl brine, 4.47 μm at 0.5 M NaCl brine and 1.55 μm at 0 M NaCl brine. The thickness of adsorped oil is slightly lower when brine resides between crude oil and mineral surface than when it is absent **Figure 7.12.** In particular, the absorbed oil has a thickness of 4.47 μm when brine is present compared with 4.80 μm it is absent. The crude oil start to be adhesive at short time interaction when the brine film between oil

and mineral surface become acidic with lower pH. The adsorption thickness increased to 14.2 μm compared with 4.468 μm when the brine is neutral pH **Figure 7.13**. Increasing the temperature results in a sharp increase of the adsorption layer from 4.47 μm to 97 μm **Figure 7.14**. The thickness is increased from 4.47 μm to 22.2 μm when asphaltene is removed from the crude oil **Figure 7.14**. Mixing the crude oil with heptane yields a thickness of 125 μm compared to 7.4 μm when it is mixed with toluene **Figure 7.16**.

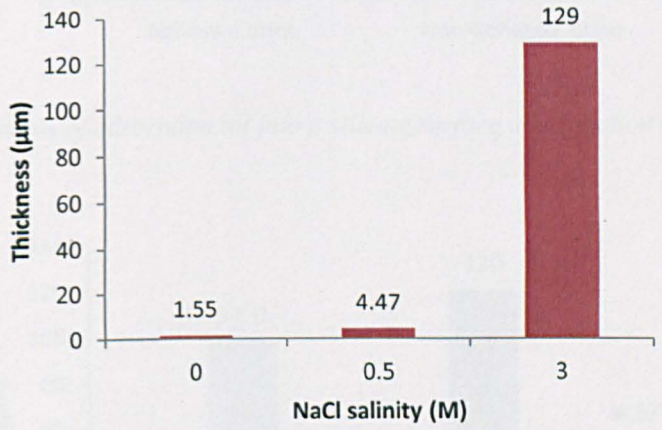

Figure 7.11 *Thickness of adsorbed oil as a function of NaCl salinity.*

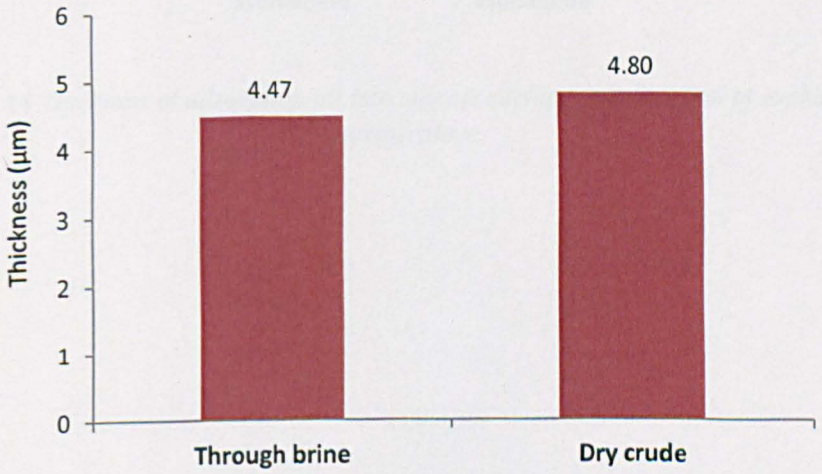

Figure 7.12 *Thickness of adsorption oil into a silicate surface as function of brine contact.*

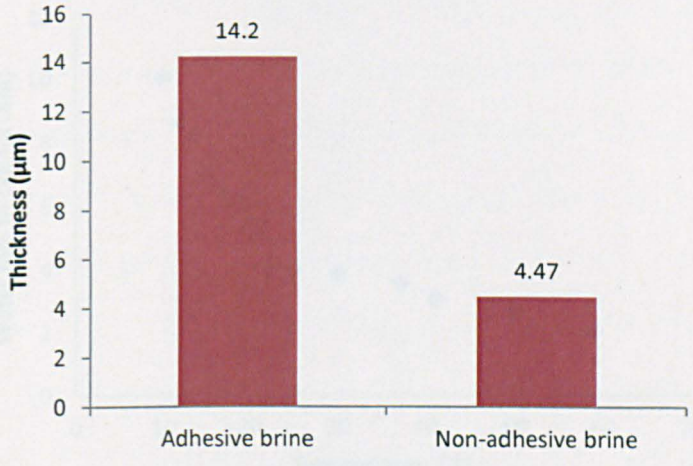

Figure 7.13 *Thickness of adsorption oil into a silicate surface as a function of brine stability.*

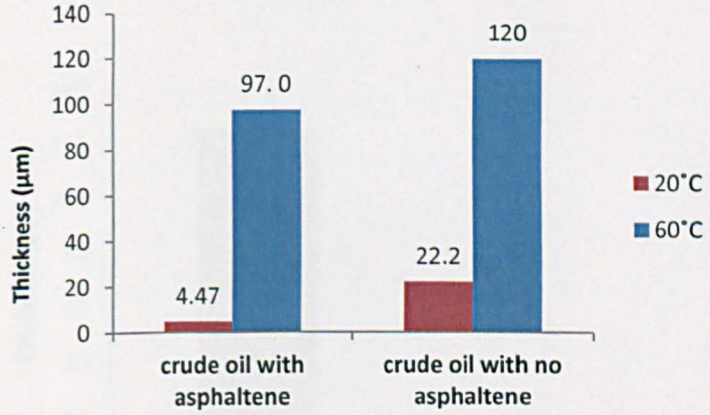

Figure 7.14 *Thickness of adsorption oil into silicate surface as a function of asphaltene and temperature.*

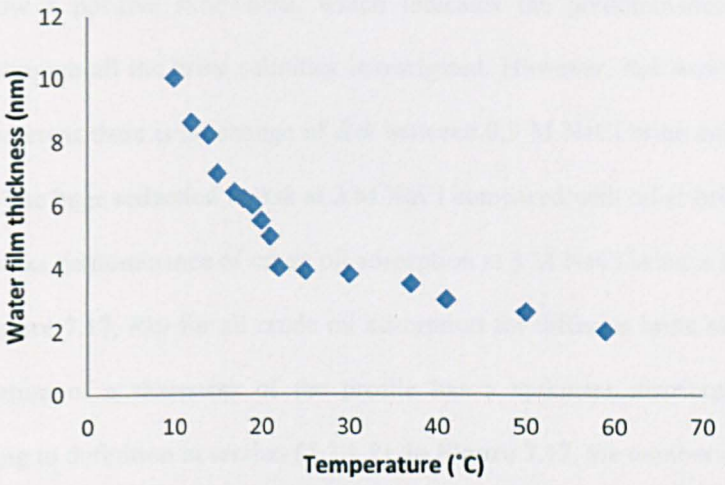

Figure 7.15 *The thickness of water film residing in fused silica as function of temperature after Derjaguin (1987).*

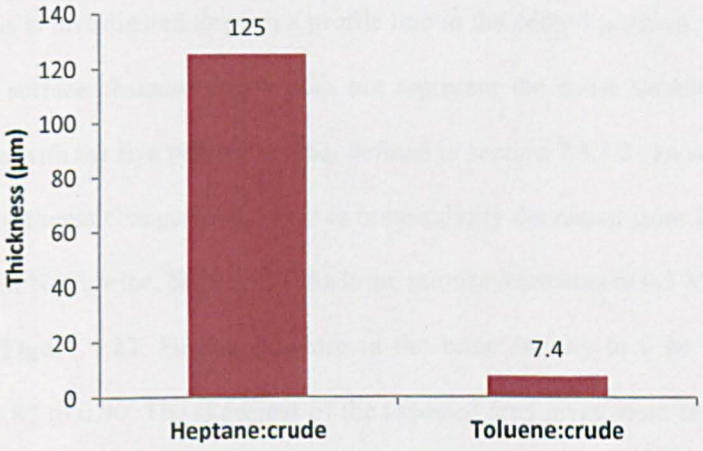

Figure 7.16 *Thickness of adsorption oil into silicate surface as a function of oil solvency.*

7.5 2D and 3D dimensional surface characterisation

7.5.1 Effect of brine salinity

Rq shows a continuous increasing as brine salinity decreased from 3 M NaCl to 0 M NaCl brine. At 3 M NaCl, *Rq* is 0.14 µm whereas it is increased five times at 0.5 M NaCl brine to reach 0.70 µm **Figure 7.17**. At 0 M NaCl brine, a further increase in *Rq* to 2.1 µm which is three times increasing of 0.5 M NaCl. In **Figure 7.17**, *Rsk* shows that all the crude oil adsorption through the three different

brine salinities show a positive sknewness, which indicates the predominance of peaks in the adsorption profile through all the brine salinities investigated. However, *Rsk* was the lowest at 3 M NaCl brine (0.16) whereas there is no change of *Rsk* between 0.5 M NaCl brine and 0 M NaCl brine, for which *Rsk* is 1. The huge reduction in *Rsk* at 3 M NaCl compared with other brines is an indicator that the degree of peaks predominance of crude oil adsorption at 3 M NaCl brine is lower compared to others brines. In **Figure 7.17**, *Rku* for all crude oil adsorption for different brine salinities is above 3 which is an indication of a sharpness of the profile has a spikiness distribution not a bumpy distribution according to definition in section (7.3.1.2). In **Figure 7.17**, the number of peaks during oil adsorption through the three different salinities 3 M, 0.5 M and 0 M NaCl show two distinctive behaviours. *Rpc* values indicate four peaks per 1 mm are present for the 3M NaCl brine. At a salinity of 0.5 M and 0 M NaCl, 2 peaks per 1 mm are determined.

Since the 2D analysis is investigated through a profile line in the central position, there is an inherent uncertainty that the surface characterisation does not represent the entire sample surface. Here 3D areal characterisation with the five parameters that defined in section 7.3.1.3 can serve to mitigate this risk. The 3D areal roughness changes noticeably as brine salinity decreased from 3 M NaCl brine to 0 M NaCl brine. At 3 M NaCl brine, *Sq* is 0.425. As brine salinity decreases to 0.5 M NaCl brine, the *Sq* is doubled to 0.82 **Figure 7.22**. Further decrease in the brine salinity to 0 M NaCl shows minor change in *Sq* from 0.82 to 0.90. The skewness of the assessed area gives more insight into the shape of topographic height distribution after crude oil adsorption, which shows two clear distinctive topographies at 3 M NaCl brine case compared with 0.5 M and 0 M NaCl brine case. At 3 M NaCl brine, *Ssk* is -0.31 whereas it is similar for 0.5 M and 0 M brine at 6.4 and 6.0 respectively. The negative *Ssk* at 3 M brine means the adsorption of oil mainly appeared as less frequent peaks compared to crude oil adsorption through brine salinity of 0.5 M NaCl brine and 0 M NaCl brine. *Skr* reveals more topographic information regarding the degree of spikiness of oil adsorption peaks in all the three previous brine salinity. From **Figure 7.22**, it is very clear that all crude oil adsorption peaks show a higher *Sku* than 3 which means a high degree of peak spike is exist for all the brine salinity. However, the degree of spikiness was the least 12.9 with 3 M NaCl brine compared with 0.5 M NaCl

brine (59.1) and 0 M NaCl brine (49.2). The texture of the adsorbed crude oil is inferred from *Str* which shows a definite alteration to less uniform texture as brine salinity decrease to 0 M NaCl brine. The texture pattern is evident from change in *Str* from 0.9 at 3 NaCl M brine and 0.7 at both 0.5 M and 0 M NaCl brine. However, none of the crude oil adsorption textures shows a directional lay texture pattern as *Str* in all brines is above>0.5.

The feature areal parameter used here is the adsorption mass per planer area, $\Delta\Gamma$, **Figure 7.23**. It decreases as brine salinity diluted. At 3 M NaCl brine salinity, 394 ng/cm^2 is adsorb in the surface. At 0.5 M NaCl salinity, $\Delta\Gamma$ is reduced by four times to reach 91.7 ng/cm^2. At 0 M NaCl brine salinity, $\Delta\Gamma$ had undergone a huge reduction to reach 0.155 ng/cm^2.

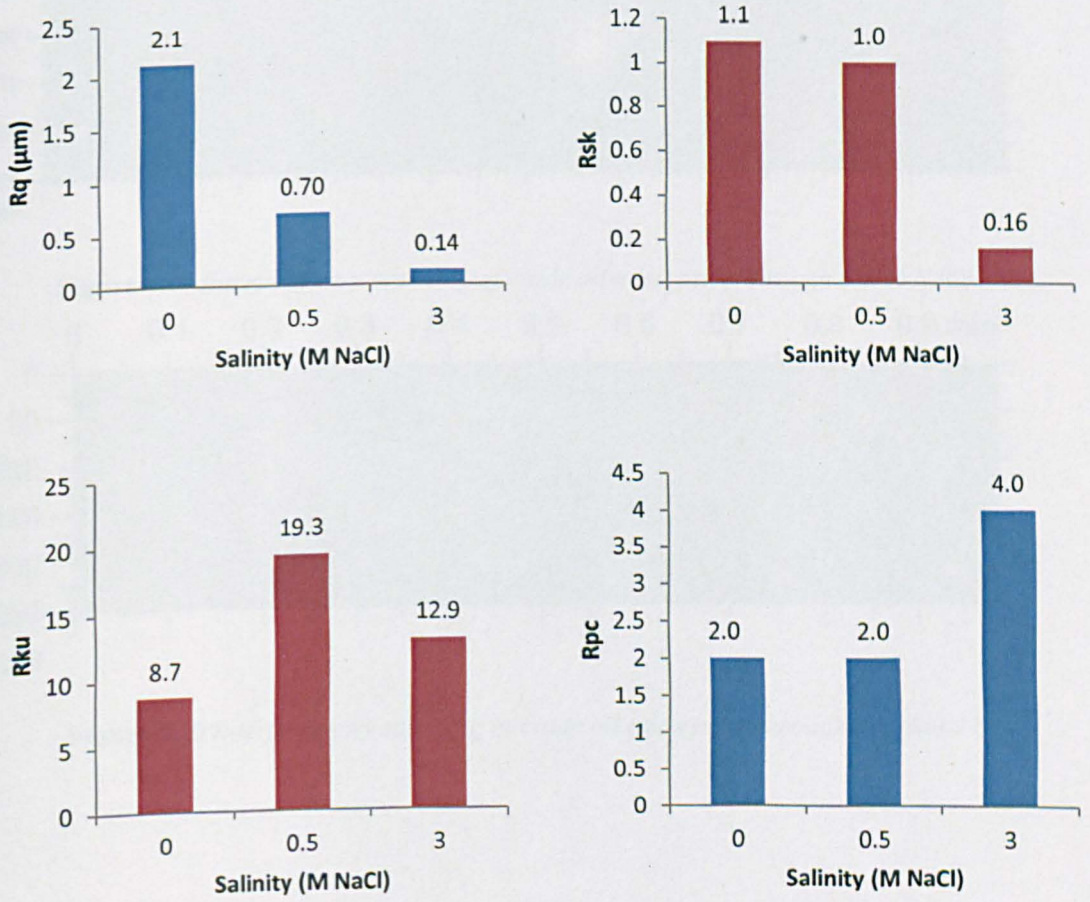

Figure 7.17 *2D profile analysis of crude oil treated silica surfaces as a function of brine salinity; Root mean square, Skewness, Kurtosis and number of peaks of the crude oil adsorption.*

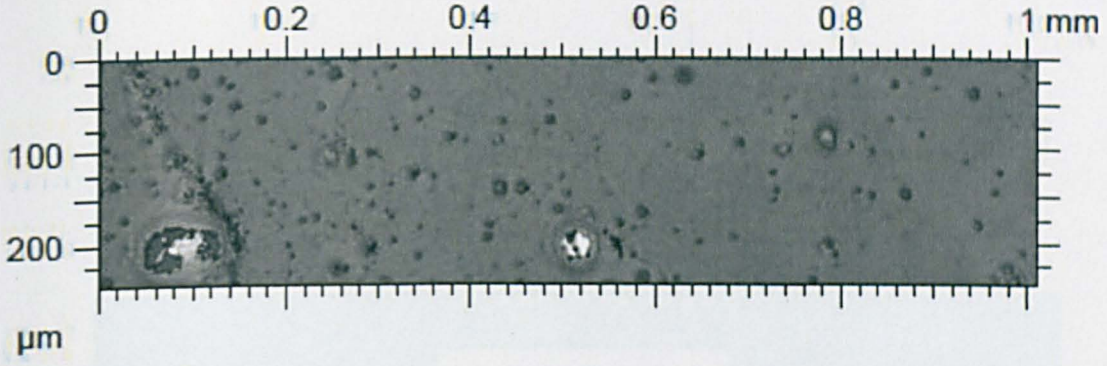

Figure 7.18 *Interferometry scanning of crude oil adsorption through 0 M NaCl brine.*

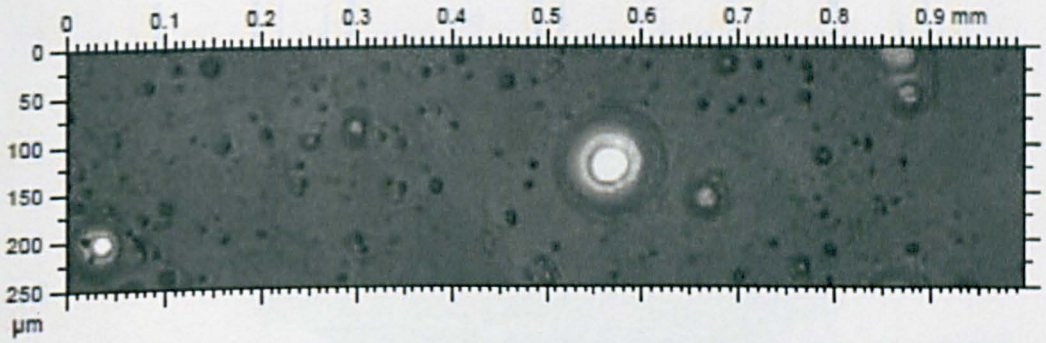

Figure 7.19 *Interferometry scanning of crude oil adsorption through 0.5 M NaCl brine.*

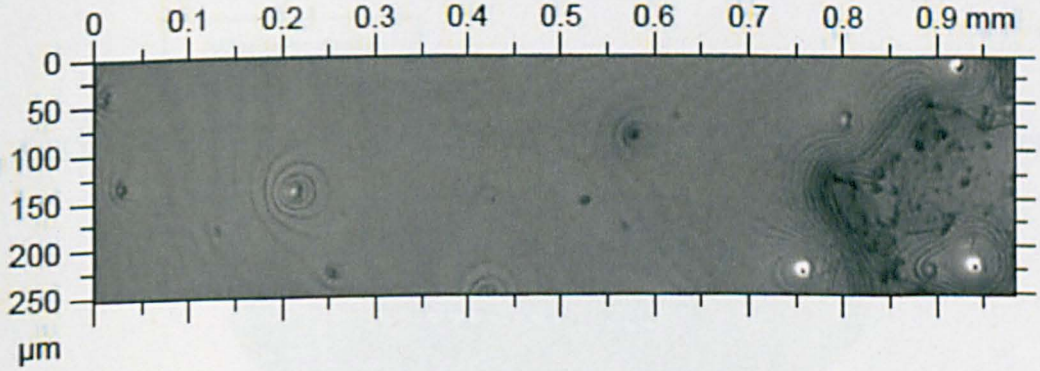

Figure 7.20 *Interferometry scanning of crude oil adsorption through 3 M NaCl brine.*

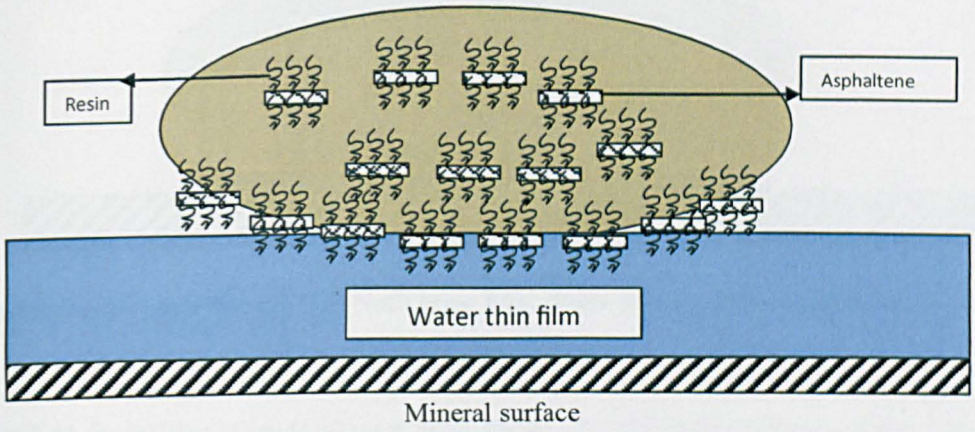

(a) Crude oil before adsorption through brine film

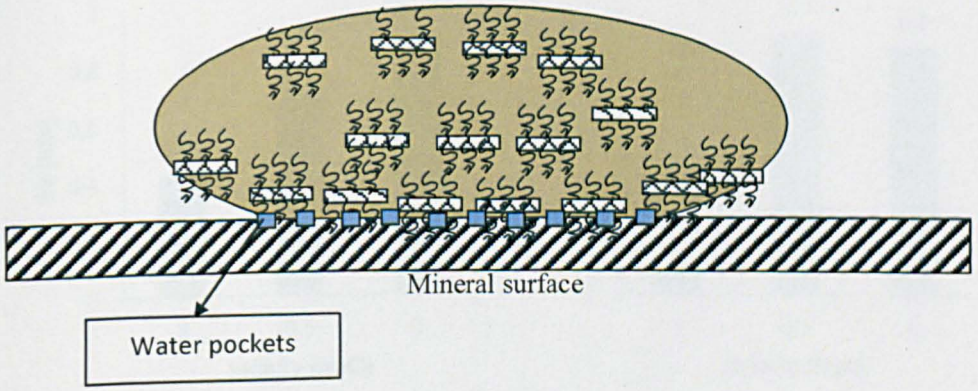

(b) Crude oil after adsorption through 3 M NaCl brine film. Water pockets appear at discrete sites.

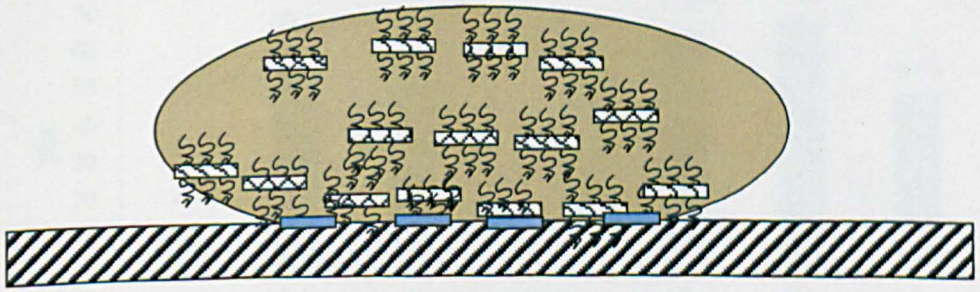

(c) Crude oil adsorption through 0.5 M NaCl brine film. Water pockets expand its size between crude oil and solid surface.

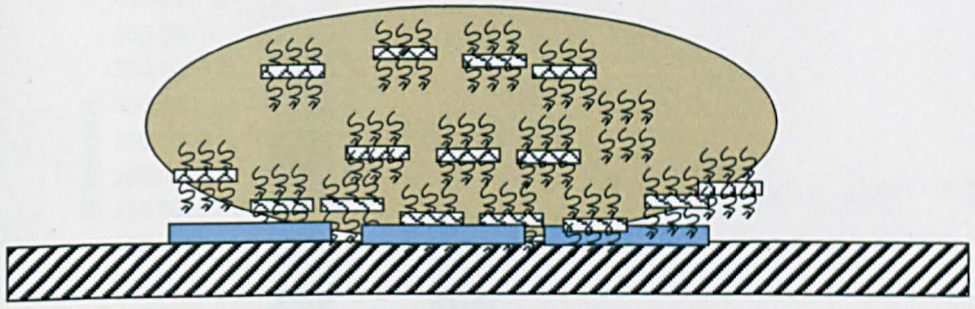

(d) Crude oil adsorption through 0 M NaCl brine film. Water pockets expand its size more compared to previous brines.

Figure 7.21 *Deposition of crude oil on mineral surface through different brine salinity 3 M, 0.5 M and 0 M NaCl brines.*

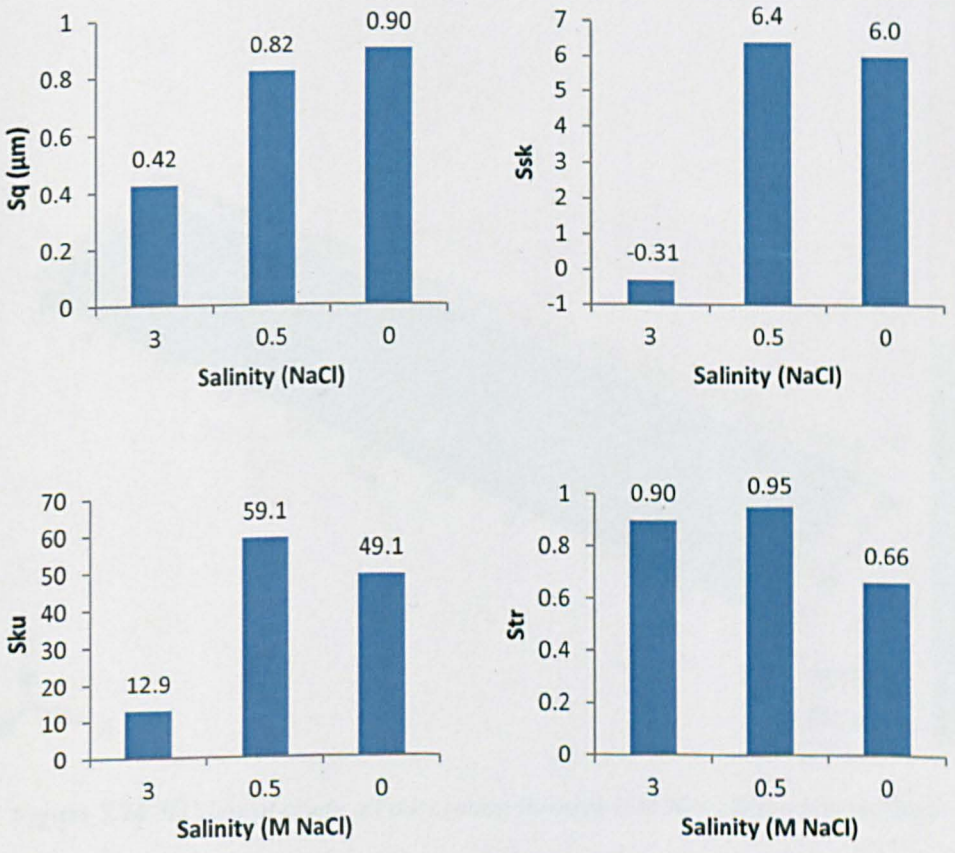

Figure 7.22 *Areal root mean square, skewness, kurtosis and texture aspect ratio of roughness of deposited oil as brine salinity change.*

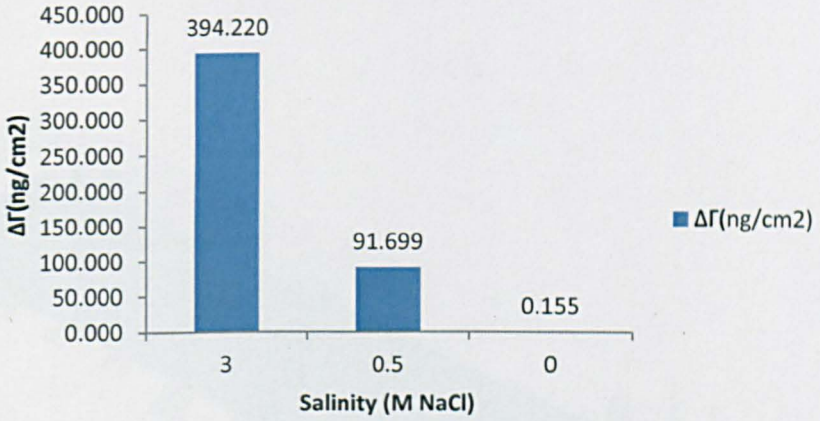

Figure 7.23 *Oil adsorption amount into silicate surface as brine salinity change.*

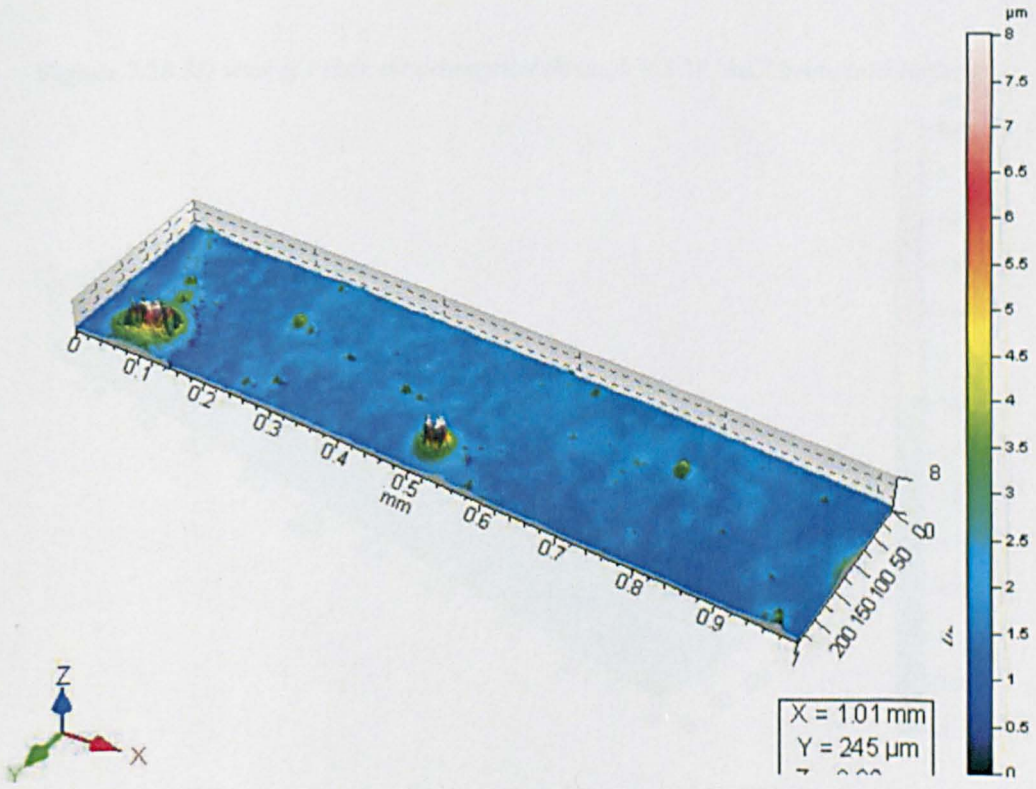

Figure 7.24 *3D view of crude oil adsorption through 0 M NaCl brine into surface.*

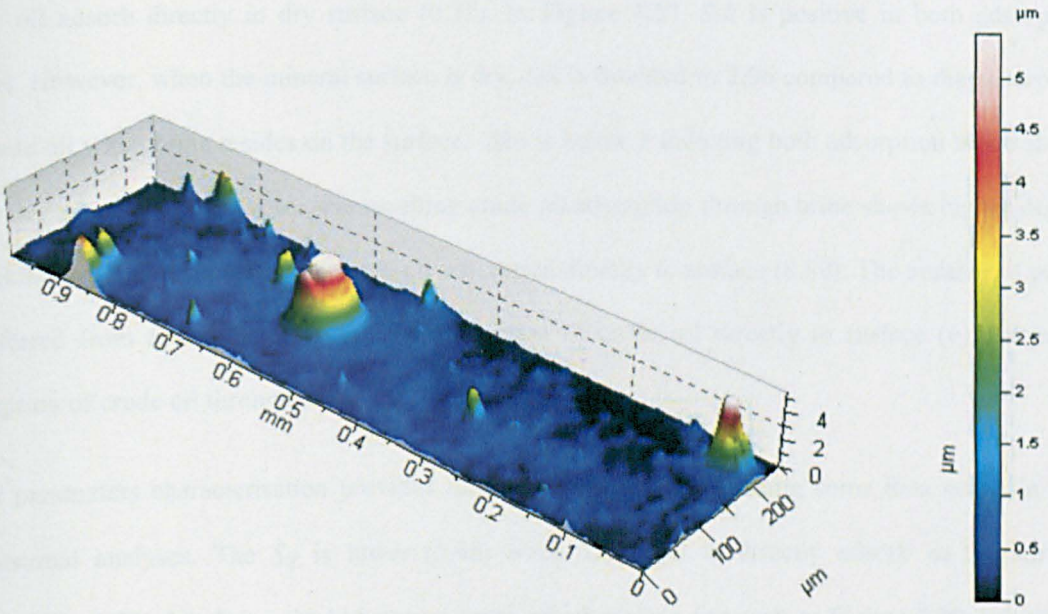

Figure 7.25 *3D view of crude oil adsorption through 0.5 M NaCl brine into surface.*

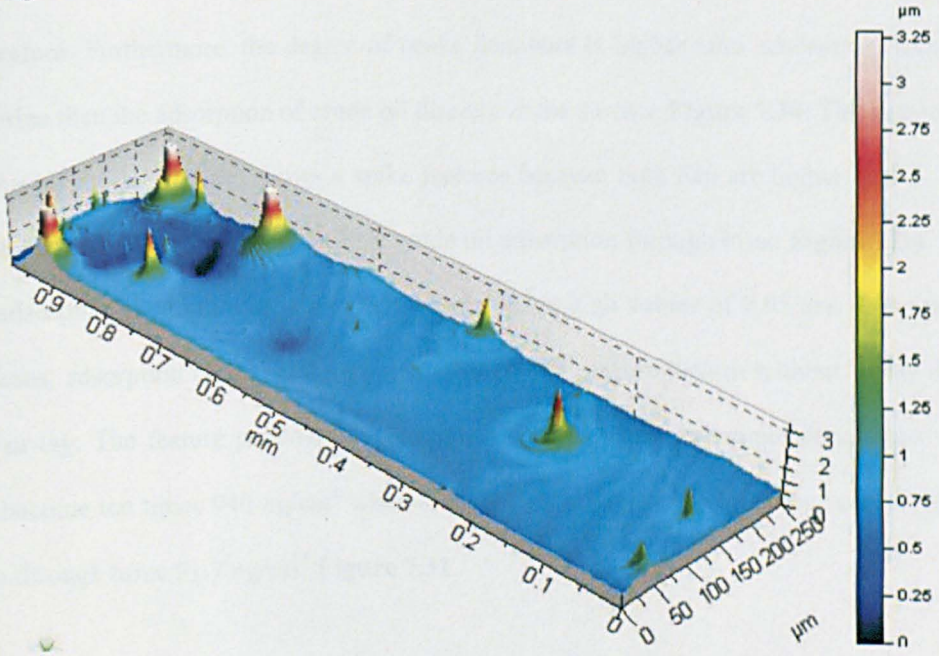

Figure 7.26 *3D view of crude oil adsorption through 3 M NaCl brine into surface.*

7.5.2 Effect of brine contact

To investigate the effect of brine existence on crude oil adsorption, two adsorption mode initiated by direct adsorption of crude oil into mineral surface and adsorption of crude oil through brine into mineral surface. In **Figure 7.27**, *Rq* is higher (0.70) when crude oil adsorbs through brine than when

crude oil adsorb directly in dry surface (0.22). In **Figure 7.27**, *Ssk* is positive in both adsorption modes. However, when the mineral surface is dry, *Ssk* is doubled to 2.06 compared to the adsorption of crude oil when brine resides on the surface. *Sku* is below 3 indicting both adsorption mode shows sharp degree of peaks. However, the resulting crude oil adsorption through brine shows higher degree of spikiness (19.3) compared with crude oil adsorption directly to surface (8.89). The number of peaks as inferred from *Rpc* is higher when the adsorption of crude oil directly to surface (6) compared adsorption of crude oil through brine (2).

Areal parameters characterisation provides full information without losing some data set as in two dimensional analyses. The *Sq* is lower (0.48) when crude oil is directly adsorb in the surface compared to 0.82 when brine shield between crude oil adsorption and surface **Figure 7.30**. *Ssk* shows that crude oil adsorption is dominated by peaks rather than valleys because both skewnesses yield positive values. Furthermore, the degree of peaks dominate is higher after adsorption from crude oil through brine than the adsorption of crude oil directly in the surface **Figure 7.30**. The sharpness of the topography height distribution shows a spike features because both *Sku* are higher than 3. However, the degree of spikiness appears higher after crude oil adsorption through brine **Figure 7.30**. *Str* shows for both adsorption mode through brine and without brine high values of 0.95 and 0.84 respectively. In both cases, adsorption mode shows a uniform degree of texture pattern without strong directional structure or lay. The feature parameters, selected to describe the three dimensional view in **Figure 7.29**, $\Delta\Gamma$ become ten times 940 ng/cm^2 when crude oil adsorbs directly to surface compared to crude oil adsorb through brine 91.7 ng/cm^2 **Figure 7.31**.

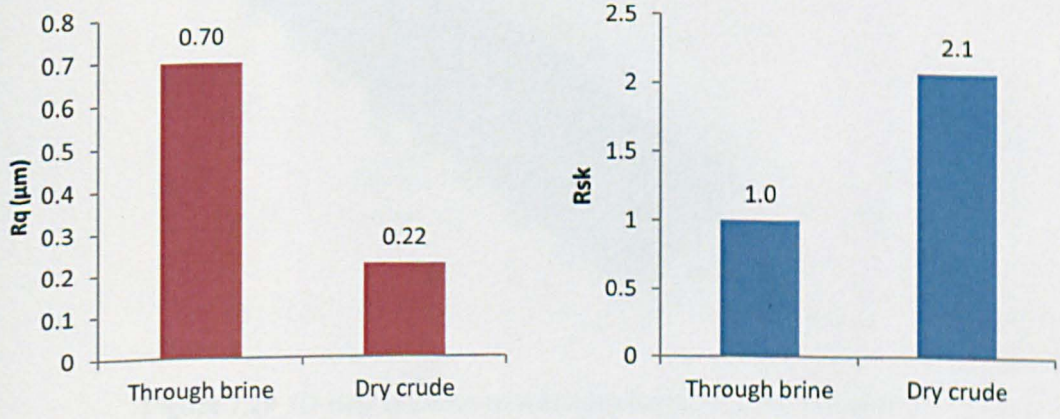

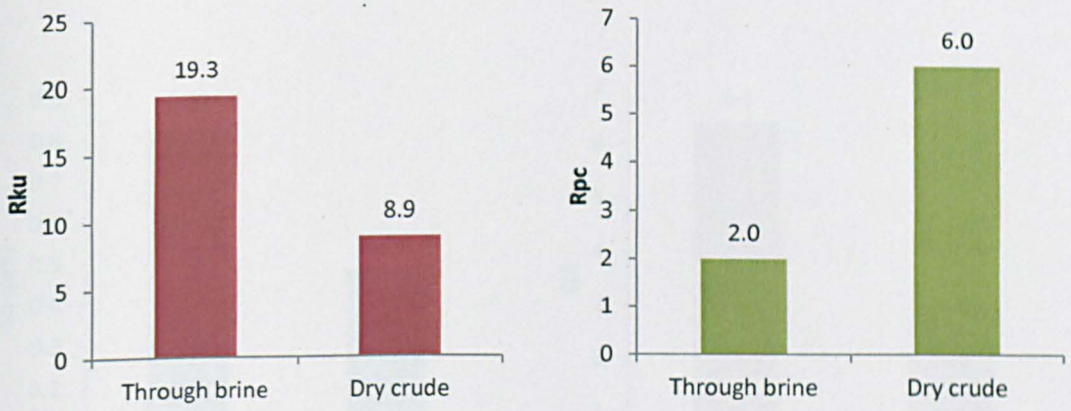

Figure 7.27 *2D profile analysis of crude oil treated silica surfaces as a function of brine contact; root mean square, skewness, kurtosis and number of peaks of the crude oil adsorption.*

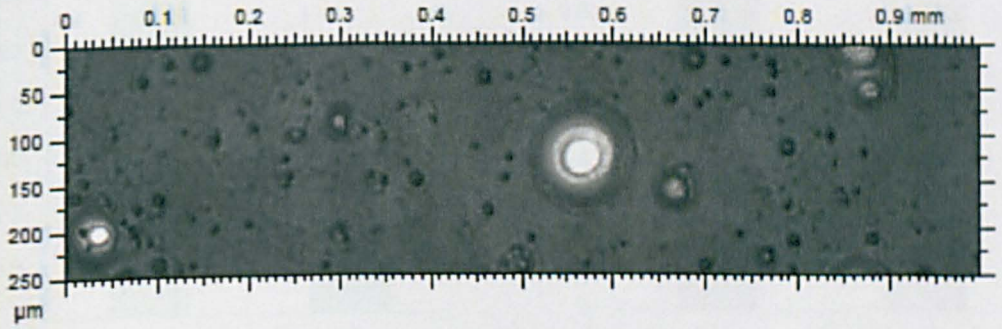

Figure 7.28 *Interferometry scanning of crude oil adsorption through brine into surface.*

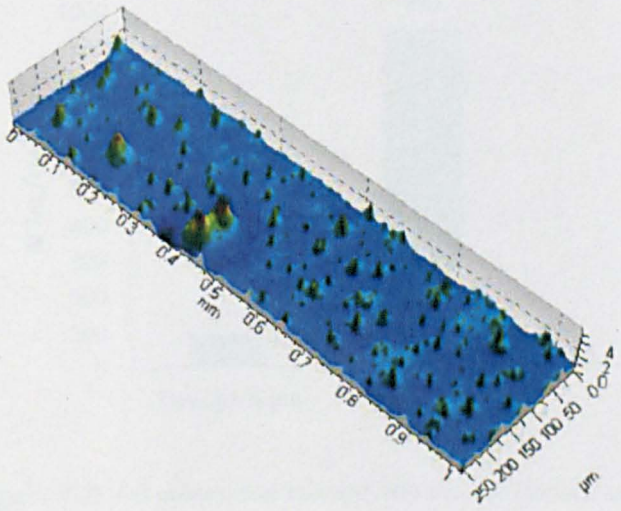

Figure 7.29 *3D view of crude oil adsorption into dry silicate surface.*

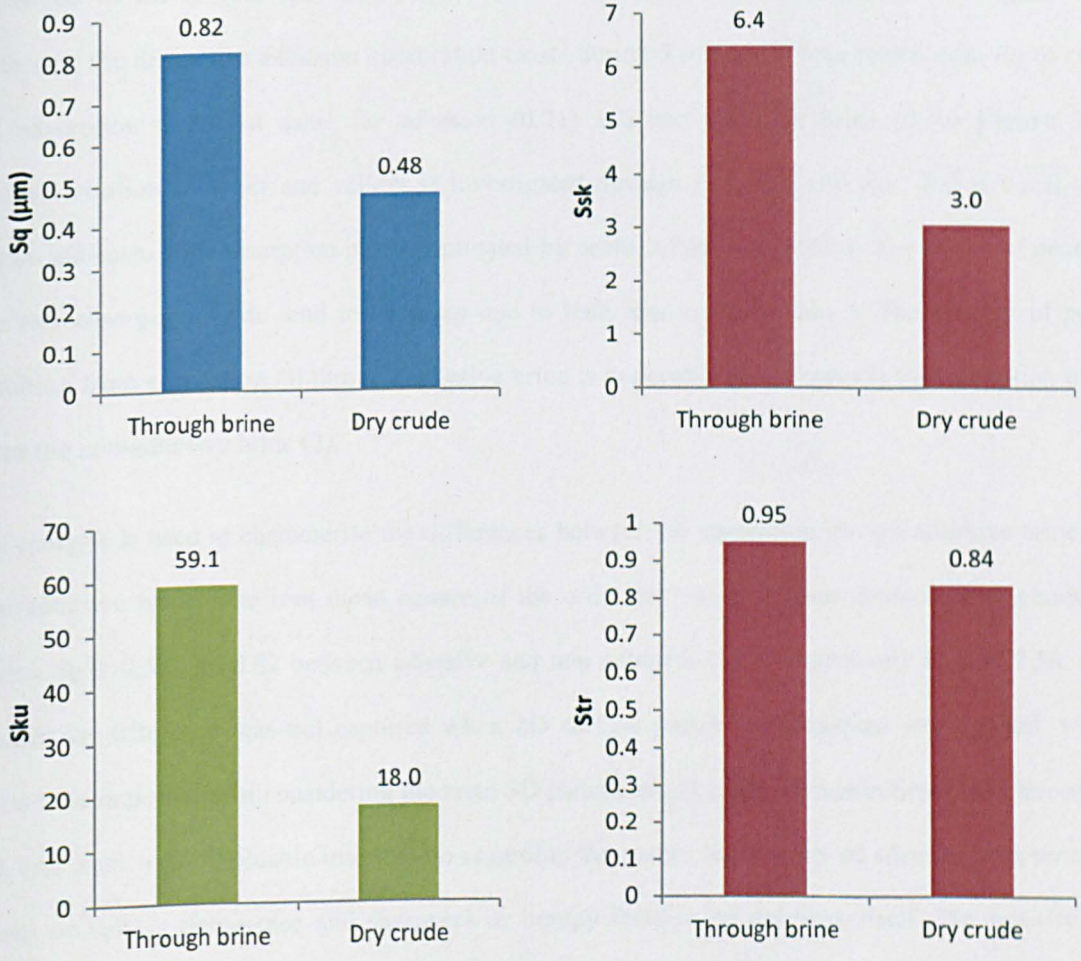

Figure 7.30 *Areal root mean square roughness, skewness, kurtosis and texture aspect ratio of topography height distribution of adsorption oil as function of water existence.*

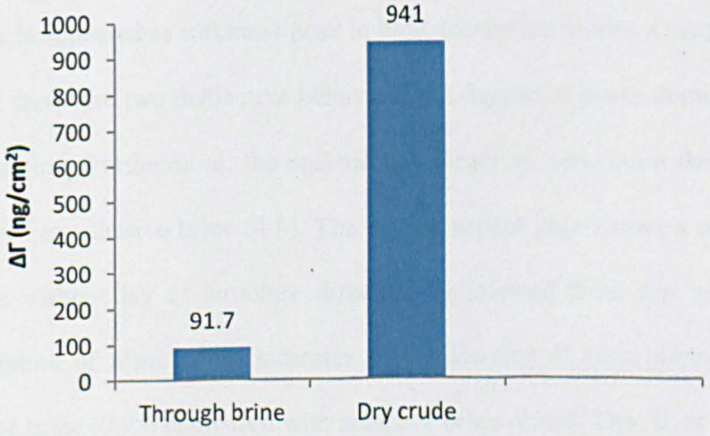

Figure 7.31 *Oil adsorption amount into silicate surface as brine exist.*

7.5.3 Effect of adhesion

Adhesion of oil is observed during short time interaction with brine and surface **Figure 7.32**. Although the distinctive adhesion observation exists during 2 min short time interaction, *Rq* of crude oil adsorption is almost same for adhesion (0.71) and non adhesion brine (0.70) **Figure 7.33**. Characterisation of peaks and valleys is investigated through *Rsk*, *Rku* and *Rpc*. *Rsk* is equal to 1, which indicates both adsorption mode dominated by peaks rather than valleys. The nature of peaks in the two adsorption mode tend to be sharp due to both *Rku* is larger than 3. The number of peaks resulting from adsorption oil through adhesive brine is noticeably four times (8) the adsorption of oil from the non-adhesive brine (2).

3D analysis is used to characterise the differences between oil adsorption though adhesive brine and non-adhesive brine. The root mean square of the ordinates shows a clear distinctive roughness in which *Sq* is 0.58 and 0.82 between adhesive and non adhesive brine respectively **Figure 7.36**. This distinctive difference was not captured when 2D surface profile measurement was applied, which shows the importance of considering the areal 3D parameters in crude oil adsorption characterisation. *Ssk* and *Skuk* o give valuable information regarding the nature topography of adsorption in terms of peaks or valleys dominance and sharpness or bumpy features of the peak itself. The positive *Ssk* indicates the peak is dominating feature more than valleys after adsorption of oil at both brines. However, the degree of dominant peaks is six times (6.39) during adsorption through non-adhesive brine. The sharpness is appeared as spikiness peak in both adsorption modes. Compared to 2D surface analysis, it does not show the two distinctive behaviours in degree of peaks dominance as shown by 3D areal characterisation. Furthermore, the spikiness is larger in adsorption through non-adhesive brine (59.1) compared to adhesive brine (4.8). The texture aspect ratio shows a strong uniformity of adsorption structure without lay or structure direction as inferred from *Str*, are both above 0.5. Furthermore, the texture of aspect ratio indicates the uniformity of adsorption structure is higher through non adhesive brine (0.95) compared with adhesive brine (0.84). The $\Delta\Gamma$ of 977 ng/cm^{2}through adhesive brine is around ten times the value of 91.7 ng/cm^2 formed through non adhesive brine (**Figure 7.37**.

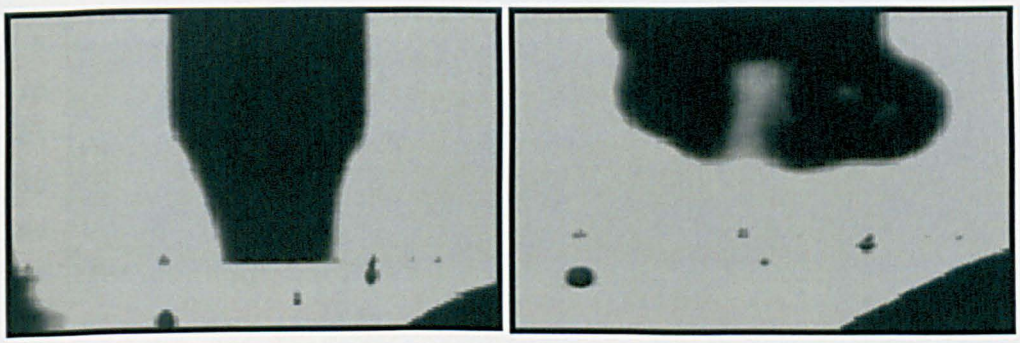

Figure 7.32 *Adhesion of oil droplets onto a mineral surface surrounding by aqueous brine (left) and non adhesion (right).*

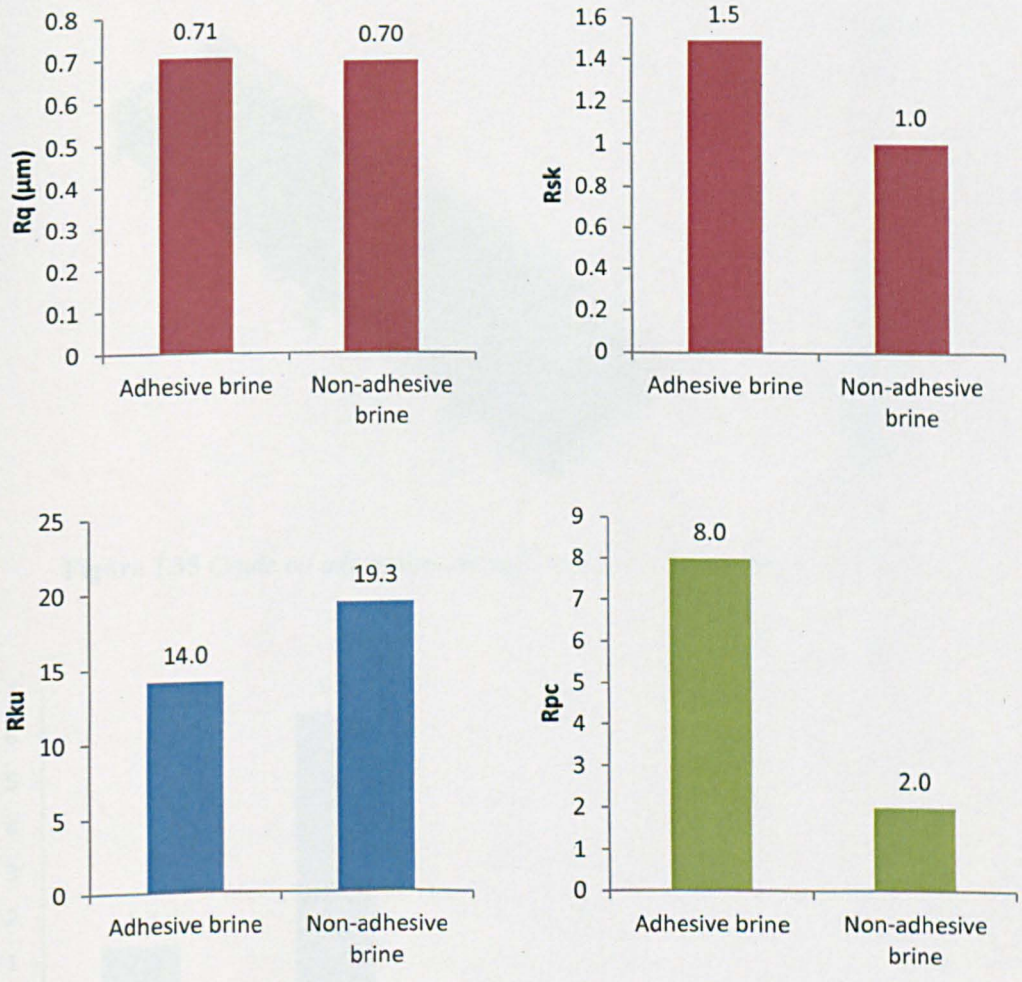

Figure 7.33 *Two dimensional profile analysis of crude oil treated silica surfaces as a function of brine adhesivity; root mean square, skewness, kurtosis and number of peaks of the crude oil adsorption.*

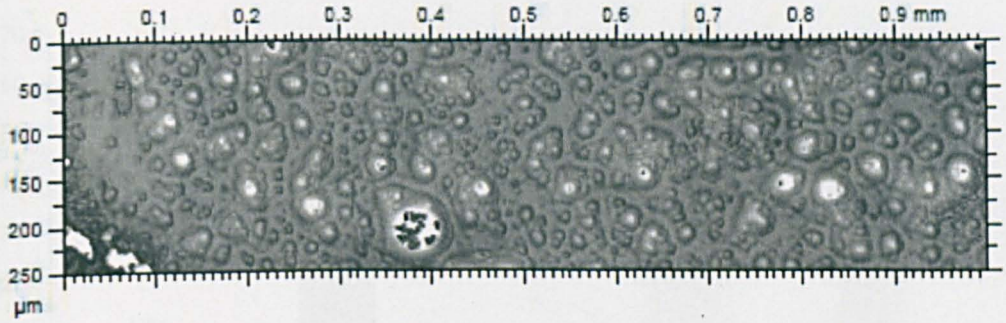

Figure 7.34 *Interferometry scanning of crude oil adsorption through adhesive brine.*

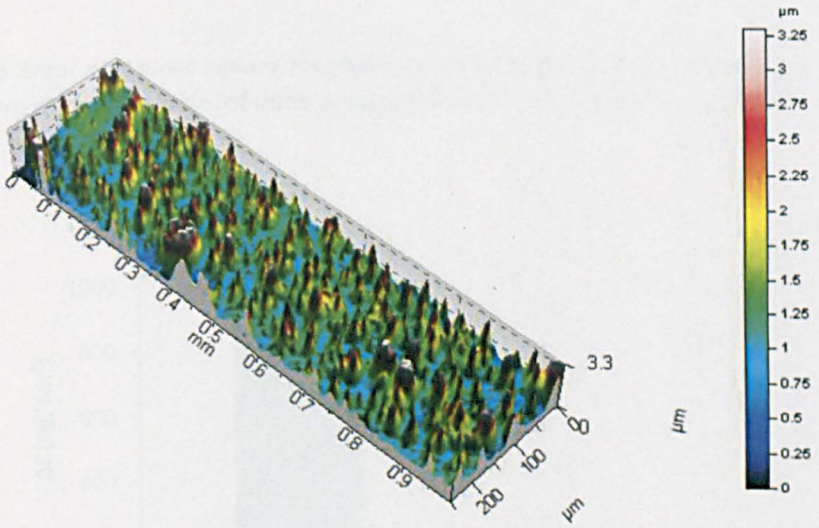

Figure 7.35 *Crude oil adsorption through adhesive brine into silicate surface.*

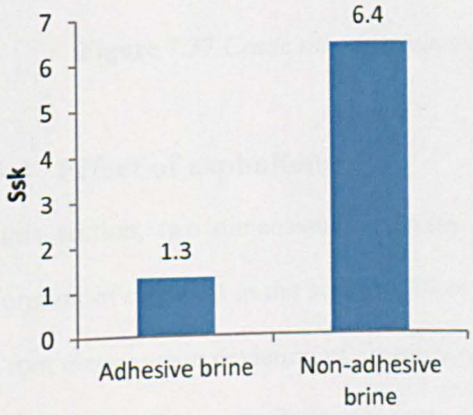

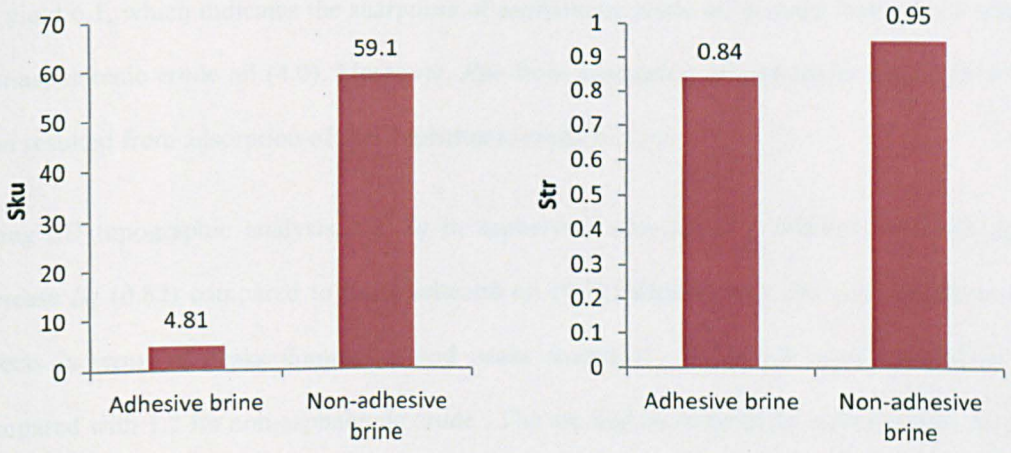

Figure 7.36 *Areal root mean square roughness, skewness, kurtosis and texture aspect ratio of topography height distribution of adsorption oil as function brine adhesivity.*

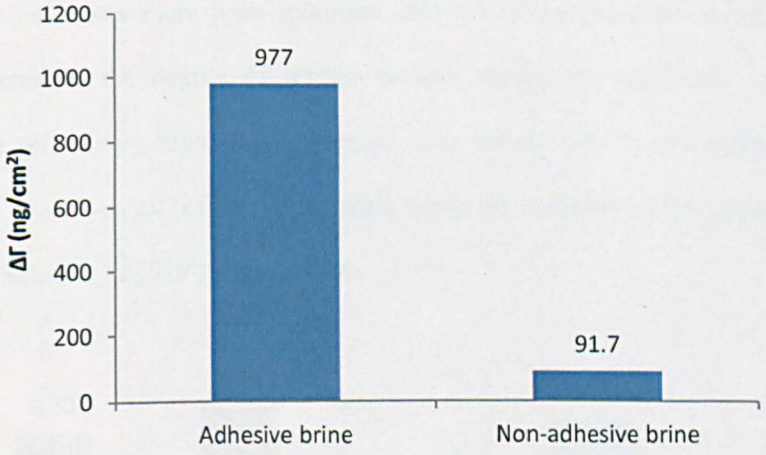

Figure 7.37 *Crude oil adsorption amount into silicate surface as brine adhesivity.*

7.5.4 Effect of asphaltene

In this section, two dimensional analyses are conducted to understand the role of asphaltene in adsorption of crude oil in the surface. When asphaltene macromolecules are removed from crude oil, the root mean square deviation of adsorption profile of asphaltenic crude oil is 0.70) very close to the value of 0.74 for non-asphaltenic crude oil **Figure 7.38**. Other amplitude parameters such as skewness and kurtosis reveal information into the aggregation type of adsorption and the degree of peak sharpness. *Rsk* of the asphaltenic crude oil adsorption has more dominate peaks (1.1) than the non asphaltenic crude oil adsorption (0.87). Similarly for peaks sharpness, *Rku* of asphaltenic crude

oil yield 6.1, which indicates the sharpness of asphaltenic crude oil is more than that of adsorption of non-asphaltenic crude oil (4.0). Moreover, *Rpc* from adsorption of asphaltenic crude oil is higher (2) than resulted from adsorption of non-asphaltenic crude oil (1).

Using 3D topographic analysis, the *Sq* in asphaltene adsorption is different. Asphaltene tends to increase *Sq* (0.82) compared to deasphaltened oil (0.72) **Figure 7.43**. *Ssk* and *Sku* show distinctive effects in terms of peaks dominance and peaks sharpness. *Ssk* is 6.4 when asphaltene is present compared with 1.2 for non-asphaltenic crude . The six fold increase in *Sq* indicates that the adsorption of asphaltenic crude oil is predominating by peaks more than non-asphaltenic crude, which shows wider degree of valleys **Figure 7.42**. However, such a large difference in *Ssk* is not evident from 2D surface profile which shows the uncertainty in trusting only the 2D surface profile. Similarly the asphaltenic crude oil shows more peak spikiness (*Sku*=59.1) compared to deasphaltene crude oil (*Sku*=4.1). Furthermore, the degree of texture pattern shows the uniformity of adsorption of asphaltenic crude oil is very high (0.95) whereas it is clearly less in non-asphaltenic crude oil adsorption (0.52). However, $\Delta\Gamma$ of non-asphaltenic crude oil is higher (3102 ng/cm^2) compared to crude with asphaltene (91.7 ng/cm^2) **Figure 7.44**.

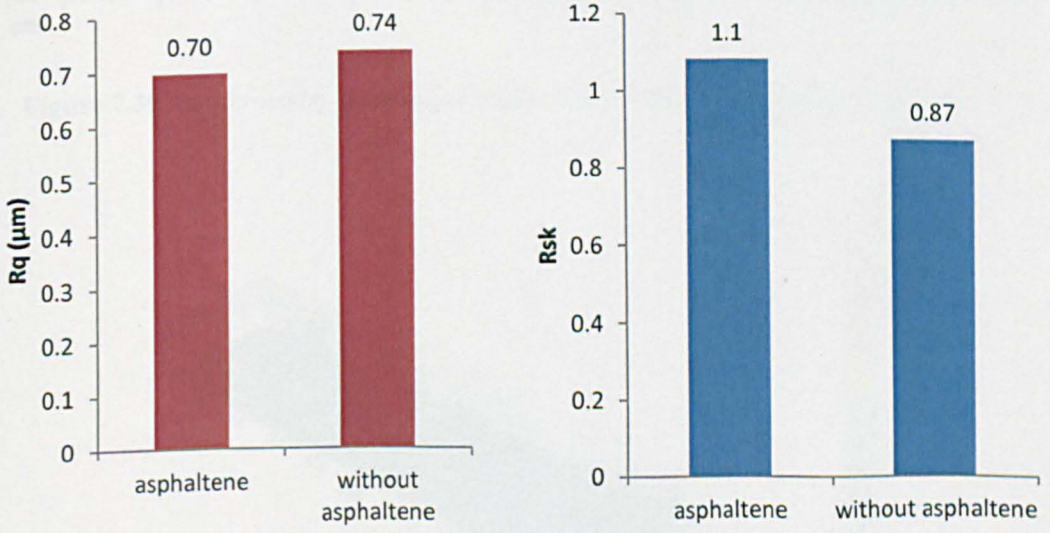

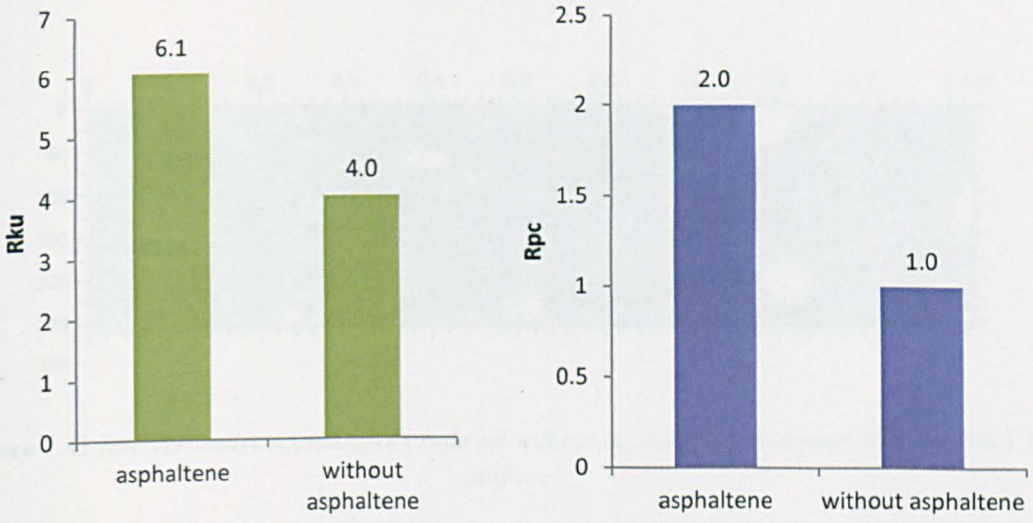

Figure 7.38 *2D profile analysis of crude oil treated silica surfaces as a function of asphaltene content; root mean square, skewness, kurtosis and number of peaks of the crude oil adsorption.*

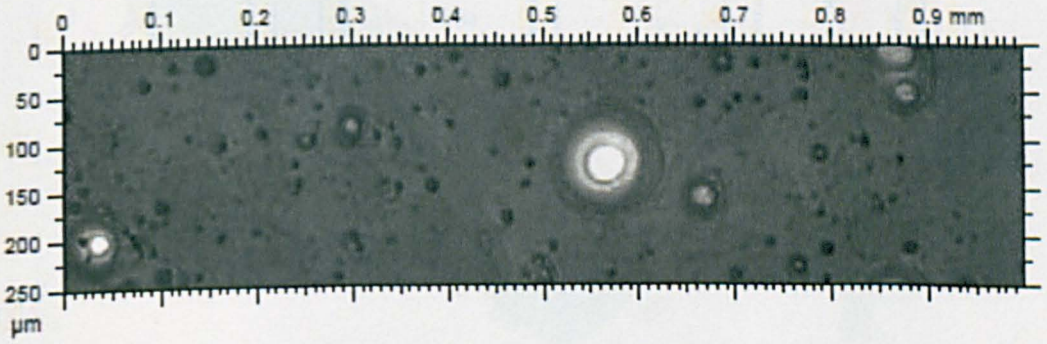

Figure 7.39 *Interferometry scanning of crude oil adsorption through 0.5 M NaCl brine.*

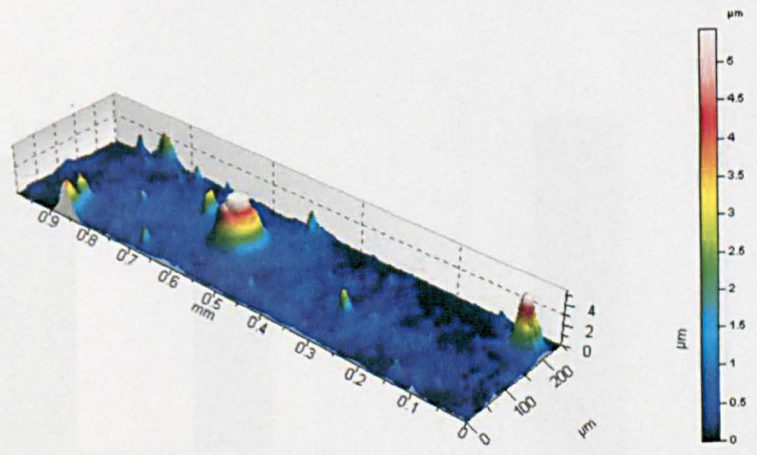

Figure 7.40 *3D view of crude oil adsorption into silicate surface through 0.5 M NaCl brine into surface.*

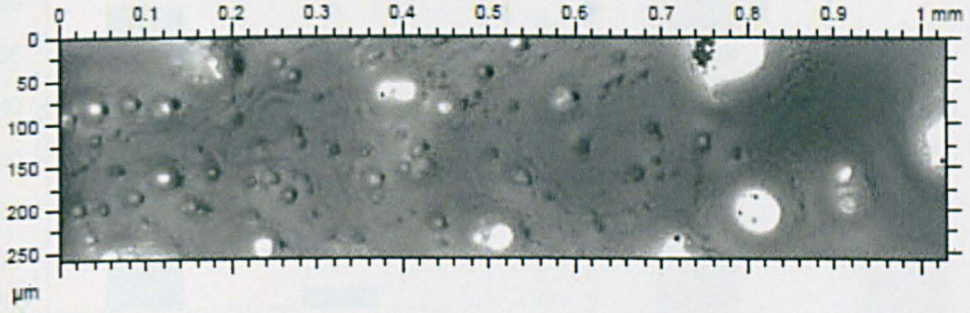

Figure 7.41 *Interferometry scanning of crude oil without asphaltene adsorption through brine into surface.*

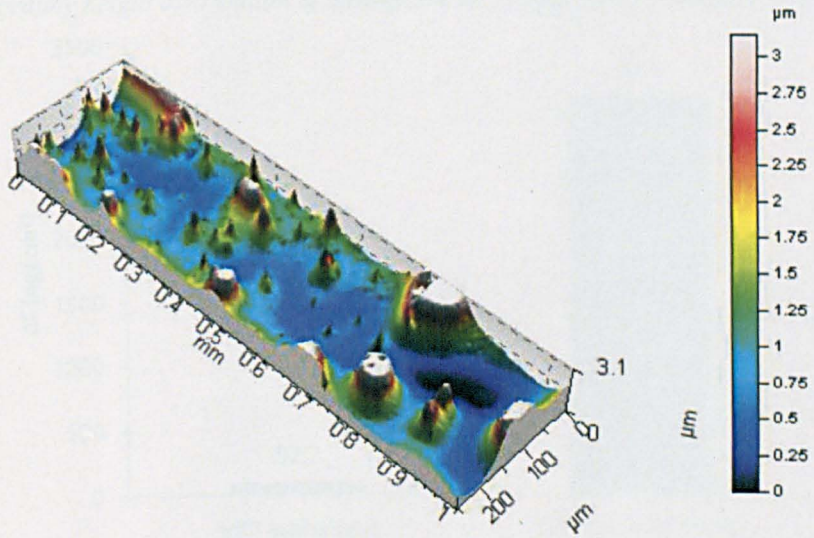

Figure 7.42 *3D view of crude oil adsorption without asphaltene into silicate surface.*

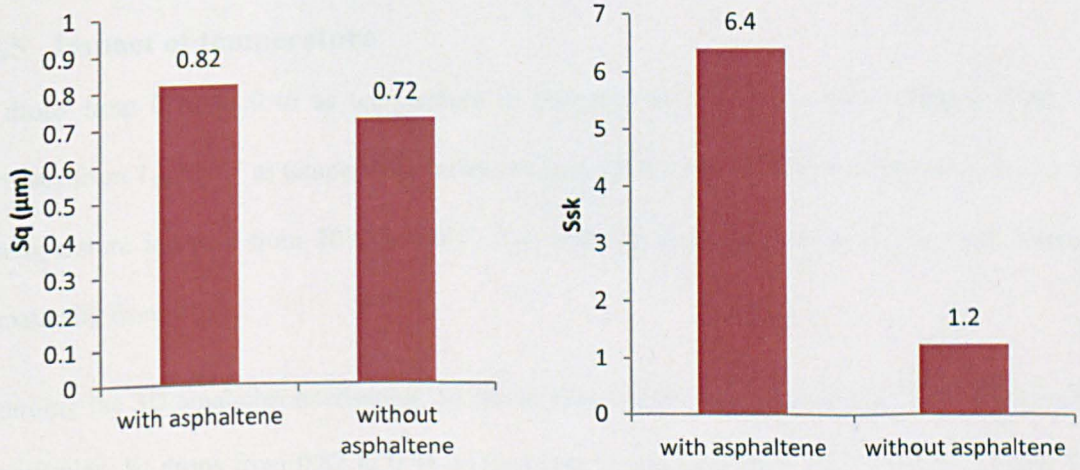

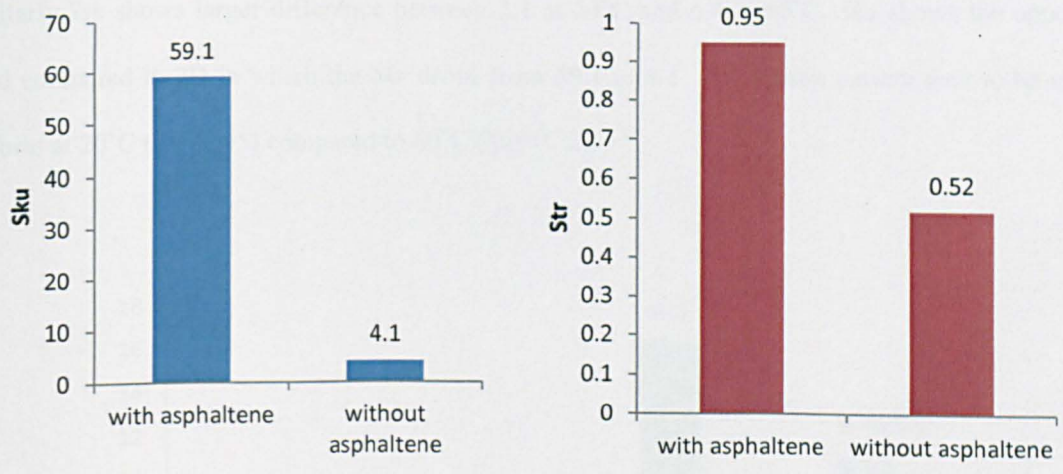

Figure 7.43 *Areal root mean square roughness, skewness, kurtosis and texture aspect ratio of topography height distribution of adsorption oil as function of asphaltene content.*

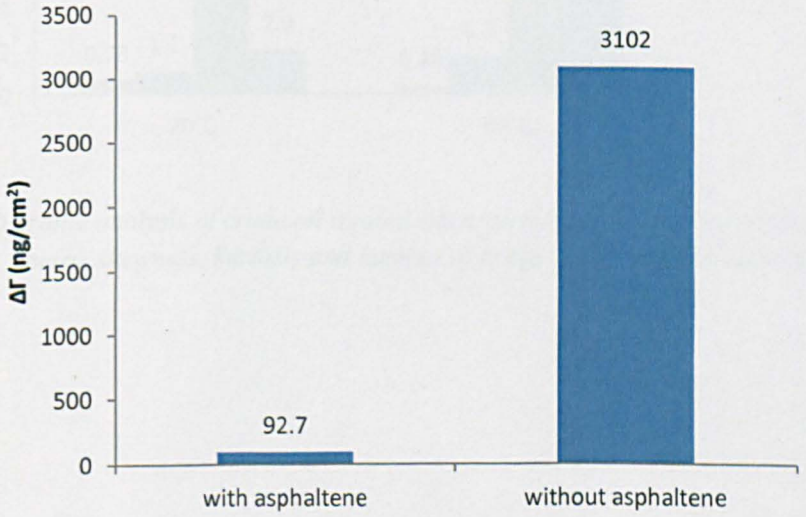

Figure 7.44 *Oil adsorption amount into silicate surface as function of asphaltene content.*

7.5.5 Impact of temperature

Rq drops from 0.70 to 0.40 as temperature is increased from 20°C to 60°C (**Figure 7.45**). *Rsk* increases from 1.1 to 1.7 as temperature increased from 20°C to 60°C. *Rku* increases from 6.1 to 16.5 as temperature increase from 20°C to 60°C. *Rpc* resulting from adsorption of crude oil increased dramatically from 2 to 6.

Regarding the 3D areal characterisation, *Sq* shows larger difference compared to 2D surface profile. In particular, *Sq* drops from 0.82 to 0.44 as temperature increased from 20°C to 60°C **Figure 7.48**.

Similarly,*Ssk* shows larger difference between 2.1 at 20°C and 6.4 at 60°C. *Sku* shows the opposite trend compared to 2D in which the *Skr* drops from 59.1 to 8.1. The texture pattern tend to be more uniform at 20°C (*Str*=0.95) compared to 60°C (*Str*=0.72).

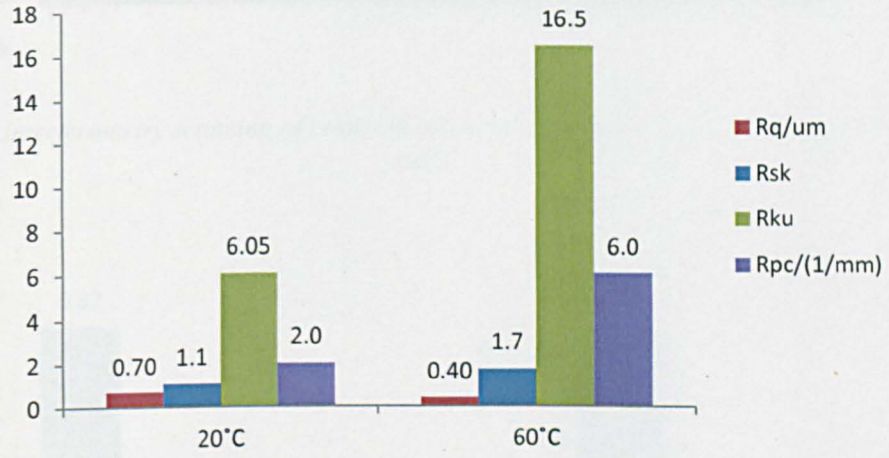

Figure 7.45 *2D profile analysis of crude oil treated silica surfaces as a function of temperature; root mean square, skewness, kurtosis and number of peaks of the crude oil adsorption.*

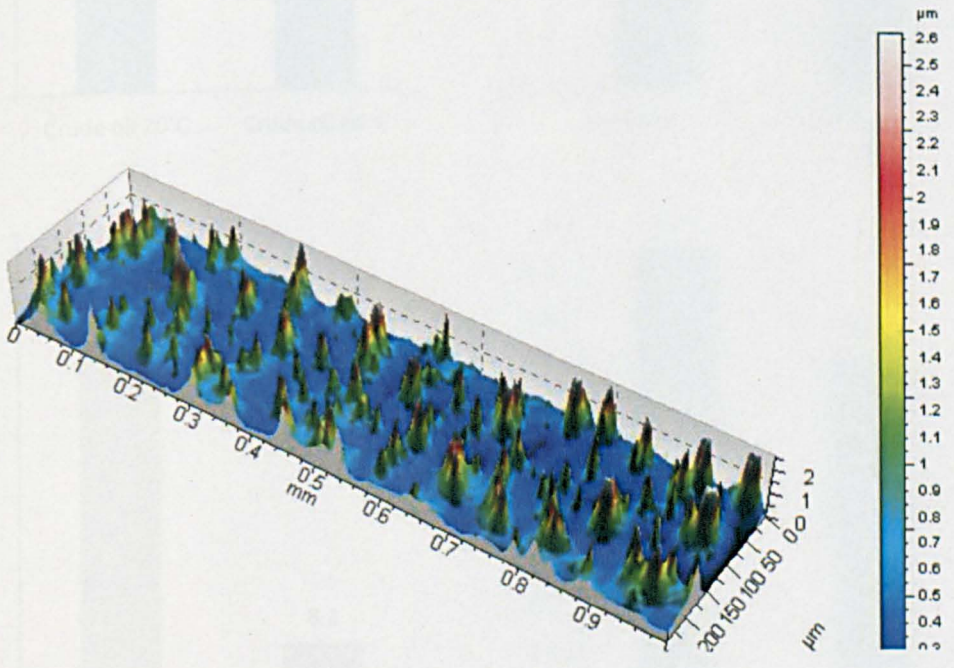

Figure 7.46 *3D view of crude oil adsorption into silicate surface at high temperature 60°C.*

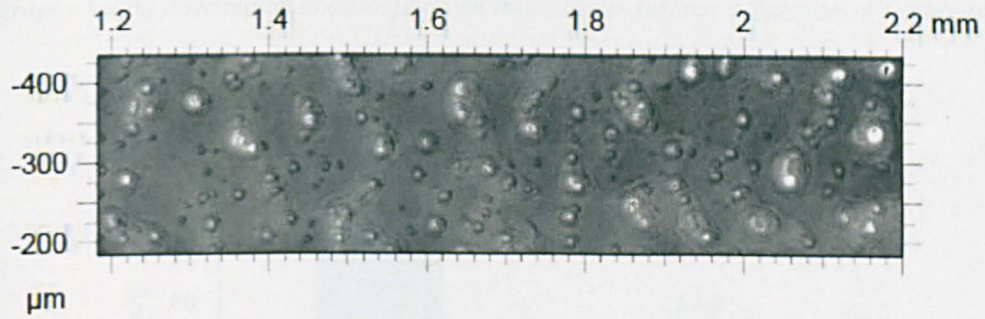

Figure 7.47 *Interferometry scanning of crude oil adsorption into silicate surface at high temperature 60°C.*

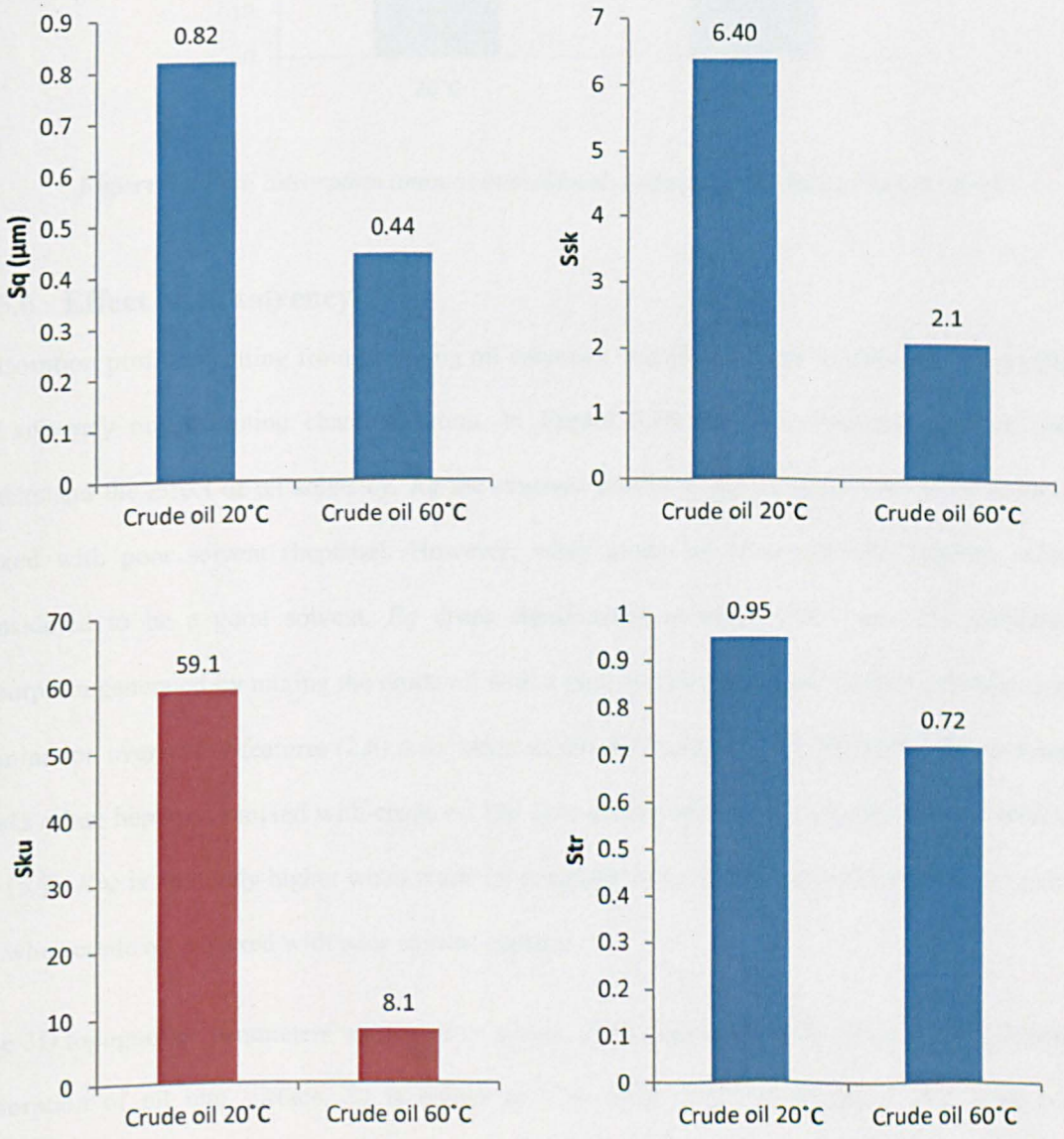

Figure 7.48 *Areal root mean square roughness, skewness, kurtosis and texture aspect ratio of topography height distribution of adsorption oil into silicate surface as function of temperature.*

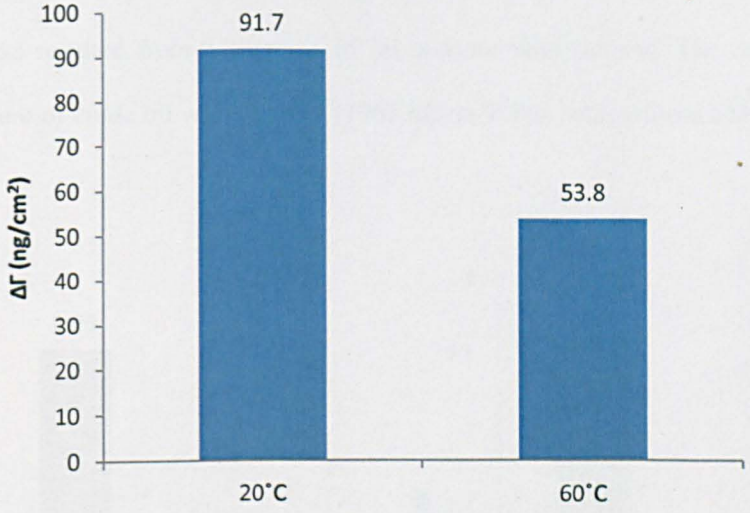

Figure 7.49 *Oil adsorption amount into silicate surface as function of temperature.*

7.5.6 Effect of oil solvency

Adsorption profile resulting from changing oil solvency was investigated to understand the effect of oil solvency on adsorption characterisation. In **Figure 7.50** *Rq*, *Rsk*, *Rku* and *Rpc* are used to understand the effect of oil solvency. *Rq* the assessed profile is higher (0.25 μm) when crude oil is mixed with poor solvent (heptane). However, when crude oil is mixed with toluene, which is considered to be a good solvent, *Rq* drops significantly to reach 0.013 μm. *Rsk* indicates the adsorption generated by mixing the crude oil with a poor solvent (heptane) resulted into higher peaks domination over valley features (2.6) than when mixed with toluene (1.0). Similarly, the sharpness of peaks when heptane is mixed with crude oil (20.2) is greater than when toluene is mixed with crude oil (5.9). *Rpc* is relatively higher when crude oil is mixed with good solvent toluene (16) compared to 11 when crude oil is mixed with poor solvent heptane.

The 3D topographic parameters were used to aid the characterisation of the effect of oil solvency on adsorption of oil into surface. *Sq* is higher at 0.34 when crude oil is mixed with poor solvent (heptane)and drops to 0.069 when crude oil is mixed with toluene. *Ssk* is 5.9 from the mixture of

crude oil with good solvent which is higher than when mixed with heptane (3.4). Nevertheless, both adsorption modes show peak dominance due to positive *Ssk*. Similarly, *Sku* yields 51 when crude oil is mixed with toluene compared to 25 when mixed with heptane. This indicate the sharpness degree is higher in the peaks resulted from adsorption of oil mixture with toluene. The $\Delta\Gamma$ is significantly higher when mixture of crude oil with heptane (1063 ng/cm^2) than with toluene (202 ng/cm^2) **Figure 7.58**.

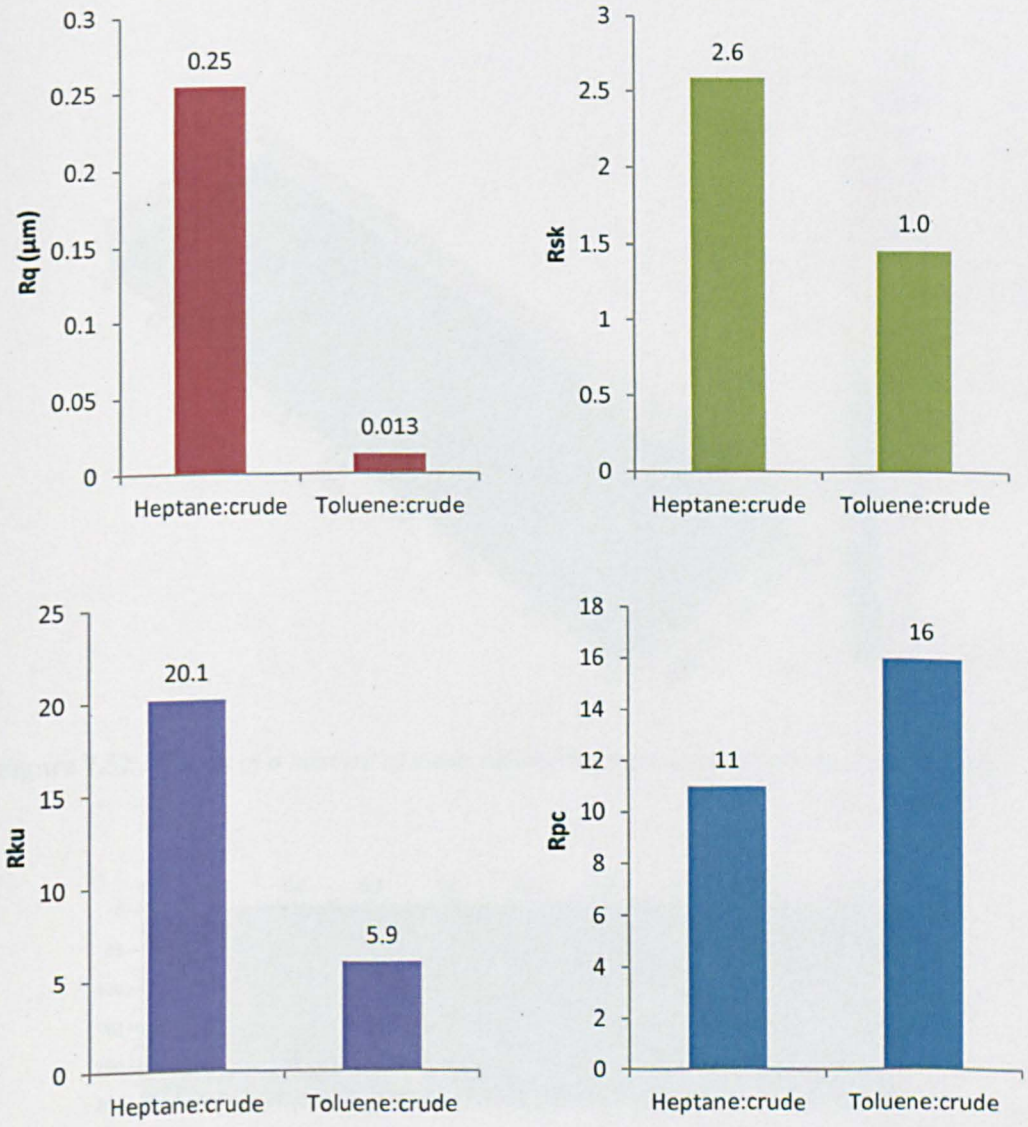

Figure 7.50 *2D profile analysis of crude oil treated silica surfaces as a function of oil solvency; root mean square, skewness, kurtosis and number of peaks of the crude oil adsorption.*

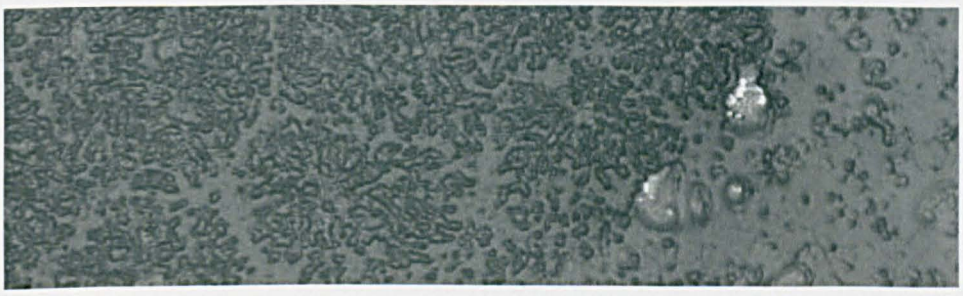

Figure 7.51 *Interferometry scanning of a mixture of crude oil and heptane adsorption through brine into silicate surface.*

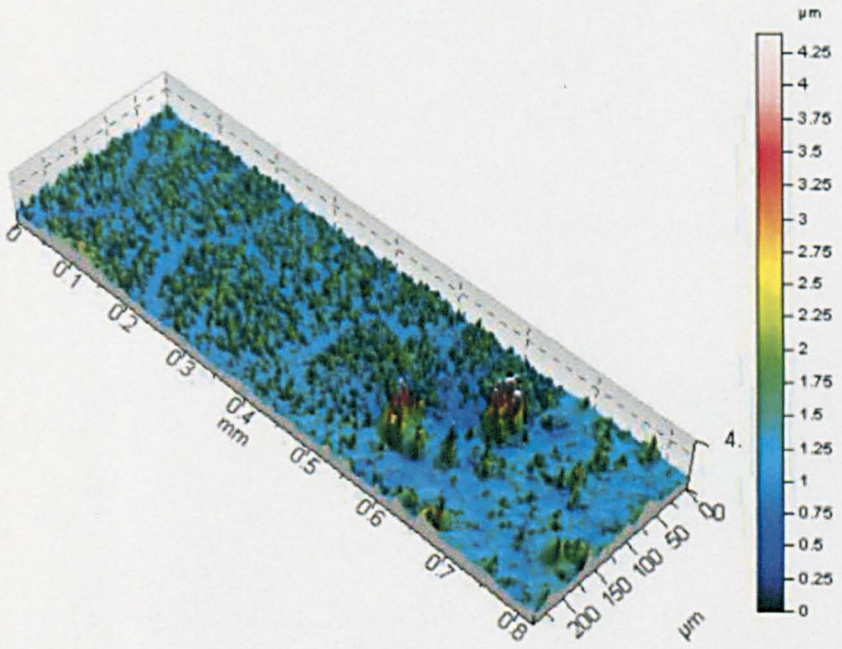

Figure 7.52 *3D view of a mixture of crude oil and heptane adsorption into silicate surface.*

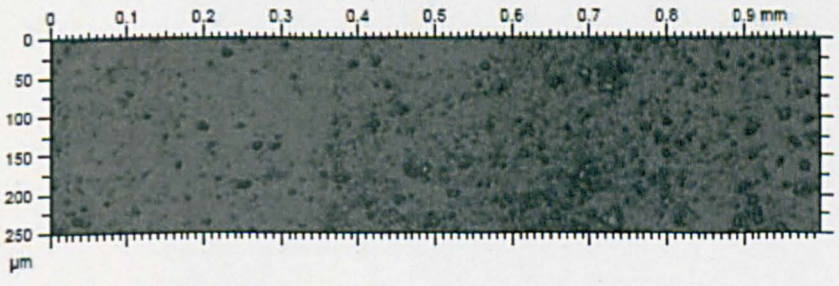

Figure 7.53 *Interferometry scanning of a mixture of crude oil and toluene adsorption through brine into silicate surface.*

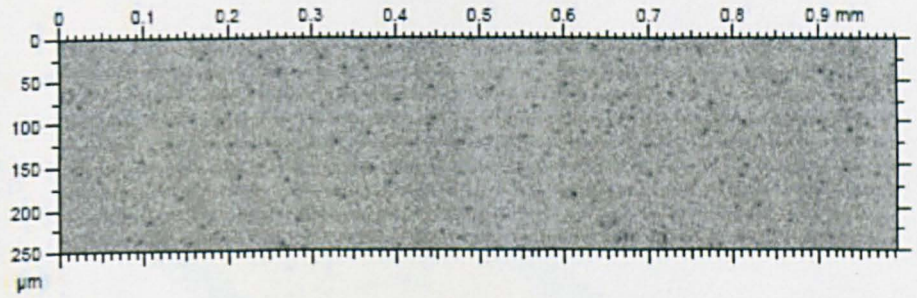

Figure 7.54 *Interferometry scanning of a bare clean glass surface.*

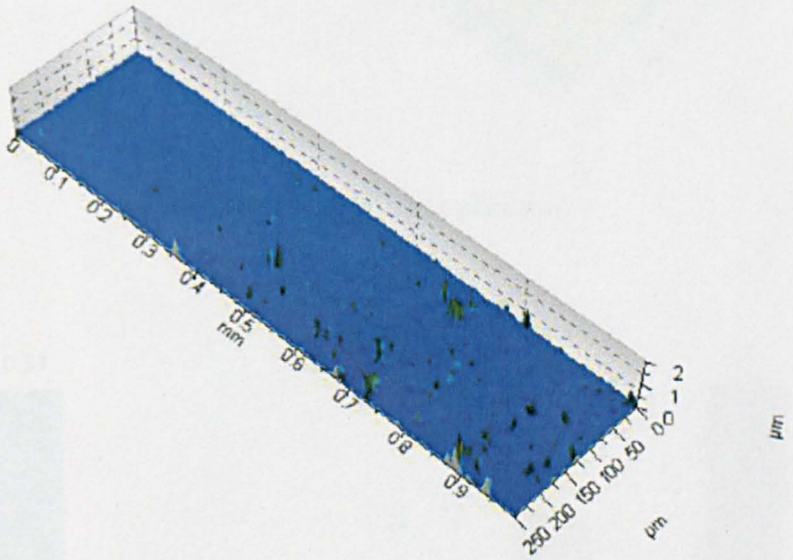

Figure 7.55 *3D view of a mixture of crude oil and toluene adsorption into silicate surface.*

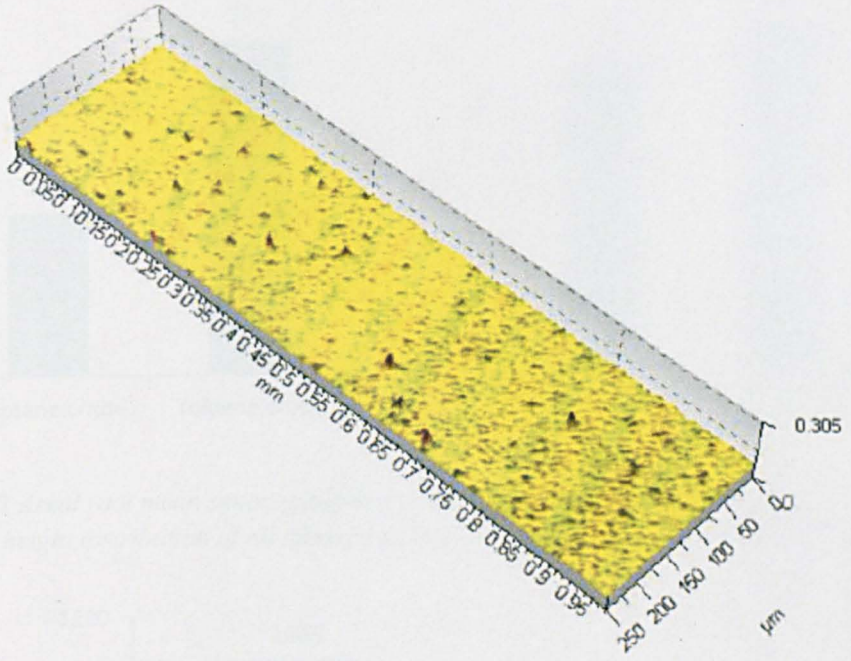

Figure 7.56 *3D view of clean glass surface.*

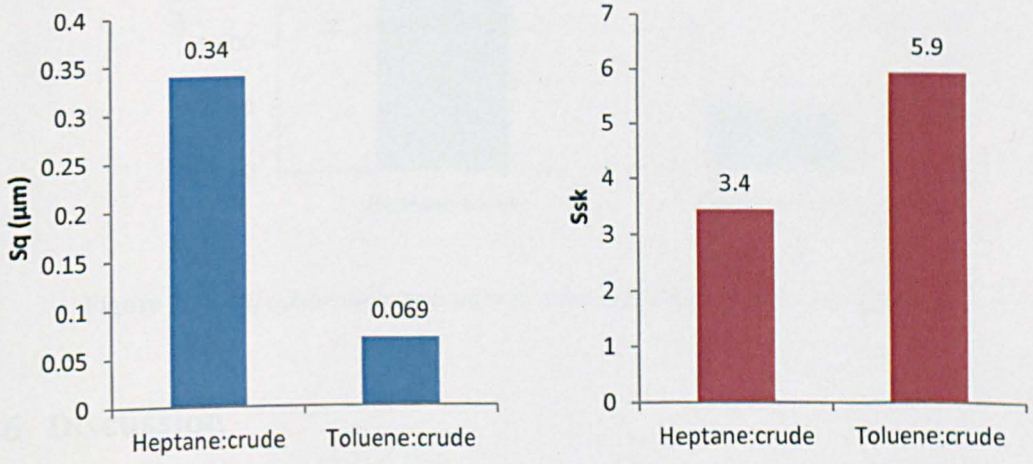

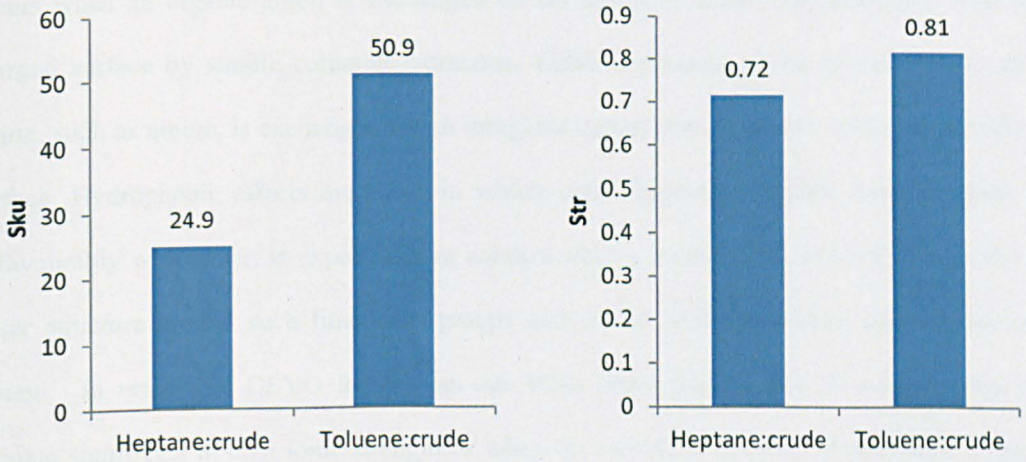

Figure 7.57 *Areal root mean square roughness, skewness, kurtosis and texture aspect ratio of topography height distribution of oil adsorption into silicate surface as function of oil solvency.*

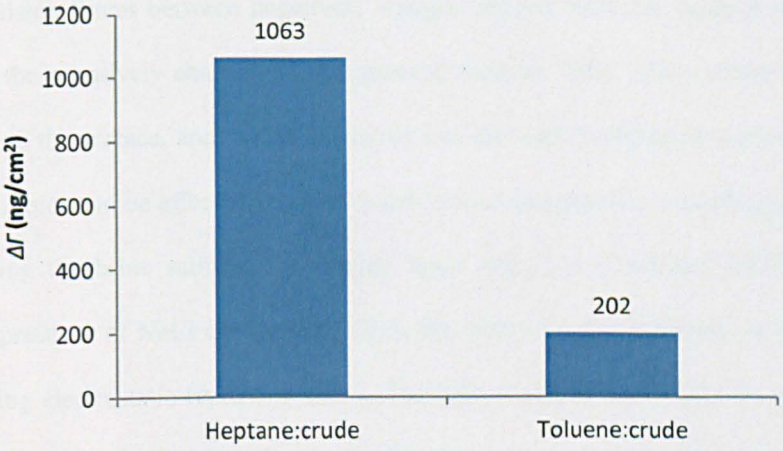

Figure 7.58 *Oil adsorption amount into silicate surface as function of oil solvency.*

7.6 Discussion

7.6.1 Thickness of adsorption layer

It is clear that adsorption of oil through brine is affected by salinity. Arnarson and Keil (2000) summarise six mechanisms for adsorption of organic material into mineral surfaces: (i)ligand exchange, (ii) cation bridges, (iii) anion exchange, (iv) cation exchange, (v) hydrophobic effect and (vi) DLVO forces. Ligand exchange means the exchange of acidic hydroxyl groups of organic matter for hydroxyl groups on surface. Cation bridges are formed when a cation creates a bridge between negative charges of the mineral surface and polar groups of the organic material. Anion exchange

occurs when an organic anion is exchanged for an inorganic anion and associates with positively charged surface by simple columbic attraction. Cation exchange is the process which an organic cation, such as amine, is exchanged for an inorganic cation and associates with a negatively charged surface. Hydrophobic effects are those in which polar functional organic matter, which interacts unfavourably with water, is expelled from solution onto a surface. The process relaxes the imposed water structure around such functional groups and results in a favourable gain in entropy of the system. In respect of DLVO forces, van der Waal interactions which is a short range and only become significant at high ionic strength or when the system is allowed to dehydrate. According to Arnarson and Keil (2000), van der Waals interactions are potentially important in high salinity brine because at high ionic strength the double-layer thickness decreases, leading to a reduction in electrostatic repulsion forces between negatively charged organic material. such as carboxyl groups, in crude oil and the negatively charged silicate mineral surfaces. This allows closer approach of the organic material to the surface, and hence, increased van der wall bonding. Based on DLVO theory, the stability of colloids can be affected by three major forces: electrostatic, van der walls and structure forces. By varying the brine salinity, the double layer, which is controlled by Dubey length, is screened by the presence of NaCl electrolytes. Thus, the Dubey length decreases as the brine salinity increases, reducing electrostatic repulsive forces. The reduction of electrostatic force and increasing of short range forces such as van der Waals promotes deposition of crude oil. This is consistent with the dramatic increase in adsorption thickness layer thickness (129 μm) at high brine salinity (3 M NaCl).

It is believed that the extience of brine film can slow the adsorption of oil to mineral surfaces compared to direct contact of crude oil to mineral surfaces (Collins and Melrose, 1983). In terms of mechanisms, silicate surfaces (SiO_2) become hydroxylated when exposed to aqueous brine solutions, and the surface hydroxyl groups, represented here in glass surface by (SOH) can be exchange for acid functional groups such as –COOH, by reactions such as like:

$$-SOH + HOOCR \rightleftharpoons SOOCR + H_2O$$

However when pH=6, ligand exchange lowers the adsorption thickness (4.5 μm) compared to direct adsorption from crude oil in which the adsorption thickness is (4.8 μm) and is only govern by van der Waals' interaction (Buckley et al., 1998).

On the other hand, when exposed to an adhesive brine with low pH, the oil/brine interface becomes cationic because the basic groups in crude oil become protonated. The cationic oil-brine interface is attracted to the anionic brine/solid interface causing the brine to become unstable and rupture. Rupture exposes the silica to crude oil allowing three times the adsorption thickness to developcompared to brine with neutral pH. However it is not clearly known how the exact scenario of brine rupture occurs. In particular, it is uncertain whether the film is ruptured prior to protnated basic groups from the crude oil anchoring to the surface or whether a Dalmation wettability developes as crude oil adsorption progresses with a residual water trapped as a pocket.

Asphaltenes and resins are known to be large, polar, poly-nuclear molecules consisting of condensed aromatic ring systems and heteroatoms like sulfur, nitrogen, and oxygen (Mullins et al., 2007). Asphaltene and resin content is clearly playing a major rule in the development of a skeleton of crude oil adsorption on the mineral surface. This is evident from increasing thickness of oil adsorption from 4.5 μm when asphaltene is present in crude oil to reach 22.2 μm when asphaltene is absent but resins exist. The five fold increase in thickness when asphaltene is removed indicates that asphaltene suppresses the thickness of adsorption. This suppression of adsorption can be explained by the high rigidity asphaltene structures, which results in a close packings of round disks or rod-shaped components **Figure 7.51**. Conversely, when asphaltene is absent, the adsorped layer thickness increases due to the high degree of compressibility of resin. This results in a multilayer thickness compared to close packed structure in the asphaltene. These experimental results agree quantitatively with measurements of surface pressure using Langmuir Blodgett conducted by Ese et al. (1999). In particular, they observed that the de-asphaltene crude oil did not show a sharp increase in surface pressure as the deasphaltene oil/air interface was compressed by trough of Langmuir Blodgett. This indicates the high degree of compressibility in the deasphaltene crude oil. Conversely, if asphaltene is

present at the interface, a sharp increase in the surface pressure is observed, which indicates the high rigidity.

The increasing of adsorption layer as function of temperature can be attributed to a reduction in the water film that separates the oil/solid interfaces. Derjaguin (1987) noticed a reduction of water thin film thickness on a fused silica surface as temperature was increased. In particular, as temperature increased from 20°C to 60°C, the thickness of water film decreased from 5 nm to 2 nm (**Figure 7.15**). The higher thickness of adsorption layer observed for crude oil at high temperature (97 μm) is believed to be a result of more polar components anchoring their functional groups into the mineral surface. Similarly when resin is liberated from asphaltene, the thickness of crude oil adsorption increased from 22.2 μm to 120 μm as temperature is increased from 20°C to 60°C. Increasing the thickness of asphaltene and deasphaltene crude oil, as temperature increased, indicates that asphaltene itself does not contribute much in terms of surface activity with temperature. In fact, it is the thinning of brine film as function of temperature that contributes to the adsorped layer thickness.

The impact of crude oil solvency is investigated in terms of adsorption layer thickness. Two different solvents have been used to characterise the impact of oil solubility on the build up of adsorption layer thickness. The solvents may be characterised according to three intermolecular forces between solvent molecules: dispersion, polar and hydrogen bonding. Heptane is an aliphatic hydrocarbon; a class with low dispersion forces, no polar forces and no ability for hydrogen bonding. Toluene falls into the category of aromatic hydrocarbons. This class of solvents have high dispersion but low polar forces and considered to be weak acceptor for hydrogen bonding. As crude oil is mixed with heptane, the crude oil adsorption thickness becomes 125 μm **Figure 7.16**. However, when crude oil is mixed with toluene, the adsorption thickness drops sharply to be 7.4 μm. The huge difference in adsorption layer thickness can be explained according to a modified Yan model presented by Mullins (2010) in which the asphaltenes are concentrated in the centre of an aggregate and are surrounded by resins. There is a smooth transition between a moderate sized polycyclic aromatic hydrocarbon (PAH) ring system in the centre of the aggregate and the continuous medium, which is more alkane substituent. If heptane solvent is added to the solution, the resins are removed from the aggregate and an accelerated

asphaltene aggregation takes places. The aggregation reach to a stage that form flocs which become heavy to be sustain disperse in the heptane solution, a sedimentation of the flocs start on the mineral surface. The thick adsorption layer when crude oil is mixed with heptane (125 μm) compared to crude oil used without additives (4.5 μm) indicates that a multilayer of aggregated asphaltene is present on the mineral surface during the sedimentation step. However, asphaltene aggregation does not occur when toluene is mixed with crude oil because toluene has a high dispersion force that prevents any large self assembly of asphaltenes; this results in a relatively thin adsorption layer thickness (7.4 μm). The decrease in the adsorption layer thickness when mixed with toluene solution can be attributed to the high dielectric constant of the toluene, which is 2.44 at 20°C compared to 1.89 at 20°C when crude oil is mixed with heptane (Whim and Johnson, 1996). Moschopedis et al. (1976) observed a reduction of 50% of molecular weight of Alberta asphaltenes when the dielectric constant of the solution is increased. Moreover, the tendency of toluene to act as weak acceptors for hydrogen bonds facilitates the dissolution of asphaltenes.

7.6.2 2D and 3D dimensional surface characterisation

7.6.2.1 *Effect of brine salinity*

The increasing of *Rq* as the brine is diluted reveals the way that oil adsorbs though the brine film and explains the pattern of wettability that initiated is by crude oil adsorption. Dalmation wettability can explain the COBR interaction . This was first proposed and observed by (Kaminsky et al., 1996) but since then there has been a lack of experimental quantification that supports the Dalmation scenario. Freer et al. (2003) confirmed the observation of Dalmation wettability by using AFM over a very limited area (5 μm x 5 μm). Roughness parameters used in this chapter, *Rq* and *Sq*, both describe the variation of elevation that is caused by crude oil adsorption in 2D and 3D. Since the crude oil type is the same used to generate the adsorption and the only variable was brine salinity, the change of elevation of height can only be attributed to water pockets that became trapped during oil adsorption. The existence of water pocket seems to be minimised when crude oil adsorption occurs through 3 M NaCl brine and it become extreme when oil adsorption occurred through 0 M NaCl brine. The water pockets are reduced because of the increased crude oil adsorption through high brine salinity (3 M

NaCl) as the electrostatic double layer reduces to a minimum. As brine salinity decreases to 0.5 M NaCl, the water pockets establish a resistance to be penetrated at some of its sites, which generates a pattern of wettability that is totally different than wettability generated through 3 M NaCl brine. The pattern of wettability is also evident in 3D view in **Figure 7.18-7.20** especially at coordinate locations of (0.22 μm, 150 μm), (0.57 μm, 100 μm) and (0.8 μm, 125 μm). Further decrease in brine salinity to 0 M increases the resistance of water pockets, which reduces crude oil adsorption to its minimum. The existence of water pockets is also supported through the number of peaks. Two peak regimes were identified for the adsorption profiles. The first, with 3 M NaCl brine in which 4 peaks formed. Second, with 0.5 M and 0 M NaCl brine when 2 peaks formed. The presence of peaks in the adsorption profile is a manifestation of the size of water pockets trapped between the adsorped oil and mineral surface. Small water pockets are formed in the presence of 3 M brine resulting in an increased number of peaks and a more discrete undulose adsorption profile **Figure 7.21**. The opposite is true when exposed to lower salinity brines. The texture pattern indicated from *Str* shows the adsorped oil does not show a specific directionality to itsstructure (i.e. $Str>0.5$) suggesting perhaps that the water pockets trapped beneath the adsorped oil do not accumulate at specific locations. In fact, it appears that the brine spreads beneath the adsorped oil with a specific spacing, which makes the texture more uniform. The uniformity of water pockets increases with brine salinity. This way of quantifying the texture pattern is applied for the first time and may also explain the texture pattern obtained from AFM scans (e.g. Yang and Hirasaki, 1999; Buckley and Lord, 2003; Freer et al., 2003).

Measuring $\Delta\Gamma$ enhances our understating of how repulsion forces minimizes adsorption of oil aggregates when exposed to low brine salinity. The results of the current study can be compared with $\Delta\Gamma$ measurements conducted using the highly sensitive quartz crystal microbalance (QCM-D) (e.g. Farooq et al., 2011). In particular, the latter study, monitored the $\Delta\Gamma$ over 60 min. Their results indicate oil aggregates are not released from the crude in the presence of high brine salinity (4000 ppm of 3% NaCl brine). However, when diluting the high salinity brine from 4000 ppm of 3% NaCl brine to 1500 ppm of 3% NaCl brine, 2 mg/m^2 is released from the crude oil aggregation.The results

presented above and published by Farooq et al., (2011) are consistent with the existence of repulsion forces that minimise the adhesion of oil aggregates to silica surfaces.

7.6.2.2 *Effect of brine contact*

The adsorption of crude oil compenents directly into dry mineral surfaces is clearly suppressing the roughness profile compared to adsorption of oil through brine. This is attributed to the presence of water pockets that become trapped when adsorption occurs through brine. Trapped water pockets elevate the surface roughness compared to when adsorption occurs directly onto the mineral surface. This understanding is also enhanced by the sharp reduction in the mass of adsorption when brine resides on the mineral surface; water trapping reduces penetration of crude oil components and their subsequent anchoring on the surface.

7.6.2.3 *Effect of adhesion*

The short time interaction of adhesion between crude oil and mineral surfaces does not affect the overall surface roughness, which might indicate the adsorption behaviour is the same. However, the story is different when the characterisation of surface profile is investigated by parameters, such as *Rpc*, that characterise the spacing. It indicates the adsorped layer through adhesive brine has four times more peaks than that formed through stable non-adhesive brine. This may indicate that the water pockets trapped during oil adsorption are more scattered than those formed through stable brine. Activity at the brine/oil interface would be much higher than at a neutral oil/brine interface due to the nature of cationicity adhesive brine. This is reflected in a higher $\Delta\Gamma$ that is 10 fold higher than from the non-adhesive brine. An interface with a higher cationicity would generate more adsorption at close spacing, which is reflected in the high value of *Rpc*..

7.6.2.4 *Effect of asphaltene*

Absence of asphaltene does not seem to contribute significantly to the surface roughness. A possible reason is that the asphaltene packing structure tends to cluster the adsorption elevation on the mineral surface. Clustering of adsorped asphaltene adsorption is magnified through small increases in the number of peaks compared to the single peak generated when asphaltene is absent.

The most striking observation is the 30 fold increase in $\Delta\Gamma$ for a deasphaltened crude compared to asphaltenic crude oil. The type of aggregation of deasphaltene a crude oil tends to be a more multilayer aggregation compared to asphaltenic crude oil. Although the 3D surface profile of deasphaltene crude oil in **Figure 7.42** shows lots of areas not covered by aggregate adsorbate, $\Delta\Gamma$ is higher. This means the volume of peaks in asphaltenic crude oil excced those of deasphaltened crude, which can be explained by the higher degree of multilayer formation of adsorption than when asphaltenic crude oil is present. The question remains as to what causes multilayer aggregation where asphaltene macromolecules are absent. The disruption of aliphatic structures in the asphaltenic crude oil is well known to prevent initiation of the staking of polar components. This is due to steric alkane repulsion effect which reduces the aggregation degree of the components (Buenrostro-Gonzalez et al., 2001). Conversely, the ability in deasphaltene crude oil to cause a disruption by aliphatic structure is reduced due to weaker repulsion steric forces. This encourages the polar components, such as aromatic rings, to stake through π-bond between polar components. This generates a multilayer aggregation on the surface. The result agrees with Labrador et al. (2007) who showed that the asphaltenic crude oil results in double the adsorption compared to free resin crude oil. The experimental approach was different in Labrador et al., (2007) who isolated the resin from the adsorption process whereas in our work asphaltene is isolated from the adsorption. Nevertheless it highlights the role of resin in generating higher $\Delta\Gamma$.

Another key question relates to how the asphaltenic crude oil increases oil-wetness despite generating a lower mass of absorbed mass than the deasphaltened crude oil. It is possible that the chemical structure of the adsorped components from the asphaltenic crude oil causes the surface to become more hydrophobic to water. In other words, the amount of material deposited by a crude oil may not be a good indicator of the extent of wetting alteration if crude oil composition is manipulated. This observation can explain why there is a lack of correlation between I_{AH} indicators of organic deposition obtained by SEM (e.g. Wolcott et al., 1993). It also explains discrpency between contact angle measurements and organic aggregation coverage obtained by AFM described by Buckley and Lord (2003).

7.6.2.5 *Effect of temperature*

Thinning of the brine film with increasing temperature (e.g. Derjaguin, 1987) can cause the water pockets, trapped between the mineral surface and the bulk crude oil, to be minimized. If the size of water pockets is reduced, the elevation of the adsorbed layer is likely to reduce as temperature is increased. Indeed, *Rq* was threefold lower at 60°C compared to 20°C. Furthermore, the spacing between peaks on the adsorbed oil profile is reduced by 3 orders as temperature increases to 60°C, which is reflected by the high number of peaks count at 60°C. 3D analysis shows that the peak adsorption elevation become less spiky at 60°C compared to 20°C. So if bulk oil is trapped during displacement at 60°C, it would be trapped between the cavities located between peaks more than cavities at the tips of each peak.

There is a little difference in $\Delta\Gamma$ as a function of temperature (i.e. 91.7 ng/cm^2 at 20°C compared to 53.8 ng/cm^2 at 60°C). Although the thin water film is diminished as temperature increases, which means water pockets between crude oil adsorption and mineral surface decrease in size, $\Delta\Gamma$ does not change much. In fact, $\Delta\Gamma$ tends to decrease at 60°C. The 3D view in **Figure 7.46** reveals that the integrity of the adsorbed layer at 60°C tends to be less than that at 20°C. This is indicated from the wider valleys that appeared with high peaks, which dominate the speckled oil adsorption especially at coordinate location (400 μm, 250 μm), (500 μm, 150 μm) and (50 μm, 100 μm). Conversely, at 20°C, the 3D view **(Figure 7.40)** shows no evidence of wide valleys features, which explains the higher $\Delta\Gamma$.

7.6.2.6 *Effect of oil solvency*

Mixing heptane with crude oil increases the solubility of alkyl chains., Asphaltene starts to agglomerate and subsequently adsorb to the surface when alkyl chains are not present. The adsorption in 3D view **Figure 7.51** tends to be amorphous with dendritic branches. This is totally different when toluene is mixed with crude oil, which shows almost the bare mineral surface with only a few patches with oil aggregation (e.g location coordinates (0.5, 150) μm, (0.7, 250) μm, (0.7, 50) μm and (0.9, 250) μm in **(Figure 7.55-7.56)**. The reduced number of patches of aggregates is that toluene cannot remove the alkyl chains from the crude oil due to its aromatic degree. This reflected in very poor

staking of asphaltene in crude oil, which limits the subsequent adsorption of crude oil components. The varible staking of asphaltene and subsequent adsorption type can explain the very high roughness 0.25 μm of created from the heptane: crude oil mixture compared the 0.013 μm from thecrude oil: toluene mixture. The variable staking of asphaltene also explains why $\Delta\Gamma$ of crude oil: heptane is five times the adsorption of crude oil:toluene. This finding agrees with previous work of Alboudwarej et al. (2005) who found increasing heptane to toluene ratios doubled adsorption compared to toluene only.

7.7 Conclusion

Several novel results have been presented in this chapter and are summarized below:

- White light interferometry (VSI) provides a promising non-contact tool that can be used to determine parameters such as the thickness and roughness of the adsorbed layer as well as the adsorption mass per planar area. VSI is superior to other surface analysis techniques, such as AFM and SFA in determining the surface texture of minerals resulting from COBR interaction.
- Surface roughness shows a direct relationship with brine salinity in which *Rq* and *Sq* increase as brine is diluted. The Dalmation wettability model for mixed wet systems has been confirmed quantitatively through 2D and 3D surface analysis.
- For the first time, 3D parameters, established by the International Organization for Standardization (ISO), have been used to describe the adsorption features resulting from interaction between a mineral surface and crude oil. The new insight, at nanoscale resolution, enables direct visualisation of role of asphaltene in controlling the wettability of mineral surfaces. Absence of asphaltene is evident by an adsorption morphology that has distinctive features compared to that produced when asphaltene is present in the crude.
- Changes in brine salinity have a severe effect in the thickness of oil components adsorb to the mineral surface. As salinity is diluted, there is a sharp decreasing in adsorped layer thickness. This provides a direct confirmation of the benefit of diluting brine to enhance oil recovery.

- Two main texture patterns are observed when oil solubility is changed. If oil solubility changes where asphaltene start to precipitate, a dendritic oil adsorption pattern is formed on the rock surface. However, this dendritic oil adsorption pattern is not apparend when asphaltene is dissolved.

Chapter 8
Conclusions and Recommendations

8.1 Introduction

This thesis has presented work from an extensive experimental program conducted to assess the impact of wettability on petroleum recovery. More specifically, the role of brine and temperature in wettability alteration has been investigated by four main approaches. **Chapter 4** investigated the basic understanding of wettability alteration of homogenous mineral surfaces. Contact angle measurements were utilised as a direct indication of wettability. **Chapter 5** increased the complexity by including the role of capillary forces in 2D glass micromodels. Combining pressure measurements and visualisation of fluid interfaces provided very informative results. Extrapolating previous results would be highly uncertain without considering the real rock surface. **Chapter 6** used rock samples from outcrops and an Omani reservoir. This third approach studied the displacement behaviour as a function of brine salinity and temperature. **Chapter 7** investigated the morphology resulting from the reaction of crude oil and a mineral surface. Nanoscale resolution of wettability alteration is extensively investigated using a novel scanning interferometry technique. In the following, further discussions and conclusions of the previous chapters are presented.

8.2 Further Discussion and conclusion

8.2.1 Effective wettability of mineral surfaces

Contact angle measurements provide a universal indication of the wettability of mineral surfaces. Advancing and receding contact angle measurements were used to describe the movement of oil and brine interface inside the reservoirs . The main conclusion that emerge from **Chapter 4** are:

Asphaltene content:

Asphaltene presence and solubility both play an important role in wettability alteration. Removing asphaltene from crude oil results in less oil-wet silicate surfaces but the oil-wetness still dominates the glass surface. However, mixing the crude oil with a good asphaltene solvent (toluene) results in more water-wet glass surface whereas mixing crude oil with an asphaltene precipitant (heptane) results in extremely oil-wet silicate surfaces. Therefore, understanding the conditions that result in asphaltene precipitation in crude oil is critical to predicting wettability alteration.

Impact of brine composition:

The composition of the brine film which covers mineral surfaces has a strong impact on wettability alteration. This role was investigated extensively through short-time (adhesion test) and long time (deposition test) interaction tests. Diluting brine in the presence of crude oil renders silicate surfaces more water-wet. Furthermore, the degree of hysteresis between advancing and receding contact angle is increased significantly when exposed to adhesive brine compared to stable brine film.

Impact of temperature:

Increasing the temperature increased the contact angles of silicate surface (i.e. made them more oil-wet). The lack of wettability reversal as a function of temperature, when asphaltene is absent from crude oil, indicates the presence of asphaltene in crude oil is a critical factor. In extracting the water-soluble components from crude oil, temperature does not have any effect on wettability alteration of silicate surface.

Oil/brine interface:

The wettability alteration of rock surfaces is affected by the interfacial activity between the oil and brine. Thus, it is important to study the behaviour of IFT with brine composition. The

interfacial tension behaviour is classified into two main categories based on brine pH and brine salinity:

Brine pH:

There is a strong interplay between the acid and base number crude oil of the crude oil and the pH of brine in controlling wettability alteration. Crude oils with the highest acid number experienced greater reduction in IFT when exposed to alkaline brine. Conversely, crude oil with a high base number shows a sharp reduction in IFT when in contact with more acidic brine. This indicates the wettability altering acids and bases that exist in the crude oil control the interfacial activity especially if the pH of reservoir brine is changed.

Brine salinity:

IFT passes through a minimum at a specific ionic strength. The alteration of interfacial activity as a function of brine salinity was only observed when polar components are present in the crude oil. The sensitivity of interfacial tension to acid and base number as well as brine pH and salinity has a major implication for the estimation of recoverable oil where the interfacial tension is a critical parameter in defining the capillary pressure. Dealing with interfacial tension as a constant parameter through the entire reservoir, without considering the change of brine pH during CO_2 injection or the change of brine salinity during low salinity waterflooding, should be revisited.

8.2.2 Micromodel investigation of wettability alteration

Micromodels have been significant in providing an indepth understanding of immiscible displacement flow inside rock crevices. A 2D structures were etched in glass to mimic the pore structure of reservoir rock in terms of pore throats and pore bodies. In this study micromodels have been utilised toidentify how changing brine salinity, temperature and flow rate affect mutiphase flow processes. This is instructive when examining the rationale for some of the screening programmes in EOR methods (Taber et al., 1997). Understanding flow

mechnisms at the pore-scale provides the reservoir engineer with a fundamental knowledge of physical chemistry of enhanced oil recovery.

The main conclusions that emerge from **Chapter 5** are:

- A specific salinity-dependent flow regime in multiphase flow in petroleum reservoir has been identified for the first time. The three flow mechanisms identified were pinch off, frontal advance and stripping flow regimes. Residual oil saturation, S_{or}, is a maximum in the case of pinch off flow whereas it minimised in the case of stripping off oil flow behaviour.
- Temperature plays a major role in controlling pore-scale flow regimes. Increasing temperature in situ prior to water invasion results in dendritic flow controlling the multiphase displacement. This flow regime occurs as a result of oil blocking the streaming water through pore throats, which creates an early sharp water front. If the temperature increased prior to invading into oil reservoir, sub-singlet water flow behaviour controls the multiphase displacement.
- The wettability of the medium was found to control flow mechanisms and the distribution of the fluid phases. Flow behaviour during imbibition can be classified into two main flow regimes depending on the injection rate and contact angles:
    - **Grain jump** describes the situation where water peels oil from grain surface and subsequently water jumps from grain to grain until the water breakthrough. Water clearly occupies the smaller pores and occurs as a thin film on the solid surface. This flow behaviour is limited to a very low rates (0.04 cc/min).
    - **Frontal advance**: describes flow when oil is mainly swept from pore bodies. This flow behaviour dominated at 0.1 cc/min and 1 cc/min rate.
- Flow behaviour is not sensitive to rate when contact angle is increased to 60° and 170° using crude oil and silane agent respectively.

8.2.3 Core scale investigation of wettability alteration

EOR requires careful engineering design. Screening criteria for EOR are designed based on laboratory investigations (Al-Mjeni et al., 2011). Cores extracted from reservoir were utilised to define the screening criteria for EOR implementations. Thus, the purpose of **Chapter 6** is to investigate the core scale response as brine salinity and temperature are altered. For the first time, wettability measurement based on spontaneous imbibition and nuclear magnetic resonance (NMR) were conducted on the same cores. The main conclusions are:

- Reducing the salinity of brine with monovalent cations increases oil recovery in sandstones. The presence of clay is not a necessary condition to observe the increased recovery. Increased oil recovery occurs by shifting the wettability of mineral surfaces towards a more water-wet state.
- Increasing temperature from 20°C to 60°C in sandstones causes a large decrease (50%) of recovery factor I_{AH} and I_{NMR} and suggests that the wettability is shifted towards a more oil-wet state.
- Increasing temperature in carbonates increases recovery factor by less than 4%. I_{AH} and I_{NMR} indicate the wettability is shifted by less degree towards water-wet.
- The viscous force produces two patterns of injectivity to sweep the residual oil as brine salinity changes. The first is sweeping the oil with high injectivity, which occurs between 0.5 M and 0.1 M NaCl brine. The second is sweeping the oil with loss of water injectivity between 0.1 M and 0.01 M NaCl brine. The potential reason of losing injectivity is attributed to detachment of clay that coats the grains leading to a blockage of pore throats.

8.2.4 Adsorption Morphology of wettability alteration

Advancement of surface engineering technology takes the studies of wettability to a new era, which includes the nanoscale observation of wettability alteration. Previous studies on the

impact of wettability on petroleum recovery infer the reservoir wettability from either indirect measurements (I_{AH}) or macroscopic measurements (contact angle). **Chapter 7** assesses wettability of petroleum reservoir at nanoscale resolution. Vertical scanning interferometry is used to probe the morphology of the layer of material adsorbed from crude oil without damaging weak material as happens when using AFM (Bowen and Hilal, 2009). Several novel conclusions emerge:

- Brine salinity variations have a major effect on the thickness of the adsorbed oil layer on mineral surfaces. There is a sharp decreasing of oil adsorption thickness as brine salinity is reduced. Reduction of the thickness of adsorbed oil provides direct evidence of enhancing oil recovery.
- Mineral surfaces have a microscopic texture that varies depending on the brine salinity used during equilibraton with crude oil. The texture of the adsorbed layer is consistent with the Dalmation wettability model. It is consistent with the model in which water accumulates as pockets on the mineral surface during interaction with crude oil. Some pockets of water remain trapped underneath the adsorbed oil layer. This Dalmation wettability scenario is supported by quantitative parameters, such as surface roughness profile, which shows a continuous increase as brine salinity diluted.
- For the first time, 3D parameters, established by International Organization for Standardization (ISO), are used to describe the features resulting from adsorption of crude oil. The new insight, at nanoscale resolution, highlights the role of asphaltene in altering the wettability of mineral surfaces. The texture of the absorbed layer is different when created by reaction with asphaltene-rich and asphaltene-free crude oil.
- Two main texture patterns were observed when aspheltene solubility in oil is changed. A dendritic oil adsorption pattern is formed on the mineral surface if asphaltene starts to precipitate. However, a uniform layer is produced when asphaltene is dissolved in the crude.

8.3 Practical significance

The experimental studies carried out in this thesis have significant implications for the interpretation of core floods and also for data input parameters in grid block characterisation for numerical models, at both core plug and field scale.

Most of experimental work performed in the literature to measure the interfacial tension between brine and oil assumes equilibrium status is achieved after short time (minutes) of contact (Jasper et al., 1970; Janczuk, 1993). **Chapter 4** indicates equilibration time between immiscible phases requires at least one hour of contact. In assessment of oil reserves, underestimation of interfacial tension between oil and brine will impact the determination of oil saturations above the free water level in the underground reservoirs. The consequence of uncertainty in estimation of oil columns could lead to mistakes during drilling and well completion. Furthermore, changing of interfacial tension with brine salinity requires a careful consideration of such variables when a salinity gradient exists in a reservoir. For example, surfactant EOR uses a salinity gradient design, in which the salinity of brine reservoir is controlled, to keep as much surfactant as possible in the active region and to minimize surfactant retention on the mineral surface (Hirasaki et al., 1983). This salinity gradient scheme will impact the interfacial tension and consequently requires an update feeding to dynamic reservoir model which forecast the behaviour of surfactant injection.

In field development plans, the use of relative permeability derived from laboratory measurement should always be coupled with a rate function. Fluids exhibit high flow rate in vicinity of injection wells and low rates in the bulk reservoir (Heaviside et al., 1987). These two extreme situations should be incorporated in numerical simulation with separate relative permeability curves. Failure to incorporate representative relative permeability data into numerical models will give a totally erroneous interpretation of the flood process, and hence an incorrect prediction of EOR. This study shows visually, in **Chapter 5,** the role of flow rate on microscale displacement behaviour in water-wet, mixed-wet and oil-wet rocks.

The combination of macroscopic and microscopic studies is complementary and necessary. This appears during **Chapter 6** when results on experiments on rocks draw important conclusions from the micromodel work in **Chapter 5.** The assessment of oil reservoir mineralogy, the presence of clay in the rock surface is not a necessary condition to select the reservoir candidate to EOR by low salinity brine. Furthermore, the way that heat is introduced to a reservoir may affect wettability. For example, wettability may vary depending upon whether heating occurs via cyclic steam injection or continuous steam flooding.

Surface engineering technology undoubtedly will advance the understanding of the EOR process to new levels. The results that emerge from utilising vertical scanning interferometry enrich our understanding of various EOR techniques. Hydrocarbon co-injection to oil reservoir has implemented for 30 years (Stalkup, 1983). The ultimate goal is to achieve misciblity between an injected solvent and the oil in the reservoir. This involves dramatically reducing interfacial tension so that economic sweep is achieved. The results of **Chapter 7** indicate the type of solvent mixed with oil have a dramatic impact in the thickness of layer of oil adsorped to the mineral surface. Increasing the thickness of oil adsorption as a result of heptane injection to oil reservoir is anticipated to be 15 times the oil adsorption thickness if toluene is injected into the oil reservoir. Such results have a practical significance in planning miscible displacements. In particular, they suggest that it is important to establish screening criteria solvent used in miscible displacements. The optimal solvent to achieve a miscible displacement is one that would reduce the interfacial tension without encouraging the oil retention on rock surface. Thus, successful integration between surface analytical techniques such as VSI and special core analysis will reduce the uncertainty of EOR implementation programme.

There is a practical significance regarding the understanding of the distribution of hydrocarbons in subsurface formations. In the past, the normal presumption was that the hydrocarbon is present in the subsurface formation as a homogenous fluid (Høier and Whitson, 2001). Recently, the advancement of fluid sampling technique indicates that the

hydrocarbons are frequently highly graded compositionally in the subsurface. The new view is that "hydrocarbons in the formation are considered compositionally graded unless otherwise proven" (Mullins et al., 2005). **Chapter 4** and **Chapter 7** address this issue through investigation of the role of asphaltenes components in crude oil, which shows a dramatic difference in the adsorption morphology when asphaltene is absent from crude oil. The distinctive difference of wettability (more water-wet) when asphaltene is absent has a practical significance in the flow behaviour via the type aggregation that occurs on the pore surface.

8.4 Recommendations

There are still many questions remaining regarding the process of wettability alteration and how wettability impacts petroleum recovery. The motivation of researchers should be carried out to find solutions to persistent technical challenges in EOR. Here recommendations are summarised for future researches:

New frontier for crude oil impact in wettability

A standard way of treating crude oils is divide their components within the SARA classification (saturates, aromatics, resin and asphaltenes). These designations are focused on operational procedures associated with solubility and adhesion in column chromatography. However, clear chemical designation for crude oil components in terms of elements and functional groups is not captured in details by the SARA test. Petroleomics, the establishment of structure-function relations for asphaltenes and crude oils, is being implemented (Rodgers and Marshall, 2007). The development of Fourier-transform - ion-cyclotron-resonance - mass spectroscopy (FT-ICR-MS) has pushed the resolution and mass accuracy of mass spectroscopy beyond the SARA test. The new mass spectral and other analytical technique are of sufficient resolution that generation of the full details of crude oil is in sight. Thus, FT-ICR-MS enables petroleomic molecular structure of crude oil components and especially of their mysterious constituents asphaltenes must be understood as

the root source of wettability effect in petroleum recovery. Simply stated, petroleum companies sell molecules and consequently, an oils composition determines its economic value. Therefore, compositional knowledge equals power: to produce oil reserves more efficiently. In wettability research, petroleomic science may be used to investigate correlations between chemical function, structure and contact angle. If there is a definite correlation, the wettability of the oil reservoir can be challenged from crude oil sampling. This will enhance the results of other wettability measurements such as I_{AH}, USBM index and I_{NMR}.

Another output from researching the wettability by applying petroleomics science is defining the chemical mechanism of EOR specific techniques. For example, the role of brine salinity in desorption the oil components from silicate surface. If the ability of revealing each crude oil components is available by FT-ICR-MS, then analysis of effluent crude oil produce from the outlet of flow experiments may be very informative. The analysis of dynamic desorption of crude oil after different brine salinity will explain which parts of crude oil are desorbed.

Effect of brine salinity in Carbonate reservoir

In this thesis, the effect of brine salinity was studied in outcrop and reservoir sandstone. More than 50% of known petroleum reserves are trapped in carbonate reservoirs, which can be divided into limestone, chalk and dolomite (Austad, 2012). Until recently, there are no studies of the effect of brine salinity on carbonate reservoir except (Yousef et al., 2011). It is recommended to study the role of brine salinity in carbonate reservoir rocks as these are still the most common reservoir rock and are likely to contain large amounts of oil remaining after primary and secondary recovery.

Phase behaviour of asphaltene on mineral surfaces

Vertical scanning interferometry offer fascinating results that shows distinctive wettability pattern as the solvent mixed with crude oil is switched from heptane to toluene (**Figure 7.52 & 7.55**). The two extreme adsorption morphologies indicate the crude oil might undergo

different steps in phase behaviour. The kinetic process of phase behaviour of crude oil with respected to asphaltene precipitation deserve more in-depth study before the final adsorption occurs. Ideally, it is a great advantage for a reservoir engineer to detect the precursor of asphaltene flocculation, which is the formation of microscopic particles. This is important when reservoir pressure decreases towards the bubble point of the oil, the solubility of asphaltenes in the crude oil decreases and they may precipitate and adsorb on the rock (Buckley, 1995). Early warning of such flocculation will avoid a major economic lost in production. These particles are generally believed to originate from asphaltene molecular self-association. Unfortunately, the knowledge that we have about asphaltenes is limited, and the mechanisms of nucleation and deposition are not completely understood. Thus, the asphaltene self-association is an important a phenomenon to investigate and understand. Yen (1988) proposed a hypothetical model that explicitly describes the evolution of the particle size from nano size aggregates to macroscopic particles observed in precipitates. Yen model is based on length scale and elemental particles, as Yen named then, are nanoscale aggregates arising from molecular self-association. This aggregation step forms the nano size precursors that flocculate later and then coat the surface of minerals. The self-association of asphaltenes in well characterised solvents can be studied using glass micromodels. Such experiments offer a direct measure of particle size as asphaltene aggregates with time. This will enhance the understanding to asphaltene self-association before adsorption.

9 References

Adamson, A.W. and Gast, A.P., 2007, Physical Chemistry of Surfaces. Wiley, New York.

Alboudwarej, H., Pole, D., Svrcek, W.Y. and Yarranton, H.W., 2005, Adsorption of Asphaltenes on Metals. Industrial & Engineering Chemistry Research, 44: 5585-5592.

Alireza Emadi, M.S., Hamon, Gerald. and Jamiolahmady, Mahmoud., 2010, Mechanistic Study Of Improved Heavy Oil Recovery By Alkaline Flood And Effect Of Wettability. Proc. 2010 SCA International Symp., Halifax, Nova Scotia, Canada.

Al-Bahlani, A.M. and Babadagli, T., 2009, SAGD laboratory experimental and numerical simulation studies: A review of current status and future issues. Journal of Petroleum Science and Engineering, 68: 135-150.

Al-Hadhrami, H. and Blunt, M., 2001, Thermally Induced Wettability Alteration To Improve Oil Recovery in Fractured Reservoirs SPE Reservoir Evaluation & Engineering, 4: 179-186.

Al-Mahrooqi, S.H., Grattoni, C.A., Muggeridge, A.H., Zimmerman, R.W. and Jing, X.D., 2006, Pore-scale modelling of NMR relaxation for the characterization of wettability. Journal of Petroleum Science and Engineering, 52: 172-186.

Al-Mutairi, S.M. and Kokal, S.L., 2011, EOR Potential in the Middle East: Current and Future Trends, SPE 143287 Annual conference, Vieena, 23-26 May.

Al-Mjeni, R., Arora, S., Cherukupalli, P., Wunnik, J.V., Edwards, J., Felber, B.J., Gurpinar, O., Hirasaki, G., Miller, C., Jackson, C., Kristensen, M., Lim, F. and Ramamoorthy, R., 2011, Has the time come for EOR? Oilfield Review Winter, 22: 16.

Amott, E., 1959, Observations Relating to the Wettability of Porous Rock. Published in Petroleum Transactions, AIME, Vol. 216, 1959, pages 156-162.

Amyx, J. M., Bass, D. M. and Whiting, R. L.,1960, *Petroleum Reservoir Engineering - Physical Properties*, McGraw-Hill Book Company, New York.

Anderson, W.G., 1986a, Wettability Literature Survey- Part 1: Rock/Oil/Brine Interactions and the Effects of Core Handling on Wettability. SPE Journal of Petroleum Technology, 38: 1125-1144.

Anderson, W., 1986b, Wettability Literature Survey- Part 2: Wettability Measurement. SPE Journal of Petroleum Technology, 38: 1246-1262.

Anderson, W.G., 1986c, Wettability Literature Survey-Part 3: The Effects of Wettability on the Electrical Properties of Porous Media. SPE Journal of Petroleum Technology, 38: 1371-1378.

Anderson, W.G., 1987a, Wettability Literature Survey- Part 4: Effects of Wettability on Capillary Pressure. SPE Journal of Petroleum Technology, 39: 1283-1300.

Anderson, W.G., 1987b, Wettability Literature Survey Part 5: The Effects of Wettability on Relative Permeability. SPE Journal of Petroleum Technology, 39: 1453-1468.

Anderson, W.G., 1987c, Wettability Literature Survey-Part 6: The Effects of Wettability on Waterflooding. SPE Journal of Petroleum Technology, 39: 1605-1622.

Arnarson, T.S. and Keil, R.G., 2000, Mechanisms of pore water organic matter adsorption to montmorillonite. Marine Chemistry, 71: 309-320.

ASTM 664-89, 1989, Annual Book of ASTM Standards, American Society Testing Materials, Section 5, Philadelphia.

ASTM 2896-88, 1988, Annual Book of ASTM Standards, American Society Testing Materials, Section 5, Philadelphia.

Austad, T., Rezaeidoust, A. and Puntervold, T., 2010, Chemical Mechanism of Low Salinity Water Flooding in Sandstone Reservoirs. Society of Petroleum Engineers, Tulsa, Oklahoma, USA.

Austad, T., 2012, Water Based EOR in Carbonates and Sandstones: New Chemical Understanding of the EOR-Potential Using "Smart Water". Short course in SPE Enhanced Oil Recovery at Oil and Gas West Asia, Muscat 14th April 2012.

Avraam, D.G. and Payatakes, A.C., 1995, Flow regimes and relative permeabilities during steady state two-phase flow in porous media. Journal of Fluid Mechanics, 293: 207-236.

Babadagli, T., Sahin, S., KALFA, U., Celebioglu, D., Karabakal, U. and Topguder, N.N.S., 2008, Development of Heavy Oil Fractured Carbonate Bati Raman Field: Evaluation of Steam Injection Potential and Improving Ongoing CO2 Injection, SPE 115400, Annual technical conference, Denver, 21-24 Septemper.

Barge, D.L., Carreras, P.E., Uphold, D.D., Al-Yami, F.M., Deemer, A.R. and Al-Anezi, T., 2009, Steamflood Piloting the Wafra Field Eocene Reservoir in the Partitioned Neutral Zone, Between Saudi Arabia and Kuwait, SPE 120205 Middle East Oil and Gas Show and Conference, Bahrain.

Barron, A.R. ed. 2009, Physical method in inorganic and nanochemistry. CONNEXIONS, Rice univesity, Houston.

Bernard, G.G., 1967, Effect of Floodwater Salinity on Recovery Of Oil from Cores Containing Clays, SPE 1725 Annual California Regional Meeting, Los Angles, October 26-27.

Berg, S., Cense, A.W., Jansen, E. and Bakker, K., 2009, Direct experimental evidence of Wettability modification by low salinity. Proc. 2009 SCA International Symp.,Noordwijk,The Netherlands.

Bobek, J.E., Mattax, C. and Denekas, M.O., 1958, Reservoir Rock Wettability – Its Significance and Evaluation. Published in Petroleum Transactions, AIME., 213: 155-160.

Bowen, W.R. and Hilal, N., 2009, Atomic Force Microscopy in Process Engineering - An Introduction to AFM for Improved Processes and Products. Elsevier.

Brown, R.J.S. and Fatt, I., 1956, Measurements of Fractional Wettability of Oil Fields Rocks by the Nuclear Magnetic Relaxation Method American Institute of Mining, Metallurgical, and Petroleum Engineers, SPE 743-G 31st Annual Fall Meeting, Los Angeles, October 14-17.

Brzoska, J.B., Azouz, I.B. and Rondelez, F., 1994, Silanization of Solid Substrates: A Step Toward Reproducibility. Langmuir, 10: 4367-4373.

Buckley, J.S. and Lord, D.L., 2003, Wettability And Morphology Of Mica Surfaces After Exposure To Crude Oil. Journal of Petroleum Science and Engineering, 39: 261-273.

Buckley, J.S., Liu, Y., Xie, X. and Morrow, N.R., 1996, Asphaltenes and crude oil wetting - the effect of oil composition. The SPE/DOE Improved Oil Recovery Symposium held in Tulsa-SPE 35366.

Buckley, J.S., 2001, Effective Wettability Of Minerals Exposed To Crude Oil. Current Opinion in Colloid & Interface Science, 6: 191-196.

Buenrostro-Gonzalez, E., Groenzin, H., Lira-Galeana, C. and Mullins, O.C., 2001, The Overriding Chemical Principles that Define Asphaltenes. Energy & Fuels, 15: 972-978.

Butler, R.M., 1991, Steam Assisted Gravity Drainage. In *Thermal Recovery of Oil and Bitumen, 258-359.*Englewood Cliffs, New Jersey: Prentice Hall.

Caruana, A. and Dawe, R.A., 1996, Flow behaviour in the presence of wettability heterogeneities. Transport in Porous Media, 25: 217-233.

Chang, Y.C., Mohanty, K.K., Huang, D.D. and Honarpour, M.M., 1997, The impact of wettability and core-scale heterogeneities on relative permeability. Journal of Petroleum Science and Engineering, 18: 1-19.

Chatenever, A. and Jr., J.C.C., 1952, Visual Examinations of Fluid Behavior in Porous Media Part I. Petroleum Trans. AIME, 195: 149-156.

Chatzis, I. and Morrow, N.R., 1984, Correlation of Capillary Number Relationships for Sandstone. Society of Petroleum Engineers Journal, 24: 555-562.

Christenson, H.K. and Yaminsky, V.V., 1995, Solute Effects on Bubble Coalescence. The Journal of Physical Chemistry, 99: 10420-10420.

Chukwudeme, E. and Hamouda, A., 2009, Enhanced Oil Recovery (EOR) by Miscible CO_2 and Water Flooding of Asphaltenic and Non-Asphaltenic Oils. *Energies, 2:* 714-737.

Chen, J., Hirasaki, G.J. and Flaum, M., 2006, NMR wettability indices: Effect of OBM on wettability

and NMR responses. Journal of Petroleum Science and Engineering, 52: 161-171.

Chilingar, G. V. And T.F. Yan, "Some notes on wettability and relative permeabilities of carbonate reservoir rocks," Energy sources, (1983)7: 67.

Cissokho, M., Boussour, S., Cordier, P., Bertin, H. and Hamon, G., 2009, Low salinity oil recovery on clayey Sandstone: experimental study. Proc. 2009 SCA International Symp.,Noordwijk,The Netherlands.

Cissokho, M., Bertin, H., Boussour,S, Cordier,P and Hamon,G., 2010, Low Salinity Oil Recovery On Clayey Sandstone: Experimental Study. Petrophysics, 51:305-313.

Coates, G.R., Xiao, L. and Prammer, M.G., 1999, NMR logging : principles and applications. Halliburton Energy Services, Houston, Texas.

Craig, F.F., 1971, The Reservoir Engineering Aspects of Waterflooding, Dallas, Texas

Cratin, P.D., 1993, Mathematical Modelling of Some pH-Dependent Surface and Interfacial Properties of Stearic Acid. Journal of Dispersion Science and Technology, 14: 559-602.

Cuiec, L.E.,1984, Rock/Crude-Oil Interactions and Wettability: An Attempt to Understand Their Interrelation SPE 13211 Annual Technical Conference and Exhibition, 16-19 September 1984, Houston, Texas.

Cuiec, 1991, Evaluation of Reservoir Wettability and its effects on Oil Recovery. In: Interfacial Phenomena in Petroleum Recovery, edited by Norman R. Morrow: 319-375.

Cuiec, L.E., Bourbiaux, B., Kalaydjian, F.,1994, Oil Recovery by Imbibition in Low-Permeability Chalk SPE Formation Evaluation, 9: 200-208.

Dawe, R.A., 1991, Enhancing oil recovery. Journal of Chemical Technology & Biotechnology, 51: 361-393.

Dawe, R., Caruana, A. and Grattoni, C., 2011, Microscale Visual Study of End Effects at Permeability Discontinuities. Transport in Porous Media, 86: 601-616.

Derjaguin, B.V., 1987, Surface Forces. Consultants Bureau, New York And London

Denekas, M.O., Mattax, C.C. and Davis, G.T., 1959, Effects of Crude Oil Components on Rock Wettability. Trans. AIME, 216: 330-333.

Donaldosn, E.C., Thomas, R.D. and Lorenz, P.B., 1969, Wettability Determination and Its Effect on Recovery Efficiency. Society of Petroleum Engineers Journal: 13-20.

Donaldson, E.C. and Thomas, R.D., 1971, Microscopic observations of oil displacement in water-wet and oil-wet systems, SPE 3555, the 46th Annual Fall Meeting, New Oleans.

Donaldson, E.C., Chilingar, G.V. and Yen, T.F., 1985, Enhanced Oil Recovery: Fundamentals and analysis I. Elsevier.

Donaldson, E.C., Chilingar, G.V. and Yen, T.F. eds., 1985, Enhanced Oil Recovery II. Elsiver.

Dong, W.P., Davis, E.J., Butler, D.L. and Stout, K.J., 1995, Topographic features of cylinder liners an application of three-dimensional characterization techniques. Tribology International, 28: 453-463.

Drummond, C. and Israelachvili, J., 2004, Fundamental studies of crude oil-surface water interactions and its relationship to reservoir wettability. Journal of Petroleum Science and Engineering, 45: 61-81.

Dullien, F.A.L., 1992, Porous media Fluid transport and pore structure. Academic Press.

Edmondson, T.A., 1965, Effect of Temperature on Waterflooding. Journal of Canadian Petroleum Technology, 4: 236-242.

Ese, M.H., Sjoblom, J., Djuve, J. and Pugh, R., 2000, An atomic force microscopy study of asphaltenes on mica surfaces. Influence of added resins and demulsifiers. Colloid & Polymer Science, 278: 532-538.

Espinat, D., Fenistein, D., Barr, L., Frot, D. and Briolant, Y., 2004, Effects of Temperature and Pressure on Asphaltenes Agglomeration in Toluene. A Light, X-ray, and Neutron Scattering Investigation. Energy & Fuels, 18: 1243-1249.

Fan, T. and Buckley, J.S., 2002, Rapid and Accurate SARA Analysis of Medium Gravity Crude Oils. Energy & Fuels, 16: 1571-1575.

Fang, J. and Christenson, H.K., 1990, Viscosity And Adsorption Studies Of Australian Crude Oils In Thin Films. Journal of Dispersion Science and Technology, 11: 97-114.

Farooq, U., Sjblom, J. and Ye, G., 2011, Desorption of Asphaltenes from Silica-Coated Quartz Crystal Surfaces in Low Saline Aqueous Solutions. Journal of Dispersion Science and Technology, 32: 1388-1395.

Fathi, S.J., Austad, T., Strand, S. and Puntervold, T., 2010, Wettability Alteration in Carbonates: The Effect of Water-Soluble Carboxylic Acids in Crude Oil. Energy & Fuels, 24: 2974-2979.

Fleury, M. and Deflandre, F., 2003, Quantitative evaluation of porous media wettability using NMR relaxometry. Magnetic Resonance Imaging, 21: 385-387.

Fogden, A., 2009, Experimental Investigation Of Deposition Of Crude Oil Components In Brine-Filled Pores. Proc. 2009 SCA International Symp, Noordwijk, The Netherlands.

Freedman, R., Heaton, N., Flaum, M., Hirasaki, G.J., Flaum, C. and Hurlimann, M., 2003, Wettability, Saturation, and Viscosity From NMR Measurements. SPE Journal, 8: 317-327.

Freer, E.M., Svitova, T. and Radke, C.J., 2003, The role of interfacial rheology in reservoir mixed wettability. Journal of Petroleum Science and Engineering, 39: 137-158.

Hamouda, A.A., Karoussi, O. and Chukwudeme, E.A., 2008, Relative permeability as a function of temperature, initial water saturation and flooding fluid compositions for modified oil-wet chalk. Journal of Petroleum Science and Engineering, 63: 61-72.

Heaviside, J., Brown, C.E. and Gamble, I.J.A., 1987, Relative Permeability for Intermediate Wettability Reservoirs, Dallas, 62nd Annual technical conference held in Dallas, September 27-30.

Heiba, A.A., Davis, H.T. and Scriven, L.E., 1983 Effect of Wettability on Two-Phase Relative Permeabilities and Capillary Pressures SPE 12172 Annual technical,San Francisco, October 5-8, 1983.

Hirasaki, G.J., van Domselaar, H.R. and Nelson, R.C., 1983, Evaluation of the Salinity Gradient Concept in Surfactant Flooding. Society of Petroleum Engineers Journal, 23: 486-500.

Hirasaki, G.J., 1991, Wettability: Fundamentals and Surface Forces. SPE Formation Evaluation, 6: 217-226.

Hirasaki, G., Miller, C., Jackson, C., Kristensen, M., Lim, F. and Ramamoorthy, R., 2011, Has the time come for EOR? Oilfield Review Winter, 22: 16.

Hirasaki, G. and Zhang, D.L., 2004, Surface Chemistry of Oil Recovery from fractured, Oil-Wet, Carbonate formations SPE Journal, 9: 151-162.

Holbrook, O.C.B., George G., 1958, Determination of Wettability by Dye Adsorption. AIME, 213: 261-264.

Hsu, W.-F., Li, X. and Flumerfelt, R.W., 1992, Wettability of Porous Media by NMR Relaxation Methods, SPE 24761, 67th Annaul technical conference in Washington,October 4-7.

Hurlimann, M.D., 1998, Effective Gradients in Porous Media Due to Susceptibility Differences. Journal of Magnetic Resonance, 131: 232-240.

Høier, L. and Whitson, C.H., 2001, Compositional Grading-Theory and Practice. SPE Reservoir Evaluation & Engineering, 4: 525-535.

Jadhunandan, P.P. and Morrow, N.R., 1995, Effect of Wettability on Waterflood Recovery for Crude-Oil/Brine/Rock Systems. SPE Reservoir Engineering, 10: 40-46.

Jańczuk, B., Wójcik, W. and Zdziennicka, A., 1993, Determination of the Components of the Surface Tension of Some Liquids from Interfacial Liquid-Liquid Tension Measurements. Journal of Colloid and Interface Science, 157: 384-393.

Jasper, J.J., Nakonecznyj, M., Swingley, C.S. and Livingston, H.K., 1970, Interfacial tensions against water of some C10-C15 hydrocarbons with aromatic or cycloaliphatic rings. The Journal of Physical Chemistry, 74: 1535-1539.

Jerauld, G.R. and Rathmell, J.J., 1997, Wettability and Relative Permeability of Prudhoe Bay: A Case Study in Mixed-Wet Reservoirs. SPE Reservoir Engineering, 12: 58-65.

Jeribi, M., Almir-Assad, B., Langevin, D., Hénaut, I. and Argillier, J.F., 2002, Adsorption Kinetics of Asphaltenes at Liquid Interfaces. Journal of Colloid and Interface Science, 256: 268-272.

Johnson, E.F., Bossler, D.P. and Naumann, V.O., 1959, Calculation of Relative Permeability from Displacement Experiments, SPE 1023-G Petroleum Trans., 370-372.

Kaminsky, R., Milter, J. and Radke, C.J., 1996, Thin Films and Wettability Alteration of Silica and Calcite Surfaces. Proc. 1994 3rd International Symposium on Evaluation of Reservoir Wettability and Its Effect on oil Recovery, Wyoming.

Kao, R.L., Wasan, D.T., Nikolov, A.D. and Edwards, D.A., 1988, Mechanisms of oil removal from a solid surface in the presence of anionic micellar solutions. Colloids and Surfaces, 34: 389-398.

Karoussi, O., Skovbjerg, L.L., Hassenkam, T., Stipp, S.L.S. and Hamouda, A.A., 2008, AFM study of calcite surface exposed to stearic and heptanoic acids. Colloids and Surfaces A: Physicochemical and Engineering Aspects, 325: 107-114.

Kleinberg, R. L., and Vinegar, H.J. (1996), NMR properties of reservoir fluids, The Log Analyst, 37: 20-32.

Kovscek, A.R., H. Wong, C. J. Radke, 1993, A pore-level scenario for the development of mixed wettability in oil reservoirs. AIChE Journal, 39: 1072-1085.

Kovscek, A.R., 2006, Enhanced Oil Recovery Using Aqueous Phase Chemicals, Miscible Gas Injection, And Thermal Means. Encyclopedia of Life Support Systems (EOLSS). Retrieved from (http://www.eolss.net/).

Kowalewski, E., Boassen, T. and Torsaeter, O., 2003, Wettability alterations due to aging in crude oil; wettability and Cryo-ESEM analyses. Journal of Petroleum Science and Engineering, 39: 377-388.

Krauskopf, K.B. and Bird, D.K., 1994, Introduction to Geochemistry. McGraw-Hill Science.

Kumar, K., Dao, E. and Mohanty, K.K., 2005, AFM study of mineral wettability with reservoir oils. Journal of Colloid and Interface Science, 289: 206-217.

Kumar, K. Dao, E. and Mohanty, K.K., 2008, Atomic Force Microscopy Study of Wettability Alteration by Surfactants. SPE Journal, 13: 137-145.

Kumar, M., Senden, T.J., Sheppard, A.P., Middleton, J.P. and Knackstedt, M.A., 2009, Visualizing and Quantifying the Residual Phase Distribution in Core Material. Proc. 2009 SCA International Symp.,Noordwijk,The Netherlands.

Kumar, M. and Fogden, A., 2010, Patterned Wettability of Oil and Water in Porous Media. Langmuir,26: 4036–4047.

ISO 4287:2000, Geometrical product specifications (GPS)-surface texture: profile method-Terms, definitions and surface texture parameters (International organisation of standardization).

ISO/DIS 25178 part 2: 2007 Geometrical product specification (GPS) – Surface texture: Areal- Part 2: Terms, definitions and surface texture: Areal – Part 2: Terms, definitions and surface texture parameters (International Organization for Standardization).

Labrador, H., Fernndez, Y., Tovar, J., Muoz, R. and Pereira, J.C., 2007, Ellipsometry Study of the Adsorption of Asphaltene Films on a Glass Surface. Energy & Fuels, 21: 1226-1230.

Lager, A., Webb, K. and Seccombe, J., 2011, Low Salinity Waterflood, Endicott, Alaska, 16th European Symposium on Improved Oil Recovery. Cambridge, United Kingdom.

Lahooti, S., Rio, O.I.D., Neumann, A.W. and P.Cheng, 2010, Axisymmetric Drop Shape Analysis (ADSA). In: Neumann, A.W. and Spelt, J.K. (eds.), Applied surface thermodynamic.

Leach, R., 2010, Fundamental Principles of Engineering Nanometrology. Elsevier.

Lenormand, R., Zarcone, C. and Sarr, A., 1983, Mechanisms of the displacement of one fluid by another in a network of capillary ducts. Journal of Fluid Mechanics, 135: 337-353.

Lenormand, R. and Zarcone, C., 1984, Role Of Roughness And Edges During Imbibition In Square Capillaries. 59th Annual Technical Conference and Exhibition of society of Petroleum Engineers,Houston,Texas.

Lever, A. and Dawe, R.A., 1987, Clay migration and entrapment in synthetic porous media. Marine and Petroleum Geology, 4: 112-118.

Li, K. and Firoozabadi, A., 1998, Wettability Change To Gas-Wetness In Porous Media. Proc. 1998 Society of core analysts.

Lo, H.Y. and Mungan, N., 1973, Effect of Temperature on Water-Oil Relative Permeabilities in Oil-Wet and Water-Wet Systems, SPE 4505 48th Annual fall meeting of the society of petorluem engineers, Las Vegas, 30 October.

Loahardjo, N., Xie, X., Yin, P. and Morrow, N.R., 2007, Low Salinity Waterflooding of a Reservoir Rock. Proc. 2009 SCA International Symp., Calgary, Canada.

Lord, D.L. and Buckley, J.S., 2002, An AFM Study Of The Morphological Features That Affect Wetting At Crude Oil-Water-Mica Interfaces. Colloids and Surfaces A: Physicochemical and Engineering Aspects, 206: 531-546.

Luttge, A., 1999, An Interferometric Study Of The Dissolution Kinetics Of Anorthite: The Role Of Reactive Surface Area. American Journal of Science, 299: 652-678.

Luttge, A., 2004, Crystal dissolution kinetics studied by Vertical Scanning Interferometry (VSI) and Monte Carlo simulations: A brief review and outlook. Kluwer, New York..

Ma, S. and Morrow, N.R., 1994, Effect of Firing on Petrophysical Properties of Berea Sandstone. SPE Formation Evaluation: 213-218.

Macaulay, R.C., et al., 1995. Design of a steam pilot in a fractured carbonate reservoir — Qarn Alam field, Oman. SPE 30300, International heavy oil symposium , Calgary, 19-21 June.

Maini, B.B. and Batycky, J.P., 1985, Effect of Temperature on Heavy-Oil/Water Relative Permeabilities in Horizontally and Vertically Drilled Core Plugs. SPE Journal of Petroleum Technology.

Martin, J.C., 1959, The Effects of Clay on the Displacement of Heavy Oil by Water, SPE 1411-G, Venezuelan 3rd Annual meeting, Caracas, October 14-16th.

Manual Book, 2004, Drop Shape Analysis, KRUSS Company, Germany.

Masalmeh, S.K., 2003, The effect of wettability heterogeneity on capillary pressure and relative permeability. Journal of Petroleum Science and Engineering, 39: 399-408.

Masalmeh, S.K. and Oedai, S., 2009, Surfactant Enhanced Gravity Drainage: Laboratory Experiments and Numerical Simulation Model. Proc. 2009 SCA International Symp.,Noordwijk,TheNetherlands.

Mattax, C.C. and Kyte, J.R., 1961, Ever see a water flood. Oil and Gas Journal, 59: 115-128.

McCaffery, F.G. and Bennion, D.W., 1974, the Effect of Wettability On Two-Phase Relative Permeabilities. 13.

McGuire, P.L., Chatham, J.R., Paskvan, F.K., Sommer, D.M. and Carini, F.H., 2005, Low Salinity Oil Recovery: An Exciting New EOR Opportunity for Alaska's North Slope. SPE 93903, Wstern regional meeting held in Irvine, 30th March – 1 April.

Merdha, A. and Yassin, A., 2009, Scale formation due to water injection in Berea sandstone. Journal of applied science, 9: 3298-3307.

Mogensen, K. and Stenby, E., 1998, A Dynamic Pore-Scale Model of Imbibition. SPE 39658, SPE/DOE Improved oil recovery symposium held in Tulsa,19-22 April.

Mohanty, K.K., 1983, Multiphase Flow in Porous Media: III. Oil Mobilization, Transverse Dispersion, and Wettability, SPE 12127, 58th Annual technical conference, San Franciso , October 5-8.

Morris, E.E. and Wieland, D.R., 1963, A Microscopic Study Of The Effect Of Variable Wettability Conditions On Immiscible Fluid Displacement. Fall Meeting of the Society of Petroleum Engineers of AIME, New Orleans, Louisiana.

Morrow, N.R., 1979, Interplay of Capillary, Viscous And Buoyancy Forces In the Mobilization of Residual Oil. Journal of Canadian Petroleum Technology, 18: 35-46.

Morrow, N.R. and Nguyen, M.D., 1982, Effect of interface velocity on dynamic contact angles at rough surfaces. Journal of Colloid and Interface Science, 89: 523-531.

Morrow, N., Lim, Hau T., Ward, Jill S., 1986, Effect of Crude-Oil-Induced Wettability Changes on Oil Recovery SPE Formation Evaluation, 1: 89-103.

Morrow, N.R., Lim, Hau T., Ward, Jill S., 1986, Effect of Crude-Oil-Induced Wettability Changes on Oil Recovery SPE Formation Evaluation, 1: 89-103.

Morrow, N., 1990, Wettability and Its Effect on Oil Recovery. Journal of Petroleum Technology, 42: 1476-1484.

Morrow, N. and Buckley, J., 2011, Improved Oil Recovery by Low-Salinity Waterflooding. SPE Journal of Petroleum Technology, 63.

Morrow, N.R., Cram, P.J. and McCaffery, F.G., 1973, Displacement Studies in Dolomite With Wettability Control by Octanoic Acid. Society of Petroleum Engineers Journal, 13: 221.

Morrow, N.R., 1976, Capillary Pressure Correlations For Uniformly Wetted Porous Media,. Journal of Canadian Petroleum Technology, 15, 4, 49-69.

Morrow, N.R., Lim, Hau T., Ward, J., 1986, Effect of Crude-Oil-Induced Wettability Changes on Oil Recovery SPE Formation Evaluation, 1: 89-103.

Morrow, N., 1990, Wettability and Its Effect on Oil Recovery. Journal of Petroleum Technology, 42: 1476-1484.

Morrow, N.R. and Mason, G., 2001, Recovery of oil by spontaneous imbibition. Current Opinion in Colloid & Interface Science, 6: 321-337.

Moschopedis, S.E., Fryer, J.F. and Speight, J.G., 1976, Investigation of asphaltene molecular weights. Fuel, 55: 227-232.

Mullins, O.C., Sheu, E.Y., Hammami, A. and Marshall, A.G., 2007, Asphaltenes, Heavy Oils, and Petroleomics. Springer.

Mullins, O.C., 2010, The Modified Yen Model. Energy & Fuels, 24: 2179-2207.

Nasiri, K.S., and Arne Skauge, 2009, Use of enzymes to improve waterflood Performance. Proc. 2009 SCA International Symp., Noordwijk, The Netherlands.

Nasr, T.N., Beaulieu, G., Golbeck, H. and Heck, G., 2003, Novel Expanding Solvent-SAGD Process "ES-SAGD", Journal of Canadian Petroleum Technology, 42:13.

Neumann, A.W., 2010, Applied Surface Thermodynamics. CRC Press.

Owens, W.W., Archer, D.L., 1971, The Effect of Rock Wettability on Oil-Water Relative Permeability Relationships Journal of Petroleum Technology, 23:873.

Petzing, J., Coupland, J. and Leach, R., 2010, The Measurement of Rough Surface Topography using Coherence Scanning Interferometry, Good Practice Guide No. 116, National Physical Labortaory, London.

Penney, R.K., Lawati, S.B.A., Hinai, R., Ravesteijn, O.P.V., Rawnsley, K., Putra, P.H., Geneau, M.D., Ikwumonu, A., Harrasy, H. and Al-Habsi, M., 2007, First Full Field Steam Injection in a Fractured Carbonate at Qarn Alam, Oman, SPE 105406, SPE Middle East Oil and Gas Show and Conference.

Petroleum Development Oman, 2008, Amal West and East Thermal Field Development Plan. Private communication.

Rangel-German, E.R. and Kovscek, A.R., 2006, A micromodel investigation of two-phase matrix-fracture transfer mechanisms. Water Resources Research. 42, American Geophysical Union.

Rao, D.N., 1999, Wettability Effects in Thermal Recovery Operations SPE Reservoir Evaluation & Engineering, 2: 420-430.

Rathmell, J. J., Braun, P.H. and Perkins, T.K., 1973, Reservoir waterflooding residual oil saturation from laboratory tests, JPT, pp: 175-185.

Raza,S.H. ,Treiber, and D.L. Archer, 1968, Wettability of reservoir rocks and its evaluation, Producers Monthly, 32:4.

Robin, S., E. Rosenberg, and Omar Fassi-Fihri 1995, Wettability Studies at the Pore Level: A New Approach by Use of Cryo-SEM SPE Formation Evaluation, 10: 11-19.

Rosen, M., 1989, Surfactant and Interfacial Phenomena. John Wiley and Sons, NewYork

Salathiel, R.A., 1973, Oil Recovery by Surface Film Drainage in Mixed-Wettability Rocks Journal of Petroleum Technology, 25:1261.

Salimi, H., Kraan, G.M.v.d., Laros, M. and Bruining, J., 2008, Construction of glass micromodels with pore-size distributions in the 10-100 μm range using wet- and dry-etching techniques for the observation of counter-current imbibition. Wettability international Symposium in Abu Dhabi.

Sanyal, T., 2009, Meeting The Challenges Of Planning A Thermal Pilot For Ratqa Lower Fars Heavy Oil Field, SPE 126796, Kuwait International Petroleum Conference and Exhibition.

Sayyouh, M.H., Hemeida, A.M., Al-Blehed, M.S. and Desouky, S.M., 1991, Role of polar compounds in crude oils on rock wettability. Journal of Petroleum Science and Engineering, 6: 225-233.

Schembre, J.M., Tang, G.-Q. and Kovscek, A.R., 2005 Effect of Temperature on Relative Permeability for Heavy-Oil Diatomite Reservoirs SPE 93831,Western regional meeting held in Irvince, 30 Marth – 1 April.

Seccombe, J., Lager, A., Jerauld, G., Jhaveri, B., Buikema, T., Bassler, S., Denis, J., Webb, K., Cockin, A. and Fueg, E., 2010, Demonstration of Low-Salinity EOR at Interwell Scale, Endicott Field, Alaska, SPE 129692, SPE Improved Oil Recovery Symposium, Tulsa.

Shahin, G.T., Moosa, R., Al-Kharusi, B.S. and Chilek, G., 2006, The Physics of Steam Injection in Fractured Carbonate Reservoirs: Engineering Development Options That Minimize Risk, SPE 102186, SPE Annual Technical Conference and Exhibition.

Sharma, B., Maerefat, N. and Crocker, M.E., 1985, Geosciences Application to the Prediction of Reservoir Variations, US-DOE Contracts for Field Projects and Supporting Research on Enhanced Oil Recovery, Vol. 44, p. 85.

Sharma, M.M. and Filoco, P.R., 2000, Effect of Brine Salinity and Crude-Oil Properties on Oil Recovery and Residual Saturations. Society of Petroleum Engineers Journal, 5: 293.

Shouxiang, M., Morrow, N., Zhang, X. and Zhou, X., 1999, Characterization of Wettability from Spontaneous Imbibition Measurements. Journal of Canadian Petroleum Technology, 38.

Skauge, A., 2004, Experimental evidence of different Intermediate wetting states. Proc. 2004 SCA International Symp.,Abu Dhabi,UAE.

Sorbie, K.S., Wat, R.M.S. and Rowe, T.C., 1987, Oil Displacement Experiments in Heterogeneous Cores: Analysis of Recovery Mechanisms. SPE Annual Technical Conference and Exhibition, Dallas, Texas.

Stalder, J.L., 2007, Cross SAGD (XSAGD) - An Accelerated Bitumen Recovery Alternative. SPE Reservoir Evaluation & Engineering: 12.

Standnes, D.C. and Austad, T., 2003, Wettability alteration in carbonates: Interaction between cationic surfactant and carboxylates as a key factor in wettability alteration from oil-wet to water-wet conditions. Colloids and Surfaces A: Physicochemical and Engineering Aspects, 216: 243-259.

Stegemeier, G. And Jessen, F.W.,1959, The relationship of relative permeability to contact angle, Proc. of Conference on the theory of Fluid Flow in Porous Media, U. Of Oklahoma, Norman, Mar.

Strand, S., Standnes, D.C. and Austad, T., 2006, New wettability test for chalk based on chromatographic separation of SCN- and SO42. Journal of Petroleum Science and Engineering, 52: 187-197.

Snell, J.S. and Close, A.D., 1999, Yates Field Steam Pilot Applies Latest Seismic and Logging Monitoring Techniques, SPE 56791, Annual technical conference held in Houston, Texas 3-6 October.

Sorbie, K.S., Ryazanov, A.V. and Dijke, M.I.J.v., 2011, The structure of residual oil as a function Of wettability alteration using pore-scale Network modelling. proc. 2011 SCA International Symp., Austin, Texas,USA.

Spildo, K. and Buckley, J.S., 1999, Uniform and mixed wetting in square capillaries. Journal of Petroleum Science and Engineering, 24: 145-154.

Stalkup Jr., F.I., 1983, Status of Miscible Displacement. SPE Journal of Petroleum Technology, 35: 815-826.

Standard No. D-2006 (1978) Annual book of ASTM standards, part 24. American Society for Testing and Materials, Philadelpia.

Sun, W. and Tang, G.Q., 2006, Visual Study of Water Injection in Low Permeable Sandstone. Journal of Canadian Petroleum Technology, 45: 21.

Sohrabi, M., Tehrani, D.H., Danesh, A. and Henderson, G.D., 2001, Visualisation of Oil Recovery by Water Alternating Gas (WAG) Injection Using High Pressure Micromodels - Oil-Wet & Mixed-Wet Systems. SPE Annual Technical Conference and Exhibition.

Starov, V.M., Velarde, M.G. and Radke, C.J., 2007, Wetting and Spreading Dynamics. CRC Press.

Stover, R.L., Tobias, C.W. and Denn, M.M., 1997, Bubble coalescence dynamics. AIChE Journal, 43: 2385-2392.

Taber, J.J., Martin, F.D. and Seright, R.S., 1997, EOR Screening Criteria Revisited - Part 1: Introduction to Screening Criteria and Enhanced Recovery Field Projects. SPE Reservoir Engineering, 12: 189-198.

Tang, G.Q. and Morrow, N.R., 1997, Salinity, Temperature, Oil Composition, and Oil Recovery by Waterflooding SPE Reservoir Engineering, 12: 269-276.

Tang, G.Q. and Morrow, N.R., 1999, Influence of brine composition and fines migration on crude oil/brine/rock interactions and oil recovery. Journal of Petroleum Science and Engineering, 24: 99-111.

Tang, G.Q. and Kovscek, A.R., 2002, Wettability Alteration of Diatomite Induced by Hot-Fluid Injection, SPE 77461, SPE Annual Technical Conference and Exhibition, San Antonio.

Tiab, D. and Donaldson, E.C., 2011 Petrophysics, Third Edition: Theory and Practice of Measuring Reservoir Rock and Fluid Transport Properties. Gulf Professional Publishing.

Tie, H. and Morrow, N.R., 2005, Oil recovery by spontaneous imbibition before and after wettability alteration of three carbonate rocks by a moderately asphaltic crude oil. Proc. 2005 SCA International Symp.,Toronto, Canada., SCA 2005-11.

Thum, M., Leith, E.S., Wunnik, J.N.M.V., Mandhari, M.S. and Clark, H.P., 2010, Thermal Developments in Petroleum Development Oman's Southern Fields - An Update. SPE 129143, SPE EOR Conference at Oil & Gas West Asia.

Tong, Z. and Morrow, N.R., 2005 Wettability control by adsorption from crude oil - aspects of temperature and increased water saturation Proceedings of the 2005 International Symposium of the Society of Core Analysts.

Toulhoat, H., Prayer, C. and Rouquet, G., 1994, Characterization by atomic force microscopy of adsorbed asphaltenes. Colloids and Surfaces A: Physicochemical and Engineering Aspects, 91: 267-283.

Treiber, L.E., Owens, W.W., Amoco Production Co., 1972, A Laboratory Evaluation of the Wettability of Fifty Oil-Producing Reservoirs, SPE Journal, 12: 531.

Tsukamoto, K., 1993, In situ observation of crystal growth from solution. Faraday Discussions, 95: 183-189.

Valavanides, M.S. and Payatakes, A.C., 2001, True-to-mechanism model of steady-state two-phase flow in porous media, using decomposition into prototype flows. Advances in Water Resources, 24: 385-407.

Vekilov, P.G., Kuznetsov, Y.G. and Chernov, A.A., 1992, Interstep interaction in solution growth; (101) ADP face. Journal of Crystal Growth, 121: 643-655.

Vledder, P., Gonzalez, I.E., Fonseca, J.C.C., Wells, T. and Ligthelm, D.J., 2010, Low Salinity Water Flooding: Proof Of Wettability Alteration On A Field Wide Scale, SPE 129564, SPE Improved Oil Recovery Symposium,Tulsa.

Wang, F.H.L., 1988, Effect of Wettability Alteration on Water/Oil Relative Permeability, Dispersion, and Flowable Saturation in Porous Media. SPE Reservoir Engineering, 3: 617.

Wang, W., and Gupta, A., 1995, Investigation of the Effect of Temperature and Pressure on Wettability Using Modified Pendant Drop Method, paper SPE 30544, Annual Technical Conference and Exhibition, Dallas, TX, 22–25 October.

Webb, K.J., 2005, Low Salinity Oil Recovery - The Role of Reservoir Condition Corefloods. Proc. 13th European Symposium on Improved Oil Recovery — Budapest, Hungary.

Webb, K.J., Black, C.J.J. and Al-Ajeel, H., 2004, Low Salinity Oil Recovery - Log-Inject-Log, SPE 89379, SPE/DOE Symposium on Improved Oil Recovery.

Wei, M., R.S. Bowman, J.L. Wilson, and N.R. Morrow, 1993, Wetting properties and stability of silane-treated glass exposed to water, air and oil, Journal of Colloid and Interface Science., 157:154-159.

Weinbrandt, R.M., JR,H.J.Ramey, and Casse, F.J., 1975, The Effect of Temperature on Relative and Absolute Permeability of Sandstones, Society Of Petroleum Engineers Journal , SPE 4142.

Wickramathilaka, S., Howard, J.J., Morrow, N.R. and Buckley, J., 2011, An Experimental Study of Low Salinity Waterflooding and Spontaneous Imbibition. 16th European Symposium on Improved Oil Recovery. Cambridge, United Kingdom.

Wunderlich, R.W., 1991, Obtaining Samples with Preserved Wettability. In: Morrow, N.R. (ed.), Interfacial Phenomena in Petroleum Recovery. Marcel Dekker.

Xie, X., Morrow, N.R. and Buckley, J.S., 2002, Contact angle hysteresis and the stability of wetting changes induced by adsorption from crude oil. Journal of Petroleum Science and Engineering, 33: 147-159.

Yang, S.Y., Hirasaki, G.J., Basu, S. and Vaidya, R., 1999, Mechanisms for contact angle hysteresis and advancing contact angles. Journal of Petroleum Science and Engineering, 24: 63-73.

Yen, T.F. (1988). In: M. Grayson and J.I. Krochwitz (eds.), *Encyclopedia of Polymer Science and Engineering*, 2nd edn., Vol. 1. Wiley, New York.

Yildiz, H.O. and Morrow, N.R., 1996, Effect of brine composition on recovery of Moutray crude oil by waterflooding. Journal of Petroleum Science and Engineering, 14: 159-168.

Yousef, A.A., Al-Saleh, S.H., Al-Kaabi, A. and Al-Jawfi, M.S., 2011, Laboratory Investigation of the Impact of Injection-Water Salinity and Ionic Content on Oil Recovery From Carbonate Reservoirs. SPE Reservoir Evaluation & Engineering, 14: pp. 578-593.

Yokoyama, E., Okada, K. and Tsukamoto, K., 1998, Precise Visualization of the Non-Steady State Concentration Field around a Growing Crystal in Solution. Forma, 13: 363-374.

Yu, L. and Wardlaw, N.C., 1986, The influence of wettability and critical pore-throat size ratio on snap-off. Journal of Colloid and Interface Science, 109: 461-472

Zhang, X., Morrow, Norman R., Ma, Shouxiang, 1996, Experimental Verification of a Modified Scaling Group for Spontaneous Imbibition. SPE Reservoir Engineering, Volume 11, Number 4: Pages 280-285.

Zhang, G.Q., Waylon, V.H. and Hirasaki, G.J., 2000, Internal Field Gradients in Porous Media. Society of Petrophysicists & Well Log Analysts.

Zhou, X., N.R. Morrow, and S. Ma, 2000, Interrelationship of wettability, initial water saturation, aging time and oil recovery by spontaneous imbibition and waterflooding, Society of Petroleum Engineers Journal, 5:199-207.